CENTRO INTERNACIONAL DE ESTUDOS
DE DOUTORAMENTO E AVANZADOS
DA USC (CIEDUS)

TESE DE DOUTORAMENTO

SEARCHING FOR THE BASIC PATTERN OF MORPHOGENESIS IN THE INNER EAR: STUDY IN A BASAL VERTEBRATE, THE SHARK *SCYLIORHINUS CANICULA*

SANTIAGO PEREIRA GULDRÍS

ESCOLA DE DOUTORAMENTO INTERNACIONAL

PROGRAMA DE DOUTORAMENTO EN NEUROCIENCIA E PSICOLOXÍA CLÍNICA

SANTIAGO DE COMPOSTELA

2018

USC UNIVERSIDADE DE SANTIAGO DE COMPOSTELA

CENTRO INTERNACIONAL DE ESTUDOS DE DOUTORAMENTO E AVANZADOS DA USC (CIEDUS)

DECLARACIÓN DO AUTOR DA TESE

Searching for the basic pattern of morphogenesis in the inner ear: study in a basal vertebrate, the shark *Scyliorhinus canicula*

D. Santiago Pereira Guldrís

Presento a miña tese, seguindo o procedemento axeitado ao Regulamento, e declaro que:

1) *A tese abarca os resultados da elaboración do meu traballo.*
2) *De selo caso, na tese faise referencia ás colaboracións que tivo este traballo.*
3) *A tese é a versión definitiva presentada para a súa defensa e coincide coa versión enviada en formato electrónico.*
4) *Confirmo que a tese non incorre en ningún tipo de plaxio de outros autores nin de traballos presentados por min para a obtención doutros títulos.*

En Santiago de Compostela, 18 de outubro de 2018

Fdo. Santiago Pereira

CENTRO INTERNACIONAL DE ESTUDOS DE DOUTORAMENTO E AVANZADOS DA USC (CIEDUS)

AUTORIZACIÓN DA DIRETORA DA TESE

Searching for the basic pattern of morphogenesis in the inner ear: study in a basal vertebrate, the shark *Scyliorhinus canicula*

Dna. Isabel Rodríguez-Moldes Rey

INFORMA:

Que a presente tese, correspóndese co traballo realizado por D. ***Santiago Pereira Guldrís****, baixo a miña dirección, e autorizo a súa presentación, considerando que reúne os requisitos esixidos no Regulamento de Estudios de Doutoramento da USC, e que como diretora desta non incorre nas causas de abstención establecidas na Lei 40/2015.*

En Santiago de Compostela, 18 de outubro de 2018

Fdo. Isabel Rodríguez-Moldes

La investigación realizada fue financiada gracias a los siguientes proyectos:

Proyecto: Buscando la condición ancestral dela organización general de gnatóstomos: regionalización, migración, proyecciones y asimetrías en el cerebroen desarrollo de un tiburón.
Entidad finaciadora: Ministerio de Economía y Competitividad-FEDER (BFU2010-15816-P)
Entidades participantes: Universidad de Santiago de Compostela
Duración: 2010-2014
Investigador principal: Isabel Rodríguez-Moldes Rey

Proyecto: Estudio de la neurogénesis en cerebro embrionario y adulto desde una perspectiva evolutiva
Entidad financiadora: Ministerio de Economía y Competitividad-FEDER (BFU2014-58631-P)
Entidades particioantes: Universidad de Santiago de Compostela
Duración: 2015-2018
Investigador principal: Isabel Rodríguez-Moldes Rey/Eva Candal Suárez

Proyecto: Descodificación de las bases moleculares de la neurogénesis en el adulto mediante el análisis de la dinámica transcripcional de nichos neurogénicos de larga duración.
Entidad financiadora: Ministerio de Economía y Competitividad-FEDER (BFU2017-89861-P)
Entidades participantes: Universidad de Santiago de Compostela
Duración: 2018-2020
Investigador principal: Isabel Rodríguez-Moldes Rey/Eva Candal Suárez

La realización de esta tesis fue posible gracias a la concesión de contratos de investigación asociados a proyectos:

Contrato a cargo de proyecto BFU2014-58631-P, Ministerio de Economía y Competitividad-FEDER; plaza 2014-PN172, convocatoria nº 7/2016. Septiembre 2016 - junio 2017.
Contrato a cargo de proyecto BFU2017-89861-P, Ministerio de Economía y Empresa-FEDER; plaza 2017-PN093.00, convocatoria nº 7/2018). Septiembre 2018 - mayo 2019.

La disponibilidad de las sondas de los genes ha sido posible gracias al proyecto de secuenciacion EST del genoma de pintarroja, coordinado por la Dra. Sylvie Mazan (CNRS, Observatoire Océanologique, Banyuls-sur-Mer, Francia).

El escaneo y obtención de las imágenes tomográficas de las muestras ha sido posible gracias a la colaboración del Prof. Dr. Victoriano Urgorri y de la Dra. María Candás de la Estación de Biología Marina de la USC de A Graña (Ferrol, España) y a la disponibilidad del equipo de micro-CT.

Yo, Santiago Pereira Guldrís, con DNI 44823407H y con domiciliación a efectos de notificación Rego do Cebro 2, Pardiñas, Santiago de Compostela, **declaro** que esta tesis no presenta conflictos de interés. Y para que así conste firmo a día 18 de octubre de 2018.

Firmado:

Santiago Pereira Guldrís

Con muchas prisas y apuros de última hora, pero ya ha llegado el momento de terminar esta tesis y de agradecer a muchas personas el haber llegado hasta aquí y haber podido compartir al menos una parte de esta etapa. Gracias.

En primer lugar a Isa, mi directora. Muchas gracias por haberme dado la oportunidad de empezar esta tesis. Muchísimas gracias por todo tu trabajo, dedicación y entusiasmo sin límites, sobre todo esta última temporada tan intensa. No fue fácil, pero lo conseguimos.

A María, muchas gracias por tu trabajo con los escaneos y hacer posible que tenga unas imágenes tan buenas. A Vituco, gracias por llevar tantas veces las muestras a Ferrol y traerlas de vuelta con los DVDs. A Marcos, también gracias por encargarte de que las muestras llegaran bien y por los consejos para tratar las imágenes.

Muchas gracias a todos los profesores del Departamento de Biología Funcional, a Eva, Miguel, Fátima, Celina, Antón, Suso y Manolo. A Ramón, muchas gracias por tu revisión, por tener siempre la respuesta a cualquier duda y por tu interés y buena disposición siempre. A Eva, responsable de mil cosas y una de las claves de que el lab funcione, muchas gracias por tu trabajo e interés. Miguel, muchas gracias por los ánimos en esta etapa y los cafés. A Fátima, gracias por tu buen humor y encargarte de que no nos falte nada en el lab. A Celina, gracias por estar al tanto y preguntar siempre.

A mis compañeros del lab 3. Muchas gracias a Idoia, Sol, David y Gabi por todo lo aprendido y la compañía en mis inicios en el laboratorio. A Nuri, muchísimas gracias por todo. Por ayudarme en mis comienzos de tesis y por tu interés y ánimo siempre, también ahora en la distancia. Desde luego que sin ti estos años no habrían sido lo mismo y seguramente no habría viajado tanto ni comido tantas tartas, a ver cuándo toca la próxima. A Yara y Sheila, porque aunque no fue mucho tiempo, fue agradable. A Alberto, con quien compartí estos años de tesis y sobre todo esta etapa final, muchas gracias por tu buena disposición e interés y por tu ayuda con todo lo que hiciera falta. A Isma y Natalia, las nuevas generaciones y llenos de entusiasmo y ganas de aprender, muchas gracias por tan buena compañía y los ánimos en esta etapa final.

A los lampreys del lab 4. A Blanca, los Danis y Rocío. Porque da gusto tener unos vecinos tan alegres y que las risas se escuchen desde nuestro lab. A Dani Romaus por esos chistes tan malos. A Dani Sobrido, capaz de hacer mil experimentos a la vez, pero siempre de buen humor y dispuesto a echar una mano en lo que haga falta, muchas gracias. A Rocío, gracias por tan buena compañía y humor.

A los chicos del lab 2, Fran, Alejandra, Ilenia y Vero, porque este último mes de agosto en el lab fue mucho más llevadero con vuestra compañía.

Muchas gracias también a Xoa y Ana del Departamento de Genética, por hacernos un hueco en vuestro congelador cuando el nuestro no funcionaba.

A David Hernández, muchas gracias por tu rapidez al arreglar una matrícula que se había quedado a medias y que casi me provoca un infarto.

A Carlos, Fina, Espe, Suso, Sheila y demás compañía de la cafetería, porque parte de esta tesis es gracias a la energía en forma de cafés y pulgas de serrano.

A Nelson y Ando, por tantos años de amistad y tantos buenos momentos.

A Pedro, Noe, Adri y Rubén, por ser un grupo estupendo y al que pronto se unirá el pequeño León. Por todos estos años juntos y tantas cenas, anécdotas y diversión. Y por muchos años más.

A David y Katia, porque no me imagino sin vosotros y porque sea donde sea, no hay mejor lugar que cuando nos reunimos. Por todas las churruscadas habidas y por haber y por estar siempre ahí. Y a Maribel, Aurora y Manolo, porque estar en Chave es como estar en casa.

Gracias especialmente a mi familia. A mis padres José Manuel y Loli, por todo, por vuestro cariño y apoyo incondicional, sin el que hoy no estaría escribiendo estas líneas. A mi hermano Fran, por apoyarme y animarme siempre, no puedo imaginarme un hermano mejor.

CONTENTS

CONTENTS

GENERAL INTRODUCTION

GENERAL INTRODUCTION

The inner ear. General structure

The inner ear or labyrinth is the sensorial organ responsible for the detection of sound, balance and acceleration in all the craniates. It dates back at least 600 million years ago, at times of the early evolution of the vertebrates, and exists in all the craniates, from jawless vertebrates (agnathans: hagfishes and lampreys) to jawed vertebrates (gnathostomes; fishes, amphibians, reptiles, birds and mammals), but not in other chordates or deuterostomes. The origin of all of the components of the inner ear are the otic placode, a pair of thickened regions of the ectoderm next to the hindbrain which invaginate or cavitate to form the otic vesicle, a round hollow structure which later suffers a series of morphological changes that originate the chambers and semicircular canals which will house the sensorial patches containing the sensorial hair cells. The dorsal of vestibular region of the inner ear is composed by a series of semicircular canals (one or two in agnathans, three in gnathostomes) which perceive the movement and acceleration. The ventral or acoustical region is composed by a series of chambers which contain otholitic and non-otholitic sensorial patches that perceive vibrations and sound. This region is quite more variable among vertebrates, but is usually formed by two large sacs, the utricle an the saccule, with a variable number of macular and accessorial chambers, being the most remarkable one the acoustic specialized cochlea of mammals and birds. The sensorial hair cells of the cristae and maculae of the inner ear are innervated by prolongations of neurons of the statoacoustic ganglion, which

receives the information and transmits it to certain central nuclei by a central projection to the brain.

Development of the inner ear

Although the inner ear is a complex structure, it completely arises from two simple epithelial regions adjacent to the hindbrain, the otic placodes, which form that multiple-patched structure with mechanosensory cells for the perception of position, acceleration and auditory information (Torres and Giráldez, 1998; Streit, 2001). The otic placodes, in turn, derive as all the cranial placodes, from a common preplacodal region surrounding the neural plate at neurula stages (reviewed in Schlosser, 2006; Streit, 2007). The melanocyte cells of the *stria vascularis* (the secretory epithelium of the cochlea) are the unique cellular components that have a neural crest origin instead of a placodal origin (Torres and Giráldez, 1998). The preplacodal region is a part of the ectoderm located in the anterior border of the neural plate that generates all the cranial placodes, including the otic placodes, by expressing appropriated factors and receiving inducing signals from surrounding tissues (Whitfield, 2015). The otic placodes are approximately centered over the rhombomere 4, the one where the root of the statoacoustic nerve reaches the hindbrain, but there are differences in the position of the otic vesicle between vertebrate species and also along the development (reviewed in Whitfield and Hammond, 2007). The otic placode invaginates or cavitates and originates the otic vesicle or otocyst and the neuronal precursors that migrate and form the statoacoustic ganglion (reviewed in Torres and Giráldez, 1998; Schlosser, 2006). The potential of the placodes to

originate any sense organ is maintained as long as they are placed in an appropriated environment (Jacobson, 1966). The placode is fully determined after the closure of the neural tube, by the acquisition of the specification and commitment via inductive signals from surrounding tissues and the capacity of the ectoderm to form the ear depends on its proximity to the prospective otic region (Yntema, 1933; Waddington, 1937; Jacobson, 1963). The successive acquisition of the placodal competence, the specification of the otic field and the functionally isolation from surrounding tissues, make the otic field competent to acquire its identity and finally making irreversible its determination to form the inner ear, independently of the surrounding environment (Waddington, 1937; Jacobson, 1963; Vazquez et al., 1996). Some of the processes acting in the formation of the inner ear may be redundant, because despite the great number of mutations affecting to the ear isolated in mouse and zebrafish (Steel, 1995; Whitfield et al., 1996) there is no single mutation that can cause the complete agenesis of the otic vesicle or its sensorial organs (Torres and Giráldez, 1998).

The formation of the otic vesicle differs between vertebrates. While in lampreys, amphibians and non-reptile amniotes the placode invaginates into a cup just before closing and forming a vesicle, in teleost fish and reptiles the placodal cells form a solid sphere under the ectoderm that later forms a inner lumen inside itself (Thornhill, 1972; Haddon and Lewis, 1996).

The semicircular canals are formed from vertical and horizontal pouches that emerge in the dorsolateral regions of the otic vesicle. Those pouches form protrusions that grow into the lumen from opposite sites of

the wall and meet each other, forming pillars that are surrounded by the newborn semicircular canals. The protrusions are composed by hyaluronan-enriched extracellular matrix and its shape varies from long fingers in teleosts and amphibians to low hillocks in amniotes (Haddon and Lewis, 1991, 1996; Becerra and Anadón, 1993a; Whitfield, 2015). Similar processes of hyaluronan production and accumulation are observed in other structures like the heart, neural tube and crest and the secondary palate (Haddon and Lewis, 1991). In the lamprey, the anterior canal develops the first (Thornhill, 1972), but in most teleosts (*Danio rerio*, *Salmo trutta fario)* the anterior canal develops the before the others, followed by the posterior and the finally the lateral one (Waterman and Bell, 1984; Becerra and Anadón, 1993a). Although that seems to be the most frequently in teleosts, there are some exceptions like the first appearance of the horizontal canal in flat fishes (maybe due to the head torsion that these species suffer) or the last appearance of the posterior canal in primitive fishes like *Polypterus* (Thomot and Bauchot, 1987). There are even some contradictions in *Danio rerio*, where some authors consider that the horizontal canal appears the first (Waterman and Bell, 1984), while others propose that it appears the last (Haddon and Lewis, 1996). In *Xenopus* the lateral canal develops the first, followed by the anterior and finally the posterior canal (Haddon and Lewis, 1991), but in salamanders it develops simultaneously to the anterior canal (Norris, 1892). The horizontal canal develops the last in chicken (Bissonnette and Fekete, 1996), opossum (Larsell et al., 1935), mouse (Morsli et al., 1998) and human (Streeter, 1906).

The apparition of the saccule and lagena occurs late in development and also presents high variability between vertebrate groups and even between species within a group (Haddon and Lewis, 1996). In *Salmo trutta* (Becerra and Anadón, 1993a,b) and many other teleosts (Vasconcelos et al., 2016) the saccule and lagena are formed by evagination of the otocyst. A constriction separates the ventral saccule from the utricle, which remain connected only by a narrow duct, except in some derived features like *Cottus pollux* or *Scophthalamus maximus*, where the utriculo-saccular connection closes completely (Iwasaki, 1937; Becerra et al., 1990). By contrast, the lagena is not separated from the saccule in most teleosts, except in some derived cases like *Cyprinus carpio* or *Danio rerio,* although a communicating foramen remains (Iwasaki, 1937; Bever and Fekete, 2002). In cyprinids fishes the saccule also emits a medial projection under the hindbrain that contacts with a corresponding protrusion from the other side and forms an endolymphatic sinus which communicates both ears (Haddon and Lewis, 1996, Bever and Fekete, 2002). In chicken, a ventral protrusion of the saccule grows ventrally and medially and forms the cochlear duct that contains the basilar papilla, occupying almost all the duct; and the lagena, located at the duct´s tip (Bissonnette and Fekete, 1996). In mouse the cochlear duct emerges as a ventral protrusion before the formation of the semicircular canals. Ventral to the utricle, the saccule appears as a dilatation of the proximal part of the cochlea and maintains its connections to the utricle and the cochlea, while the distal part of the cochlea begins to coil until complete one and three-quarters turns (Morsli et al., 1998). The endolymphatic duct differs considerably between species. In some teleosts is

absent, while in others like *Salmo trutta fario* or *Danio rerio* appears relatively late and is a rudimentary tubular blind structure located at the medial part of the otocyst (Becerra and Anadón, 1993a; Bever and Fekete, 2002). In *Xenopus*, birds, and mammals, the endolymphatic duct forms a dilatation at its end, the endolymphatic sac (Haddon and Lewis, 1991, Bissonnette and Fekete, 1996; Morsli et al., 1998), which is located out of the bony labyrinth contacting with extralabyrinthine fluids. Despite the differences among vertebrates, the basic pattern of the inner ear is the same in all of them, being the major difference the lagena modified into the cochlea in mammals and into the basilar papilla in reptiles and birds (Popper, 2011).

Chondrichthyans belong to the most ancient radiation of gnathostomes, but, despite its phylogenetic position, there are scarce studies about the development of its inner ear. Chondrichthyans are teh only vertebrates where the endolymphatic duct is open externally, which has been considered a derived feature (Maisey, 2001), and although they present all the characteristics of the gnathostome inner ear, they also present some particularities, like the almost totally circularized posterior semicircular canal or the presence of the utricular recess (reviewed in Baird, 1974, Maisey, 2001). Among the chondrichthyans, the lesser spotted dogfish *Scyliorhinus canicula* represents and ideal model for searching for the ancestral condition due to its evolutionary position and appropriated characteristics as a model organism (Coolen et al., 2009).

Perception of mechanical stimuli. Mechanosensorial cells of the inner ear

The sensorial hair cells and supporting cells are located in various sensorial patches which vary in position and number in the otic epithelia among taxa (Fritzsch et al., 2002). The origin and evolution of the mechanosensorial cells has been nicely revised by Fay and Popper (2000), Fritzsch and Beisel (2001) and Fritzsch et al. (2002, 2006).

The neurosensory transduction process of mechanical stimuli by the sensorial hair cells depends on the regulation of the volume and concentration of the perilymph and endolymph within the ear, which are regulated by different aquaporins located in the membranous labyrinth (reviewed in Eckhard et al., 2012). Aquaporins mediate water permeability between perilymph and endolymph. There are scarce studies about secretory structures in the inner ear of fishes, but it seems that the secretory pattern of Cl-, HCO3- and Na+/K+ in the cerebrospinal fluid, aqueous humor and endolymph is well stablished in elasmobranchs and is performed by carbonic anhydrase and Na+-K+-ATPase (Maren et al., 1975; Maren, 1977; Garvin et al., 1988).

The main structures secreting endolymph are the dark cells and plana semilunata in teleosts (Becerra and Anadón, 1992, 1993b), three types of cells in the semicircular canals of elasmobranchs (Garvin et al., 1988) and the dark cells located in the ampullae of semicircular canals in amphibians

(Bernard et al., 1986), in the *tegmentum vasculosum* in birds and in the *stria vascularis cochleae* in mammals (Anniko and Bagger-Sjöbäck, 1982).

Evolution of the inner ear

Different studies concerning the labyrinth have stablished that the inner ear shows orderly sequences of histological, cytological and morphological changes that can be correlated with the phylogenetic position of the different species (Baird, 1974). Morphological characterization of the inner ear may be reliable to the taxonomic level of family, while histological patterns have been shown in numerous genera (Baird, 1974). In the same way, the neuroepithelium of vestibular and auditory receptors shows consistent characteristics throughout the vertebrates, with the supporting cells extending from an underlying basal lamina and the hair cells with the stereocilia and kinocilium projecting to the lumen of the labyrinth and revealing the evident morphological and functional polarization of the hair cells (Baird, 1974).

The actual craniates include jawless vertebrates (Agnatha: hagfishes and lampreys) and jawed vertebrates (Gnathostomata), but the origin of the inner ear dates back to the early vertebrate evolution, at least 600 million years ago (Fritzsch and Beisel, 2001). The origin of the inner ear may be related to the statocyst and hydrodynamic receptors of invertebrates, due to the conservation of developmental regulatory genes (athonal and Math1) between some invertebrate mechanosensory neurons and vertebrate hair cells (Fritzsch and Beisel, 2001), but how those mechanosensory cells gave

origin to the inner ear sensorial cells remains unclear (Fritzsch et al., 2006). There is a pan-vertebrate evolutionary and developmental conservation between cranial placodes, which share a common ancestry and are derived from a unique pan-placodal region that is later divided into the different placodes (Streit, 2001; O´Neill et al., 2007; reviewed in Baker et al., 2008). In the same way, the otic, epibranchial and lateral line placodes share a common origin and function (Baker et al., 2008). There are various hypothesis to explain the origin of the otic placode; but it is not clear if the inner evolved as a modification of the lateral line in fishes ("acousticolateralis hypothesis", Wilson and Mattocks, 1897, reviewed in Baird, 1974; Wever, 1974; Streit, 2001) or vice versa (reviewed in Baker et al., 2008) or if both systems evolved independently from an ancestral mechanosensorial pore (Wever, 1974; Streit, 2001, reviewed in Duncan and Fritzsch, 2012), maybe related to mechanoreceptor cells of some Urochordates (Bone and Ryan, 1978; reviewed in Maisey, 2001 and Streit, 2001) Regardless the relationship between the inner ear and the lateral line system, their bifurcation is very ancient because the lateral line system has disappeared many times along evolution without affecting the inner ear (Streit, 2001; Baker et al., 2008). It has been suggested that the evolution of the vertebrate inner ear has happened in two steps: (1) the formation of a statocyst-like gravistatic organ followed by (2) the generation of canal cristae without otoconia (Fritzsch et al., 2006).

Imaging techniques for studying complex three-dimensional (3D) structures. Micro-computed tomography (micro-CT):

There are many methods for studying the structure and development of different biological samples. Classical histological slices for optic or electron microscope are a very common one. Light or fluorescence microscopy provides a high resolution and allows specific immunostaining or i*n situ* hybridization for detecting specific molecular markers and electron microscopy even reaches higher resolutions. However, the complete visualization of most of the samples requires its physical slicing, what supposes the destruction of the sample and the individual analysis of each slice. The reconstruction of a 3D model from those slices is quite complicate an requires so much time. Moreover, the slices usually present important anatomical distortions or ruptures, due to the manipulation and sectioning, especially in complex and delicate three-dimensional structures like the inner ear. The appearance of nondestructive three-dimensional imaging techniques, such as magnetic resonance imaging (MRI) and X-ray computed tomography (CT) allowed the generation of realistic two-dimensional and three-dimensional images of intact biological structures. Both, MRI and CT, allow a good resolution for 3D imaging with medical purposes, but not enough for histological purposes. Optical projection tomography (OPT) is similar to CT, but based on the transmission of visible light, so it requires almost transparent samples (Metscher, 2009a). The development of high resolution scanners with resolutions down to a few micrometers allowed the improvement of MRI and CT, making them available for histological studies, known as micro-MRI and micro-CT (Pauwels et al., 2013). Micro-

MRI is a harmless technique that allows the study of living organisms, however, micro-CT offers easier access and lower maintenance costs than equivalent micro-MRI (Pauwels et al., 2013).

Micro-CT is based on the application of the X-rays, electromagnetic radiation with wavelengths between 0,01 and 10 nm discovered by W. C. Roentgen in 1895 and shares the same physical principles as clinical CT scanning. It is based on a X-ray beam crossing a sample and projecting an image on a scintillator or other x-ray-sensitive detector, obtaining resolutions of a few microns, similar to light microscopy (Metscher, 2009a). The use of a synchrotron as source of X-rays increases the flux of the beam and therefore the resolution, which reaches 60 nm and below (Badea et al., 2008). The use of area detectors capturing 2D images meanwhile the sample rotates and the analysis of the divergence of the cone of radiation improved the resolution and introduced the possibility of a three-dimensional imaging (Feldkamp et al., 1984; Badea et al., 2008). The results of those multiple projections are combined by a reconstruction algorithm that produces a 3D matrix of high resolution voxels (volume pixels) smaller than 100 μm3 with individual values of attenuation of the x-ray beam or “brightness”. This matrix can be oriented in any direction and sliced, revealing the inner view of the anatomy (Badea et al., 2008).

Micro-CT is useful for analyzing bones, shells and other mineralized structures, but the visualization of soft tissues, especially if the sample contains mineralized and non-mineralized tissues, is quite more difficult (Badea et al., 2008; Pauwels et al., 2013). The use of different contrast-

enhancing agents as gallocyanin-chromalum, osmium tetroxide, Lugol´s solution, etc. notably improves the images obtained from soft and non-mineralized tissues (Badea et al., 2008; Metscher, 2009b; Lusic and Grinstaff, 2012). Some of those contrast-enhancing agents can cause the shrinking of the samples, but the use of stabilization hydrogels can minimize it (Chung et al., 2013; Wong et al., 2013). Other methods like drying the sample by freeze drying or critical-point drying improve the visualization of soft tissues, but require specialized devices to control pressure and temperature (Pauwels et al., 2013). Micro-CT also allows 3D imaging of specific immunostaining through metallic precipitation associated to antibody-antigen binding reaction and applying and additional threshold that differentiates unstained tissue from antibody signal, with a resolution similar to light microscopy immunostained samples (Metscher and Müller, 2011).

The use of micro-CT allows a high resolution study of the inner structures all along the developmental and adult stages and is especially valuable for those organs which present a complex structure, like the inner ear. There are numerous studies of model organisms analyzed through micro-CT (zebrafish: Bruneel and Witten, 2015; Babaei et al., 2016; *Xenopus*: Moosmann et al., 2013; Porro and Richards, 2017; chick: Henning et al., 2011; Kim et al., 2011; Metscher, 2011; mouse: Holsworth and Thornton, 2002; Wong et al., 2012; Hsu et al., 2016), but studies concerning chondrichthyans are scarce (Maisey, 2001, 2004; Schnetz et al., 2017) and do not comprise the whole study of the embryological stages as far as we know.

LITERATURE CITED

- Alba-Tercedor, J, Sánchez-Tocino, L (2011) “The use of the SkyScan 1172 high-resolution micro-CT to elucidate if the spicules of the sea slugs (Mollusca: Nudibranchia, Opisthobranchia) have a structural or a defensive function”. *SkyScan Users Meeting* 2011, 113-121.
- Anniko M, Bagger-Sjöbäck D (1982) “Maturation of junctional complexes during embryonic and early postnatal development of inner ear secretory epithelia”. *Am. J. Otolaryngol*. 3: 242-253.
- Babaei F, Hong TLC, Yeung K, Cheng SH, Lam YW (2016) “Contrast-enhanced X-ray micro-computed tomography as a versatile method for anatomical studies of adult zebrafish”. *Zebrafish* 13: 310-316.
- Badea CT, Dragonva M, Holdsworth DW, Johnson GA (2008) “In vivo small animal imaging using micro-CT and digital subtraction angiography”. *Phys. Med. Biol.* 53: 319-350.
- Baird IL (1974) “Some aspects of the comparative anatomy and evolution of the inner ear in submammalian vertebrates”. *Brain Behav. Evol.* 10: 11-36.
- Baker CVH, O’Neill P, McCole RB (2008) “Lateral line, otic and epibranchial placodes: developmental and evolutionary links?” *J. Exp. Zool. B. Mol. Dev. Evol*. 310: 370-383.
- Becerra M, Anadón R, Rodríguez-Moldes I, De Miguel E, Caruncho H, Corujo A, Rodicio C (1990) “Desarrollo del laberinto en la larva del rodaballo *(Scophthalmus maximus*)”. Actas 111 Congreso Nacional Acuicultura, pp. 289-294.
- Becerra M, Anadón R (1992) “The structure and development of the “plana semilunata” of the labyrinth of the trout”. *J. Anat.* 180: 247-253.
- Becerra M, Anadón R (1993a) “Development of the inner ear of the brown trout (*Salmo trutta fario*): I. Gross morphology and sensory cell proliferation”. *Journal of Morphology*, 216: 209-223.
- Becerra M, Anadón R (1993b) “Fine structure and development of ionocyte areas in the labyrinth of the trout (*Salmo trutta fario*)”. *J. Anat.* 183: 463-474.

- Bernard C, Ferrary E, Sterkers O (1986) “Production of endolymph in the semicircular canal of the frog *Rana esculenta*”. *J. Physiol.* 371: 17-28.
- Bever MM, Fekete DM (2002) “Atlas of the development of the inner ear in zebrafish”. *Dev. Dynam.* 223: 536-543.
- Bissonnette JP, Fekete DM (1996) “Standard atlas of the gross anatomy of the developing inner ear of the chicken”. *J. Comp. Neurol.* 368: 620-630.
- Bone Q, Ryan KP (1978) “Cupular sense organs in Ciona (Tunicata: Ascidiacea)”. *J. Zool.* 186: 417-429.
- Bruneel B, Witten PE (2015) “Power and challenges of using zebrafish as a model for skeletal tissue imaging”. *Connect. Tissue Res.* Early Online: 1-13.
- Chung K, Wallace J, Kim S-Y, Kalyanasundaram S, Andalman AS, Davidson TJ, Mirzabekov JJ, Zalocusky KA, Mattis J, Denisin AK, Pak S, Bernstein H, Ramakrishnan C, Grosenick L, Gradinaru V, Deisseroth K (2013) “Structural and molecular interrogation of intact biological systems”. *Nature* 497: 332-337.
- Duncan JS, Fritzsch B (2012) “Evolution of sound and balance perception: innovations that aggregate single hair cells into the ear and transform a gravistatic sensor into the organ of Corti”. *Anat. Rec.* 295: 1760-1774
- Eckhard A, Gleiser C, Arnold H, Rask-Andersen H, Kumagami H, Müller M, Hirt B, Löwenheim H (2012) “Water channel proteins in the inner ear and their link to hearing impairment and deafness”. *Mol. Aspects Med.* 33: 612-637.
- Fay RR, Popper AN (2000) “Evolution if hearing in vertebrates: the inner ears and preocessing”. *Hearing res.* 149: 1-10.
- Fritzsch B, Beisel KW (2001) “Evolution of the nervous system. Evolution and development of the vertebrate inner ear”. *Brain Res. Bull.* 55: 711-721.
- Fritzsch B, Beisel KW, Jones K, Fariñas I, Maklad A, Lee J, Reinhardt LF (2002) “Development and evolution of inner ear sensory epithelia and they innervation”. *J. Neurobiol.* 53: 143-156.
- Fritzsch B, Pauley S, Beisel KW (2006) “Cells, molecules and morphogenesis: The making of the vertebrate ear”. *Brain Res.* 1091: 151-171.

- Garvin JL, Spring KR, Santi PA (1988) “Secretion of endolymph by semicircular canals of the shark”. *Am. J. Physiol.* 255: 711-719.
- Haddon C, Lewis J (1991) “Hyaluronan as a propellant for epithelial movement: the development of semicircular canals in the inner ear of *Xenopus*”. *Development* 112: 541-550.
- Haddon C, Lewis J (1996) “Early ear development in the embryo of the zebrafish, *Danio rerio*”. *J. Comp. Neurol.* 365: 113-128.
- Henning AL, Jiang MX, Yalcin HC, Butcher JT (2011) “Quantitative three-dimensional imaging of live avian embryonic morphogenesis via micro-computed tomography”. *Dev. Dynam.* 240: 1949-1957.
- Holdsworth DW, Thornton M (2002) “Micro-CT in small animal and specimen imaging”. *Trends Biotechnol.* 20: 34-9.
- Hsu C-W, Wong L, Rasmussen TL, Kalaga S, McElwee ML, Keith LC, Bohat R, Seavitt JR, Beaudet AL, Dickinson ME (2016) "Three-dimensional microCT imaging of mouse development from early post-implantation to early postnatal stages". *Dev. Biol.* 419: 229-236.
- Iwasaki I (1937) “Entwicklungsgeschichtliche Untersuchungen uber das hautige Labyrinth der Knochenfische”. *Jpn. J. Med. Sci. (Anat.)* 6: 301-419.
- Jacobson AG (1963) “The determination and positioning of the nose, lens and ear”. *J. Exp. Zool.* 154: 273-303.
- Jacobson AG (1966) “Inductive processes in embryonic development”. *Science* 152: 25-34.
- Jørgensen JM, Shichirit M, Genesert FA (1998) “Morphology of the hagfish inner ear”. *Acta Zool-Stockholm* 79: 251-256.
- Kim JS, Min J, Recknagel AK, Riccio M, Butcher JT. (2011) “Quantitative three-dimensional analysis of embryonic chick morphogenesis via microcomputed tomography”. *Anat. Rec.* 294: 1-10.
- Larsell O, McCrady E Jr, Zimmermann (1935) “Morphological and functional development of the membranous labyrinth in the opossum”. *J. Comp. Neurol.* 63: 95-118.
- Lowenstein O, Osborne M, Wersall J (1964) “Structure and innervation of the sensory epithelia of the labyrinth in the thornback ray (*Raja clavata*)”. *Proc. R. Soc. Lond. B. Biol. Sci.* 160: 1-12.
- Lusic H, Grinstaff MW (2012) “X-ray-computed tomography contrast agents”. *Chem. Rev.* 113: 1641-1666.

- Maisey JG (2001) “Remarks on the inner ear of elasmobranchs and its interpretation from skeletal labyrinth morphology”. *J. Morphol.* 250: 236-264.
- Maisey JG (2004) “Morphology of the braincase in the broadnose sevengill shark *Notorynchus* (Elasmobranchii, Hexanchiformes), based on CT scanning”. *Am. Mu. Novit.* 3429**:** 1-52.
- Maren TH, Swenson ER, Addink AD (1975) “Rates of in movement from plasma to endolymph in the dogfish”. *Ann. Otol. Rhinol. Laryngol.* 84: 847-858.
- Maren TH (1977) “Physiology and chemistry if cerebrospinal fluid, aqueous humor and endolymph in *Squalus acanthias*”. *J. Exp. Zool*. 199: 317-324.
- Mazan S, Jaillard D, Baratte B, Janvier P (2000) “Otx1 gene-controlled morphogenesis of the horizontal semicircular canal and the origin of the gnathostome characteristics”. *Evol. Dev.* 2: 186-193.
- Metscher BD (2009 a) “MicroCT for developmental biology: a versatile tool for high-contrast 3D imaging at histological resolutions”. *Dev. Dynam.* 238: 632-640.
- Metscher BD (2009 b) “MicroCT for comparative morphology: simple staining methods allow high-contrast 3D imaging of diverse non-mineralized animal tissues”. *BMC Physiol*. 9: 11 doi: 10.1186/1472-6793-9-11.
- Metscher BD, Müller GB (2011) “MicroCT for molecular imaging: quantitative visualization of complete three-dimensional distributions of gene products in embryonic limbs”. *Dev. Dynam.* 240: 2301-2308.
- Metscher BD (2011) "X-ray microtomographic imaging of intact vertebrate embryos”. *Cold Spring Harbor Protoc*. 12: 1462-1471.
- Moosmann J, Ershov A, Altapova V, Baumbach T, Prasad MS, LaBonne C, Xiao X, Kashef J Hofmann R (2013) “X-ray phase-contrast in vivo microtomography probes new aspects of *Xenopus* gastrulation”. *Nature* 497: 374-377.
- Morsli H, Choo D, Ryan A, Johnson R, Wu DK (1998) “Development of the mouse inner ear and origin of its sensory organs”. *J. Neurosci.* 18: 3327-3335.
- Norris HW (1892) “Studies on the development of the ear of Amblysoma”. *J. Morphol*. 7: 23-34.

- O´Neill P, McCole RB, Baker CVH (2007) “A molecular analysis of neurogenic placode and cranial sensory ganglion development in the shark, *Scyliorhinus canicula*”. *Dev. Biol.* 304: 156-181.
- Pauwels E, Van Loo D, Cornillie P, Brabant L, Van Hoorebeke L (2013) “An exploratory study of contrast agents for soft tissue visualization by means of high resolution X-ray computed tomography imaging”. *J. Microsc*. 250: 21-31.
- Popper AN (2011) “Auditory system morphology”. In *Encyclopedia of Fish Physiology: From Genome to Environment*. Ed. Farrel AP. San Diego: Academic, 252-261.
- Porro LB, Richards CT (2017) “Digital dissection of the model organism *Xenopus laevis* using contrast-enhanced computed tomography”. *J. Anat.* 231: 169-191.
- Poznyakovskiy AA, Zahnert T, Kalaidzidis Y, Schmidt R, Fischer B, Baumgart J, Yarin YM (2008) “The creation of geometric three-dimensional models of the inner ear based on micro computer tomography data”. *Hearing Res.* 243: 95-104.
- Schlosser G (2006) “Induction and specification of cranial placodes”. *Dev. Biol.* 294: 303-351.
- Schnetz L, Kriwet J, Pfaff C. (2017) “Virtual reconstruction of the skeletal labyrinth of two lamnid sharks (Elasmobranchii, Lamniformes)”. *J. Fish. Biol*. 90: 1083-1089.
- Steel KP (1995) “Inherited hearing defects in mice”. *Ann. Rev. Genet.* 29: 675-701.
- Streeter GL (1906) “On the development of the membranous labyrinth and the acoustic and facial nerves in the human embryo”. *Am. J. Anat.* 6: 139-165.
- Streit A (2001) “Origin of the vertebrate inner ear: evolution and induction of the otic placode”. *J. Anat.* 199: 99-103.
- Streit A (2007) “The preplacodal region: an ectodermal domain with multipotential progenitors that contribute to sense organs and cranial sensory ganglia”. *Int. J. Dev. Biol.* 51: 447-461.
- Thomot A, Bauchot R (1987) “L´organogenesis du labyrinthe membraneux chez *Polypterus senegalus* Cuvier, 1829 (Pisces, Holostei, Polypteridae)”. *Anat. Anz.* 164: 189-211.

- Thornhill RA (1972) “The development of the labyrinth of the lamprey (*Lampetra fluviatilis* Linn. 1758)”. *Proc. R. Soc. Lond. B.* 181: 175-198.
- Torres M, Giráldez F (1998) “The development of the vertebrate inner ear”. *Mech. Develop.* 71: 5-21.
- Vasconcelos RO, Alderks PW, Sisneros JA (2016) “Development of structure and sensitivity of the fish inner ear”. *Adv. Exp. Med. Biol.* 877: 291-318.
- Vazquez E, Guijo E, Schimmang T, Giráldez F (1996) “Compartmental structure of the otic placode: junctional permeability and clonal restriction”. *Intl. J. Dev. Supply.* 1, 236-237.
- Waddington CH (1937) “The determination of the auditory placode in the chick”. *J. Exp. Biol.* 14: 232-239.
- Waterman RE, Bell DH (1984) “Epithelial fusion during early semicircular canal formation in the embryonic zebrafish, *Brachydanio rerio*”. *Anat. Rec.* 210: 101-114.
- Wever EG (1974) “The evolution of vertebrate hearing. Handbook of sensory physiology vol. V/1 (ed. Seidel WD, Neff WD), pp. 423-454. Berlin. Springer”.
- Whitfield TT, Granato M, van Eden FJM, Schach U, Brand M, Furutani-Seiki M, Haffter P, Hammerschmidt M, Heisenberg CP, Jiang YJ, Kane DA, Kelsh RN, Mullins MC, Odenthal J, Nusslein-Volhard C (1996) “Mutations affecting the development of the zebrafish inner ear and lateral line”. *Development* 123: 241-254.
- Whitfield TT, Hammond KL (2007) “Axial patterning in the developing vertebrate inner ear”. *Int. J. Dev. Biol.* 51: 507-520.
- Whitfield TT (2015) “Development of the inner ear”. *Curr. Opin. Genet. Dev.* 32: 112-118.
- Wong MD, Dorr AE, Walls JR, Lesch JP, Henkelman RM (2012) "A novel 3D mouse embryo atlas based on micro-CT". *Development* 139: 3248-3256.
- Wong MD, Spring S, Henkelman RM (2013) “Structural stabilization of tissue for embryo phenotyping using micro-CT with iodine staining”. PLoS ONE 8(12): e84321. doi:10.1371/journal.pone.0084321.
- Yntema CL (1933) “Experiments on the determination of the ear ectoderm in the embryo of *Amblystoma punctatum*”. *J. Exp. Zool.* 65: 317-357.

RATIONALE AND AIMS

RATIONALE AND AIMS OF THE THESIS

Morphogenesis is the set of processes by which the embryonic form and structure are generated. As indicated in the Thesis title, in this work we have search for the basic pattern of morphogenesis in the inner ear of the shark *Scyliorhinus canicula*, used as a model of basal vertebrates.

The inner ear is the structure responsible for functions as important for survival as the detection of sound, balance and acceleration. It exists in all craniate vertebrates and is composed by a complex three-dimensional epithelia containing various sensorial patches encaged in as osseous or cartilaginous capsule. The inner ear of all gnathostomes comprises a dorsal region with three semicircular canals, but the ventral regions is quite variable. While in fishes contains the utricle, saccule, lagena and macula neglecta, in tetrapods contains variable sensorial papillae and reaches its major complexity in mammals, which present the cochlea with the organ of Corti, responsible for the auditory sensitivity (Schneider-Maunoury and Pujades, 2007).

In spite of differences, the inner ears of all the vertebrates seem to share a common developmental pattern, which transforms the otic placode into the complex inner ear. The loss of hearing sense or alterations in the balance can be caused by molecular alterations during the development of the inner ear. Due to the conservation of molecular mechanisms responsible for development of the inner ear along the evolution, the knowledge of the basic

and shared morphogenetic mechanisms will help to understand the alterations in this sense organ.

The information available on the temporal sequence of the morphogenetic mechanisms that occur during the development of the inner ear of vertebrates comes mainly from mouse and chicken studies while in fish such studies are almost exclusively restricted to zebrafish. This bony fish has been disproportionately considered the canonical model representative of all fish groups for developmental studies in spite of that the ancient and highly diversified group of “fishes” includes both the cartilaginous (such as sharks and rays) and bony fishes, which often show highly divergent features. The great differences between both fish groups make the use of a single teleost species to represent all the fishes is a clear limitation. In fact, important events as the formation of the otic vesicle in zebrafish happen by a morphogenetic process (cavitation) that is markedly different of that takes places in cartilaginous fishes (by invagination), incidentally, similar of which occurs in amphibians, birds and mammals.

Cartilaginous fish (or chondrichthyans) has great evolutionary relevance due to its phylogenetic position as an outgroup of vertebrates with a bone skeleton, being the oldest radiation of the vertebrates with jaws (gnathostomes) since it appeared in the Ordovician period 455 million years ago. The apparition of the inner ear at the early evolution of vertebrates, at least 600 million years ago, and the phylogenetic position of this fish group at the base of gnathostome lineage, thus closer to its ancestral condition,

makes it an ideal model to study the origin, development and evolution of the inner ear.

Among chondrichthyans, the catshark *Scyliorhinus canicula* is an ideal subject for morphogenetic–studies for several reasons: the availability of obtaining embryos from Aquaria and Marine Biological Stations; its lengthy development and relative large size of embryos (which allow the identification of details that go unnoticed in species with rapid development and small size as zebrafish); its easy maintenance under laboratory conditions; and the transparency of the eggs shells, which facilitates the identification of the embryonic stages. All these characteristics have contributed to increase the interest for *S. canicula* studies in the last decades in different biological fields such as physiology, comparative embryology or molecular evo-devo studies (Coolen et al., 2009). It has helped the availability of specific literature concerning this species, among which highlight the normal developmental series (Ballard et al., 1993) and the detailed review of anatomical and functional characteristics of its central nervous system (CNS), including the organization of fiber connections between inner ear and brain (Smeets et al., 1983) .There are also many other neurochemical and genoarchitectonic studies that have provided an important amount of information about the organization and development of its CNS (reviewed in Rodríguez-Moldes, 2009; Rodríguez-Moldes et al., 2017), many of them carried out by the research group in which this Thesis has been performed (G-1853 of the Catalog of Researcher-Groups of the University of Santiago de Compostela, http://imaisd.usc.es/grupoficha.asp?idpersoatipogrupo=88770&i=en&s=-126-191-196-235). The group benefits of

the collaborative relationships that maintains with Dr. Mazan (Sorbonne Université-CNRS-UPMC UMR 7232, Observatoire Océanologique, Banyuls, France) who provides with access to a unique collection of genomic resources for *S. canicula*.

Based on the knowledge about *S. canicula*, its appropriated characteristics as a model organism, the scarce information about the development of the inner ear in chondrichthyans, the access to genomic resources for this species, and the access to facilities for micro-computed tomography (micro-CT) at the Marine Biology Station of the University of Santiago de Compostela, we have proposed as the **main aim** of this Thesis to know the origin and destination of the components of the inner ear of cartilaginous fish, its regionalization and the development of its innervation.

More specifically, we have established a **series of objectives** for this Thesis:

1º.- To determine the most effective and simple protocol for contrast-enhancing and desiccation methods for scanning of samples (embryos and dissected inner ears from juveniles) of *S. canicula* through micro-CT, which will allow us to obtain high-resolution two and three-dimensional images suitable for evolutionary developmental studies. This is the central aim of chapter 1 and allows the obtention of results for chapter 2.

2º.- To apply the appropriated contrast-enhancing protocol on our samples for analyzing them through micro-CT at different embryological stages, from early embryos (with soft tissues) to late developmental stages (with mineralized skeletons) to obtain consistent high-resolution 2D and 3D images to elaborate a precise and realistic description of the morphological events which take place during the development of a highly complex three-dimensional structure like the inner ear.

3º.- To study the expression pattern of different molecular markers which participate in the processes that the conversion of the otic placode into the complex inner ear. The use of specific antibodies and genetic probes through immunohistochemistry and *in situ* hybridization, respectively, will enable to decipher the origin and development of the different cells that constitute the inner ear, particularly the innervating neurons of the statoacoutic ganglion and the hair cells of the sensorial patches. This study will contribute to gain knowledge about the development and regionalization if the inner ear of *S. canicula* and also evaluate the evolutionary degree of conservation of the developmental patterns.

LITERATURE CITED

- Ballard WW, Mellinger J, Lechenault H (1993) “A series of normal stages for development of *Scyliorhinus canicula*, the lesser spotted dogfish (Chondrichthyes: Scyliorhinidae)”. *J. Exp. Zool.* 267: 318-336.
- Coolen M, Menuet A, Chassoux D, Compagnucci C, Henry S, Lévèque L, Da Silva C, Gavory F, Samain S, Wincker P, Thermes C, D’Aubenton-Carafa Y, Rodríguez-Moldes I, Naylor G, Depew M, Sourdaine P, Mazan S (2009) “The dogfish *Scyliorhinus canicula*, a reference in jawed vertebrates. In: Behringer RR, Johnson AD, Krumlauf RE (eds) Emerging model organisms. A laboratory manual, vol 1. CSHL Press, Cold Spring Harbor, pp 431-446.
- Rodríguez-Moldes I (2009) “A developmental approach to forebrain organization in elasmobranchs: new perspectives on the regionalization of the telencephalon”. *Brain Behav. Evol.* 74:20-29.
- Rodríguez-Moldes I, Santos-Durán GN, Pose-Méndez S, Quintana-Urzainqui I, Candal E (2017) ‘‘The brains of cartilaginous fishes’’. *Evolution of Nervous Systems* (Vol. 1), ed. J. Kaas (Oxford: Elsevier), 77-97.
- Schneider-Maunoury S, Pujades C (2007) “Hindbrain signals in otic regionalization: walk on the wild side” *Int. J. Dev. Biol.* 51: 495-506.
- Smeets WJAJ, Nieuwenhuys R, Roberts BL (1983) “The central nervous system of cartilaginous fishes. Structural and functional correlations”. Springer-Verlag Berlin Heidelberg. Chapter 6, pp 40-41.

CHAPTER 1

Microcomputed tomography for studying the chondrichthyans development: standardizing its application from early (soft) embryos to fully chondrified juveniles

INTRODUCTION

The study of any kind of 3D structure requires methods that provide steady, rapid easily reproducible reconstructions of internal and external morphological features. Moreover, such methods should cause the minimal distortion to the sample, providing size-calibrated 3D images and preserving the volumetric relationships within the original specimen (Metscher, 2009a). Despite the good resolution of classical histological techniques, the destruction of the sample during these processes avoids the possibility of further studies over it. The same problem is found with more recent techniques like confocal or episcopic microscopy. The development of techniques for obtaining 3D images like magnetic resonance imaging (MRI) and computed tomography (CT) has provided a faster, more reliable and influential tool to the anatomical study of structures with complex 3D organization, because they are non-destructive and may provide high-contrast images with high spatial resolution, allowing 3D imaging even in structures formed by soft tissues. Such techniques allow the standardization and reproducibility of the image acquisition which, together with other advantages (commercial availability, high spatial resolution, contrast enhancement, multi-sample handling) has become them crucial for anatomical, developmental and evolutionary studies (Nieman et al., 2011; Gregg and Butcher, 2012; Wise et al., 2013).

Among the different non-destructive techniques for 3D imaging, the micro computed tomography (micro-CT) appears to be the most

advantageous for comparative anatomical evolutionary studies (Metscher 2009 a, b, 2011; Alba-Tercedor and Sánchez-Tocino, 2011; Metscher and Müller, 2011). This technique is a X-ray imaging in 3D that allows to observe fine details of internal structures, being of easier access and lower maintenance costs than equivalent micro-MRI, and can reach resolutions similar to a light microscope (Metscher, 2009a; Handschuh et al., 2010). It has the added value that can also be applied for the study of living samples with the appropriated contrast agents (de Crespigny et al., 2008; Badea et al., 2008) and combined with immunocytochemistry (Metscher, 2011a; Metscher and Müller, 2011). Among other advantages, it helps in the interpretation of section planes and the scanned sample can be used in other techniques from simple histological method to immunohistochemical. This is really important to make profitable studies about species in which there are limitations for obtaining a number of samples and also for meeting the ethical requirement of reducing to minimum the numbers of specimens object of study.

Digital imaging and analysis of high-resolution CT scanning have been crucial for the evolutionary comparative studies based on the anatomy of complex 3D structures, as those related to skeletal structures because they facilitate the study of fossils (Liu et al., 2015). Moreover, micro-CT has revealed to be a really useful tool when applied to study the mature organization of species representatives of different vertebrate groups as bony fishes (Berquist et al., 2012; Bruneel and Witten, 2015; Babaei et al., 2016), amphibians (Porro and Richards, 2017), birds (Lautenschlager et al.,

2014), and mammals (Holdsworth and Thornton, 2002; Majka et al., 2018). Its application has been crucial to gain knowledge about the development of complex 3D structures as the inner ear of some fishes (Schulz-Mirbach et al., 2013, 2014), and other vertebrate species (Poznyakovskiy et al., 2008; Bonsmann et al., 2015). In chondrichthyans (cartilaginous fishes) such techniques have been applied to study the adult skeletal components of the inner ear (Maisey, 2001, 2004; Schnetz et al., 2017). The phylogenetic position of this fish group as basal gnathostomes (jawed vertebrates) makes its study crucial to provide information about the origin of the main characteristics of vertebrates, especially through the knowledge of their embryonic development. Hovewer, as far as we know, there are no developmental studies using micro-CT in fishes, although they are relatively frequent in other vertebrate groups. In fact, micro-CT has revealed to be a really useful tool applied to study the embryonic development of some model organisms as the mouse (Wong et al., 2012; Hsu et al., 2016), chick and quail (Henning et al., 2011; Kim et al., 2011, Metscher, 2011; Tahara and Larsson, 2013), *Xenopus* (Moosmann et al., 2013), and zebrafish (Silvent et al., 2017). These studies have been specially focused to the imaging of the process of skeletogenesis during embryonic development or performed in late embryos that have developed skeletons. Its application to early developmental stages presents additional challenges since, despite all the advantages of this technique for analyzing mineralized structures and its capability for scanning any kind of sample indistinctly of its composition, its application in soft tissues requires certain previous procedures to improve the contrast. The soft and extremely high water content tissue of early

embryos are almost "invisible" to the X-ray without contrast-enhancers, and differs significantly from later embryos, which present solid and dense structures, like the otic cartilage.

The catshark *Scyliorhinus canicula* is a recognized model for evolutionary developmental studies (Coolen et al., 2009) and, in fact, studies in this species have provided abundant information about the main developmental events in cartilaginous fishes and helped to better understand the similarities and differences with other model organisms (revised in Rodríguez-Moldes et al., 2017). Such developmental studies have been based on 2D imaging of serial sections obtained with traditional methods. The obtaining of 3D images appears very helpful to gain knowledge about the development of structures characterized by complex spatial arrangement of its components in the three axes because gives support for cito-, chemo- and geno-architectonic studies about. In the developing catshark, 3D representations of the embryonic telencephalon have been obtained from reconstructions of the 2D sections using the RECONSTRUCTTM software developed by Fiala (2005) (Quintana-Urzainqui et al., 2015, Figs. 1-3). Pioneering studies of 3D imaging in the developing catshark have been performed by Carrera et al. (2012) by using optical projection tomography (OPT) microscopy.

In this study we have tested different contrast-enhancing and desiccation methods for micro-CT imaging of fixed embryos and juveniles of the shark *Scyliorhinus canicula*. Our aim has been to determine the most

effective and simple protocol for scanning different embryonic stages and dissected structures with complex three-dimensional structures, as the inner ear, in order to obtain consistent imaging for comparison of their spatiotemporal organization. This work shows the usefulness of 3D studies for gaining knowledge about the development of complex structures and lays the groundwork for the implementation of an atlas of the developing inner ear of *S. canicula* (**see chapter 2**).

MATERIAL AND METHODS

Experimental animals

A total of 20 embryos from stages 18 to 33 (prehatching at stage 34, not processed) and 7 juveniles (from 10 to 11 cm in total length) of the catshark (also known as lesser spotted dogfish, *Scyliorhinus canicula*) were used in this study. Embryos from different broods, supplied by the Marine Biological Model Supply Service of the CNRS UPMC Roscoff Biological Station (France), were raised in seawater tanks in standard conditions (temperature: 15–16ºC; pH: 7.5–8.5; salinity: 35 g/L). The embryos were staged based on their external characteristics according to Ballard et al. (1993). The following stages were analyzed: **stage 18** (first and second pairs of pharyngeal pouches visible and appearance of a shallow buccal groove), **stage 19** (third pair of pharyngeal pouches visible and deeping of the buccal groove), **stage 20** (four pairs of unopened pharyngeal pouches visible by translucence), **stage 21** (second pharyngeal clefts and mouth opened), **stage 22** (two pairs of pharyngeal clefts open), **stage 24** (diamond- shaped mouth), **stages 26** (five pairs of open pharyngeal clefts, simple gill bars), **stage 27** (diamond-shaped mouth and primordial gill filaments), **stage 28** (transverse oval mouth, gills with external filaments), **stage 29** (mandibular arches crowded into the mouth opening and initial eye pigmentation), **stage 30** (eyeballs circled with black pigment), **stage 31** (detectable rostrum and long branchial filaments), **stage 32** (regression of branchial filaments), and **stage 33** (decreased volume of the yolk sac; prehatching). The beginning of

stage 32 corresponds to the beginning of the second half of embryonic development. Hatching occurs after the emptying of the external yolk sac in embryos at stage 34. The mineralized cartilaginous tissue starts to be evident in the parachordal cartilages at the base of the hindbrain at stage 27 (Ballard et al., 1993), including the parachordal cartilage the inner ear, which continues to grow and constitute the main portion of the skull and otic capsule.

The relationship of embryonic stages with body size, gestation and birth, are described in Table 1 in Ferreiro-Galve et al. (2010). Adequate measures were taken to minimize animal pain or discomfort. All procedures conformed to the guidelines established by the European Communities Council Directive of 22 September 2010 (2010/63/UE) and by the Spanish Royal Decree 53/2013 for animal experimentation, and were approved by the Ethics Committee of the University of Santiago de Compostela.

Sample preservation

Embryos from stages 18 to 32 were deeply anaesthetized with 0,5% tricaine methane sulphonate (MS-222, Sigma) in seawater and separated from the yolk before fixation by immersion in 4% paraformaldehyde (PFA) in 0.1 M phosphate buffer (PB; pH 7.4) containing 1.75% urea (elasmobranch PB) for 48–72 h depending on the stage of development. Stage 33 embryos and juveniles were deeply anaesthetized with MS-222 and fixed by intracardial perfusion with the same fixative after being rinsed with

elasmobranch Ringer´s solution. The fixative was removed by washing several times with PB saline for 2 days (PBS). In six juveniles, the otic capsule was dissected out containing the whole inner ear. Heads of one juvenile and of large embryos, whole embryos at stages 19-31 and juvenile inner ear capsules were dehydrated in increasing concentrations of methanol and preserved in absolute methanol at -20ºC.

Staining. Contrast media

We consider six groups of samples depending on the contrast agents used and the drying protocol applied (tables 1 and 2). To prevent the sample from moving or dry during the scanning process, it was wrapped in a wet paper with water or methanol, according to the immersion media of each sample. Different contrast agents (lugol, iodine or phosphotungstic acid) and enhancing-contrast techniques (desiccation with hexamethyldisilazane) were tested (see table 2 for details):

Control samples. One early embryo (stage 19) and one inner ear dissected from a juvenile were scanned *unstained and non-desiccated as controls* and a methanol-stored inner ear of one juvenile was rehydrated in decreasing concentrations of methanol and scanned immersed in PBS with no contrast agent. Three non-stained embryos were dried with hexamethyldisilazane (HMDS) before scanning (*unstained HMDS-desiccated samples*).

Lugol staining. One inner ear dissected from a juvenile was rehydrated to PBS in decreasing concentrations of methanol and stained with Lugol´s

solution 0,1N for 1 hour, then washed in PBS for 1 day and dehydrated to methanol and scanned. This process was repeated over the same inner ear with staining times in Lugol´s solution of 4, 10 and 24 hours.

Iodine staining. Two embryos and other three inner ears were stained with alcoholic iodine (1% iodine in methanol) for 1, 4, 14, and 24 hours before scanning. Due to the loss of contrast of the samples stained with alcoholic iodine during its storage in methanol, some of these samples were stained again with alcoholic iodine for 1, 3 and 5 days and immediately scanned.

Phosphotungstic acid staining. Two isolated inner ears were stained with 1% phosphotungstic acid (PTA) in methanol for 4 days and scanned twice, once at 40 KV and a second time at 55 KV. Ten whole embryos or its heads at different developmental stages were stained with 1% PTA in methanol for 1 day before scanning. Three embryos and one isolated inner ear embryo stained with PTA were also immersed for 2 hours in hexamethyldisilazane (HMDS), allowed to dry overnight, according to Alba-Tercedor and Sánchez-Tocino (2011), and scanned (PTA-stained and HMDS-desiccated samples).

Imaging parameters for Micro-CT scanning

All stained samples were transferred to absolute methanol after staining and scanned within methanol, except a preliminar test with a non-stained sample which was scanned within PBS. The scans were performed with a Bruker Skyscan 1172 microtomograph (Bruker, Kontich, Belgium) located

at the Marine Biology Station of the USC in A Graña. The samples were stored in 100% methanol after scanning and some of them were used for further experiments. The conditions applied in the Micro-CT scanning of each sample are indicated in Table 1.

3D Digital Reconstruction

All the images were reconstructed digitally with NRecon software (Bruker, Kontich, Belgium) and processed with CTAnalyzer software (Bruker, Kontich, Belgium). For displaying data, CTVox and DataViewer softwares (Bruker, Kontich, Belgium) were used. Serial images of the three axis and 3D reconstructed images and videos of each sample were obtained.

RESULTS

The results presented here show the possibilities of micro-CT to obtain realistic morphological information from samples without damaging them. We have tested different contrast agents and a drying method and after scanning and image reconstruction, the results obtained were different according on the contrast media used, the desiccation or not of the sample and the stage of embryonic development. We have comparatively analyzed such differences in order to stablish the optimal procedure. For such comparison, we have considered six groups depending on the contrast media and drying protocol applied: unstained samples, HMDS-desiccated samples, Lugol´s solution stained samples, alcoholic (methanol) iodine (I2M) stained samples, PTA-stained samples and PTA-stained and HMDS-desiccated samples. Some samples stained with I2M and Lugol´s solution lost their staining during the storage in methanol, so they were stained again with iodine. Another sample was scanned unstained and merged in PBS, but the obtained images were extremely poor. Although the 3D reconstructions of all the samples show a detailed vision of their external morphology (independently of the shrinkage suffered by the sample during its manipulation), there are important differences between the internal images of the samples according to the applied protocol.

The 3D reconstruction of the **unstained and undried** early embryo (stage 19) reveals a clear view of its surface, where some structures like the otic pit (Fig. 1A, B, asterisks) are recognized. It is also evident the collapse

of the skin over the hindbrain (Fig. 1B, arrow), which is an artifact probably caused by the procedure. Artifacts are not apparent in other brains regions like the forebrain, as appreciated in a frontal 3D view (Fig. 1C). The inner view presents a low contrast and undifferentiated tissue without appreciated structures (Fig. 1D). An inner ear dissected from a juvenile was also scanned and analyzed in the same conditions, unstained and undried, but although this is a relative dense and rigid structure because the cartilage of the otic capsule is completely formed at this stage, the result was very poor, almost indistinguishable from the background.

The **unstained and desiccated** embryos (stages 19, 27, 29, 31) also present important distortions, but seem to have a better definition than the untreated one (Fig. 2, compare with Fig. 1). Although they present lower contrast than the embryos stained with iodine (see below, figs. 5-6), they seem to have higher contrast than the unstained and undried one. The external surface shows several wrinkles, especially in the midhead and the eyes (Fig. 2 A-C up, arrows). With this treatment, the hindbrain ventricle also appears collapsed (Fig. 2 A-C middle, arrows) but not the forebrain (Fig. 2 A middle left, asterisk). The contrast in inner tissues is low and, except the neural tube, other inner structures like the statoacoustic ganglion, related to the inner ear (Fig. 2 B middle, arrowheads) are hard to differentiate from the surrounding tissues. The poor visualization of the inside of these embryos is more evident in individual transverse sections, where the low-dense and granulated aspect of the sample allows to identify only the main structures, but no vessels, nervous fibers or other thin

elements (Figs. 2 A-C, down). It is remarkable that the most developed embryo treated with this procedure (stage 31) presents the most important distortions, maybe duet to the presence at this stage of numerous and large gill filaments which suffer great deformations if desiccated. However, the inner ear dissected from a juvenile specimen (with its cartilaginous capsule) unstained and HMDS-desiccated presents an excellent 3D image where the thinnest details are well appreciated and identified (Fig. 3). The most remarkable structures are the otoliths (Fig. 3 A-D, asterisks), that appear bright white due to their high density composition of calcium carbonate in calcite form (Coleman, 1990; Campana, 1999). The muscular tissue appears clear grey (Fig. 3 A, arrow) and the cartilage of the otic capsule is the darker structure. Nervous structures like the VIII nerve present a contrast similar to that observed in the cartilage (Fig. 3 C, star). The membranous labyrinth is clearly identified, especially in two-dimensional sections (Figs. 3 C, D; arrowheads), where appears close to the cartilage or separated by a wide space.

Embryos **stained with PTA** and **desiccated with HMDS** (stages 19, 24, 26) provide a good 3D reconstruction. External structures are well recognized, even those of small size in small embryos (fig. 4). In a stage-24 embryo, the branquial arches and otic vesicle are well recognized externally (Fig. 4 A, arrows). Transverse sections of this embryo show highly contrasted gross structures and the collapsed ventricle of the hindbrain (Figs. 4 B, C, arrows). The treatment appears not suitable for larger embryos in which external structures as olfactory pit and gill buds are evident (Fig. 4

D, arrows) and gross internal structures appear highly contrasted (Figs. 4 E, F), but the thinner structures are not appreciated and the tissue presents a low-dense appearance, especially in the deeper regions of the head. It is also noticeable the collapsed ventricle (Figs. 4 E, F, arrows).

The **alcoholic iodine stain (I2M)** is easy to prepare, penetrates quickly in the tissues and gives good contrast. When applied in **undesiccated** samples (stages 18 and 22 and dissected juvenile inner ear), the results have been uneven depending on the stage of development and the staining time. The images of early embryos (stage 18, Fig. 5) present a very good 3D reconstruction and contrast, with no significant collapsed cavities (Fig. 5 A). The inner structures appear clearly differentiated (Fig. 5 B), with the nervous structures and the somites specially stained and other structures like the gut less stained (Figs. 5 B, C). In contrast, a little more developed embryo (stage 22) stained in the same way that present a proper and well-detailed 3D external image (Fig. 5 D), shows internally a very dense and homogenous appearance with no recognizable inner structures (Fig. 5 E). It is noticeable the collapsed ectoderm over the hindbrain (Fig. 5 E, arrow). The over-stained look is maintained in the entire specimen (Figs. 5 E, F). The use of this contrast-enhancing method in isolated juvenile inner ears gave satisfactory results, but with some differences according to the staining time. These samples were merged in I2M for 1, 3 and 5 days and all of them provided detailed 3D rendered images. The mayor differences are appreciated in sectioned 3D renders. Thus, the sample stained for one day shows a mid-intense grey image with the canals, chambers and membranous

labyrinth clearly visible (Fig. 6 A) and the otoliths almost white (Fig. 6 A, asterisks). The sample stained for 3 days presents a much more enhanced contrast, with bright white otoliths (Fig. 6 B, asterisks) and notably white maculae (Fig. 6 B, arrowheads) and well contrasted nerves (Fig. 6 B, arrow). It is also remarkable the high contrast acquired by the muscular tissue (Fig. 6, star). Interestingly, the sample stained for 5 days presents a lower contrast (Fig. 6 C), similar to that observed in the sample stained for 1 day. In this case the otoliths are not evident, but there are some high dense particles that could be parts of disintegrated otoliths (Fig. 6C, arrowheads).

Contrast enhancing with **Lugol´s solution** in **undessicated** samples has been applied only in a dissected inner ear from a juvenile which was repeatedly stained and scanned at different staining times (1, 4, 10 and 24 hours). It provides 3D reconstructions with good resolution, being clearly visible thin details like nerves (Fig. 7 A). However, individual sections across this sample reveal a low dense image (Fig. 7 B), with a barely distinguishable cartilage from the surrounding tissue (Fig. 7 B). The membranous labyrinth is slightly appreciated in some parts separated from the cartilage (Fig. 7 B, arrowheads) and the statoacoustic nerve appears next to the saccule, a little more stained than the cartilage (Fig. 7, arrow).The most remarkable structure are the otoliths (Figs. 7 B-D, asterisks). If the image is false- colored (Fig. 7 C, D) some parts are better appreciated, like the otoliths or the statoacoustic nerve (Fig 7 C, asterisk and arrow, respectively). The otolith is specially remarked if the color of the image reflects the density of the tissue (Fig. 7 D, asterisk).

The **PTA-staining of undessicated** samples is the simplest staining procedure applied and it has provided the best 3D reconstructions in all of the tested samples, which ranged from the fragile stage 20 to the robust stage 33 (prehatching) embryos, juveniles and one dissected juvenile inner ear. However, some differences can be noted according to the developmental stage, mainly referred to their internal view. Early embryos at stages 20, 21, and 24 present a reasonable sounded external appearance (Fig. 8). The main external characteristics are the otic pit/vesicle (Fig. 8 A-C, asterisks) and branchial clefts (Fig. 8 A-C up, arrows). Internal sections reveal a high-density in the largest structures (otic epithelium, neural tube, ganglia) while other smaller are not well distinguished (Fig. 8 A-C mid). Individual transverse sections of these early stages (Fig. 8 A-C, down) reaffirm the high dense appearance of the neural tube, otic vesicles and ganglia, surrounded by less dense tissue. It is remarkable the very homogeneous and dense appearance of the earliest embryo tissue with a slight ring effect (Fig. 8 A, down). Ring artefacts are an intrinsic trouble for 3D micro-CT imaging based on 2D X-ray detectors because of the divergence of the cone-beam, but varying the scanning parameters or applying correction methods can reduce these artefacts (Eldib et al., 2017). In the same way, it is also common to these samples the collapsed ventricle of the hindbrain (Fig. 8, arrowheads). The intensity of the stain seems to be reduced along the development. The best PTA-stained images have been obtained from mid-late embryos (stages 27-28) (Fig. 9 A, B, left). The 3D reconstruction of these embryos provided good resolution of its superficial characteristics, although some distortions appear as wrinkles in the earlier one (Fig. 9 A left,

arrows). It is remarkable the resolution of the gill buds (Fig. B left, arrows). Individual sections of these samples evidence an intense staining of the brain and other structures like the otic vesicles (Fig. 9 A, B, asterisks), while the low-stained cranial cartilage is visible within the non-stained surrounding tissue (Fig. 9 A, B center and right, arrows). There is also a moderate collapse of the roof of the ventricle of the hindbrain (Fig. 9, A, B center and right, arrowheads). Later embryos (stages 29 and 31), which present solid and dense structures, like the otic cartilage, offer a good 3D view (Fig. 10 A-F), although some samples show a moderate sinking of the ectoderm over the hindbrain (Fig. 10 A-C, arrows). Transverse sections of 3D images show intense staining of the retina, lens, brain and ganglia (Fig. 10 B), while individual sections evidence the low contrast of the deep tissue between the main structures (Fig. 10 C). Later samples (stage 31) share these characteristics (Fig. 10 D-E), but the deformation of the head over the hindbrain seems to be reduce as the skull develops, although some superficial wrinkles are visible (Fig. 10, D, E, arrows). Individual sections show the low dense but visible skull (Fig. 10 F, arrowheads). In stage 32 and onwards, there is not any deformation of the cranium and the surface of the head appear smooth and without wrinkles (Fig 10 G). Sections through 3D reconstructions of this more developed embryo reveal not only the major structures but also gills or mandibular muscles (Fig. 10 H, arrowheads) which appear well developed. Two-dimensional transverse sections evidence even better the development of the mandibular muscles, where the muscle fibers can be identified (Fig. 10 I, arrowheads). The brain is clearly visible although it is not as stained as in previous samples treated with this

procedure, it. As the development progresses, thinner structures are evident in the surface of the reconstructed embryo, like the pores containing the neuromasts of the lateral line system (Fig. 11 A, arrowheads). In 3D transverse sections, the brilliant white-colored otoliths highlight within the inner ears (Fig. 11 B, arrowheads), which contrast with the low density of the cartilages of the otic capsule and brain. The cavities of the inner ear and of the brain ventricles are clearly visualized in a two-dimensional slice (Fig. 11 C), although a slight ring effect is also appreciated. In a juvenile specimen, the most remarkable characteristic of its 3D view are the numerous scales covering all the skin (Fig. 11 D). The 3D transverse section evidences that the brain is poorly stained (Fig. 11 E, asterisk), while other dense structures like mandibular and ocular muscles present a clear grey color in contrast to the cartilage, being their density more evident in a two-dimensional view (Fig. 11 F, arrows). By inverting the colors the image the visualization of the brain can be slightly improved (Fig. 11 G), but appearing or increasing a ring effect. When isolated inner ears were processed with this procedure, the images reveal a very homogeneous intense staining along the samples (Fig. 12) where the membranous labyrinth is visible and shows the sensorial patches in the vestibular chambers and the semicircular canals (Fig. 12 A, B; arrowheads). The statoacoustic nerve is clearly appreciated and seems as stained as the cartilage (Fig. 12 A, B; asterisks). The otolith is evident, but its contrast is not more intense than the other tissues (arrows). This sample was scanned at two different voltages (A at 40KV and B at 55 KV) but we do not appreciate significant differences between them.

The control sample in figure 1 was also **scanned dried with HMDS and stained with PTA and dried with HMDS** (Fig. 12). Both scannings show as well a sharp defined image of the surface of this embryo. The more evident external characteristics are again the otic cup (Figs. 12A-D, asterisks) and the collapsed skin over the dorsal region of the head (Figs. 12B, D, arrows). Due to the successive manipulations of this sample, some differences are appreciated in the images, like some lumps in the surface of the stained embryo (Figs. 12 C, D, arrowheads). The inner sections of the unstained desiccated sample are very similar to that of the non-desiccated one, showing an undifferentiated low-dense tissue but with more brilliant edges (Fig. 12 E, F). In the PTA-stained sample the differences are more evident, with a very low-dense inner tissue and a blurred appearance (Figs. 12 G, H).

DISCUSSION

After testing different methods of drying and contrast enhancement for micro-CT imaging of fixed embryos and juveniles of the shark *Scyliorhinus canicula*, we have determined the most efficient and simple protocol for the scanning of different embryonic stages and complex 3D structures, as inner ear, that can produce consistent images for comparative studies.

In that follows, we first examine the steps followed and discuss about the advantages and disadvantages of the use of some substances and methodologies. Finally, we state the basic protocol what has been applied for the study of the inner ear development of the catshark included in chapter 2.

To carry out the objective of this study, that is, to determine the best micro-CT protocol for shark embryos, the first decision was to establish the starting point for the scans. Micro-CT is useful for analyzing bones, shells and other unstained mineralized structures, but the visualization of soft tissues is not as good, especially if the sample contains mineralized and non-mineralized tissues. We firstly performed a test scanning a PBS-embedded unstained sample and the obtained results were extremely poor (no images were available). Then we tested unstained methanol-merged samples, which provided a relative good external view, although the inner view clearly needed to be improved. Nevertheless, these inner images were better than the images obtained from the PBS-embedded sample. Due to these firsts

attempts, we decided to continue using methanol-stored samples, that also presented the advantage of the larger conservation power compared to the samples merged in PBS. The conservation in methanol also facilitates the next tried attempt by desiccating the samples to improve the results. Although drying the samples often causes shrinking of the tissue and structural changes, these can be minimized by using freeze drying or critical-point drying, but these methods are complicated and require special devices to control temperature and pressure (Pauwels et al., 2013). A simpler way to dry the samples is desiccating them with hexamethyldisilazane (HMDS) according to Alba-Tercedor and Sánchez-Tocino (2011). Although the suggested protocol recommends ethanol-based dehydrations, we tried methanol-based dehydrations, achieving dry samples for scanning too. The desiccation with HMDS was planned as a simple next step to easily increase contrast without staining, avoiding at the same time possible complications caused by the contrast- enhancing media. Despite other authors achieved satisfactory results with this procedure (Alba-Tercedor and Sánchez-Tocino, 2011; Alba-Tercedor, 2013), in our samples the results were not good for whole embryos and only the images from isolated inner ears were acceptable. This may be due to the different kind of samples analyzed. While the hard exoesqueleton of insects processed by these authors can resist the collapse after the evaporation of the body water, the soft body of our shark embryos specially the earliest (with soft tissues, without cartilage differentiated) presented several important deformations, although the external wrinkled aspect could be appreciated with high detail. Apart of the wrinkled surface or the collapse of the walls of inner cavities caused by the

desiccation, the inner view presented also a low contrast that did not allow an appropriated visualization of the internal organs and only the biggest structures were visible. In the case of the isolated inner ears, we do not appreciate any collapse due to the resistance of the otic cartilage and the 3D reconstruction of the inner ears provided a reasonable defined image where the most visible structures were the mineralized ones, as seen in by other authors in previous studies (Alba-Tercedor and Sánchez-Tocino, 2011; Schulz-Mirbach et al., 2013), but also less dense parts were appreciated, but with a much lower contrast. The combined use of desiccation and staining was expected to increase the contrast, and in fact it was, but only the larger inner structures presented a high contrast. The rest of the tissues, specially the deepest ones, were very poorly stained and no thin elements were appreciated. A positive aspect that this procedure seemed to provide was the good external view, well stained and where the wrinkled aspect of the unstained and desiccated samples was reduced. Maybe the PTA-staining before desiccation prevented someway the shrinking of the tissue, but not enough for avoiding the collapse of the ventricle of the hindbrain, a common alteration to the most of our samples.

As the desiccation seemed not to necessarily improve the images of our samples, we also tried other contrast-enhancing agents without desiccation. There are several contrast agents and protocols to improve tissue contrast, but some of them were not tested due to practical or security reasons. Gallocyanin-chromalum is a histological stain that can be used to give contrast in micro- CT analysis, but not enough to fully differentiate samples

from background (Metscher, 2009a). Osmium tetroxide is commonly used for electron-microscopy and micro-CT applications and gives excellent contrast to samples, but it was not used in this study due to its toxicity, volatility, high cost, equipment requirement and uselessness with alcohol-stored samples (Metscher, 2009a; Pauwels et al., 2013). The simple preparation and staining process with alcoholic iodine (I2M) of our methanol-stored samples indicated that it could be a easy way for getting good micro-CT images. Some authors report tissue shrinking when stained with alcoholic iodine (Alba-Tercedor, 2013), this was not observed in the present study. Samples showed a reasonably good contrast with differentiated tissues from the background. Although some authors refer a "stain bleeding" when the sample is stained for large periods (Smith et al., 2016), we found that this contrast-enhancing agent easily over stains the sample, but not to the point of creating blurred edges, at least for the staining periods we tested (max. 5 days). In the case of juvenile inner ears there was the opposite situation, the contrast of the inner sections was not very high but relatively satisfactory. We saw the variation in the contrast according to the staining time and, contrarily to that observed in the embryos, over-staining was not perceived.

Other contrast-enhancing agent tested was the Lugol´s solution (iodine potassium iodide, IKI) in isolated inner ears. Although this solution is water-based, samples can be scanned in water or dehydrated to alcohol (Metscher, 2009a). It has been referred that this staining agent provides good results in formalin-fixed samples (Metscher, 2009a), although some authors

mentioned the weak stain of the inner ears with this substance (Schulz-Mirbach et al., 2013). Lugol´s stained samples can also suffer important shrinking processes that can be reduced by using stabilization protocols (Wong et al., 2013; Chung et al., 2013), but they were excluded for this study due to the presence of acrylamide and bis-acrylamide in its composition, which present neurotoxic and carcinigenetic effects (LoPachin and Gavin, 2012; NTP Technical Report, 2012). In our case the samples were mainly composed by thick cartilage and we did not appreciate shrinking even without using any stabilization protocol. Although the low contrasted inner appearance, maybe due to the great part of cartilage in these samples which prevents the staining media to penetrate into the inner parts, the external view provided a high-detailed image.

PTA-stained samples provided in general acceptable results for the widest variety of developmental stages. Although the PTA concentration seems not to be critical (Metscher, 2011b) and prolonged staining time does not cause “stain bleeding” (Smith et al., 2016), we have noticed some differences according to the developmental stage of the samples that may be corrected by adjusting the staining periods. For the same staining time, the earliest embryos appear highly stained. Staining overnight seemed appropriated for intermediate embryos (from stage 24 to 32 approximately), while the largest ones may require largest periods merged in the PTA solution.

Multiple treatments and scans of the same sample showed that is possible to try different contrast- enhancing methods for a single sample. Although the multi-treated sample only showed slightly superficial alterations, the quality of its internal images was not significantly improved, perhaps due to the early stage of the selected embryo.

A proposal of micro-CT scanning protocol for studying the embryonic development of cartilaginous fishes

1 · Fix embryos by immersion in 4% paraformaldehyde in 0.1 M phosphate buffer (PB; pH 7.4) containing 1,75% urea (elasmobranch PB) for 1-2 days depending on its size. Large embryos (st32 onwards) can be fixed by perfusion with 4% paraformaldehyde.

2 · Remove he fixative washing several times with PB saline.

3 · Dehydrate the samples by merging in increasing concentrations of methanol in PBS. Ethanol dehydration is also possible and should not mean any significant difference.

2 hours in 30% methanol in PBS.

2 hours in 50% methanol in PBS.

2 hours in 70% methanol in PBS.

2 hours in 90% methanol in PBS.

Transfer to absolute methanol.

4 · Stain in 1% PTA in methanol for 1 day. PTA does not overstain and the staining time is not critical. Large embryos or juveniles may need more staining time, up to 4 days.

5 · Transfer to absolute methanol and mount in the micro-CT device in a apropriated size eppendorf to scan. The sample can be wrapped in soft paper within the eppendorf tube to avoid moving during the scanning time.

6 · Set the scan parameters (in our samples: voltage: 40-55 kV, amperage: 165-250 µA, rotation step: 0.20º, exposure time: 900-1000 ms)

7 · Run the tomography. For our size samples and scan parameters it takes about 1.5 - 2 hours.

8 · Reconstruct and process images with NRecon software and CTAnalyzer software (Bruker, Kontich, Belgium).

CONCLUSSIONS

After testing different methods for staining and scanning samples of the shark *Scyliorhinus canicula* at different developmental stages, we conclude that more than one method can be valid for enhancing the contrast of the samples. Attending to our results, the best contrast enhancing method for embryos at different developmental stages is the staining with PTA. Early embryos stained with I2M also provided acceptable results. The study of isolated inner ears showed that these ones provide good results stained with PTA, but also stained with iodine and even those unstained but desiccated with HMDS.

The use of contrast-enhancing methods associated for scanning samples through micro-CT has proved to be an efficient way to obtain two-dimensional and 3D images of the embryonic development of *S. canicula*, from the soft tissue of the earlier stages to the fully chondrified juvenile samples, and particularly, for the study of complex and fragile 3D structures as the inner ear. This shows the applicability of this technique for different kind of samples, not only for hard samples like shells, bones or teeth, but also soft tissues, although some contrast-enhancing method must be applied.

LITERATURE CITED

- Alba-Tercedor, J, Sánchez-Tocino, L (2011) “The use of the SkyScan 1172 high-resolution micro- CT to elucidate if the spicules of the sea slugs (Mollusca: Nudibranchia, Opisthobranchia) have a structural or a defensive function”. *SkyScan Users Meeting 2011*, 113-121.
- Alba Tercedor J (2013) “Study of the anatomy of the common housefly *Musca domestica* Linnaeus, 1758 (Insecta: Diptera, Muscidae) scanned with the Skyscan 1172 high resolution micro-CT”. *Bruker Micro-CT Users Meeting 2013*, 275-289.
- Babaei F, Hong TLC, Yeung K, Cheng SH, Lam YW (2016) “Contrast-enhanced X-ray micro-computed tomography as a versatile method for anatomical studies of adult zebrafish”. *Zebrafish* 13 :310-316.
- Badea CT, Dragonva M, Holdsworth DW, Johnson GA (2008) “In vivo small animal imaging using micro-CT and digital subtraction angiography”. *Phys. Med. Biol.* 53: 319-350.
- Ballard WW, Mellinger J, Lechenault H (1993) “A series of normal stages for development of *Scyliorhinus canicula*, the lesser spotted dogfish (Chondrichthyes: Scyliorhinidae)”. *J. Exp. Zool.* 267: 318-336.
- Berquist RM, Gledhill KM, Peterson MW, Doan AH, Baxter GT, Yopak KE, Kang N, Walker HJ, Hastings PA, Frank LR. 2012 The Digital Fish Library: using MRI to digitize, database, and document the morphological diversity of fish. PLoS One 7:e34499.
- Bonsmann A, Stoffel MH, Burkhard M, Hatt JM (2015) “Anatomical atlas of the quail´s ear (*Coturnix coturnix*)”. *Anat. Histol. Embryol.* 45: 399-404.
- Bruneel B, Witten PE (2015) “Power and challenges of using zebrafish as a model for skeletal tissue imaging”. *Connect. Tissue Res.* Early Online: 1-13.
- Campana SE (1999) “Chemistry and composition of fish otoliths: pathways, mechanisms and applications”. *Mar. Ecol. Prog. Ser*. 188: 263-297.
- Carrera I, Moss J, Davidson D, Rodríguez-Moldes I (2012) “Three-dimensional (3D) modeling of the embryonic shark brain: A basic anatomical tool for studying the development of neuronal systems in a basal vertebrate”. *Int. J. Dev. Neurosci.* 30: 670-670.

- Chung K, Wallace J, Kim SY, Kalyanasundaram S, Andalman AS, Davidson TJ, Mirzabekov JJ, Zalocusky KA, Mattis J, Denisin AK, Pak S, Bernstein H, Ramakrishnan C, Grosenick L, Gradinaru V, Deisseroth K (2013) “Structural and molecular interrogation of intact biological systems”. *Nature* 497: 332-337.
- Coleman JR (1990) “Development of sensory systems in mammals”. *Ed. Wiley Interscience*. Chapter 9: (“Development of the vestibular system”, Matti Anniko) pp. 341-400.
- Coolen M, Menuet A, Chassoux D, Compagnucci C, Henry S, Lévèque L, Da Silva C, Gavory F, Samain S, Wincker P, Thermes C, D’Aubenton-Carafa Y, Rodriguez-Moldes I, Naylor G, Depew M, Sourdaine P, Mazan S (2009) “The dogfish *Scyliorhinus canicula*, a reference in jawed vertebrates. In: Behringer RR, Johnson AD, Krumlauf RE (eds) Emerging model organisms. A laboratory manual, vol 1. CSHL Press, Cold Spring Harbor, pp 431-44.
- de Crespigny A, Bou-Reslan H, Nishimura MC, Phillips H, Carano RA, D'Arceuil HE (2008) “3D micro-CT imaging of the postmortem brain”. *J. Neurosci. Meth.* 171: 207-213.
- Eldib ME, Hegazy M, Mun YJ, Cho MH, Cho MH, Lee, SY (2017) “A ring artifact correction method: validation by micro-CT imaging with flat-panel detectors and 2D Photon-counting detector". *Sensors* 17: 269.
- Ferreiro-Galve S, Rodríguez-Moldes I, Anadón R, Candal E (2010) “Patterns of cell proliferation and rod photoreceptor differentiation in shark retinas”. *J. Chem. Neuroanat.* 39: 1-14.
- Fiala JC (2005) “Reconstruct: a free editor for serial section microscopy”. *J. Microsc.* 218: 52-61.
- Gregg CL, Butcher JT (2012) "Quantitative in vivo imaging of embryonic development: opportunities and challenges”. *Differentiation* 84: 149-162.
- Handschuh S, Schwan T, Metscher BD (2010) “Showing their true colors: a practical approach to volume rendering from serial sections”. *BMC Dev. Biol.* 10:41.
- Henning AL, Jiang MX, Yalcin HC, Butcher JT (2011) “Quantitative three-dimensional imaging of live avian embryonic morphogenesis via micro-computed tomography”. *Dev. Dyn.* 240: 1949-1957.

- Holdsworth DW, Thornton M (2002) “Micro-CT in small animal and specimen imaging”. *Trends Biotechnol.* 20: 34-9.
- Hsu C-W, Wong L, Rasmussen TL, Kalaga S, McElwee ML, Keith LC, Bohat R, Seavitt JR, Beaudet AL, Dickinson ME (2016) "Three-dimensional microCT imaging of mouse development from early post-implantation to early postnatal stages". *Dev. Biol.* 419: 229-236.
- Kim JS, Min J, Recknagel AK, Riccio M, Butcher JT. (2011) “Quantitative three-dimensional analysis of embryonic chick morphogenesis via microcomputed tomography”. *Anat. Rec.* 294: 1-10.
- Lautenschlager S, Bright JA, Rayfield EJ (2014) “Digital dissection - using contrast-enhanced computed tomography scanning to elucidate hard- and soft-tissue anatomy in the common buzzard *Buteo buteo”*. *J. Anat.* 224 :412-431.
- Liu Y, Scholtz G, Hou X (2015) “When a 520 million-year-old Chengjiang fossil meets a modern micro-CT--a case study”. *Sci. Rep*. 5: 12802-12809.
- LoPachin RM, Gavin T (2012) "Molecular mechanism of acrylamide neurotoxicity:lessons learned from organic chemistry". *Environ. Health Perspect.* 120: 1650-1657.
- Maisey JG (2001) “Remarks on the inner ear of elasmobranchs and its interpretation from skeletal labyrinth morphology”. *J. Morphol.* 250: 236-264.
- Maisey JG (2004) “Morphology of the braincase in the broadnose sevengill shark *Notorynchus* (Elasmobranchii, Hexanchiformes), based on CT scanning”. *Am. Mu. Novit.* 3429**:** 1-52.
- Majka P, Chlodzinska N, Turlejski K, Banasik T, Djavadian RL, Węglarz WP, Wójcik DK. 2018 A three-dimensional stereotaxic atlas of the gray short-tailed opossum (*Monodelphis domestica*) brain. *Brain Struct. Funct*. 223: 1779-1795.
- Metscher BD (2009a) “MicroCT for developmental biology: a versatile tool for high-contrast 3D imaging at histological resolutions”. *Dev. Dynam.* 238: 632-640.
- Metscher BD (2009b) “MicroCT for comparative morphology: simple staining methods allow high-contrast 3D imaging of diverse non-mineralized animal tissues”. *BMC Physiol.* 9: 11.

- Metscher BD (2011) "X-ray microtomographic imaging of intact vertebrate embryos". *Cold Spring Harb. Protoc.* 12: 1462-1471.
- Metscher BD, Müller GB (2011) "MicroCT for molecular imaging: quantitative visualization of complete three-dimensional distributions of gene products in embryonic limbs". *Dev. Dynam.* 240: 2301-2308.
- Moosmann J, Ershov A, Altapova V, Baumbach T, Prasad MS, LaBonne C, Xiao X, Kashef J Hofmann R (2013) "X-ray phase-contrast in vivo microtomography probes new aspects of *Xenopus* gastrulation". *Nature* 497: 374-377.
- National Toxicology Program (2012) "NTP Technical Report on the toxicology and carcinogenesis studies of acrylamide (CAS No. 79-06-1) in F344/N rats and B6C3F1 mice (feed and drinking water studies)". NIH Publication No. 12-5917. National Institutes of Health Public Health Service U.S. Department of health and human services.
- Nieman BJ, Wong MD, Henkelman RM (2011) "Genes into geometry: imaging for mouse development in 3D". *Curr. Opin. Genet. Dev.* 21: 638-646.
- Pauwels E, Van Loo D, Cornillie P, Brabant L, Van Hoorebeke L (2013) "An exploratory study of contrast agents for soft tissue visualization by means of high resolution X-ray computed tomography imaging". *J. Microsc*. 250: 21-31.
- Porro LB, Richards CT (2017) "Digital dissection of the model organism *Xenopus laevis* using contrast-enhanced computed tomography". *J. Anat*. 231: 169-191.
- Poznyakovskiy AA, Zahnert T, Kalaidzidis Y, Schmidt R, Fischer B, Baumgart J, Yarin YM (2008) "The creation of geometric three-dimensional models of the inner ear based on micro computer tomography data". *Hearing Res.* 243: 95-104.
- Quintana-Urzainqui I, Rodríguez-Moldes I, Mazan S, Candal E (2015) "Tangential migratory pathways of subpallial origin in the embryonic telencephalon of sharks: evolutionary implications". *Brain Struct. Funct.* 220: 2905-2926.
- Rodríguez-Moldes I, Santos-Durán GN, Pose-Méndez S, Quintana-Urzainqui I, Candal E (2017) ''The brains of cartilaginous fishes'' *Evolution of Nervous Systems* (Vol. 1), ed. J. Kaas (Oxford: Elsevier), 77-97.

- Schulz-Mirbach T, Heß M, Metscher BD (2013) “Sensory epithelia of the fish inner ear in 3D: studied with high-resolution contrast enhanced microCT”. *Front. Zool.* 10: 63.
- Schulz-Mirbach T, Ladich F, Plath M, Metscher BD, Heß M (2014) “Are accessory hearing structures linked to inner ear morphology? Insights from 3D orientation patterns of ciliary bundles in three cichlid species”. *Front. Zool.* 11: 25.
- Schnetz L, Kriwet J, Pfaff C. (2017) “Virtual reconstruction of the skeletal labyrinth of two lamnid sharks (Elasmobranchii, Lamniformes)”. *J. Fish. Biol*. 90: 1083-1089.
- Silvent J, Akiva A, Brumfeld V, Reznikov N, Rechav K, Yaniv K, Addadi L, Weiner S (2017) “Zebrafish skeleton development: High resolution micro-CT and FIB-SEM block surface serial imaging for phenotype identification”. PLoS One 12:e0177731.
- Smith DB, Bernhardt G, Raine NE, Abel RL, Sykes D, Ahmed F, Pedroso I, Gill RJ (2016) "Exploring miniature insect brains using micro-CT scanning techniques". *Sci. Rep.* 6: 21768-21777.
- Tahara R, Larsson HC (2013) “Quantitative analysis of microscopic X-ray computed tomography imaging: Japanese quail embryonic soft tissues with iodine staining”. *J. Anat.* 223: 297-310.
- Wise LD, Winkelmann CT, Dogdas B, Bagchi A (2013) “Micro−computed tomography imaging and analysis in developmental biology and toxicology”. *Birth Defects Res. C* 99: 71-82.
- Wong MD, Dorr AE, Walls JR, Lesch JP, Henkelman RM (2012) "A novel 3D mouse embryo atlas based on micro-CT". *Development* 139: 3248-3256.
- Wong MD, Spring S, Henkelman RM (2013) "Structural stabilization of tissue for embryo phenotyping using micro-CT with iodine staining". PLoS ONE 8(12): e84321.

TABLE LEGENDS

Table 1.- Scanning parameters applied on the samples. Non-desiccated samples were scanned within methanol. HMDS-desiccated sampled were scanned dried. Every sample was scanned every 0.18º. Color of the boxes indicates the protocol applied: white: unstained and non-dessicated control samples, yellow: staining with alcoholic iodine, blue: staining with Lugol´s solution, yellow: unstained samples desiccated with hexamethyldisilazane (HMDS), purple: staining with phosphotungstic acid (PTA), green: staining with PTA and desiccation with HMDS.

Table 2.- Combinations of the contrast-enhancers and desiccation applied. Color of the boxes indicates the protocol applied: white: unstained and non-dessicated control samples, yellow: staining with alcoholic iodine, blue: staining with Lugol´s solution, yellow: unstained samples desiccated with hexamethyldisilazane (HMDS), purple: staining with phosphotungstic acid (PTA), green: staining with PTA and desiccation with HMDS.

FIGURE LEGENDS

Fig. 1.- Unstained and non-desiccated *S. canicula* stage 19 embryo. Lateral (A), dorsal (B) and frontal (C) 3D reconstructions of the embryo showing the surface and main external features like the otic cups (asterisks) and the collapsed skin over the hindbrain. Note the undifferentiated inner tissue without appreciated structures in a transverse section (D). The white line in B indicates the level of the section in D.

Fig. 2.- Unstained and HMDS-desiccated *S. canicula* embryos at stages 27 (A), 29 (B) and 31 (C). Lateral 3D views (up) evidence the presence of several wrinkles around the eyes and mid head (arrows). Transverse sections through the 3D reconstructed embryos (middle) show that the ventricle of the hindbrain collapsed (arrows) while the forebrain did not (asterisk). Apart from the neural tube, only some inner structures like the otic ganglia (arrowheads) are barely visible (B, middle). Individual transverse sections reveal a very poor visualization of the inner tissues (A-C, down), with a low-dense granulated appearance where only the main structures can be appreciated, like the otic vesicles (asterisks) or the skull in the later one (arrow). The white lines indicate the level of the sections below the 3D reconstructions.

Fig. 3.- Unstained and HMDS-desiccated isolated inner ears of juvenile *S. canicula*. Horizontal (A) and transverse (B) sections of 3D reconstructed inner ears and transverse individual images of the inner ear (C, D). The most dense structures are the bright white otoliths inside the otic chambers (asterisks). The membranous labyrinth is clearly visible in the two- dimensional images (C, D, arrowheads). Out of the otic capsule, the muscular tissue appears strongly stained (A, arrow).

Fig. 4.- PTA-stained and HMDS-desiccated *S. canicula* embryos stages 24 (up; A-C) and 26 (down; D-F). Lateral view of a reconstructed stage 24 embryo (A) and transverse individual (B) and 3D (C) sectioned images. Same views of a stage 26 embryo (D-E). The external view of the stage 24 embryo shows the branchial clefts and optic vesicle (A, arrows) as the main external features, while the inner reveal the intense staining of the brain, otic vesicles and ganglia (B,C) and the collapsed ventricle of the hindbrain (arrows). The stage 26 embryo shows the gill buds and olfactory pits (D, arrows) as external main news, but internally looks like the earlier embryo (E, F) and presents the collapse of the ventricle too (arrows). The white lines in A and D indicate the level of the sections in B-C and E-F, respectively.

Fig. 5.- Alcoholic iodine (I2M) stained *S. canicula* embryos stages 18 (up; A-C) and 22 (down; D-F). The reconstructed stage 18 embryo presents a well-contrasted and correct 3D view, only slight damages due to manipulation (A, asterisks) are appreciated. Transverse sections show non-collapsed cavities and, despite the early stage of development of this sample, some structures like the otic placodes (B, arrows) are clearly differentiated and empty spaces appear black. Sagittal sections evidence the staining variation along the embryo: from clear grey in neural tube and otic placodes, to darker grey in other tissues and black in empty spaces like inside the cavities (C). The stage 22 embryo presents a good external 3D view (D, up), showing as main external characteristics the branchial clefts and the otic vesicle (D up, arrows and arrowhead, respectively). However, parasagittal sections reveal an homogeneous aspect (D, down). Transverse sections evidence that the homogeneous dense aspect occupies the whole embryo (E) and the collapse of the ventricle of the hindbrain (E, arrows), while other hollow structures like the otic cups are not (E, arrowheads), although these ones connect with the exterior. The sagittal section corroborates the above (F). The white lines in A indicate the level of the sections in B. The white line in B indicates the level of the section in C. The white lines in D indicate the level of the sections in E. The white line in E indicates the level of the section in F.

Fig. 6.- Isolated inner ears of juvenile *S. canicula* stained with alcoholic iodine (I2M) for 1 (A), 3 (B) and 5 (C) days. Transversal (A-C, up), sagittal (A, B, down) and horizontal (C, down) sections through the reconstructed otic capsule provide well defined images. The sample stained for 1 day (A) presents visible cavities and membranous labyrinth in a grey tone, remarking the white color of the otoliths (A, asterisks). The sample stained for 2 days presents a much more contrasted appearance where the most dense structure are the bright-white otoliths (B, asterisks), but other structures are also well stained, like the maculae (arrowheads) and the otic nerve (arrow). Curiously, the sample stained for 5 days presents a low contrast and no otoliths are observed, but there are some dense particles that may be parts of disintegrated otoliths (B, arrowheads). The cartilage presents low contrasts in the three cases.

Fig. 7.- Lugol´s solution stained isolated inner ears of *S. canicula*. Frontal view (A), transverse individual section (B) and false colored sections through 3D reconstructed otic capsule (C, D). The external view presents a good resolution where thin structures like nerves are distinguishable (A, arrowheads) although the image presents a mid-low contrast. Individual transverse sections show a very low-dense general aspect (B) where the membranous labyrinth is hardly distinguishable in some points separated from the cartilage (B, arrowheads). The statoacoustic nerve si a little more stained (B, arrow), but the most dense structure is again the otolith (B, asterisk). False-colored images allow a better appreciation of some details like the otic nerve or the otoliths (C, arrow and asterisk, respectively). If the color reflects the density of the tissue the otolith is specially visible (D, asterisk).

Fig. 8.- PTA-stained embryos of *S. canicula* stages 20 (A), 21 (B) and 24 (C). Lateral (up) and parasagittal (middle) 3D views and transverse individual sections (down). These early embryos present an good external aspect where the main characteristics are the branchial clefts and the otic pit (A-C up, arrows and asterisks, respectively). Parasagittal sections through these reconstructions show a variation in the staining along the development (A-C, middle), where it is appreciated how the internal staining seems weaker as the development progresses. These views also evidence the collapsed ventricle of the hindbrain (A,B middle, arrowheads). Transverse individual sections show the very high-contrasted stage 20 embryo with no differentiated inner structures and a slightly collapsed ventricle (A down, arrowhead). The stage 21 shows the high staining of the neural tube and otic vesicles, but surrounded by less dense tissue (B, down), while the roof of the ventricle is also moderately collapsed (arrowhead). The latter embryo presents a high contrasted appearance too, but a little less intense than the previous one (C, down). The neural tube, otic vesicles and ganglia are more stained than the surrounding tissue. The collapse of the ventricle is more evident than in the previous samples (arrowhead). The white lines in the upper images indicate the level of the sections below.

Fig. 9.- PTA-stained embryos of *S. canicula* stages 27 (A) and 28 (B). Lateral view of reconstructed heads (left), individual transverse sections (center) and transverse sections through 3D reconstructions (right). The stage 27 embryo reconstructed head shows a detailed view of its surface, although it presents some wrinkles (A left, arrows). Individual transverse sections reveal the high contrasted brain and otic vesicles, which are not collapsed (A centre, asterisks), while the roof of the ventricle is slightly wrinkled-collapsed (arrowhead). Although the cartilage in not very stained, at this stage the skull begins to be clearly visible in the transverse images (A center and right, arrow). The stage 28 embryo presents a good 3D appearance too, remarking the resolution of external features like the gill buds (B left, arrows). Transverse sections (B, center and right) show the high contrast of the brain and also other structures like the otic vesicles and statoacoustic ganglia (asterisks and empty arrowheads, respectively). The ventricle seems more collapsed than in the previous sample (white-colored arrowheads). The white lines in the lateral views indicate the level of the sections next to them.

Fig. 10.- PTA-stained embryos of *S. canicula* stages 29 (A), 31 (B) and 32 (C). Lateral view of reconstructed heads (A, D, G), transverse sections through 3D reconstructions (B, E, H) and individual transverse sections (C, F, I). The external view of the stage 29 embryo is correct and shows the details of its surface, but it also evidences the important sinking of the ectoderm over the ventricle (A, arrow). This sinking is noticeable also in the transverse sectioned view (B, arrow), where a reasonable good reconstruction of the inside of the embryo showing the stained brain and ganglia is appreciated. It is also seen the stained and defined retinas defined (B, arrowheads). The individual transverse slice corresponding to the previous image reaffirms the well-stained structures and evidences the low-contrasted tissue between them (C). The stage 31 embryo presents as well a good 3D view, but some moderate distortions like wrinkles are appreciated, specially in the eye (D, arrow). The transverse sectioned image shows those wrinkles too (E, arrows), but the deformation over the hindbrain is only superficial. The individual transverse slice allows a better appreciation of the developing skull, showing that not only the basal part is formed, but also the lateral walls are (F, arrowheads). The 3D reconstruction of the head of the stage 32 embryo shows a smooth surface with the gill filaments and the eye as the principal external characteristics (G, arrows and asterisk, respectively), but there is no evidence of wrinkles or other kind of distortion. The transverse section through this reconstruction shows that not only the biggest structures are visible, there are other thinner elements like mandibular muscles or gills that are well-appreciated (H, arrowheads). The individual slice shows a less blurred image that provides a better identification of inner structures, although the staining in not as intense as in earlier samples. This view even allows the visualization of the fibers of the mandibular muscles (I, arrowheads). The white lines in the lateral views indicate the level of the sections next to them.

Fig. 11.- PTA-stained stage 33 embryo (A-C) and juvenile (D-G) of *S. canicula*. Lateral view of a reconstructed head (A) and transverse 3D (B) and individual slice (C) of the head of a stage 33 embryo. Lateral view of a reconstructed head (D) and transverse 3D (E) and individual slices (F,G) of the head of juvenile S. canicula. The external view of the stage 33 embryo allows the identification of individual neuromasts (A, arrowheads), while in the transverse section the most striking elements are the otoliths (B, arrowheads). The individual slice (C) evidences the dark empty cavities of the inner ear and brain, even with the low contrast of these tissues. The juvenile 3D reconstruction is characterized by the numerous scales covering its surface (D). The transverse section evidences the poorly contrasted brain (E, asterisk) while other structures like the mandibular muscles appear more stained (F, arrows). Inverting the color of the slice allows a little improvement of the brain, but at the same time a ring effect appears (G).

Fig. 12.- PTA-stained inner ears of juvenile *S. canicula* scanned at 40KV (A) and 55 KV (B). Transverse sections at different levels of the otic capsule showing the maculae and cristae of the membranous labyrinth (arrowheads) inside the cartilage and the statoacoustic nerve entering the capsule (asterisks). The otoliths are also visible (arrows). Note the homogeneous staining along the whole sample.

Fig. 13.- Control stage 19 embryo desiccated (left) and PTA-stained (right) to study the effect of successive treatments over the same sample. Both scannings show a detailed view of the surface of the sample (A-D) where the most remarkable structures are the otic cups (asterisks) and the most important distortion is the collapse of the ectoderm over the hindbrain (B, D, arrows). Some lumps are also appreciated in the surface of the desiccated and stained sample (C, D, arrowheads) as consequence of it manipulation. Transverse sections through the desiccated embryo (E,F) show a similar aspect to that observed in the unstained sample, while the stained sample presents a much more low-dense inner tissue and brighter edges (G,H). The white line in A indicates the level of the sections in E-G. The white line in C indicates the level of the sections in F-H.

TABLES

Table 1.- Scanning parameters applied on the samples. Non-desiccated samples were scanned within methanol. HMDS-desiccated sampled were scanned dried. Every sample was scanned every 0.18º. Color of the boxes indicates the protocol applied: white: unstained and non-dessicated control samples, yellow: staining with alcoholic iodine, blue: staining with Lugol´s solution, yellow: unstained samples desiccated with hexamethyldisilazane (HMDS), purple: staining with phosphotungstic acid (PTA), green: staining with PTA and desiccation with HMDS.

STAGE	STAIN	DESICCATION	VOLTAGE (Kv)	AMPERAGE (µA)	PIXEL SIZE (camera) (µm)	PIXEL SIZE (imagen) (µm)	ROTATION STEP (deg)	EXPOSURE TIME (ms)	SCAN DURATION (h:m:s)
St19	NO	NO	40 Kv	250 µA	9,01 µm	2,04 µm	0,2	0s 370ms	01:32:29
Juvenile ear	NO	NO	Kv	µA	µm	µm			
St19	NO	HMDS	40 Kv	250 µA	9,01 µm	1,15 µm	0,2	1s 0ms	01:21:08
St27	NO	HMDS	55 Kv	165 µA	9,01 µm	1.49 µm	0,2	1s	01:46:31
St29	NO	HMDS	55 Kv	165 µA	9,01 µm	1.49 µm	0,2	1s	01:41:40
St31	NO	HMDS	55 Kv	165 µA	9,01 µm	3,05 µm	0,2	0s	01:33:08
Juvenile ear	NO	HMDS	55 Kv	165 µA	9,01 µm	2,44 µm	0,2	0s	01:32:42
St19	PTA	HMDS	40 Kv	250 µA	9,01 µm	1.15 µm	0,2	1s 0ms	01:21:54
St24	PTA	HMDS	40 Kv	250 µA	9,01 µm	0,95 µm	0,2	1s	02:05:37
St26	PTA	HMDS	55 Kv	165 µA	9,01 µm	1,49 µm	0,2	1s	01:46:34
St18	Iodine	NO	40 Kv	250 µA	9,01µm	0,95 µm	0,2	1s 0ms	02:09:34
St22	Iodine	NO	40 Kv	250 µA	9,01 µm	0,95 µm	0,2	1s	02:05:36
Juvenile ear	Iodine	NO	55 Kv	165 µA	9,01 µm	3,94 µm	0,4	0s	00:47:03
Juvenile ear	Iodine	NO	55 Kv	165 µA	9,01 µm	3,94 µm	0,4	0s	00:46:09
Juvenile ear	Iodine	NO	55 Kv	165 µA	9,01 µm	3,94 µm	0,4	0s	00:46:24
Juvenile ear	Lugol	NO	55 Kv	165 µA	9,01 µm	4,07 µm	0,4	0s	00:46:12
St20	PTA	NO	40 Kv	250 µA	9,01 µm	0,88 µm	0,2	0s 990ms	02:04:12
St21	PTA	NO	40 Kv	250 µA	9,01 µm	1,15 µm	0,2	1s	02:05:55
St24	PTA	NO	40 Kv	250 µA	9,01 µm	0,95 µm	0,2	1s	02:07:13
St25	PTA	NO	40 Kv	250 µA	9,01 µm	1,97 µm	0,2	0s	01:33:48
St27	PTA	NO	40 Kv	250 µA	9,01 µm	1,70 µm	0,2	1s	01:46:28
St28	PTA	NO	40 Kv	250 µA	9,01 µm	2,58 µm	0,2	0s	02:46:15
St29	PTA	NO	40 Kv	250 µA	9,01 µm	2.44 µm	0,2	0s	01:32:24
St30e	PTA	NO	40 Kv	250 µA	9,01 µm	3,46 µm	0,2	0s	01:34:16
St31m	PTA	NO	40 Kv	250 µA	9,01 µm	3,19 µm	0,2	0s	01:30:49
St32e	PTA	NO	40 Kv	250 µA	9,01 µm	5,97 µm	0,2	1s	01:38:30
St33	PTA	NO	40 Kv	250 µA	9,01 µm	4,95 µm	0,2	0s	01:32:32
Juvenile	PTA	NO	40 Kv	250 µA	9,01 µm	6,79 µm	0,2	1s	02:07:45
Juvenile ear	PTA	NO	55 Kv	165 µA	9,01 µm	2,78 µm	0,2	0s	01:32:25
			40 Kv	250 µA	9,01 µm	2,78 µm	0,2	0s	01:33:10

Untreated	Iodine	Lugol	HMDS	PTA	PTA + HMDS

TABLE 1

Table 2.- Combinations of the contrast-enhancers and desiccation applied. Color of the boxes indicates the protocol applied: white: unstained and non-dessicated control samples, yellow: staining with alcoholic iodine, blue: staining with Lugol´s solution, yellow: unstained samples desiccated with hexamethyldisilazane (HMDS), purple: staining with phosphotungstic acid (PTA), green: staining with PTA and desiccation with HMDS.

	Stained	Unstained
Desiccated	HMDS + PTA	HMDS
Un-desiccated	I2M	Control*
	Lugol	
	PTA	

TABLE 2

FIGURES

Fig. 1.- Unstained and non-desiccated *S. canicula* stage 19 embryo. Lateral (A), dorsal (B) and frontal (C) 3D reconstructions of the embryo showing the surface and main external features like the otic cups (asterisks) and the collapsed skin over the hindbrain. Note the undifferentiated inner tissue without appreciated structures in a transverse section (D). The white line in B indicates the level of the section in D.

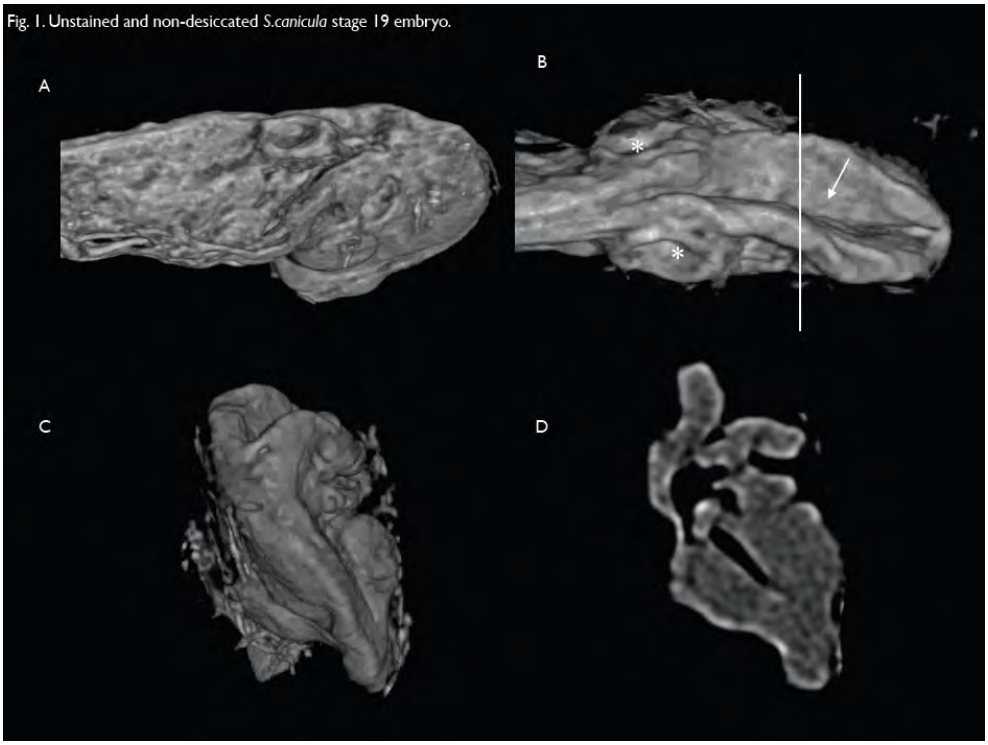
Fig. 1. Unstained and non-desiccated S.canicula stage 19 embryo.
A
B
C
D

Figure 1

Fig. 2.- Unstained and HMDS-desiccated *S. canicula* embryos at stages 27 (A), 29 (B) and 31 (C). Lateral 3D views (up) evidence the presence of several wrinkles around the eyes and mid head (arrows). Transverse sections through the 3D reconstructed embryos (middle) show that the ventricle of the hindbrain collapsed (arrows) while the forebrain did not (asterisk). Apart from the neural tube, only some inner structures like the otic ganglia (arrowheads) are barely visible (B, middle). Individual transverse sections reveal a very poor visualization of the inner tissues (A-C, down), with a low-dense granulated appearance where only the main structures can be appreciated, like the otic vesicles (asterisks) or the skull in the later one (arrow). The white lines indicate the level of the sections below the 3D reconstructions.

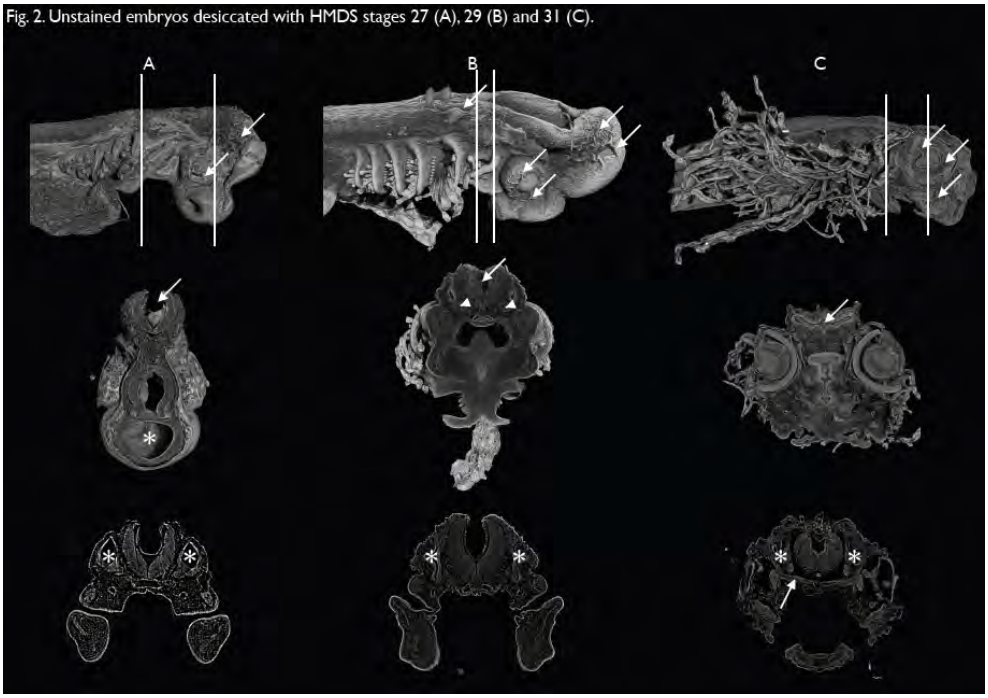
Fig. 2. Unstained embryos desiccated with HMDS stages 27 (A), 29 (B) and 31 (C).
A
B
C

Figure 2

Fig. 3.- Unstained and HMDS-desiccated isolated inner ears of juvenile *S. canicula*. Horizontal (A) and transverse (B) sections of 3D reconstructed inner ears and transverse individual images of the inner ear (C, D). The most dense structures are the bright white otoliths inside the otic chambers (asterisks). The membranous labyrinth is clearly visible in the two- dimensional images (C, D, arrowheads). Out of the otic capsule, the muscular tissue appears strongly stained (A, arrow).

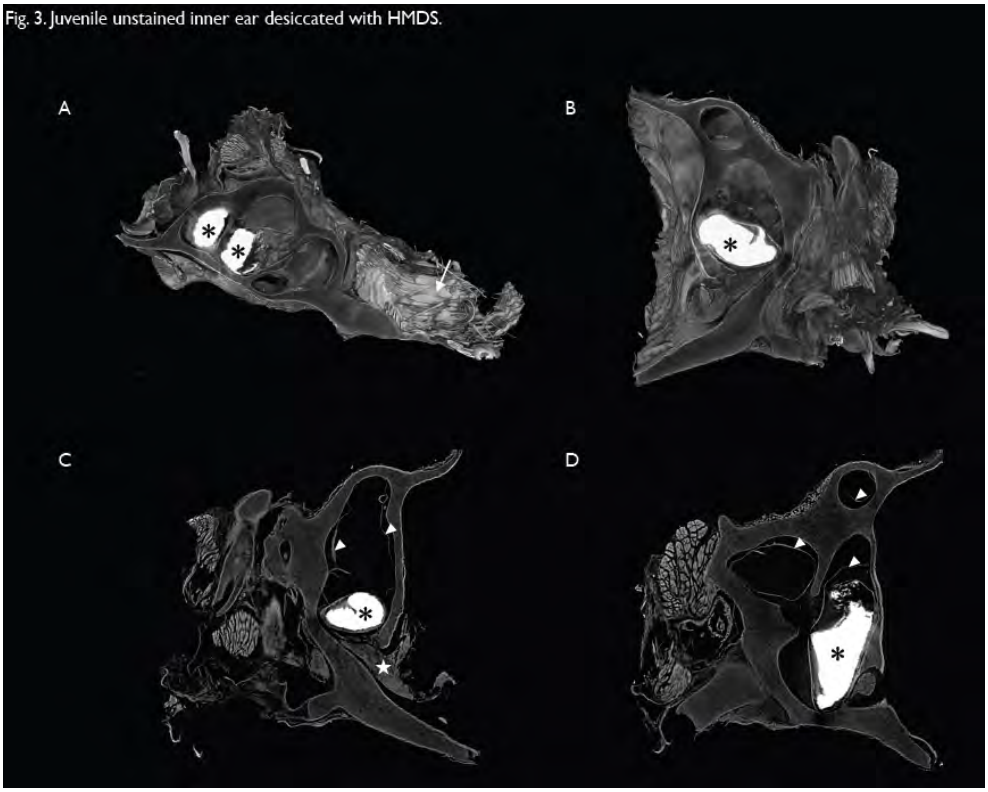
Fig. 3. Juvenile unstained inner ear desiccated with HMDS.
A
B
C
D

Figure 3

Fig. 4.- PTA-stained and HMDS-desiccated *S. canicula* embryos stages 24 (up) and 26 (down). Lateral view of a reconstructed stage 24 embryo (A) and transverse individual (B) and 3D (C) sectioned images. Same views of a stage 26 embryo (D-E). The external view of the stage 24 embryo shows the branchial clefts and optic vesicle (A, arrows) as the main external features, while the inner reveal the intense staining of the brain, otic vesicles and ganglia (B,C) and the collapsed ventricle of the hindbrain (arrows). The stage 26 embryo shows the gill buds and olfactory pits (D, arrows) as external main news, but internally looks like the earlier embryo (E, F) and presents the collapse of the ventricle too (arrows). The white lines in A and D indicate the level of the sections in B-C and E-F, respectively.

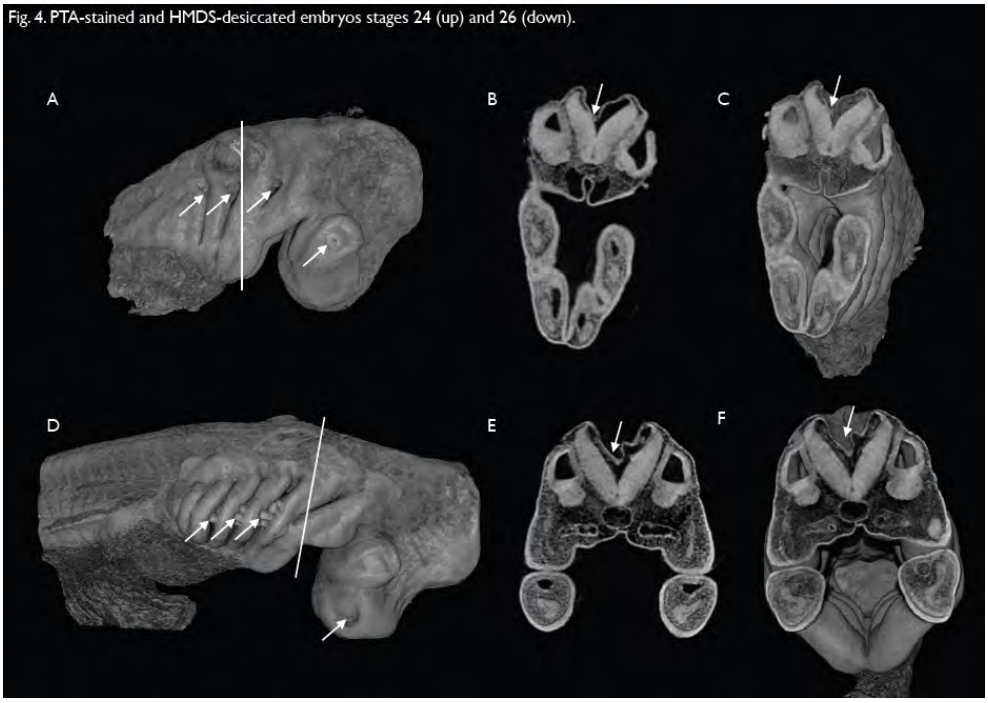
Fig. 4. PTA-stained and HMDS-desiccated embryos stages 24 (up) and 26 (down).
A
B
C
D
E
F

Figure 4

Fig. 5.- Alcoholic iodine (I2M) stained *S. canicula* embryos stages 18 (up) and 22 (down). The reconstructed stage 18 embryo presents a well-contrasted and correct 3D view, only slight damages due to manipulation (A, asterisks) are appreciated. Transverse sections show non-collapsed cavities and, despite the early stage of development of this sample, some structures like the otic placodes (B, arrows) are clearly differentiated and empty spaces appear black. Sagittal sections evidence the staining variation along the embryo: from clear grey in neural tube and otic placodes, to darker grey in other tissues and black in empty spaces like inside the cavities (C). The stage 22 embryo presents a good external 3D view (D, up), showing as main external characteristics the branchial clefts and the otic vesicle (D up, arrows and arrowhead, respectively). However, parasagittal sections reveal an homogeneous aspect (D, down). Transverse sections evidence that the homogeneous dense aspect occupies the whole embryo (E) and the collapse of the ventricle of the hindbrain (E, arrows), while other hollow structures like the otic cups are not (E, arrowheads), although these ones connect with the exterior. The sagittal section corroborates the above (F). The white lines in A indicate the level of the sections in B. The white line in B indicates the level of the section in C. The white lines in D indicate the level of the sections in E. The white line in E indicates the level of the section in F.

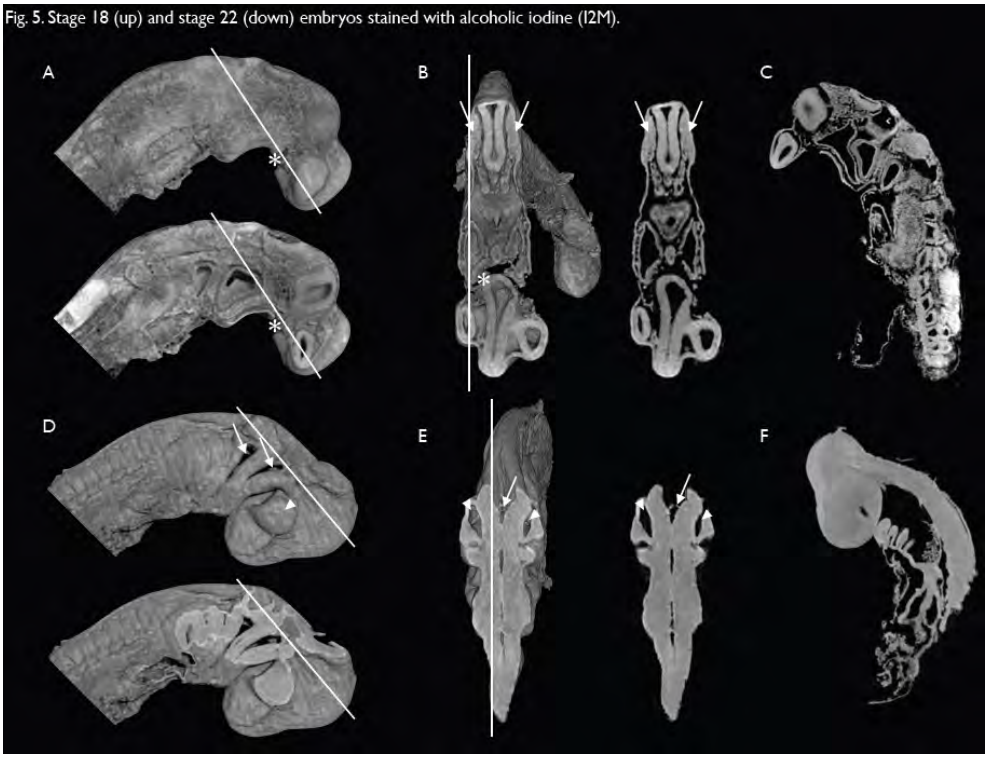
Fig. 5. Stage 18 (up) and stage 22 (down) embryos stained with alcoholic iodine (I2M).
A
B
C
D
E
F

Figure 5

Fig. 6.- Isolated inner ears of juvenile *S. canicula* stained with alcoholic iodine (I2M) for 1 (A), 3 (B) and 5 (C) days. Transversal (A-C, up), sagittal (A, B, down) and horizontal (C, down) sections through the reconstructed otic capsule provide well defined images. The sample stained for 1 day (A) presents visible cavities and membranous labyrinth in a grey tone, remarking the white color of the otoliths (A, asterisks). The sample stained for 2 days presents a much more contrasted appearance where the most dense structure are the bright-white otoliths (B, asterisks), but other structures are also well stained, like the maculae (arrowheads) and the otic nerve (arrow). Curiously, the sample stained for 5 days presents a low contrast and no otoliths are observed, but there are some dense particles that may be parts of disintegrated otoliths (B, arrowheads). The cartilage presents low contrasts in the three cases.

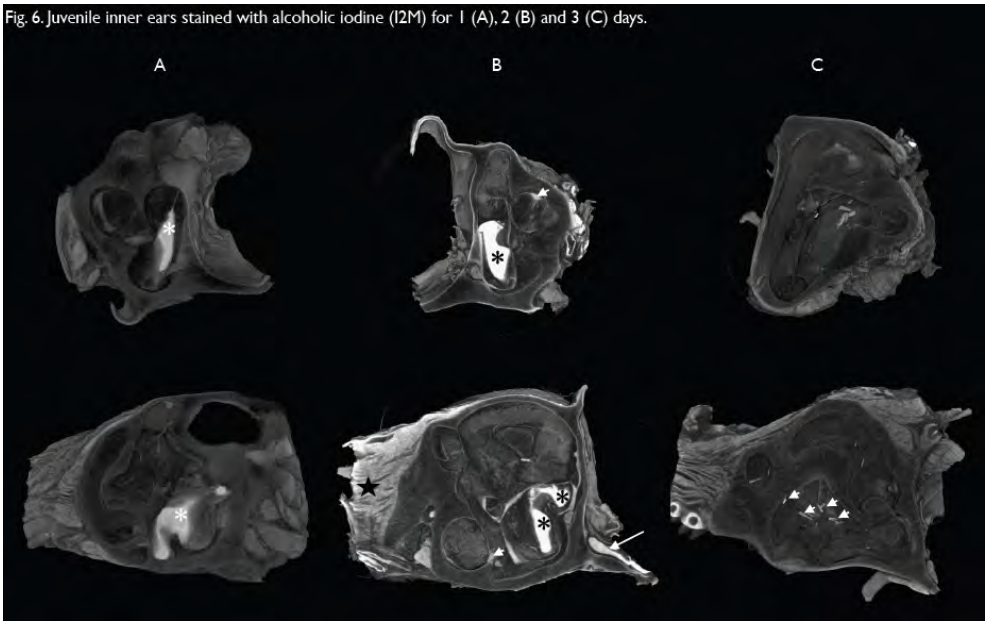

Fig. 6. Juvenile inner ears stained with alcoholic iodine (I2M) for 1 (A), 2 (B) and 3 (C) days.

Figure 6

Fig. 7.- Lugol´s solution stained isolated inner ears of *S. canicula*. Frontal view (A), transverse individual section (B) and false colored sections through 3D reconstructed otic capsule (C, D). The external view presents a good resolution where thin structures like nerves are distinguishable (A, arrowheads) although the image presents a mid-low contrast. Individual transverse sections show a very low-dense general aspect (B) where the membranous labyrinth is hardly distinguishable in some points separated from the cartilage (B, arrowheads). The statoacoustic nerve si a little more stained (B, arrow), but the most dense structure is again the otolith (B, asterisk). False-colored images allow a better appreciation of some details like the otic nerve or the otoliths (C, arrow and asterisk, respectively). If the color reflects the density of the tissue the otolith is specially visible (D, asterisk).

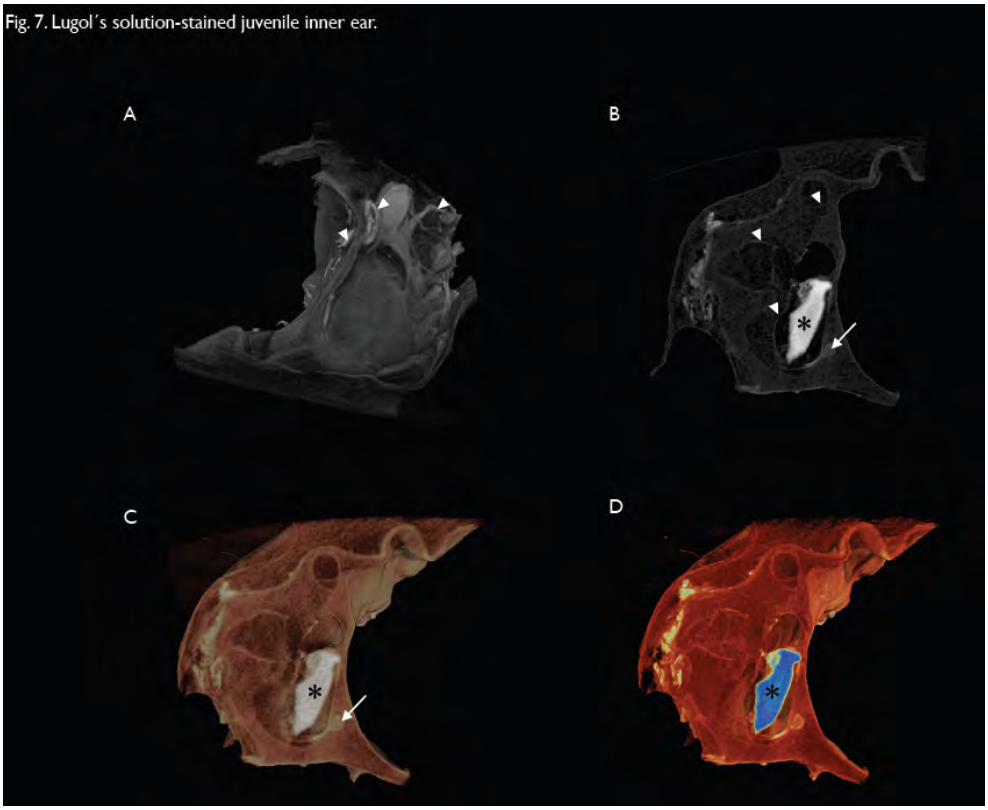

Figure 7

Fig. 8.- PTA-stained embryos of *S. canicula* stages 20 (A), 21 (B) and 24 (C). Lateral (up) and parasagittal (middle) 3D views and transverse individual sections (down). These early embryos present an good external aspect where the main characteristics are the branchial clefts and the otic pit (A-C up, arrows and asterisks, respectively). Parasagittal sections through these reconstructions show a variation in the staining along the development (A-C, middle), where it is appreciated how the internal staining seems weaker as the development progresses. These views also evidence the collapsed ventricle of the hindbrain (A,B middle, arrowheads). Transverse individual sections show the very high-contrasted stage 20 embryo with no differentiated inner structures and a slightly collapsed ventricle (A down, arrowhead). The stage 21 shows the high staining of the neural tube and otic vesicles, but surrounded by less dense tissue (B, down), while the roof of the ventricle is also moderately collapsed (arrowhead). The latter embryo presents a high contrasted appearance too, but a little less intense than the previous one (C, down). The neural tube, otic vesicles and ganglia are more stained than the surrounding tissue. The collapse of the ventricle is more evident than in the previous samples (arrowhead). The white lines in the upper images indicate the level of the sections below.

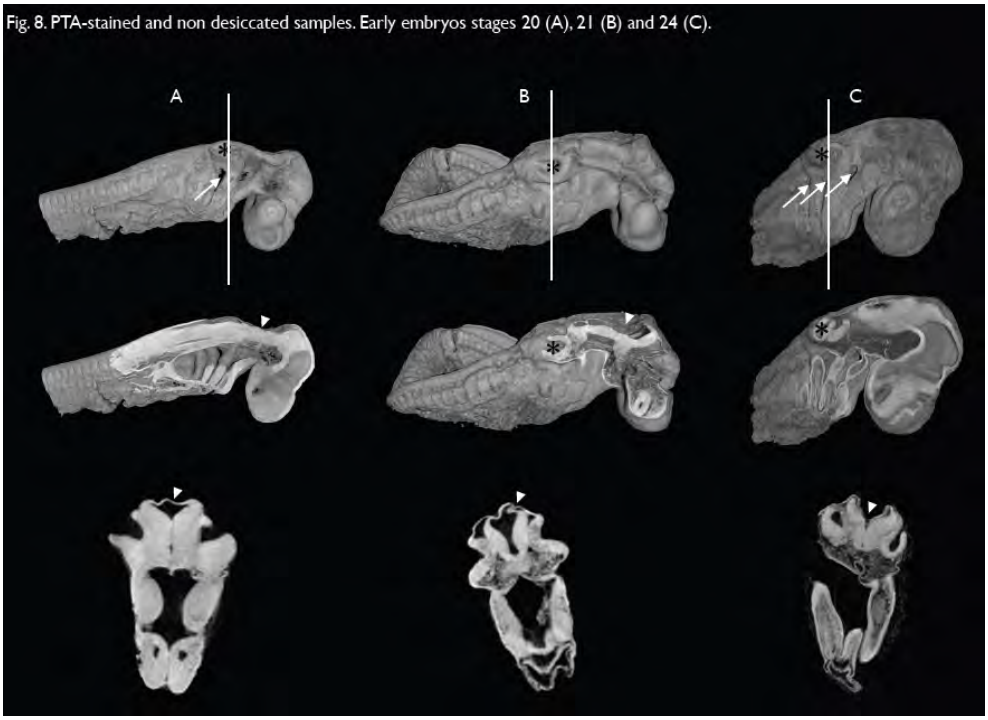
Fig. 8. PTA-stained and non desiccated samples. Early embryos stages 20 (A), 21 (B) and 24 (C).
A
B
C

Figure 8

Fig. 9.- PTA-stained embryos of *S. canicula* stages 27 (A) and 28 (B). Lateral view of reconstructed heads (left), individual transverse sections (center) and transverse sections through 3D reconstructions (right). The stage 27 embryo reconstructed head shows a detailed view of its surface, although it presents some wrinkles (A left, arrows). Individual transverse sections reveal the high contrasted brain and otic vesicles, which are not collapsed (A centre, asterisks), while the roof of the ventricle is slightly wrinkled-collapsed (arrowhead). Although the cartilage in not very stained, at this stage the skull begins to be clearly visible in the transverse images (A center and right, arrow). The stage 28 embryo presents a good 3D appearance too, remarking the resolution of external features like the gill buds (B left, arrows). Transverse sections (B, center and right) show the high contrast of the brain and also other structures like the otic vesicles and statoacoustic ganglia (asterisks and empty arrowheads, respectively). The ventricle seems more collapsed than in the previous sample (white-colored arrowheads). The white lines in the lateral views indicate the level of the sections next to them.

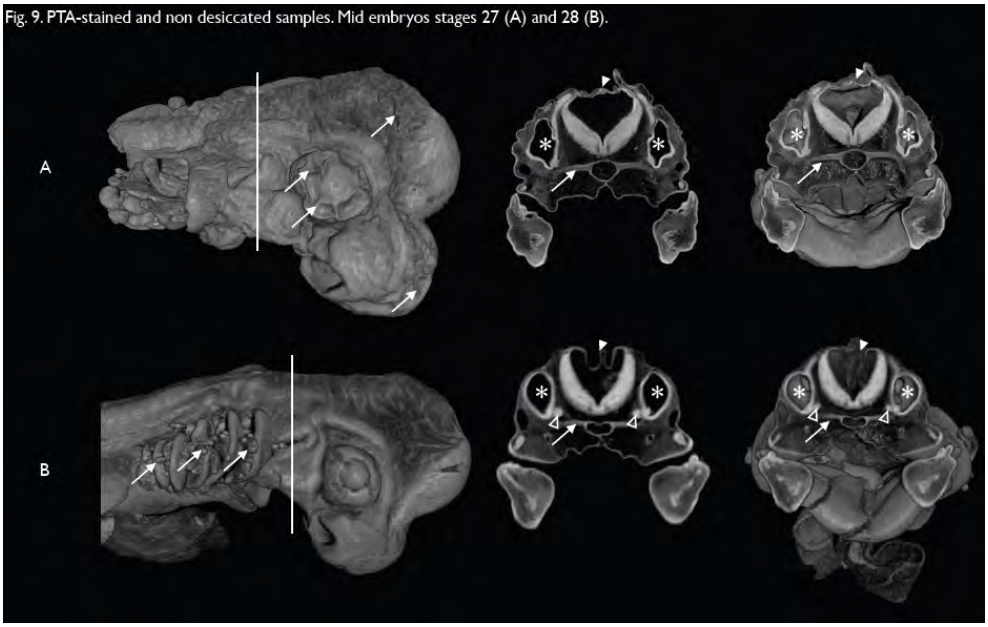
Fig. 9. PTA-stained and non desiccated samples. Mid embryos stages 27 (A) and 28 (B).
A
B

Figure 9

Fig. 10.- PTA-stained embryos of *S. canicula* stages 29 (A), 31 (B) and 32 (C). Lateral view of reconstructed heads (A, D, G), transverse sections through 3D reconstructions (B, E, H) and individual transverse sections (C, F, I). The external view of the stage 29 embryo is correct and shows the details of its surface, but it also evidences the important sinking of the ectoderm over the ventricle (A, arrow). This sinking is noticeable also in the transverse sectioned view (B, arrow), where a reasonable good reconstruction of the inside of the embryo showing the stained brain and ganglia is appreciated. It is also seen the stained and defined retinas defined (B, arrowheads). The individual transverse slice corresponding to the previous image reaffirms the well-stained structures and evidences the low-contrasted tissue between them (C). The stage 31 embryo presents as well a good 3D view, but some moderate distortions like wrinkles are appreciated, specially in the eye (D, arrow). The transverse sectioned image shows those wrinkles too (E, arrows), but the deformation over the hindbrain is only superficial. The individual transverse slice allows a better appreciation of the developing skull, showing that not only the basal part is formed, but also the lateral walls are (F, arrowheads). The 3D reconstruction of the head of the stage 32 embryo shows a smooth surface with the gill filaments and the eye as the principal external characteristics (G, arrows and asterisk, respectively), but there is no evidence of wrinkles or other kind of distortion. The transverse section through this reconstruction shows that not only the biggest structures are visible, there are other thinner elements like mandibular muscles or gills that are well-appreciated (H, arrowheads). The individual slice shows a less blurred image that provides a better identification of inner structures, although the staining in not as intense as in earlier samples. This view even allows the visualization of the fibers of the mandibular muscles (I, arrowheads). The white lines in the lateral views indicate the level of the sections next to them.

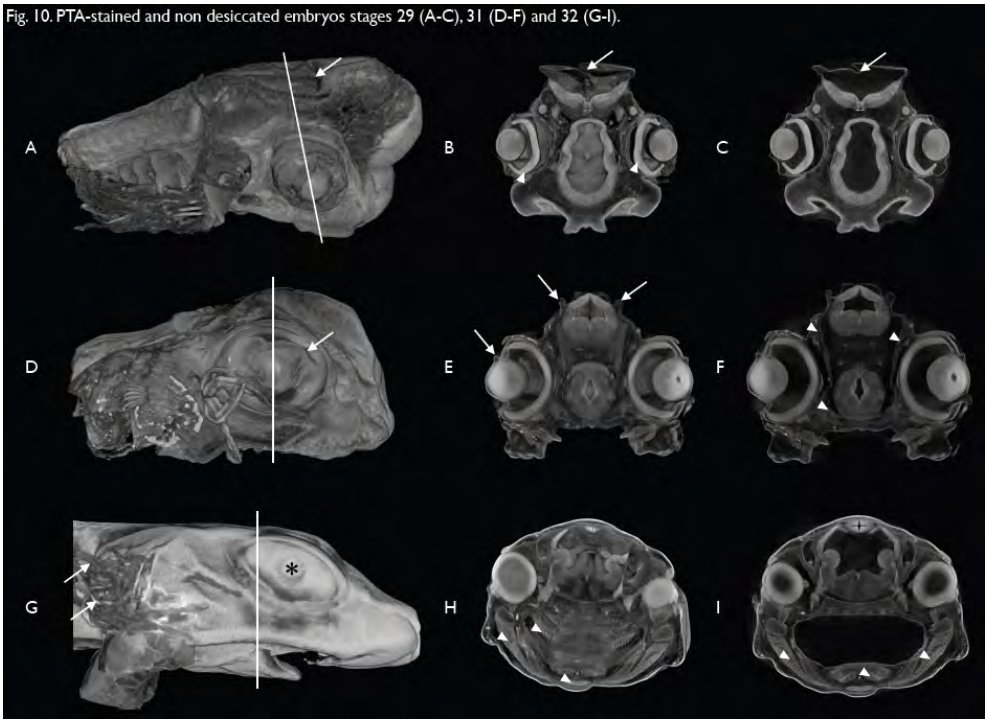
Fig. 10. PTA-stained and non desiccated embryos stages 29 (A-C), 31 (D-F) and 32 (G-I).
A
B
C
D
E
F
G
H
I
*

Figure 10

Fig. 11.- PTA-stained stage 33 embryo (A-C) and juvenile (D-G) of *S. canicula*. Lateral view of a reconstructed head (A) and transverse 3D (B) and individual slice (C) of the head of a stage 33 embryo. Lateral view of a reconstructed head (D) and transverse 3D (E) and individual slices (F,G) of the head of juvenile S. canicula. The external view of the stage 33 embryo allows the identification of individual neuromasts (A, arrowheads), while in the transverse section the most striking elements are the otoliths (B, arrowheads). The individual slice (C) evidences the dark empty cavities of the inner ear and brain, even with the low contrast of these tissues. The juvenile 3D reconstruction is characterized by the numerous scales covering its surface (D). The transverse section evidences the poorly contrasted brain (E, asterisk) while other structures like the mandibular muscles appear more stained (F, arrows). Inverting the color of the slice allows a little improvement of the brain, but at the same time a ring effect appears (G).

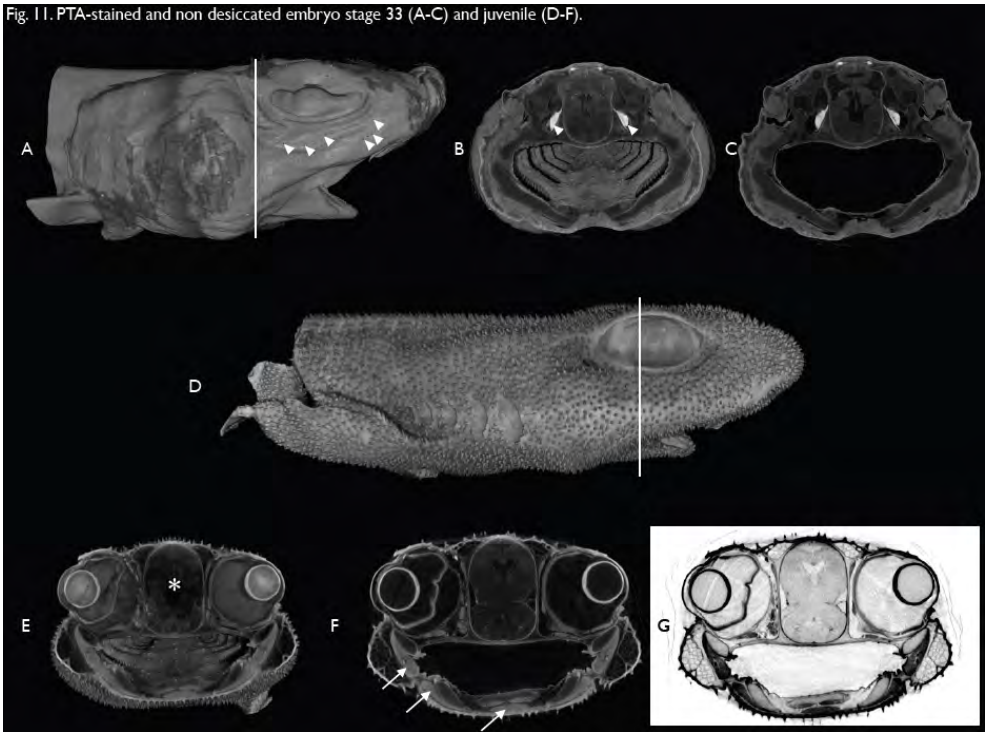
Fig. 11. PTA-stained and non desiccated embryo stage 33 (A-C) and juvenile (D-F).
A
B
C
D
E
F
G

Figure 11

Fig. 12.- PTA-stained inner ears of juvenile *S. canicula* scanned at 40KV (A) and 55 KV (B). Transverse sections at different levels of the otic capsule showing the maculae and cristae of the membranous labyrinth (arrowheads) inside the cartilage and the statoacoustic nerve entering the capsule (asterisks). The otoliths are also visible (arrows). Note the homogeneous staining along the whole sample.

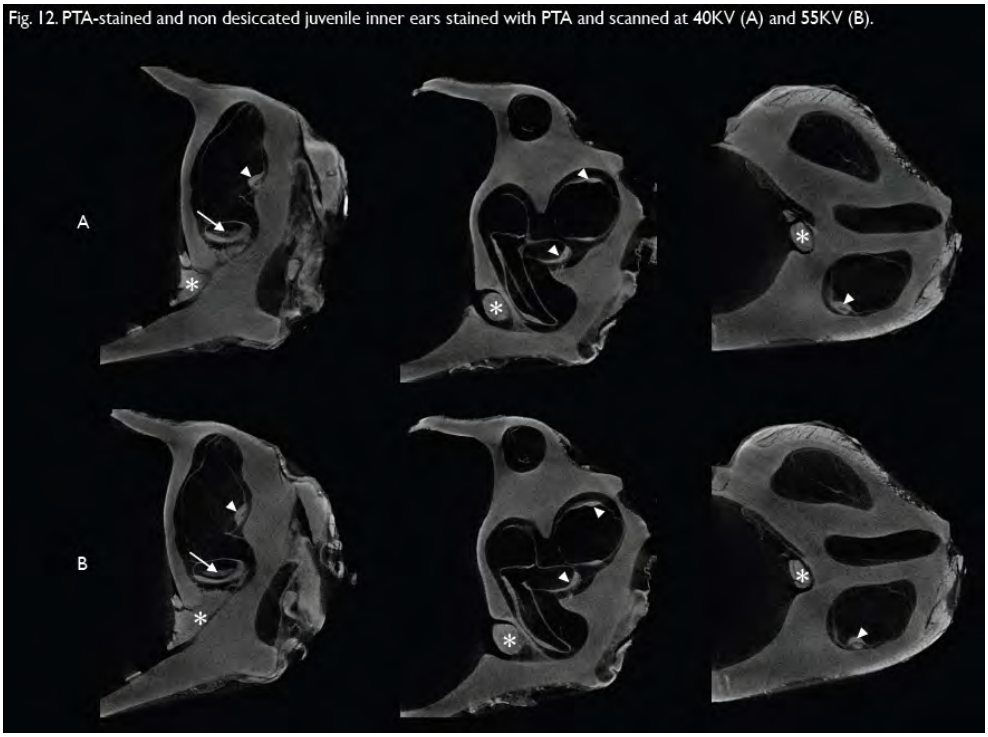
Fig. 12. PTA-stained and non desiccated juvenile inner ears stained with PTA and scanned at 40KV (A) and 55KV (B).
A
B

Figure 12

Fig. 13.- Control stage 19 embryo desiccated (left) and PTA-stained (right) to study the effect of successive treatments over the same sample. Both scannings show a detailed view of the surface of the sample (A-D) where the most remarkable structures are the otic cups (asterisks) and the most important distortion is the collapse of the ectoderm over the hindbrain (B, D, arrows). Some lumps are also appreciated in the surface of the desiccated and stained sample (C, D, arrowheads) as consequence of it manipulation. Transverse sections through the desiccated embryo (E,F) show a similar aspect to that observed in the unstained sample, while the stained sample presents a much more low-dense inner tissue and brighter edges (G,H). The white line in A indicates the level of the sections in E-G. The white line in C indicates the level of the sections in F-H.

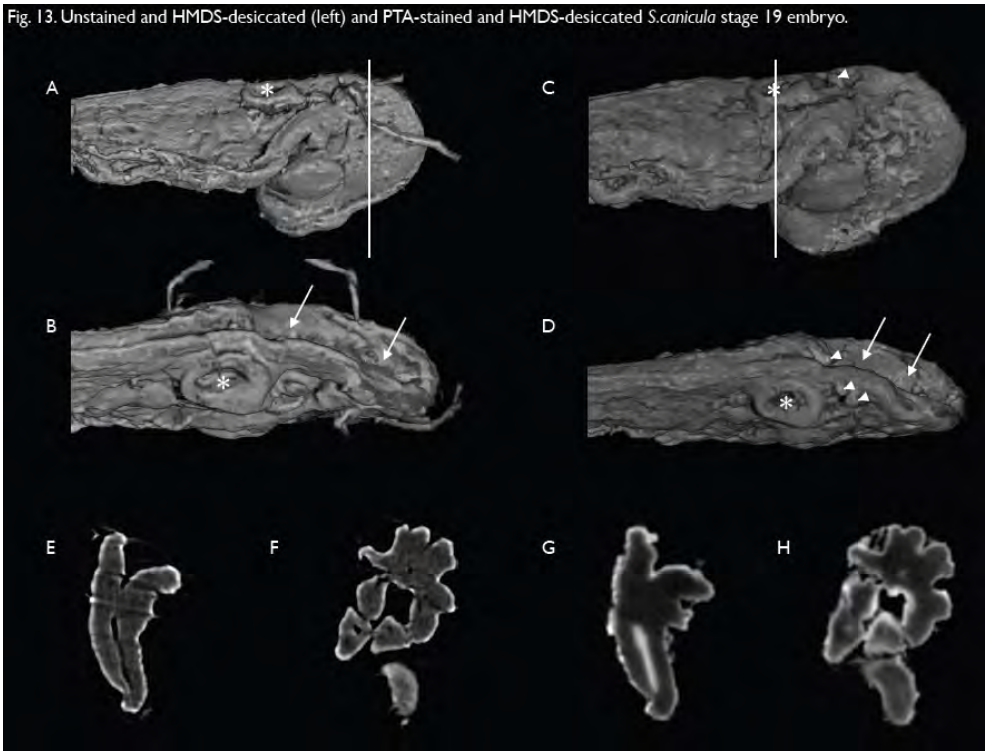
Fig. 13. Unstained and HMDS-desiccated (left) and PTA-stained and HMDS-desiccated S.canicula stage 19 embryo.
A
B
C
D
E
F
G
H

Figure 13

CHAPTER 2

Study of the development of the inner ear of the chondrychthyan *Scyliorhinus canicula* through micro-computed tomography (micro-CT)

INTRODUCTION

The inner ear is the structure responsible for the detection of sound, balance and acceleration in vertebrates. It exists in all craniates vertebrates, which include agnathans (hagfishes and lampreys) and gnathostomes (jawed vertebrates). The inner ear is composed by a three-dimensional sensory and non-sensory epithelia filled with endolymph and surrounded by perilymph that is encaged in a cartilaginous or osseous capsule (Torres and Giráldez, 1998) and presents two main regions: the dorsal or vestibular region, specialized in the perception of head movement; and the ventral or auditive part, specialized in the perception of the head position and sound perception. The dorsal region is composed by a variable number of semicircular canals with a dilatation called ampullae, which contains a sensory patch or crista. The movements of the head generate the movement of the endolymph in the canals, causing the depolarization of the hair cells of the ampullae and transmitting the information to the brain through the statoacoustic nerve. The auditory region is much more variable, being nearly absent in fish and showing increasing levels of complexity in terrestrial species, with different chambers containing otoliths or otoconia and sensory patches or maculae (Torres and Giráldez, 1998). The origin of the inner ear dates back to the early evolution of

vertebrates, at least 600 million years ago, and may be related to the statocyst and hydrodynamic receptors of invertebrates, according to some shared developmental genes between some invertebrate mechanosensory neurons and vertebrate hair cells (Fritzsch and Beisel, 2001), although how those mechanosensory cells gave rise to the vertebrate hair cells is still unclear (Fritzsch et al., 2006).

The simplest ear belongs to hagfishes, which have a single semicircular canal with two ampullae at each end and are the unique animals with two octaval nerves, the anterior one innervating the anterior crista and anterior region of the common macula and the rear one innervating the posterior crista and posterior part of the common macula (Lowenstein and Thornhill, 1970). The inner ear is irregularly ring-shaped and that forms an angle of 30º with the horizontal plane and with the anteroposterior axis of the animal (Lowenstein and Thornhill, 1970; McVean, 1991) and is enclosed in a cartilaginous capsule except in its medial side, which is covered by a membrane of connective tissue (Lowenstein and Thornhill, 1970). An endolymphatic duct departs dorsally from the ventral part of the ring and ends in an endolymphatic sac next to the medulla oblongata (Jørgensen et al., 1998; Fritzsch et al., 2006). The inner ear presents an anterior and a posterior dilatation, where

the cristae are located, and the macula communis is located in the ventromedial part and covered by an otoconia (Lowenstein and Thornhill, 1970). The inner ear of hagfishes presents only statotoconia which are structurally different from other vertebrates and are composed by partially crystallized calcium phosphate and calcium carbonate (Carlström, 1963; Maisey, 2001, Popper, 2011). Apart of the ring shape, the inner ear of the myxines is characterized by the specially high relation between the inner diameter of the canal and the curvature radium of itself, which joined to the absence of cupolae suggest the ability of their hair cells to respond independently of each other to the movement of the endolymph (Lowenstein and Thornhill, 1970; McVean, 1991). It is not clear yet if the inner ear of hagfishes is result of two fusioned vertical canals that have been reduced to the *saccus communis* and the unique semicircular canal is in fact the utriculus, as some authors propose (Jarvik, 1980, Maisey, 2001); or if this semicircular canal is homologous to both vertical canals of the other vertebrates, as most authors propose (Lowenstein and Thornhill, 1970; Maisey, 2001).

Lampreys have two vertical semicircular canals, each with an ampulla, fused in a *crus commune* and very close to the underlying utricle (Mazan et al., 2000). Below the canals, the inner ear presents two ciliated chambers where the cilia create a

vigorous circulation of the endolymph (Lowenstein et al., 1968; Thornhill, 1972; Baird, 1974). Neither hagfishes nor lampreys present a ventral recess in their labyrinths corresponding to the gnathostome saccule (Mazan et al., 2000). The inner ear of the lampreys is originated by the invagination of the otic placode that becomes an otocyst without communication to the exterior (Thornhill, 1972). Like hagfishes, lampreys have a *macula communis* that exhibits horizontal, anterior and posterior parts separated by a medial part (Baird, 1974). In contrast with the ring-shaped cristae of hagfishes, lampreys present cupolas and have tripartite cristae with vertical, horizontal and basal arms in each ampullae (Lowenstein et al., 1968; Thornhill, 1972; Fritzsch et al., 2006). Like hagfishes, the inner ear of the lampreys is characterized by the presence of calcium carbonate and calcium phosphate otoconia (Carlstöm, 1963; Maisey, 2001). Some extinct agnathans, like *Osteostracans*, share a considerable number of characteristics with gnathostomes, but none of them present any structure, including the sea canals of *Osteostracans*, that could be considered as a precursor of the horizontal semicircular canal (Mazan et al., 2000). Recent studies have proposed the existence of two “horizontal semicircular ducts” in each inner ear of *Petromyzon marinus*, but these ducts, contrarily to that observed in jawed vertebrates, are located in the medial wall of the labyrinth and in any case

are homologous to the horizontal semicircular canal of gnathostomes (Maklad et al., 2014).

The jawed vertebrates or gnathostomes present a high morphological variability in their inner ears, but share a common basic ear pattern, being the main difference among them the evolved lagena as the cochlea in mammals and as the basilar papilla in amphibians, reptiles and birds (Fritzsch et al., 2006; Popper, 2011). The main novel characteristic compared to agnathans is the appearance of a third semicircular canal, disposed horizontally and perpendicularly to the vertical ones (Mazan et al., 2000; Fritzsch et al., 2006), which is present even in Placoderms, the closest group to the common ancestor of all gnathostomes (Mazan et al., 2000). Related to the horizontal canal, the utricular recess is a rostral diverticulum of the saccule of gnathostomes where the ampullar chambers of the anterior and horizontal semicircular canals meet, which is obvious in Chondrichthyans, Arthrodires, Acanthodes and osteichthyans, but not in Osteostracans or Galeapsides; so the utricular recess may be biologically related to the origin of the horizontal semicircular canal (reviewed in Brazeau and Friedman, 2014). Like lampreys, the two vertical canals fuse in a *crus commune*, except in elasmobranchs, where the partially fused canals are the anterior and lateral ones, and in some placoderms (Mazan et al.,

2000; Evangelista et al., 2010). In some teleosts like *Salmo salar,* the three semicircular canals and the utricle make up the major vestibular parts of the ear, although in several species the utricle also participates in hearing (Popper, 2011). The sarcopterygian line that leads to tetrapods presents a new modification of the labyrinth, maybe beginning in the coelacanth *Latimeria*, a sensory epithelium associated to a perilymphatic duct that could have evolved into the actual mammalian cochlea (Fritzsch et al., 2006). It seems that the neglect papilla evolved into the amphibian papilla and that the amphibian basilar papilla is homologous to the basilar papilla of sarcopterygians and to the cochlea of mammals (Fritzsch et al., 2006). There are also other noticeable modifications in the inner ear of jawed vertebrates respect to agnathans, like the anteroposterior asymmetry of the canals and vestibular chambers, the widely curved arcs described by the canals, the subdivision of the vestibular region into communicated chambers or the presence of the non-otholitic macula neglecta, among others (reviewed in Maisey, 2001). The otolithic end organs (utricle, saccule and lagena) contain calcareous otoliths or otoconia. Otoconia do not present any particular form, but the otoliths present very specific irregular shapes that are diagnostic of particular species (Popper, 2011) and their names are derived from the shape that present in carps: sagitta (arrow), lapillus (small stone) and asterisks (star)

and are located in the sacculus, utricle and lagena, respectively (Carlström, 1963). In agnathans, sharks, rays, primitive bony fishes and terrestrial vertebrates the otoconia are embedded in a gelatinous matrix, while in modern bony fishes the crystals are fused into a solid otolith (Lovell et al., 2005; Popper, 2011). In contrast to that observed in agnathans, the composition of the otoliths in gnathostomes consists almost only in calcium carbonate in different forms.

Cartilaginous fishes (sharks, skates, rays and chimaeras) belong to the most ancient radiation of gnathostomes, but despite of their key phylogenetic position in the basis of the gnathostome radiation, studies concerning their inner ear are scarce. Although there are some studies about different aspects of the developed inner ear in elasmobranchs (Tester et al., 1972; Corwin, 1977; Maisey, 2001, 2004; Lovell et al., 2007; Evangelista et al., 2010), there is little information concerning its embryological development and usually studied along the with the rest of the cranium (de Beer, 1931; Holmgren, 1940; Jollie, 1971). Chondrichthyans have only inner ear labyrinths, without any kind of accessory hearing organ like an associated swimbladder, webberian ossicles or connections between both ears found in some bony fishes. The general characteristics of the gnathostome inner ear are displayed, but they are also

present some other peculiarities, like the isolation and almost complete circularization of the posterior vertical canal, which also presents a single communication with the vestibular region; the enlargement of the crista neglecta (reviewed in Maisey, 2001), even being duplicated in some sharks like *Carcharhinus sp.* (Tester et al., 1972; Corwin, 1977); or the horizontal semicircular canal entering the descending posterior limb of the anterior duct, contrarily to that observed in teleosts, where the horizontal duct enters the posterior limb of the utricle (Gray, 1952; Baird, 1974). There are also some exceptions, like *Chimaera monstrosa*, which presents a *common crus* similar to teleosts (Gray, 1952). Chondrichthyans are the only actual vertebrates where the endolymphatic duct is open externally, which may be a derived feature (Maisey, 2001), but while the duct to the exterior takes a simple straight course in chimaeras, in elasmobranchs (sharks, skates and rays) is frequently recurved and dilated, forming a subcutaneous otic sac below the surface opening (Baird, 1974). The open endolymphatic duct of chondrichthyans makes possible the presence exogenous sea sand in the inner ear with the endogenous otoconia, which are, unlike the single crystalline otoliths of bony fishes, a mass of elongate elliptical calcium carbonate crystals in sharks and almost perfect large spheres in chimaeras (Carlström, 1963; Maisey, 2001; Lovell et al., 2007).

The teleosts fishes have a labyrinth with a conserved dorsal region pattern with three semicircular canals with their ampullae containing the sensory cristae and connected to the utricle, which presents an anteroventral depression, perhaps reflecting the existence of an ancestral utricular recess (Baird, 1974); and three ventral otolithic organs (utricle, saccule and lagena) containing the sensory epithelium or macula, which are covered by an otolithic membrane and a solid otolith (Baird, 1974; Platt, 1983). The saccule and the utricle are close and communicated by a short utriculo-saccular foramen in most teleosts, but this communication is a long duct in ostariophysians and some deep sea species; or even is absent in holosteans and mormyrids (reviewed in Baird, 1974). Some teleost species, like ostariophysians, present an intersaccular canal that communicates both saccules and contacts posteriorly with the unpaired sinus, which receives vibratory signals from the gas bladder trough the Weberian ossicles (Baird, 1974; Platt, 1983; Bever and Fekete, 2002; Schulz-Marbach et al., 2013). Although fishes have no middle ear complex, the Weberian ossicles may be considered a functionally analogous to the middle ear (Bernstein, 2003). Apart of the otolithic maculae, the macula neglecta, consisting in a pair of non-otolithic patches, is located

next to the duct that connects the ampullae of the posterior semicircular canal to the utricle (Platt, 1983).

The formation of the otic vesicle in teleosts differs from that observed in other vertebrates. Instead of the invagination process observed in chondrichthyans, amphibians and non-reptile amniotes, the formation of the otic vesicle in teleosts like zebrafish happens by cavitation, when cells from the ectoderm form a solid sphere beneath the surface and later a small inner space appears, representing the first sign of the ear lumen (Waterman and Bell, 1984; Haddon and Lewis, 1996). The otocyst enlarges and develops various finger-shaped protrusions that grow inside the lumen (Becerra and Anadón, 1993; Haddon and Lewis, 1996). Protrusions from opposite walls of the vesicle meet each other and fuse, and the surrounding toroidal spaces become the three semicircular canals, disposed perpendicular to each other (Waterman and Bell, 1984; Haddon and Lewis, 1996). Diverse studies have stablished that bony fishes the most frequent order of formation of the semicircular canals is first the anterior canal and the horizontal canal the last (zebrafish; Waterman and Bell, 1984; Haddon and Lewis, 1996; trout: Becerra and Anadón, 1993; *Cyprinus carpio* and *Cottus pollux*: Iwasaki, 1937), with exceptions, like the primitive fish *Polypterus senegalus*, where the first canal that appears is the

anterior and the last is the posterior (Thomot and Bauchot, 1987); or flat fishes like *Scophthalamus maximus*, where the horizontal canal appears the first (Becerra et al., 1990), but this may be due to the torsion of the head they suffer. After the formation of the canals, the main chamber of the otocyst develops diverticula and constrictions that will create the utricle, saccule and lagena (Haddon and Lewis, 1996; Bever and Fekete, 2002). The saccule is the main acoustic organ in fishes, although in several species the utricle also participates in hearing (Bever and Fekete, 2002; Popper, 2011). The lagena arises as a posterior pouch of the saccule, firstly widely communicated with it, but later the utriculosaccular foramen becomes narrower (Bever and Fekete, 2002). The utricular macula originates the horizontal and anterior crests while the saccular macula originates the posterior crest before the separation of the semicircular canals, and finally the lagenar macula and the macula neglecta, which is composed by two sensorial patches (Becerra and Anadón, 1993; Bever and Fekete, 2002). The endolymphatic duct is one of the first and evident structures originated in the developing inner ear of amphibians, birds and mammals, but in teleosts like zebrafish is a rudimentary structure and emerges relatively late, after the canals are formed (Haddon and Lewis, 1996; Bever and Fekete, 2002). The endolymphatic duct begins as a small evagination in the medial wall of the otocyst and becomes a thin blind tube that

goes dorsally along the medial wall of the crus commune with no clear function (Bever and Fekete, 2002). Among actinopterygians, the inner ear of the crossopterygian fish *Latimeria chalumnae,* member of the sarcopterygian line that leads to tetrapods, presents a sensory epithelium next to the foramen sacculo-lagenar that resembles the tetrapod basilar papilla (Fritzsch, 1987). Although studies indicate that the basilar papilla is a unique feature of tetrapods, *L. chalumnae* presents a membranous structure covering the sacculo-lagenar foramen that resembles the basilar papilla of tetrapods, so it would be homologous to the basilar papilla and to the mammalian cochlea (Fritzsch, 1987; Bernstein, 2003; Fritzsch et al., 2006). This membrane also suggests that the communication between both ears is a perilymphatic space, rather than an endolymphatic duct as in teleosts, and this perilymphatic duct would facilitate the sound pressure to reach the sensory epithelia (Fritzsch, 1987; Fritzsch et al., 2006), although *Latimeria* absolutely lacks of Weberian apparatus connecting the swim bladder to the *canalis communicans* (Bernstein, 2003). Among actinopterygians, the groups *Chondrostei* and *Holostei* have statoconia and statoliths, while the group *Teleostei* presents three large crystalline statoliths composed mainly by calcium carbonate in form of aragonite, lacking statoconia; except the sun-fish *Mola mola* which presents statoconias instead of

statoliths (Carlström, 1963). On the other hand, the crossopterygian fish *Latimeria* has only a big saggita composed by aragonite and calcite (Carlström, 1963).

The inner ear of most of living amphibians (*Caudata* (salamanders and newts), *Anura* (frogs and toads) and *Gymnophiona* (caecilians), which diverged from other tetrapods 300 million years ago, presents modifications for an efficient sound perception underwater, underground and in the air, and differ from their purely aquatic ancestors in the presence of inner organs specifically receptive to sound pressure and in the anatomical changes that direct the sound pressure changes to those inner organs (Smotherman and Narins, 2004). The basic anatomy of the anuran ear comprises the external tympanic membranes, located at both sides of the head, which drive the sound via the columella to the oval window located on the lateral side of the otic capsules (Wever, 1983; Smotherman and Narins, 2004). There are four openings in the wall separating the otic and brain cavities, by which branches of the VIII nerve pass (Wever, 1983) but also may be a pression relief route or connect and acoustically couple both ears via the cerebrospinal fluid or by a direct contact present in some species, which improves the sound localization (Wever, 1978a; Mason et al., 2015). From this basic structure common to all amphibians, there are some

derived features, like the the absence of tympanum, columnelles and the middle ear cavity in all caecilians, many salamanders and some frogs; or the reduced or even entirely lost macula neglecta and basilar papilla in many *Gymnophiona* and *Caudata* (Smotherman and Narins, 2004). Inside the inner ear of amphibians there are elongated statoconias and statoliths composed by calcium carbonate in aragonite form and calcium phosphate in apatite form (Carlström, 1963). The most part of the adult amphibians present numerous elongated statoconias of pure aragonite within their inner ears, but there are some particularities, like the unusual statolith of *Amblystoma tigrinum*, consisting of densely packaged otoconia of aragonite surrounded by a thin shell of calcium phosphate in apatite form; or *Ichthyophis glutinosus*, which presents a single round otolith at larval stages, but numerous statoconia in the adulthood (Carlström, 1963).

As in all vertebrates, the inner ear of amphibian is divided in two main halves: the dorsal region, with the three semicircular canals and the utricle and responsible for the equilibrium sensitivity; and the ventral part, with the saccule, lagena, basilar papillae recess and amphibian papillae recess, and responsible for the acoustic sensitivity (Bever et al., 2003). Between both regions, the endolymphatic duct arises from the

medial wall, ending in an endolymphatic sac (Bever et al., 2003). The development of the inner ear of *Xenopus* begins at embryonic stage 23 as a placode that invaginates and forms a closed vesicle by stage 28, according to Nieuwkoop and Faber staging (1994). The expansion of dorsal pouches and the growth and central fusion of protrusions from the otocyst wall originate the semicircular canals (Haddon and Lewis, 1991; Bever et al., 2003), of which the anterior and posterior ones are fused in a *cruss commune* by stage 46 (Bever et al., 2003). The ventral region begins to differentiate by stage 47, with the formation of the three diverticula of the saccule (a medial evagination for the recess of the amphibian papilla, a postero-medial evagination for the recess of the basilar papilla and a larger medial evagination for the lagena) and by stage 52, the gross morphogenesis is complete (Bever et al., 2003). The sensory organs (cristae or maculae) are located at the ampullae, utricle, saccule, lagena, amphibian papilla recess and basilar papilla recess, but only the saccule and lagena have associated otoconial masses, which are suggested to be produced at the endolymphatic sac, which also presents an otoconial mass inside (Imoto, 1983, reviewed in Bever et al., 2003). Concerning to the amphibian papilla, it has been suggested to be homologous to the macula neglecta present in fishes, reptiles and birds, due to its position near to the utriculo-sacular duct in primitive amphibians, until Burlett in

1928 determined it was not homologous to it and it was not a macula at all (Wever, 1983). A macula neglecta has been found in amphibians only in Gymnophiona, and is very similar to the amphibian papilla of caecilians and salamanders, which has been interpreted by some author as a possibility that the amphibian papilla may be derived directly from the primitive macula neglecta (reviewed in Smotherman and Narins, 2004). In relation to the basilar papilla, its apparent connection to the lagena led some authors to postulate its homology to the basilar papilla of reptiles and birds (reviewed in Smotherman and Narins, 2004).

The development of the inner ear of reptiles takes place by a cavitation process instead of the usual invagination process that occurs in other amniotes and also in amphibians (Haddon and Lewis, 1996) and chondrichthyans. The inner ear of reptiles**, l**ike in other gnathostomes presents a dorsal region composed by the three semicircular canals with their corresponding ampullae and cristae and a ventral region containing the chambers with the sensorial epithelia or macule. The most significant phylogenetic modification is the definition of a cochlear duct in the rear part of the saccule and communicated to it by the saccule-cochlear duct (Baird, 1974). The proximal part of this cochlear duct contains the basilar papilla, capped by a tectorial membrane;

while the distal part contains the lagenar macula, like birds and monotremes (Baird, 1974). Despite sharing a common cavitation process to form the otic vesicle, the reptiles present an extraordinarily diverse auditory anatomy (Dooling et al., 2000), so three main groups of reptiles have been considered according to their inner ear type: *Archosauria* (including crocodiles, alligators and their relatives and also the birds), *Chelonia* (turtles) and *Lepidosauria* (including lizards (*Lacertilia*), snakes (*Serpentes*) and an ancestral group of fossorial animals (*Amphisbaenians*), which are placed in the monophyletic group *Squamata*; and the tuatara *Sphenodon*, placed in the group *Rhynchocephalia*) (Dooling et al., 2000; Manley, 2000). Anatomical comparisons suggest that the hearing organs in turtles and the tuatara represent the primitive stage of development, despite their early separation in the radiation of reptiles (reviewed in Dooling et al., 2000). Within the group *Lacertilia*, the most diverse group of reptiles with respect to the cochlear anatomy (Dooling et al., 2000), the chameleons present some special variations in the inner ear from the usual lizard pattern, because they do not present the external ear opening nor visible tympanic membrane, and the round window of the cochlea is usually absent (Wever, 1978 b). Snakes, Amphisbaenians and the tuatara have no external ear openings too (Dooling et al., 2000). Concerning to lizards, its hearing

organ presents the greatest variability among amniotes, possibly because it did not suffer the selective pressures of a fossorial enviroment (Baird, 1974); and has also been used with phylogenical classification purposes (Wever, 1978C). Lizards, as other amniotes, present the ventral region of the inner ear with the saccule and the cochlear duct, containing respectively the saccular macula and the lagenar macula; and the basilar papilla, which is located in the basilar membrane, next to the sacculo-cochlear duct (Manley, 2000). Despite its great variability, reptiles share the common characteristic of inner ears containing elongated crystals of aragonite with small amounts of calcite, with some exceptions like the pure aragonite otoconia of *Varanus* (Carlström, 1963).

There is a considerable similarity between the inner ears of birds and reptiles, specially the *Crocodilia* (Baird, 1974; Manley, 2000; Dooling et al., 2000) because although both groups separated 200 million years ago during the early Triassic period (Dooling et al., 2000), they belong to the *Archosauria* group (Manley, 2000). Birds present a remarkable consistency in their auditory structures and hearing abilities, with the larger birds hearing better at low frequencies and poorer at high frequencies than smaller birds (Dooling et al., 2000). Among birds, although there are descriptions of various species

(Romanoff, 1960); the chicken has been very used and recognized as a model specie for studying morphogenetic events due to to its easily accessibility for manipulation from very early stages of development (Bissonnette and Fekete, 1996). The development of the chick embryo comprises 21 days, divided in 46 stages (E1 to E46) according to Hamburger and Hamilton staging (1951). The development of its inner ear begins as a flat placode which center sinks and forms a hollow epithelial sphere, as occurs in amphibians and non-reptile amniotes (Haddon and Lewis, 1996). The early otocyst changes and presents a dorsal bulge that will form the utricle and semicircular canals; a ventral bulge that will originate the saccule and cochlear duct and a medial hollow tube that will originate the endolymphatic duct, which tip expands and forms the endolymphatic sac (Bissonnette and Fekete, 1996). By E5, the dorsal region presents two pouches: the lateral pouch, that will give rise to the horizontal semicircular canal; and a dorsal pouch, that will originate the anterior and posterior semicircular canals. The opposite epithelial walls of these pouches begin to approximate each other due to the growth of low-hillock shaped hyaluronan-enriched protrusions that meet and create the canals, being the horizontal canal formed the last (Haddon and Lewis, 1991; Bissonnette and Fekete, 1996). The cochlear duct, which extends ventrally and medially under the hindbrain; contains the

basilar papilla, occupying the mosts length of the duct and specialized in hearing; and the lagena, located at its distal tip and absent in mammals (Bissonnette and Fekete, 1996). Although birds have small statoconias within their inner ears like reptiles, these are composed by calcite instead of aragonite (Carlström, 1963).

The mammalian inner ear is a very complex organ. It arises from the otic placodes, which, as in other non-reptilian amniotes and amphibians, originates the otocyst by invagination and later morphological events originate the developed inner ear (Haddon and Lewis, 1996; Torres and Giráldez, 1998). The inner ear of a 10 dpc mouse embryo is an otocyst with two medial and ventral bulges corresponding to the endolymphatic duct and cochlear duct buds, which continue expanding at 12 dpc (Morsli et al., 1998). By this stage, significant changes take place. Cartilaginous protrusions through the vertical canal pouch begin to delimitate the vertical canals, while the horizontal canal pouch emerges in the lateral wall of the otocyst, the utricle protrudes in the anterodorsal region of the vesicle and the cochlea elongates and starts to take curved shape (Morsli et al., 1998). By 13 dpc, the three semicircular canals are formed, the cochlea coiled half a turn and the endolymphatic duct becomes thinner, but with its dorsal tip enlarged into the endolymphatic

sac. By 15 dpc, the utriculo-saccular and cochlea-saccular connections are evident and the cochlea completed one and a half turns, giving the inner ear an almost mature appearance; which is really reached by 17 dpc, with the membranous labyrinth completely mature and the cochlea coiled till one and three-quarters turns (Morsli et al., 1998). The mineralized components within the inner ear of different mammals are small single crystals (Carlström, 1963).

Due to the importance of this sense organ and the apparently common developmental pattern among vertebrate taxa, is especially important to know the basic and common morphogenesis to better understand the alterations in this organ. The major part of the information concerning the morphogenesis of the inner ear proceeds from studies in mouse, chicken and zebrafish. Despite the common pattern, there are some differences among vertebrates that make crucial the study of chondrichthyans to decipher the evolution of the inner ear development. Moreover, the zebrafish, a teleost commonly used as a developmental model for all the fishes, develops its inner ear through cavitation of the otic placode, while in mouse and chicken, other conventional model organism, it develops by invagination, similar to what happens in the chondrichthyans, as demonstrated in the present study in the shark *Scyliorhinus*

canicula. The important differences between teleosts and other vertebrates regarding to the morphogenesis of the inner ear, plus the phylogenetic position of *S. canicula* in the base of the gnathostome radiation, close to the ancestral condition, make this species an ideal model for deciphering the basic conditions of the development of the inner ear. The scarce information about the development of the inner ear of cartilaginous fishes, the appropriated characteristics of *S. canicula* as a model organism and the availability of a micro-computed tomography scan, allowed us to establish the objective of applying appropriated contrast-enhancing and scanning protocols to obtain high-resolution images at different embryological stages to elaborate a realistic and detailed description of the morphogenesis of the inner ear of *S. canicula.*

MATERIAL AND METHODS

Embryos and juveniles preservation:

A total of 10 embryos from stages 18 to 33 (prehatching at stage 34, not processed) and 2 juveniles (10 and 11cm in total length) of the catshark *Scyliorhinus canicula* were used in this study (some of them were also tested in chapter 1). Embryos from different broods, supplied by the Marine Biological Model Supply Service of the CNRS UPMC Roscoff Biological Station (France), were raised in seawater tanks in standard conditions (temperature: 15–16ºC; pH: 7.5–8.5; salinity: 35 g/L). The embryos were deeply anesthetized with 0,5% tricaine methane sulphonate (MS-222, Sigma) and staged based on their external characteristics according to Ballard et al. (1993) and the following stages were analyzed: **stage 18** (first and second pairs of pharyngeal pouches visible and appearance of a shallow buccal groove), **stage 20** (four pairs of unopened pharyngeal pouches visible by translucence), **stage 22** (two pairs of pharyngeal clefts open), **stage 24** (diamond- shaped mouth), **stages 25** (five pairs of open pharyngeal clefts), **stage 27** (diamond-shaped mouth and primordial gill filaments), **stage 29** (mandibular arches crowded into the mouth opening and initial

eye pigmentation), **stage 31** (detectable rostrum and long branchial filaments), **stage 32** (regression of branchial filaments), **stage 33** (decreased volume of the yolk sac; prehatching) and **juvenile** (post-hatching). Early embryos were fixed by immersion in 0.1 M phosphate buffer (PB; pH 7.4) containing 1.75% urea (elasmobranch PB), while late embryos (st32 and later) and juveniles were perfused with 4% paraformaldehyde after being rinsed with Ringer´s solution. The fixative was removed with PB and embryos were dehydrated in increasing concentrations of methanol and preserved in absolute methanol. All procedures conformed to the guidelines established by the European Communities Council Directive of 22 September 2010 (2010/63/UE) and by the Spanish Royal Decree 53/2013 for animal experimentation, and were approved by the Ethics Committee of the University of Santiago de Compostela.

Contrast media and micro-CT:

Despite the staining protocol with PTA described in chapter 1 appeared as the most efficient for scanning samples at any developmental stage, here we applied different contrast enhancing media. Two undesiccated early embryos (st18 and st22) stained for three days in methanolic iodine (I2M) were

also used in this study due to the acceptable results obtained with this contrast-enhancer in early embryos in the previous chapter. In the same way, an unstained and HMDS-desiccated isolated inner ear dissected from a juvenile was used. Phosphotungstic acid (PTA) was tested in previous experiments and revealed to be the most efficient staining agent for staining samples at any stage of develpment and caused the least distortions. Eight embryos (stages 20, 24, 25, 27, 29, 31, 32 and 33) and the head of a juvenile were stained with 1% PTA in methanol for up to 4 days before scanning.

As indicated in chapter 1, all stained samples were transferred to absolute methanol after staining and scanned within methanol. The scans were performed with a Bruker Skyscan 1172 microtomograph located at the Marine Biology Station of the University of Santiago de Compostela in A Graña and the samples were stored in 100% methanol after scanning. Images were reconstructed with NRecon software and processed with CTAnalyzer software. For displaying data, CTVox and DataViewer softwares were used. Serial images of the three axis and 3D reconstructed images and videos of each sample were obtained. For more detail, see Chapter 1.

RESULTS

The development of the inner ear of *S. canicula* can be subdivided in different stages for facilitating its understanding. The first signals of the otic development appear at **stage 17** according to Ballard et al., (1993), when two regions of the ectoderm next to the hindbrain become thicker and originate the otic placodes, which has been confirmed by O'Neill et al. (2007) on the basis of the expression of *Pax2*, a gene marker of early otic placode. From this stage, the placodes develop a central sinking which leads to the formation of an otic pit at **stages 20 to 22**, appearing almost closed by **stage 24**. At stage 25, the otic cup is totally closed, forming the otic vesicle or otocyst, which maintains a communication with the exterior only by a narrow duct, the persistent endolymphatic duct. From this stage, the walls of the otocyst emit various projections that grow through the lumen, originating subdivisions in the otic vesicle. Those projections are responsible for the formation of the otic chambers utricle, saccule and lagena and also the semicircular canals. By **stage 31**, the inner ear has almost completed its morphogenesis and by **stage 32** is very similar to the juvenile and adult shape. An interesting characteristic of the inner ear is the presence of solid mineral masses, the otoliths, within the vestibular chambers. These mineralized structures are located

over the sensorial patches of the utricle and saccule and its function is to transmit positional information by the stimulation of the maculae by its own weight. In this study we found remarkable otoliths from stage 33 and over, but some considerations are needed because they were not present in all the scanned samples over stage 33.

First period: from otic placodes to otocysts. Stages 18 to 25.

At **stage 18** (the earliest analyzed sample in this study) the otic placodes appear as a thickness of the ectoderm adjacent to each side of the hindbrain (Fig. 1; OP). Micro-CT scans reveal at this stage the early signs of invagination of the otic placode, marked by the existence of a central sinking irrespectively of the section plane (Fig. 1B, C; arrowheads).

The invagination of the otic cup follows and by **stage 20** it presents a very wide opening oriented dorsolaterally respectively to the body axis (Fig. 2A-C). The otic cup is located dorsally to the second pharyngeal cleft and laterally to the hindbrain, which appears collapsed (asterisks) in the image due to the manipulation of the embryo previous to its scanning. This opening presents now a larger anteroposterior axis than the

mediolateral/dorsoventral axis. The primordial presence of the statoacoustic or VIII ganglion (SAG) is morphologically appreciated at this stage, even externally, as a dense mass located ventrally and slightly rostral to the otic cup (Fig. 2B-C; SAG). Transverse three dimensional reconstructions of micro-CT scans show the close position between the cup, the primordial statoacoustic ganglion and the hindbrain (Fig. 2C-E).

At **stage 22,** the otic cup is still appreciated externally (Fig. 3A-C), but its morphology is slightly modified, being the cup deeper (Fig. 3B) and its opening a bit narrower than in previous stages, but maintaining a larger anteroposterior axis than the mediolateral one (Fig. 3B-C). The otic cup presents a wide cavity in the bottom (Fig. 3F; arrow), but a narrow inner space just below the external opening (Fig. 3F; arrowhead). The otic cup remains very close to the second pharyngeal cleft and the hindbrain (the ectoderm over the hindbrain appears artifactually collapsed; Figs. 3C, F, asterisks).

At **stage 24** the otic cup is almost closed forming the otic vesicle or otocyst, which is only slightly appreciated from the outside like a bulge (Fig. 4A; asterisk) located dorsally to the branchial arches (Fig. 4A; arrows) and to the SAG (Fig. 4B). The external opening of the vesicle is appreciated as a small

pore (Fig. 4C; arrowhead) in almost nonexistent space between the vesicle and the dorsal surface of the head. The previously wide invagination process of the otic cup is reduced to a narrower hole, the endolymphatric pore (Fig. 4D, arrowhead), that in later stages will elongate to form the endolymphatic duct. The otic vesicle remains very close to the hindbrain (Figs. 4E, F).

In an external view of the head at **stage 25,** the otic vesicle is not evident (Fig. 5A) but inner sections through the otic region at sagittal, transverse and horizontal planes (Figs. 5B, C and D, respectively) evidence its ovoid shape that contrast with the round shape of the VIII ganglion (SAG) located ventrally and slightly rostral to the vesicle (Fig. 5C, F, I, J). 3D reconstructions show the localization of both otic vesicles beside and close to the hindbrain (Figs. 5C and 5D, respectively). The most rostral structure of the auditory system is the SAG located dorsal to the facial nerve (Fig. 5E). The rear part of the SAG is located just below the rostral pole of the otic vesicle (Fig. 5F), which in its medial side maintains the connection to the exterior of the embryo through the unclosed endolymphatic duct (Fig. 5G), that goes dorsally and caudally (Fig. 5H) until it reaches the surface of the ectoderm. At this stage, the otic vesicle is located near and dorsal to the branchial clefts (Fig. 5I) and in

close contact with the SAG (Fig. 5J). In the medial wall of the otic vesicle, the endolymphatic duct extends dorsally and caudally (Fig. 5K) until it opens to the dorsal surface of the head, next to the midline (Fig. 5L).

Second period: the otocyst and the origin of the semicircualr canals. Stages 26 to 31.

The vesicle at **stage 27** presents buds of protrusions of the cartilage beginning to subdivide the vesicle (Figs. 6A-C). The posterior semicircular canal is formed the first due to the growth of cartilaginous protrusions from the ventrolateral and medial walls of the vesicle (Figs. 6B, C, asterisks), which leads to the canal connecting to the postero-medial wall of the vesicle (Figs. 6A, B; arrowheads). At this stage, the horizontal semicircular canal starts to be appreciated (Fig. 6A, asterisk). The endolymphatic duct is connecting the exterior with medial wall of the vesicle (Figs. 6A, B; arrows).

At **stage 29,** the progression of the protrusions continues and the subdivisions of the inner ear are more evident. The differentiation of the horizontal canal is more evident (Fig. 6D; asterisk). The endolymphatic duct maintains its opening to the medial wall (Figs. 6D, E; arrow) and the connection of the

vesicle to the posterior semicircular canal appears as a medial wide opening (Figs. 6D, E; arrowhead). The subdivision of the three chambers is slightly visible in a sagittal view, with the presumable utricle in the most dorsal and anterior region, the future saccule ventral to the utricle and the presumptive lagena occupying the rear and ventral part of the vesicle (Fig. 6E). A horizontal vision evidences the growth of the protrusion separating the posterior semicircular canal from the chambers (Fig. 6F; asterisk).

By **stage 31** the inner ear is clearly subdivided and presents an almost mature aspect (Fig. 6G-I). The saccule and utricle are separated but connected by a narrow duct (Fig. 6G; arrow) and the semicircular canals are well differentiated and present a diameter thinner than in previous stages due to the growth of the cartilage of the protrusions (Fig. 6G-I). The utricle presents a frontal subdivision, the utricular recess (UR), located below the anterior part of the anterior semicircular canal (Fig. 6H). The horizontal semicircular canal presents a sensorial crista near its anterior end (Fig. 6I; arrowhead), which reaches the anterior semicircular canal, not the utricle itself (Fig. 6I; asterisk).

Third period: subdivided inner ear. From stage 32 onwards.

At **stage 32** the inner ear is not visible externally (Fig. 7A), but an internal sagittal view of the head reveals its complex structure. The rostral region of the auditory capsule is located between the eye and the hindbrain, contains the frontal region of the anterior semicircular canal, where the sensory crista is present at its lateral wall (Fig. 7B, arrowhead). The root of the statoacoustic nerve is located at this level, going ventrally and next to the facial nerve root, where it leaves the braincase (Fig. 7B, VIIIr, VIIr, respectively). The horizontal canal is the most lateral structure and contacts with the anterior canal next to its rostral end, over the utricle recess and in front of the utricle (Fig. 7C, D). Near to this point, the horizontal canal has its crista (Fig. 7B, arrowhead). The saccule, located ventral to the utricle (Fig. 7C-E), has the largest cavity and communicates with the endolymphatic duct by its medial wall (Fig. 7D; arrowhead), with the utricle by a narrow dorsal canal (Fig. 7D; arrowhead) and with the posterior semicircular canal by the *ductus canalis semicircularis* (DCS) (Fig. 7E), where is located the macula neglecta (Fig. 7F; arrow). It has a sensory macula in its ventro-medial region (Fig. 7E; arrowhead). The lagena is the smallest cavity of the inner ear, located at the caudal end of the saccule

and surrounded by loose mesenchymal tissue except at its latero-ventral wall, that contacts with the cartilaginous capsule (Fig. 7F). The glossopharyngeal nerve (IX) crosses the auditory capsule by the loose mesenchymal tissue, following a latero-caudal course behind the lagena and over the lamina hypotica (Fig. 7F). The caudal region of the otic capsule contains the rear parts of the horizontal and posterior canals (Fig. 7G), with the posterior crista in the ventral part of the posterior canal (Fig. 7G; arrowhead). Transverse view of the head at stage 32 also shows the complex structure of the inner ear (Fig. 7H). The most lateral structure is the horizontal canal (Fig. 7I), containing a crista in its rostral part (Fig. 7I; arrowhead), that goes medially to converge over the utricular recess with the frontal end of the anterior canal (Fig. 7J), ventrally to its crista (Fig. 7J; arrowhead). The frontal end of the horizontal canal does not reach the utricle, but the anterior canal does (Fig. 7K). The fibers innervating the sensory patches of the inner ear meet in a point between the utricular recess and the saccule (Fig. 8K; VIII), from where they can be followed coursing ventrally to the SAG between the saccule and the hindbrain, behind the facial nerve (Fig. 7L; VII). At this stage, the posterior semicircular canal almost forms a complete ring (Fig. 7K-M), surrounding the rear part of the horizontal canal (Fig. 7K) and communicating with the ventral part of the utricle trough the

ductus canalis semicircularis (Fig. 7L). The most medial structure of the inner ear is the sinuous superficial region of the endolymphatic duct (Fig. 7N; ED), which opens to the dorsal surface of the head over the parietal fossa (Fig. 7N; arrowhead) and near to the midline (Fig. 7O; arrowheads).

By **stage 33,** the structure of the inner ear is very similar to the previous stage, but there are some new aspects. The most evident is the presence of the big and dense otoliths within the chambers, but also the clearest view of the limits between the components of the skull and otic capsule. The anterior crista inside the anterior canal represents the most rostral part of the inner ear (Fig. 8B; arrowhead). Slightly caudally, the most rostral part of the saccule is occupied by an otolith (Fig. 8C; asterisk) that also occupies its medial part, very close to the SAG (Fig. 8D; asterisk), but not the most caudal region (Fig. 8E; black asterisk). At this level, the *ductus canalis semicircularis* communicates the chambers to the frontal region of the posterior semicircular canal located medially to them (Fig. 8E). This canal is separated from the saccule by the dorsal process of the parachordal cartilage, but from the utricle only by a membranous layer of tissue (Fig. 8E; DP and arrowheads, respectively). The most caudal part of the vestibular chambers is occupied by the rear part of the utricle, just under the dorsal part

of the posterior semicircular canal, which is at the same time next to the parietal fossa (Fig. 8F, PF)). Caudally to the utricle, both branches of the horizontal semicircular canal meet between the dorsal and ventral branches of the posterior semicircular canal (Fig. 8G), which presents its crista in the lower one, being disposed from the lateral wall of the frontal region of the ampulla (Fig. 8G; arrowhead) to the ventral wall of the rear part of the ampulla (Fig. 8H; arrowhead). Lateral to the posterior ampulla, the glossopharyngeal nerve is visible going out of the otic capsule over the lamina hipotyca (Fig. 8G,H; IX and LHO, respectively). The most lateral region of the otic capsule contains the horizontal semicircular canal, under which rear branch the glossopharyngeal nerve is observed coming out of the otic capsule (Fig. 8J, IX). The utricular recess is located under the horizontal semicircular canal (Fig. 8K; UR) and contains an otolithic mass (Fig. 8L; black asterisk), similar to that observed in the saccule (Fig. 8L-N; black asterisks). The rear wall of the utricle connects to the horizontal semicircular canal (Fig. 8L,M; HSC), while its dorsal wall connects to the anterior semicircular canal and the medial wall connects to the *ductus canalis semicircularis* (Fig. 8N; ASC and DCS, respectively). The most medial region of the otic capsule is occupied by the frontal branch of the posterior semicircular canal and a wide space of mesenchymal tissue between the

cartilaginous and membranous labyrinth (Fig. 8O; PSC and asterisk, respectively).

Organization of the inner ear in juveniles

An external view of a three-dimensional reconstruction of the head of a **juvenile** *S. canicula* shows a significant change in the skin, with the presence of numerous scales all over its surface (Fig. 9A). The developed skin is a barrier for contrasts-enhancing substances, like some low-contrasted deep tissues evidence (Fig. 9B, C). Scans of a non-stained but HMDS-desiccated isolated juvenile inner ear show the benefit of removing the skin (Fig. 9D-L). The utricular otolith occupies the rostral region of the utricular recess (Fig. 9D, E; asterisks) while the saccular otolith occupies the rostral and medial region of the saccule over the lamina basiotica (Fig. 9F; LBO, black asterisk). At this stage there are several points of the inner ear where the membranous labyrinth (Fig. 9F, G; arrowheads) is quite separated from the cartilaginous labyrinth, leaving a considerable space between them (Fig. 9F, G; white asterisks). The disposition of the inner ear is very similar to the previous stage, with the posterior semicircular canal medially to the utricle and saccule and the caudal branch of the horizontal semicircular canal reaching the caudal region of the utricle (Fig.

9G; PSC and white star, respectively). The most caudal region of the otic capsule contains the rear parts of the horizontal and posterior semicircular canals, with the posterior crista located at the ventral and lateral wall of the ampulla (Fig. 9H; arrowhead). A sagittal view of the same sample shows the position of the lateral crista at the rostro-lateral part wall of the horizontal ampulla (Fig. 9I; arrowhead). At this stage, an otolithic mass is clearly seen within the utricular recess (Fig. 9J; asterisk), and two mineral masses (Fig. 9K; black asterisks), with the saccular mass are visible next to the rostral wall of the saccule. The lateral walls of the membranous saccule and lagena (Fig. 9J; S and L, respectively), with the ductus canalis semicircularis connecting to the dorsal edge of the saccule, are also evident (Fig. 9G, DCS). The most medial part of the otic capsule contains the rostral region of the posterior semicircular canal (Fig. 9L).

DISCUSSION

The results obtained in this work provide a global view of the development of the inner ear of *S. canicula* from early embryonic stages to juvenile stage, when the inner ear is a miniature of the adulthood. Despite the key phylogenetic position of sharks as basal members of the gnathostome radiation, the development of its inner ear has not been studied as deeply as in other groups. Although there are studies about its developed braincase and inner ears (Baird, 1974; Maisey, 2001, 2004; Lovell et al., 2007; Evangelista et al., 2010), there are not studies concerning its complete development as far as we know. In this study, we have analyzed the morphological development of the inner ear of *Scyliorhinus canicula* through micro-computed tomography (micro-CT), from the very early stages of its development to the juvenile stage. The use of new imaging techniques in developmental studies, like micro-CT, has been increasing in the last years due to the advances in obtaining high-resolution, reproducible and reliable 3D images of the internal and external morphology of samples (Metscher, 2009). In fact, micro-CT seems to be the most appropriated technique for comparative morphological studies (Metscher, 2009, 2011). After testing different contrast-enhancing media and propose a simple but useful scanning protocol for obtaining 2D and 3D

high-quality images along the embryological development and also post-hatching period (see chapter 1), we have applied it to obtain images with optimal quality to analyze and describe with detail the development of the inner ear of the catshark *Scyliorhinus canicula*. The results obtained have been compared to those observed in other species, thus contributing to increase knowledge about the morphogenesis of the inner ear in cartilaginous fish from an evolutionary perspective.

Similarly to other vertebrates (as gnathostomes as agnathans), the inner ear of *S. canicula* originates from initial otic placodes, a pair of thickened regions of the ectoderm that invaginate to form the otic pit, similar to that observed in lampreys and non-reptile tetrapods, but different from the cavitation process that takes place in teleosts and reptiles (Haddon and Lewis, 1996; Thornhill, 1972). Contrarily to the inner ear of agnathans, which present a simpler structure with one or two semicircular canals, lacking the horizontal semicircular canal (Lowenstein and Thornhill, 1970; Thornhill, 1972, McVean, 1991), the inner ear of *S. canicula* presents all the characteristics corresponding to gnathostomes, with the horizontal semicircular canal as one of the most relevant morphological characteristics of jawed vertebrates (Mazan et al., 2000). Some agnathans present common characteristics with

gnathostomes, but he existence of a pair of ducts in the medial wall of the labyrinth of the lamprey (Maklad et al., 2014) or the sea canals present in Osteostracans (Mazan et al., 2000) do not represent any kind of homology to the horizontal semicircular canal present in *S. canicula* and gnathostomes in general. Despite the great differences between their inner ears, in both groups, lampreys and sharks, is originated by invagination of the otic placode forming a cup or pit (Thornhill, 1972, present results), which closes to originate the otic vesicle or otocysts. Unlike the observed in lampreys and hagfishes, the otic vesicle of *S. canicula* never closes completely. While in hagfishes and lampreys it develops a blind endolymphatic duct which ends in an endolymphatic sac (Thornhill, 1972; Baird, 1974; Jorgensen et al., 1998), the inner ear of *S. canicula* communicates to the exterior through its endolymphatic duct, even in the adulthood. The inner ear of agnathans present only a *macula comunis*, a unique macula located ventro-medially and covered by otoconia (Lowenstein and Thornhill, 1970; Thornhill, 1972; Baird, 1974), which has been interpreted by some authors as corresponding to the utricular and saccular macula of teleosts (Hammond and Whitfield, 2006) but differs form the utricular, saccular and lagenar maculae present in the inner ear of *S. canicula* and other gnathostomes.

Whether they are formed by cavitation or by invagination, the inner ears of all the gnathostomes present the same basic structural pattern, with three dorsal semicircular canals for detecting head movement and a variable number of ventral chambers for detecting position and sound. However, there are variations in the order of formation of the semicircular canals and in the relative time that the inner ear takes in complete its morphogenesis in relation to the complete embryological period. The otocyst of *S. canicula* differs from agnathans and the rest of gnathostomes in that it never closes completely, although its external opening becomes progressively narrower during the development, from a wide opening at stage 20 to a pore at stage 24 and finally a long thin duct, the endolymphatic duct, from stage 25 onwards that persist the entire life of the shark. The persistence of the opened endolymphatic duct of developed sharks (Tester et al., 1972, present results) contrarily to the closed duct observed in lampreys, teleosts and tetrapods may be a derived feature unique of chondrichthyans, even if we accept that the closed endolymphatic duct of lampreys corresponds to a new evagination of the otic vesicle (Hagelin, 1974; reviewed in Maisey, 2001), instead of the invagination canal of the otocyst (Thornhill, 1972).

As in other chondrichthyans (Tester et al., 1972; Baird, 1974; Maisey, 2001), the endolymphatic duct of *S. canicula* goes dorsally through the parietal fossa and reaches the surface of the head. Contrarily to the duct of chimaeras, which describes a straight trajectory (Baird, 1974), that of *S. canicula* describes a curve trajectory at its dorsal end (a complete dextrogire loop in the left duct and levogire in the right duct) in the non-chondrified region of the chondrocranium known as the parietal fossa. The external openings of the endolymphatic ducts of *S. canicula* are located at the dorsal region of the head, next to the midline, slightly caudal to the eyes and are very small, hard to see at a glance. We found otolithic masses in the utricular recess, saccule and lagena of the inner ear, which agrees with that observed in other fishes. The role of the endolymphatic duct and sac in its formation and degradation has been studied in different species (Imoto et al., 1988), and even in sharks, where its formation has been observed in the proximal endolymphatic duct (Vilstrup, 1951). The presence of high-density material within the endolympatic duct of a juvenile inner ear of *S. canicula* supports these observations. It seems that the secretory processes and ionic exchanges that take place within the inner ear and that may be related to the formation of the endolymphatic fluid (Vilstrup, 1951; Garvin et al., 1988; Eckhardt et al., 2012) could also be related to the formation and

precipitation of the calcium carbonate that forms the otoliths (Imoto et al., 1988). The otoliths of *S. canicula* present irregular shapes and look like aggregated of small granules rather than cristalized individual pieces, contrarily to the crystalized solid otoliths found in teleost fishes or the majority presence of otoconia inside the inner ear of agnathans and tetrapods (Carlström, 1963; Popper, 2011). The open inner ear of sharks also allows the presence of exogenous granules in the inner ear, increasing the variability of the otolithic compounds and even could have some function as magnetic fields detectors (Carlstöm, 1963, Hanson et al., 1990), but the individuals used in this study were maintained in an aquarium without sand or any kind of granulated substrate, so its otoliths may have only endogenous origin. The composition of the otoliths cannot be analyzed through micro-CT, but the presence of calcium carbonate in its composition is easily revealed by its complete dissolution in hydrochloric acid with intense formation of gas bubbles. The relative size of the saccule and the relation of the semicircular canals with it, has used to elaborate a classification of the inner ear of elasmobranchs that relates its morphology and interspecific variations to a phylogeny and functional significance (Evangelista et al., 2010). According to this, the relative small saccule of *S. canicula* and the absence of ducts separating the semicircular canals from the vestibular region of

the inner ear place the catshark in the group 4 of this classification, which corresponds to benthic demersal elasmobranchs and non-raptorial foragers that feed mainly marine invertebrates (Evangelista et al., 2010).

The invagination process of the otic placode leads to the formation of an otic vesicle similar to that observed in lampreys and non-reptile amniotes (Thornhill, 1972, Haddon and Lewis, 1996). The wide opening of the otic cup of *S. canicula* suffers a progressive reduction until the otocyst is formed, when it has become a small aperture by Ballard´s stage 24, but it never completely closes. The opening persists and begins to elongate after stage 25 to form the endolymphatic duct. This event may be used as a morphological reference of the beginning of the second period of the development of the inner ear of *S. canicula*. The otocyst here formed presents an almost round shape with the statoacoustic ganglion located ventrally and medially to it and suffers several morphological changes until the developed inner ear is complete. As in other jawed vertebrates, the otocyst of *S. canicula* enlarges and also modifies its shape by evagination processes and the growth of protrusions into the lumen that lead to the formation of the semicircular canals and the ventral chambers with the otholitic and non-otholitic maculae. The buds of the three chambers are slightly appreciated

by stage 29 and are well recognizable and almost developed by stage 31, although the apparition time of the chambers is a very variable characteristic along the vertebrate groups (Bissonnette and Fekete, 1996, Haddon and Lewis, 1996; Morsli et al., 1998).

Among teleost fishes, some groups present different features, like the completely separated utricle and saccule in *Cottus pollux*, *Scophthalmus maximus*, holosteans and mormyrids (Baird, 1974; Becerra et al.,1990) or the partially separated lagena and saccule in *Cyprinus carpio* (Iwasaki, 1937) or *Danio rerio* (Bever and Fekete, 2002); but the chambers of *S. canicula* maintain the usual pattern of utricle and saccule separated by a constriction and the lagena as a caudal continuation of the saccule, only with a small protrusion separating them, but keeping a wide communication to it. The separation between the utricle and the saccule is quite evident at stage 31 and maintained in the adulthood, like in most teleosts (Haddon and Lewis, 1996). The saccule is the main acoustic organ in teleost fishes (Bever and Fekete, 2002; Popper, 2011), and some teleost groups like ostariophysians, have both saccules communicated by an unpaired sinus which also receives vibratory signals from the gas bladder by the Weberian ossicles (Baird, 1974; Platt, 1983; Bever and Fekete, 2002; Schulz-Mirbach et al., 2013), but any kind of similar structure or

communication between both inner ears has been appreciated in *S. canicula*. The inner ear of *S. canicula*, like all chondrichthyans (Baird, 1974; Maisey, 2001), presents an utricular recess, a rostral diverticula that contains a sensory macula and its corresponding otholitic mass, and no true utricle is incorporated directly in the base of the canals system (Baird, 1974; Brazeau and Friedman, 2014). Sucht diverticule is located ventrally to the horizontal ampulla, very close to it, and is a characteristic of modern chondrichthyans and dipnoans, while in actinopterygians, *Latimeria* (Crossoperygians) and tetrapods is absent (Fritzsch, 1987; Maisey, 2001). Despite this similarity between chondrichthyans and dipnoans, no more characteristics suggest a monophyletic group of chondrichthyans and dipnoans or the exclusion of dipnoans from osteichthyans (Maisey, 2001). Respect to the timing of formation of the inner ear, there is a striking difference between teleosts and *S. canicula*. In the catshark it is a large period, about 53 to 62 days of 175 of the entire embryological period, from the appearance of the otic placodes at st18 (18 to 22 days post fertilization (dpf) according to Ballard et al., 1993) to the complete gross morphology at the end of st31 (75 to 80 dpf) which corresponds to about one third of the whole embryogenesis. On the other hand, the zebrafish presents a very short embryological period, only three days (Waterman and Bell, 1984; Haddon and Lewis, 1996), but the

formation of the inner ear takes five days to complete the semicircular canals and up to 15 days to complete the development of all the ventral chambers (Bever and Fekete, 2002), which considerably overpasses the embryological period.

The inner ear of *S. canicula* is significantly different from the inner ear of tetrapods. The ventral part of the inner ear of amphibians presents some modifications respect to the inner ear of teleost and chondrichthyans fishes for a better sound perception, but also there are new external structures like tympanic membranes and columnelles that constitute a medial ear (Wever, 1983; Smotherman and Narins, 2004). That medial ear improves the perception of sound by directing it to the sensorial organs, that can be entering directly to the endolymphatic space or surrounding the saccule until the medial wall of the otic capsule, which presents four gaps in this region and allows acoustically coupling of both ears by transmitting vibrations through the cerebrospinal fluid (Smotherman and Narins, 2004). Neither *S. canicula* nor any other cartilaginous or bony fish present similar structures to the tympanic membranes or columnelles, but the non-cartilaginous membrane that separates the medial region of the inner ear of *S. canicula* from the brain could facilitate the transmission of vibrations in a similar way to that observed in amphibians. Respect to the

ventral part of the inner ear, instead of the three otholitic maculae (utricular, saccular and lagenar) and the non-otholitic macula neglecta present in *S. canicula,* amphibians have also a basilar papilla and an amphibian papilla located in posteromedial evaginations of the saccule (Bever et al., 2003), but only the saccule and lagena contain otoconia, Concerning to the macula neglecta found in *S. canicula*, the most of amphibians lack it and only is present in the group Gymnophiona (Smotherman and Narins, 2004). The similarities between the macula neglecta and the amphibian papilla of other amphibians suggested that the last one could derive from it, but it was determined that they were not homologous and even the amphibian papilla was not a macula at all (de Burlett, 1928, Wever, 1983). So, the macula neglecta of *S. canicula* and the amphibian papilla seem not to be homologous, but the amphibian basilar papilla seems to be homologous to the basilar papilla of reptiles (Smotherman and Narins, 2004).

The inner ear of *S. canicula* differs so much from the reptilian inner ear. The cavitation process by which the otic placode of reptiles becomes a vesicle is curiously shared only with bony fishes, but not with cartilaginous fishes like *S. canicula*, which inner ear is formed by invagination. Reptiles present the largest diversity among vertebrates regarding to its

inner ear morphology, being the ancestral condition the inner ear of turtles and tuataras (Dooling et al., 2000). Compared to the catfish, the inner ear of reptiles presents a much more complex ventral region, with the saccular and lagenar maculae but also the basilar papilla, which is placed in a cochlear duct (Manley, 2000). Despite its complexity, some groups of reptiles have lost their external openings or tympanic membranes, like snakes, amphisbaenians and tuataras (Wever, 1987 b; Manley, 2000). Like sharks, the most part of the otoconia are composed by aragonite (Carlström, 1963).

The inner ear of birds is very similar to the reptilian inner ear (Baird, 1974; Manley, 2000), but at difference to them, and like happens in *S. canicula*, the placode of birds becomes a vesicle by invagination, not cavitation as seen in teleosts and reptiles (Haddon and Lewis, 1996; Bissonnette and Fekete, 1996). The inner ear of the chicken needs form 29-30 hpf to the seventh day to complete its gross morphology (Hamburger and Hamilton, 1951; Bissonnette and Fekete, 1996), which represents almost one third of the whole embryologic period, similar percentage to that observed in *S. canicula*. Despite the inner ear of birds contains otoconia, these are composed by calcite instead of aragonite like occurs in reptile, amphibians and fishes (Carlström, 1963).

The mammalian inner ear is a very complex organ. It arises from the otic placode that invaginates to form a vesicle in a similar way to that observed in other animals (Morsli et al., 1998), like *S. canicula.* Respect to the timing of development of the inner ear, in the mouse it takes from the eighth dpf to the 15th dpf, which represents approximately 1/5 of the total days, percentage shorter than in *S. canicula.*

The formation of the semicircular canals in vertebrates occurs through the growth of protrusions from the wall of the otocyst until they match each other and the surrounding space becomes a semicircular canal. While it has been stablished that these protrusions have long finger shapes in teleosts, in birds and mammals take the form of low hillocks, although the developmental anatomy suggests that they share the same developmental principles (reviewed in Haddon and Lewis, 1996). Despite the same basic pattern of the semicircular canals among gnathostomes, the time and order of apparition of each canal is quite variable. In the same way, the apparition of the otoliths depends on the species. While in *S. canicula* the first evidences of otolithic masses are perceived in late developmental stages, when the labyrinth is almost developed, in teleosts like *Danio rerio* the otoliths begin to grow in the otocyst stage, before any canal or chamber formation (Haddon

and Lewis, 1996). Concerning the canals itself, the posterior semicircular canal is the first that appears in *S. canicula*, at stage 27, while the posterior and horizontal are still pouches where the protrusions did not meet yet. These ones appear later and approximately at the same time, about stage 30. Once they are formed, the growth of the inner ear makes them relative longer and thinner. Contrarily to the first appearance of the posterior semicircular canal in *S. canicula*, in most teleosts the first canal that appears is the anterior one, followed by the posterior canal and finally the horizontal one (zebrafish: Waterman and Bell, 1984; trout: Becerra and Anadón, 1993). There are some exceptions to this order of formation of the semicircular canals: in *Polypterus senegalus* the posterior semicircular canal appears the last (Thomot and Bauchot, 1987) and in *Scophthalamus maximus* the horizontal semicircular canal appears the first (Becerra et al., 1990). Curiously, the horizontal semicircular canal uses to be the first which appears in amphibians (Haddon and Lewis, 1991) or simultaneously to the anterior canal (Norris, 1892). In birds and mammals, the horizontal semicircular canal uses to appear the last (Streeter, 1906, Larsell et al., 1935; Bissonnette and Fekete, 1996; Morsli et al., 1998). In mouse, the posterior semicircular canal is the last which completes its formation (Martin and Swanson, 1993). In any case, the order of appearance of the semicircular canals of the inner ear of *S.*

canicula seems to be a characteristic not shared with other gnathostomes.

The labyrinth of *S. canicula*, like other sharks and elasmobranchs in general, presents some other particularities referred to its spatial disposition and interrelation of its different parts. The most evident is the almost complete circumference that the posterior semicircular canal describes, connecting to the medial and rear part of the saccule just by one duct (*ductus canalis semicircularis*). This disposition of the posterior semicircular canal also avoids the formation of a common cruss between the caudal branch of the anterior semicircular canal and the rostral branch of the posterior semicircular canal, which is a characteristic of all non-chondrichtyans gnathostomes, but also of non-elasmobranch chondrichthyans, the holocephalans, like *Chimaera monstrosa* (Baird, 1984, Maisey, 2001). The relation of the anterior and horizontal canals also presents other particularity, because the anterior and horizontal ampullae are in close contact and both lay over the utricular recess (Maisey, 2001), the real and functional utricle of chondrichthyans.

CONCLUSSIONS

The development of the inner ear of *S. canicula,* contrarily to that observed in bony fishes and reptiles, takes place by an invagination process of the otic placode similar to that observed in lampreys and non-reptilian tetrapods. This development begins at early stages, at least as soon as Ballard´s stage 18 and comprises approximately one third of the entire embryological period, until it reaches a mature-like aspect at the end of stage 31.

The developmental process of the inner ear of *S. canicula* can be divided in three main periods according to the morphological changes that happen. The first period comprises from the placodal stage to the formation of the otic vesicle at the end of Ballard´s stage 24. The second period comprises the transformation of the round vesicle at stage 25 into a mature-like inner ear at the end of Ballard´s stage 31. The third period begins at stage 32 and implies growth according to the body size and the maturation of the sensory organs.

The mature inner ear of *S. canicula* presents the characteristics of the gnathostome inner ear, with three perpendicular semicircular canals and the three ventral chambers: the utricle (with the utricular recess), the saccule located ventral to the utricle and connected to it by a narrow duct; and the lagena at the rear part of the saccule and connected to it by a wide space. In this study we show that this mature morphology is achieved in late embryos from stage 32 onwards.

The posterior semicircular canal is almost a complete circle, connected to the utricle by a single duct, and implies the absence of a *cruss commune* between the anterior branch of the posterior semicircular canal and the rear branch of the anterior semicircular canal, as happens in non-chondrichthyans vertebrates. In contrast to tetrapods and bony fishes, the anterior semicircular canal and the horizontal semicircular canal meet and fuse over the utricular recess.

The inner ear of *S. canicula* is communicated to the exterior by the endolymphatic duct, as a remnant of the invagination process that never closes completely, contrarily to the invagination process of other vertebrates, which invagination process closes completely and the inside of its inner ear is not communicated to the exterior. The endolymphatic duct arises from the medial wall of the saccule and goes dorsally, taking a sinuous trajectory at its dorsal region, before opening to the exterior on the top of the head, next to the midline.

LITERATURE CITED

- Baird IL (1974) “Some aspects of the comparative anatomy and evolution of the inner ear in submammalian vertebrates”. *Brain Behav. Evol.* 10: 11-36.
- Ballard WW, Mellinger J, Lechenault H (1993) “A series of normal stages for development of *Scyliorhinus canicula*, the lesser spotted dogfish (Chondrichthyes: Scyliorhinidae)”. J. *Exp. Zool.* 267: 318-336.
- Becerra M, Anadón R, Rodríguez-Moldes I, De Miguel E, Caruncho H, Corujo A, Rodicio C (1990) “Desarrollo del laberinto en la larva del rodaballo *(Scophthalmus maximus*)”. Actas 111 Congreso Nacional Acuicultura, pp. 289-294.
- Becerra M, Anadón R (1993) “Development of the inner ear of the brown trout (*Salmo trutta fario*): I. Gross morphology and sensory cell proliferation”. *J. Morphol.* 216: 209-223.
- Bernstein P (2003) “The ear region of *Latimeria chalumnae*: functional and evolutionary implications”. *Zoology* 106:233:242.
- Bever MM, Fekete DM (2002) “Atlas of the development of the inner ear in zebrafish”. *Dev. Dynam.* 223: 536-543.
- Bever MM, Jean YY, Fekete DM (2003) “Three-dimensional morphology of the inner ear development in *Xenopus laevis*”. *Dev. Dynam.* 227:422-430.
- Bissonnette JP, Fekete DM (1996) “Standard atlas of the gross anatomy of the developing inner ear of the chicken”. *J. Comp. Neurol.* 368:620-630.

- Brazeau MD, Friedman M (2014) “The characters of Paleozoic jawed vertebrates”. *Zool. J. Linn. Soci-Lond.* 170: 779-821.
- Carlström D (1963) “A crystallographic study of vertebrate otoliths”. *Biol. Bull.* 125: 441-463.
- Corwin JT (1977)”Morphology of the macula neglecta in sharks of the genus Carcharhinus”. J. Morphol. 152: 341-362.
- De Beer GR (1931) “The development of the skull of *Scyllium (Scyliorhinus) canicula* L.” *Quart. J. Microsc. Sci.* 74:591–645.
- de Burlet HM (1928) **“**Uber die Papilla neglecta”. *Anat. Anz*. 66: 199-209.
- de Burlet HM, Versteegh C (1930) “Über Bau und Funktion des *Petromyzon* Labrynthes”. *Acta Oto-Laryngol*. 13: 5-58.
- Dooling RJ, Lohr B, Dent M (2000) “Hearing in birds and reptiles”. In: Dooling R, Popper AN, Fay RR, editors. “Comparative hearing: birds and reptiles. Springer Handbook of Auditory Research” p. 308-359.
- Eckhard A, Gleiser C, Arnold H, Rask-Andersen H, Kumagami H, Müller M, Hirt B, Löwenheim H (2012) “Water channel proteins in the inner ear and their link to hearing impairment and deafness”. *Mol. Aspects Med.* 33: 612-637.
- Evangelista C, Mills M, Siebeck UE, Collin SP (2010) "A comparison of the external morphology of the membranous inner ear in eslasmobranchs". *J. Morphol.* 271: 483-495.
- Fritzsch B (1987) "Inner ear of the coelacanth fish *Latimeria* has tetrapod affinities". *Nature* 327: 153-154.

- Fritzsch B, Beisel KW (2001) “Evolution of the nervous system. Evolution and development of the vertebrate inner ear”. *Brain Res. Bull*. 55: 711-721.
- Fritzsch B, Pauley S, Beisel KW (2006) “Cells, molecules and morphogenesis: The making of the vertebrate ear”. *Brain Res.* 1091: 151-171.
- Garvin JL, Spring KR, Santi PA (1988) “Secretion of endolymph by semicircular canals of the shark”. *Am. J. Physiol.* 255: 711-719.
- Gray O (1952) “The comparative anatomy of the labyrinth; an example of the evolution of a special sense organ”. *Proc R Soc Med*. 45:794-796.
- Haddon C, Lewis J (1991) “Hyaluronan as a propellant for epithelial movement: the development of semicircular canals in the inner ear of *Xenopus*”. *Development* 112: 541-550.
- Haddon C, Lewis J (1996) “Early ear development in the embryo of the zebrafish, *Danio rerio*”. *J. Comp. Neurol.* 365: 113-128.
- Hagelin LO (1974) “Development of the membranous labyrinth in lampreys”. *Acta. Zool-Stockholm* 1-218.
- Hamburger V, Hamilton HL (1951) “A series of normal stages in the development of the chick embryo”. *J. Morphol*. 88: 49-91.
- Hammond KL, Whitfield TT (2006) “The developing lamprey ear closely resembles the zebrafish otic vesicle: otx1 expression can account for all major patterning differences”. *Development* 133:1347-1357.
- Hanson M, Westerberg H, Öblad M (1990) “The role of magnetic statoconia in dogfish (*Squalus acanthias*)”. *J. Exp. Biol.* 151: 205-218.
- Holmgren N (1940) “Studies on the head in fishes. Part I. Development of the skull in sharks and rays”. *Acta Zool-Stockholm* 21: 51-257.

- Imoto T, Rask-Andersen H, Bagger-Sjoback D (1983) “The role of the endolymphatic sac in statoconial formation and degradation”. *Acta Oto-Laryngol.* 96: 227-235.
- Iwasaki I (1937) “Entwicklungsgeschichtliche Untersuchungen uber das hautige Labyrinth der Knochenfische”. *Jpn. J. Med. Sci.* (Anat.) 6:301-419.
- Jarvik E (1980) “Basic structure and evolution of vertebrates”. *J. Vertebr. Paleontol.* 1: 389-397.
- Jollie M (1971) “Some developmental aspects of the head skeleton of the 35-37 *Squalus acanthias* foetus". *J. Morphol.* 133: 17-40.
- Jørgensen JM, Shichirit M, Genesert FA (1998) “Morphology of the hagfish inner ear”. *Acta Zool-Stockholm* 79: 251-256.
- Larsell O, McCrady E Jr, Zimmermann (1935) “Morphological and functional development of the membranous labyrinth in the opossum”. *J. Comp. Neurol.* 63: 95-118.
- Lovell JM, Findlay MM, Moate RM, Nedwell JR, Pegg MA (2005) “The inner ear morphology and hearing abilities of the paddlefish (*Polyodon spathula*) and the lake sturgeon (*Acipenser fulvescens*). *Com. Biochem. Phys. A.* 142: 286-296.
- Lovell JM, Findlay MM, Harper GM, Moate RM (2007) "The polarization of hair cells from the inner ear of the lesser spotted dogfish *Scyliorhinus canicula*". *J. Fish Biol.* 70: 362-373.
- Lowenstein O, Osborne MP, Versal J (1964) “Structure and innervation of the sensory epithelia of the labyrinth in the thornback ray (*Raja clavata*)”. *Proc. R. Soc. Lond. B. Biol. Sci.* 160: 1-12.
- Lowenstein O, Osborne MP, Thornhill RA (1968) “The anatomy and ultrastructure of the labyrinth of the

lamprey (*Lampetra fluviatilis L.*)". *Proc. R. Soc. Lond. B. Biol. Sci.* 170: 113-134.

- Lowenstein O, Thornhill RA (1970) "The labyrinth of myxine: anatomy, ultrastructure and electrophysiology". *Proc. R. Soc. Lond. B. Biol. Sci.* 176: 21-42.
- Maisey JG (2001) "Remarks on the inner ear of elasmobranchs and its interpretation from skeletal labyrinth morphology". *J. Morphol.* 250: 236-264.
- Maisey JG (2004) "Morphology of the braincase in the broadnose sevengill shark *Notorynchus* (Elasmobranchii, Hexanchiformes), based on CT scanning". *Am. Mu. Novit.* 3429**:** 1-52.
- Maklad A, Reed C, Johnson NS, Fritzsch B (2014) "Anatomy of the lamprey ear: morphological evidence for occurrence of horizontal semicircular ducts in the labyrinth of *Petromyzon marinus*". *J. Anat.* 224: 432-446.
- Manley GA (2000) "The hearing organs of lizards". In: Dooling R, Popper AN, Fay RR, editors. "Comparative hearing: birds and reptiles. Springer Handbook of Auditory Research" p. 139–196.
- Maren TH, Swenson ER, Addink AD (1975) "Rates of in movement from plasma to endolymph in the dogfish". *Ann. Oto. Rhinol. Laryn.* 84: 847-858.
- Maren TH (1977) "Physiology and chemistry in cerebrospinal fluid, aqueous humor and endolymph in *Squalus acanthias*". *J. Exp. Zool*. 199: 317-324.
- Martin P, Swanson GJ (1993) "Descriptive and experimental analysis of the epithelial remodellings that control the semicircular canal formation in the developing mouse inner ear". *Dev. Biol.* 159: 549-558.

- Mason MJ, Segenhout JM, Cobo-Cuan A, Quiñones PM, van Dijk P (2015) “The frog inner ear; picture perfect?”. *JARO-J. Assoc. Res. Otol*. 16: 171-188.
- Mazan S, Jaillard D, Baratte B, Janvier P (2000) "Otx1 gene-controlled morphogenesis of the horizontal semicircular canal and the origin of the gnathostome characteristics". *Evol. Dev.* 2: 186-193.
- McVean A (1991) “The semicircular canals of the hagfish *Myxine glutinosa*” *J. Zool. Lond.* 224: 213-222.
- Metscher BD (2009) “MicroCT for developmental biology: a versatile tool for high-contrast 3D imaging at histological resolutions”. *Dev. Dynam.* 238: 632-640.
- Metscher BD (2011) "X-ray microtomographic imaging of intact vertebrate embryos”. *Cold Spring Harb. Protoc.* 12: 1462-1471.
- Morsli H, Choo D, Ryan A, Johnson R, Wu DK (1998) “Development of the mouse inner ear and origin of its sensory organs”. *J. Neurosci.* 18: 3327-3335.
- Nieuwkoop PD, Faber J (1994) “Normal table of *Xenopus laevis* (Daudin); a systematical and chronological survey f the development from the fertilized egg till the end of metamorphosis”. *New York: Garland Publishing, Inc*.
- Norris HW (1892) “Studies on the development of the ear of *Amblysoma*”. *J. Morphol*. 7: 23-34.
- O´Neill P, McCole RB, Baker CVH (2007) “A molecular analysis of neurogenic placode and cranial sensory ganglion development in the shark, *Scyliorhinus canicula*”. *Dev. Biol.* 304: 156-181.
- Platt C (1983) “Retention of generalized hair cell patterns in the inner ear of the primitive flatfish Psettodes”. *Anat Rec*. 207:503-508.

- Popper AN (2011) “Auditory system morphology”. In *Encyclopedia of Fish Physiology: From Genome to Environment*. Ed. Farrel AP. San Diego: Academic, 252–261.
- Romanoff A (1960) “The avian embryo: structural and functional development”. New York: Macmillan.
- Schulz-Mirbach T, Heß M, Metscher BD, Ladich F (2013) “A unique swim bladder-inner ear connection in a teleost fish revealed by a combined high-resolution microtomographic and three-dimensional histological study ”. *BMC Biol.* 11: 75-87.
- Smotherman M, Narins P (2004) “Evolution of the amphibian ear”. G. A. Manley et al. (eds.), Evolution of the Vertebrate Auditory System © Springer Science+Business Media, New York.
- Streeter GL (1906) “On the development of the membranous labyrinth and the acoustic and facial nerves in the human embryo”. *Am. J. Anat.* 6: 139-165.
- Tester AL; Kendall JI, Milisen WB (1972) “Morphology of the ear of the shark genus *Carcharhinus*, with particular reference to the macula neglecta”. *Pac. Sci.* 26: 264-274.
- Thornhill RA (1972) “The development of the labyrinth of the lamprey (*Lampetra fluviatilis* Linn. 1758)”. *Proc. R. Soc. Lond. B.* 181: 175-198.
- Thomot A, Bauchot R (1987) “L’organogenesis du labyrinthe membraneux chez *Polypterus senegalus* Cuvier, 1829. (Pisces, Holostei, Polypteridae)”. *Anat. Anz.* 164: 189-211.
- Torres M, Giráldez F (1998) “The development of the vertebrate inner ear”. *Mech. Develop.* 71: 5-21.
- Vilstrup T (1951) “On the formation of the otoliths”. *Ann. Otol. Rhinol. Laryn.* 60, 974-981.

- Waterman RE, Bell DH (1984) “Epithelial fusion during early semicircular canal formation in the embryonic zebrafish, *Brachydanio rerio*”. *Anat. Record* 210: 101-114.
- Wever EG (1978a) “Sound transmission in the salamander ear”. *Proc. Natl. Acad. Sci.* 75: 529-530.
- Wever EG (1978b) “The ear of the chameleon-*Chamaeleo senegalensis* and *Chamaeleo quilensis*”. *J. Exp. Zool.* 168: 423-436.
- Wever EG (1978c) “The Reptile Ear”. Princeton, N.J.: Princeton University Press.
- Wever EG (1983) “The ear and hearing in the frog, *Rana pipiens*”. *J. Morph.* 141: 461-478.

FIGURES LEGENDS

Abbreviations: ASC: anterior semicircular canal; DCS: *ductus canalis semicircularis*; DP: dorsal process of the parachordal cartilage; ED: endolymphatic duct; Hb: hindbrain; HSC: horizontal semicircular canal; IX: glossopharyngeal nerve; IXr: root of the glossopharyngeal nerve; L: lagena; LBO: lamina basiotica; LHO: lamina hypotica; OC: otic cup; OP: otic placode; OV: otic vesicle; PF: parietal fossa: PSC: posterior semicircular canal; S: saccule; SAG: statoacoustic ganglion; U: utricle; UR: utricular recess; V: trigeminal nerve; VII: facial nerve; VIIr: root of the facial nerve; VIII: auditory nerve; VIIIr: root of the auditory nerve; X: vagus nerve; Xr: root of the vagus nerve.

Fig. 1.- Micro-CT images of a stage 18 embryo stained with alcoholic iodine (I2M). A.- Lateral view of a 3D reconstructed embryo showing the levels of the transversal (B) and horizontal (C) sectioned planes the inner ear. B, C.- Images illustrate early events of he inner ear de development corresponding at the otic placodes formation. The otic placodes appear as a thickenning of the ectoderm adjacent to each side of the hindbrain irrespectively of the section plane. The horizontal plane reveals the central sinking (arrowheads). Scale bars= 500 µm in A; 200 µm in B, C.

Fig. 2.- Micro-CT images of a stage 20 embryo treated with phosphotungstic acid (PTA). A-C: lateral (A), lateral-horizontal (B) and horizontal (C) external views. D-E: transversal sections. Lines in Fig. A indicate the level of Figs. D and E. The otic placode has formed a deep otic cup (OC) which presents a antero-posterior axis larger than the dorso-ventral one (A-C). The octaval ganglion (A-B; SAG) is seen ventrally and rostrally to the cup, and very close to it in its rostral part (D) but less close in more caudal levels (E). Scale bars= 500 µm in A-C; 200 µm in D, E.

Fig. 3.- Micro-CT images of a stage 22 embryo treated with alcoholic iodine (I2M). Lateral external view (A), parasagittal section (B), fronto-lateral external view (C),and transverse (D, E) and horizontal (F) sections. Fig. A indicates the level of Fig. F. Fig. B indicates the level of figures D and E. Due to the curvature of the body, the transverse plane to the main axis of the body (B, white lines) corresponds to the horizontal plane of the otic cup (D, E), while the horizontal plane to the main axis of the body (A, white line) corresponds to the transverse plane of the otic cup (F). Note the close relation between the otic cup and the hindbrain, as well as the severe collapse of the ectoderm over the hindbrain (asterisks). Scale bar= 500 µm in A-C; 200 µm in D-F.

Fig. 4.- Micro-CT images of a stage 24 embryo treated with phosphotungstic acid (PTA). Lateral and dorsal external views (A, D, respectively) and parasagittal (B, C), horizontal (E) and transverse (F) sections. Fig. A indicates the level of Fig. E. Fig. F indicates the level of Figs. B (more lateral) and C (more medial).The otic cup is almost a closed vesicle located almost apposed to the dorsal surface of the head and open to the exterior by a narrower opening that in previous stages (C, D; arrowheads). Note the collapsed ectoderm over the hindbrain (asterisks). Scale bars= 500 μm in A-F.

Fig. 5.- Micro-CT images of a stage 25 embryo treated with phosphotungstic acid (PTA). A-D: external view (A) and sagittal (B), transversal (C) and horizontal (D) sections. Figs. B and D indicate the level of Figs. E-H and I-L respectively. The otic vesicle presents an almost round shape with the endolymphatic duct in its medial wall opening dorsal to the exterior (K, arrow). Note the situation of the statoacoustic ganglion, located ventrally and slightly rostrally, but very close to the vesicle (J, arrowhead). Scale bars= 500 μm in A-L.

Fig. 6.- Transverse (A, D, G), sagittal (B, E, H) and horizontal (C, F, I) sections of embryos at stages 27 (A-C), 29 (D-F) and 31 (G-I) scanned with micro-CT after PTA staining showing the progression of the otic vesicle from the single vesicle to the subdivided inner ear. At stage 27 the main new visible structure is the posterior semicircular canal located in the rear region of the vesicle. At stage 29 the subdivision of the three main chambers is slightly appreciated (E). The buds of the protrusions continue to grow into the vesicle and the subdivisions are clearly visible at stage 31. Note the significative enlargement of the protrusions that delimitate the semicircular canals, making them relatively long and thin (G, I), and the narrow duct connecting the saccule and the utricle (G, arrow). Scale bars= 400 μm in A-I.

Fig. 7.- Sagittal (A) and transverse (H) sections and horizontal external view (O) of a stage 32 embryo stained with PTA and scanned with micro-CT. Fig. A and H indicate the level of Figs. B-G and I-N respectively. By this stage all the structures are completely formed, being visible not only the separated chambers (U, S, L, UR) and canals (ASC, HSC, PSC), but also the sensorial patches within them (B-E, G, I, J, L; white arrowheads). The route of the VIII and IX nerves through the otic capsule is also visible. The volume of the space between the cartilaginous and membranous labyrinths is noticeable in some regions, being occupied by loose mesenchymal tissue (*). Note also the sinuous trajectory of the endolymphatic duct (ED) at its dorsal part and its external openings located in the dorsal region of the head, next

to the midline (N, white arrowhead; O, black arrowheads). Scale bars= 2000 µm in A, H, O; 500 µm in B-G, I-N.

Fig. 8.- Sagittal (A) and transverse (I) sections of a stage 33 embryo stained with PTA and scanned with micro-CT. Fig. A and I indicate the level of Figs. B-H and J-O respectively. At this stage the inner ear is very similar to that observed in post hatching sharks, being the most remarkable new aspect the presence of the irregular-shaped and high-density mineral otoliths located within the utricular recess, the saccule and the lagena (C, D, L-N, black asterisks). Note the wide spaces between the cartilaginous and membranous labyrinths (E-G, L, N, O, white asterisks). Scale bars= 2000 µm in A-I; 500 µm in B-H, J-O.

Fig. 9.- External view (A) and sagittal and transverse sections (B, C) of the head of a juvenile *S. canicula* and transverse (D-H) and sagittal (I-L) sections through an isolated left inner ear of a juvenile scanned with micro-CT after staining with phosphotungstic acid (PTA) (A-C) and unstained after desiccating with HMDS (D-L). Figs. B and C indicate the levels of Figs. D-H and I-L respectively. The thickness of the skin makes the penetration of the PTA more difficult and gives little contrast to deep tissues (C). The desiccated inner ear presents a good contrast and shows a detailed view of all the inner components of the inner ear, specially the otolithic masses (D-F, J, K, white asterisks), and evidences the disposition of the membranous labyrinth (F, G, arrowheads), quite separated from the cartilage in various points (F, G, black asterisks). Note the communication of the horizontal semicircular canal to the posterior region of the utricle (G, star).Scale bars= 2000 µm in A-C; 500 µm in D-L.

FIGURES

Fig. 1.- Micro-CT images of a stage 18 embryo stained with alcoholic iodine (I2M). A.- Lateral view of a 3D reconstructed embryo showing the levels of the transversal (B) and horizontal (C) sectioned planes the inner ear. B, C.- Images illustrate early events of he inner ear de development corresponding at the otic placodes formation. Note as the otic placodes arise as a thickness of the ectoderm adjacent to each side of the hindbrain irrespectively of the section plane. Interestingly, the horizontal plane reveals that the placodes begin to invaginate early, showing a central sinking (arrowheads). Scale bar= 500 µm in A; 200 µm in B, C.

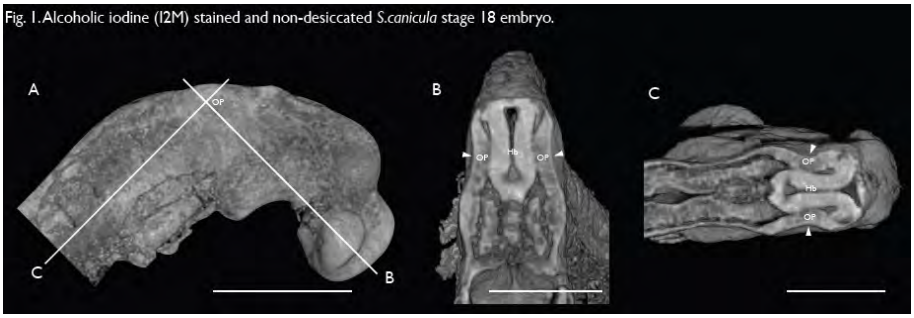
Fig. 1. Alcoholic iodine (12M) stained and non-desiccated S.canicula stage 18 embryo.
A
OP
C
B
B
OP
Hb
OP
C
OP
Hb
OP

Figure 1

Fig. 2.- Micro-CT images of a stage 20 embryo treated with phosphotungstic acid (PTA). A-C: lateral (A), lateral-horizontal (B) and horizontal (C) external views. D-E: transversal sections. Fig. A indicates the level of Figs. D and E. The initial sinking of the otic placode has progressed into a deep otic cup (OC) which presents a larger anteroposterior axis (A-C). The octaval ganglion (A-B; VIII) can be appreciated ventrally and rostral to the cup, but very close to it. Transversal sections confirm its close relation, being visible contacting to the rostral part of the cup (D; VIII), but not in a more caudal level (E). Scale bar= 500 µm in A-C; 200 µm in D, E.

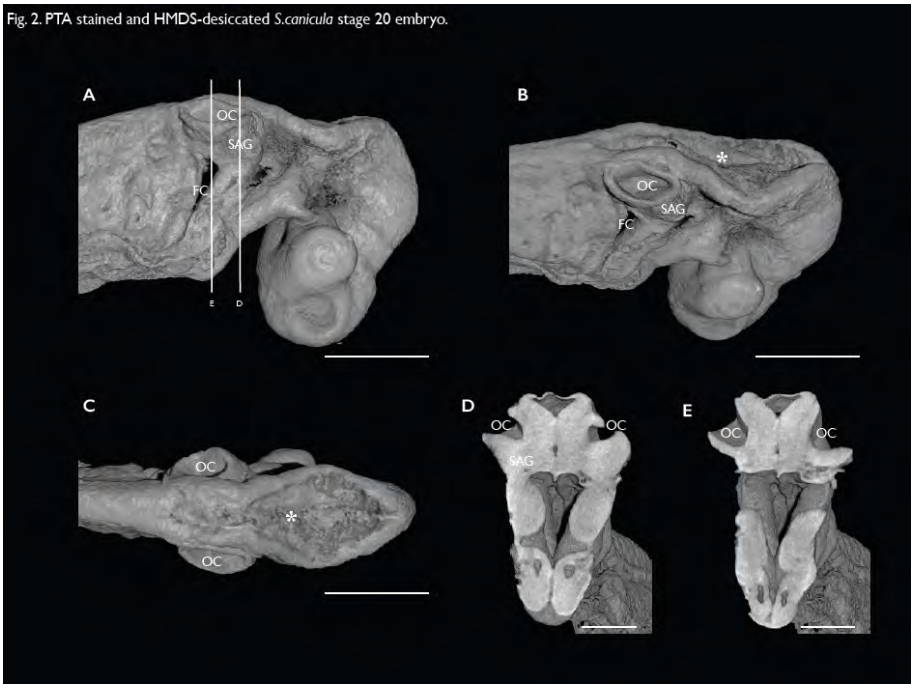
Fig. 2. PTA stained and HMDS-desiccated S.canicula stage 20 embryo.
A
OC
SAG
FC
E
D
B
OC
SAG
FC
C
OC
OC
D
OC
OC
SAG
E
OC
OC

Figure 2

Fig. 3.- Micro-CT images of a stage 22 embryo treated with alcoholic iodine (I2M). Lateral external view (A), parasagittal section (B), fronto-lateral external view (C),and transverse (D, E) and horizontal (F) sections. Fig. A indicates the level of Fig. F. Fig. B indicates the level of figures D and E. Due to the curvature of the body, the transverse plane to the main axis of the body (B, white lines) corresponds to the horizontal plane of the otic cup (D, E), while the horizontal plane to the main axis of the body (A, white line) corresponds to the transverse plane of the otic cup (F). Note the close relation between the otic cup and the hindbrain, as well as the severe collapse of the ectoderm over the hindbrain (asterisks). Scale bar= 500 μm in A-C; 200 μm in D-F.

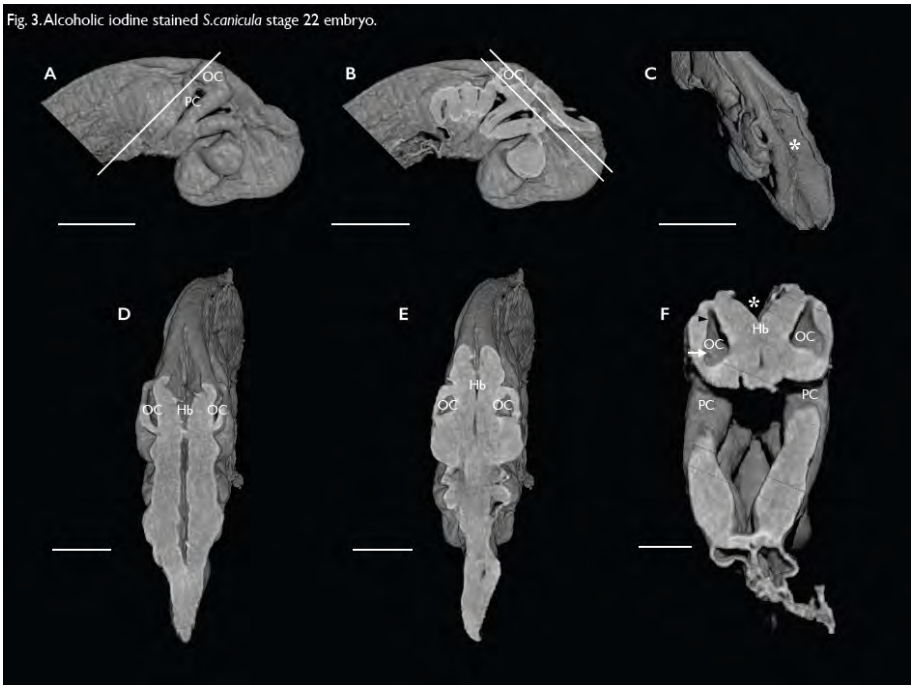
Fig. 3. Alcoholic iodine stained S.canicula stage 22 embryo.
A
OC
PC
B
OC
C
*
D
OC
Hb
OC
E
Hb
OC
OC
F
*
Hb
OC
OC
PC
PC

Figure 3

Fig. 4.- Micro-CT images of a stage 24 embryo treated with phosphotungstic acid (PTA). External view (A, D) and parasagittal (B, C), horizontal (E) and transverse (F) sections. Fig. A indicates the level of Fig. E. Fig. F indicates the level of Figs. B-C. The otic cup is almost a closed vesicle located very close to the dorsal surface of the head and open to the exterior by a narrower opening than in previous stages (C, D; arrowheads). Note the collapsed ectoderm over the hindbrain (asterisks). Scale bar= 500 μm in A-F.

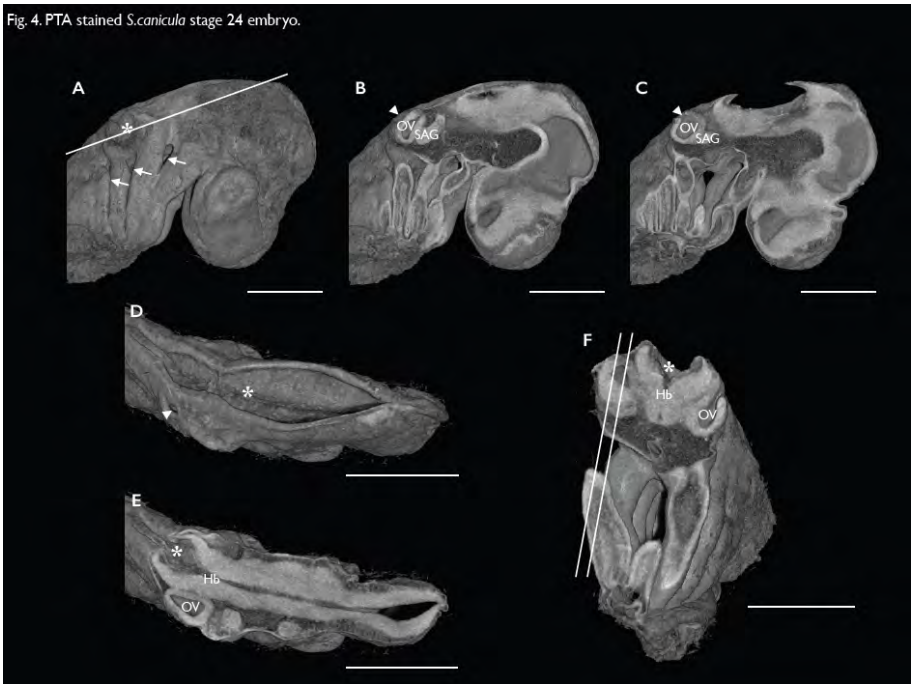
Fig. 4. PTA stained S.canicula stage 24 embryo.
A
B
C
OV
SAG
OV
SAG
D
E
Hb
OV
F
Hb
OV

Figure 4

Fig. 5.- Micro-CT images of a stage 25 embryo treated with phosphotungstic acid (PTA). A-D: external view (A) and sagittal (B), transversal (C) and horizontal (D) sections. Figs. B and D indicate the level of Figs. E-H and I-L respectively. The otic vesicle presents an almost round shape with the endolymphatic duct in its medial wall opening dorsal to the exterior (K, arrow). Note the situation of the statoacoustic ganglion, located ventrally and slightly rostrally, but very close to the vesicle (J, arrowhead). Scale bar= 500 μm in A-L.

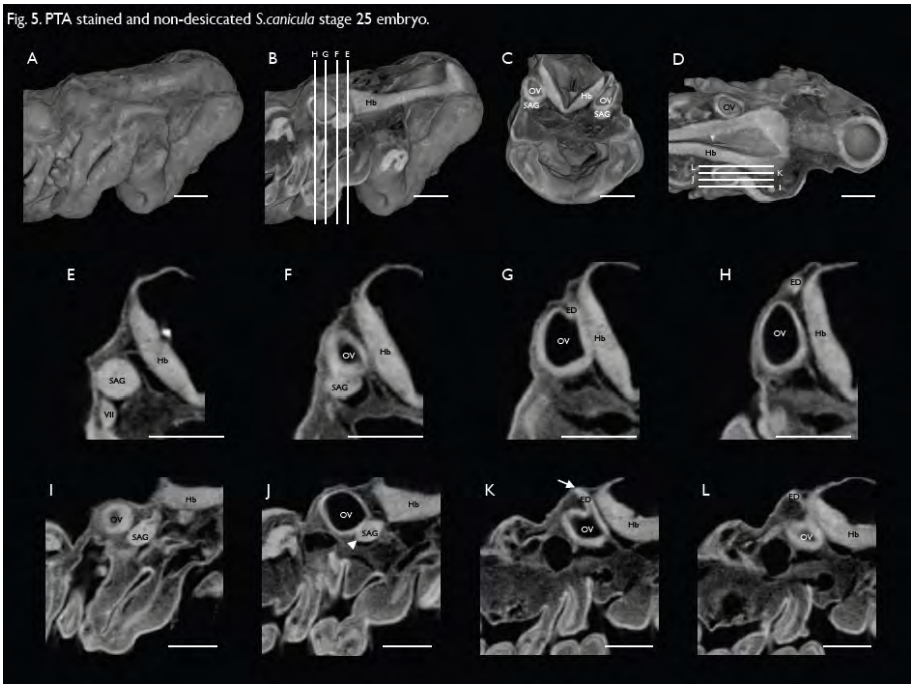
Fig. 5. PTA stained and non-desiccated S.canicula stage 25 embryo.
A
B
H G F E
Hb
C
OV
SAG
Hb
OV
SAG
D
OV
Hb
L
K
J
I
E
Hb
SAG
VII
F
OV
Hb
SAG
G
ED
OV
Hb
H
ED
OV
Hb
I
Hb
OV
SAG
J
OV
Hb
SAG
K
ED
OV
Hb
L
ED
OV
Hb

Figure 5

Fig. 6.- Transverse (A, D, G), sagittal (B, E, H) and horizontal (C, F, I) sections of embryos at stages 27 (A-C), 29 (D-F) and 31 (G-I) scanned with micro-CT after PTA staining showing the progression of the otic vesicle from the single vesicle to the subdivided inner ear. At stage 27 the main new visible structure is the posterior semicircular canal located in the rear region of the vesicle. At stage 29 the subdivision of the three main chambers is slightly appreciated (E). The buds of the protrusions continue to grow into the vesicle and the subdivisions are clearly visible at stage 31. Note the significative enlargement of the protrusions that delimitate the semicircular canals, making them relatively long and thin (G, I); and the narrow duct connecting the saccule and the utricle (G, arrow). Scale bar= 400 μm in A-I.

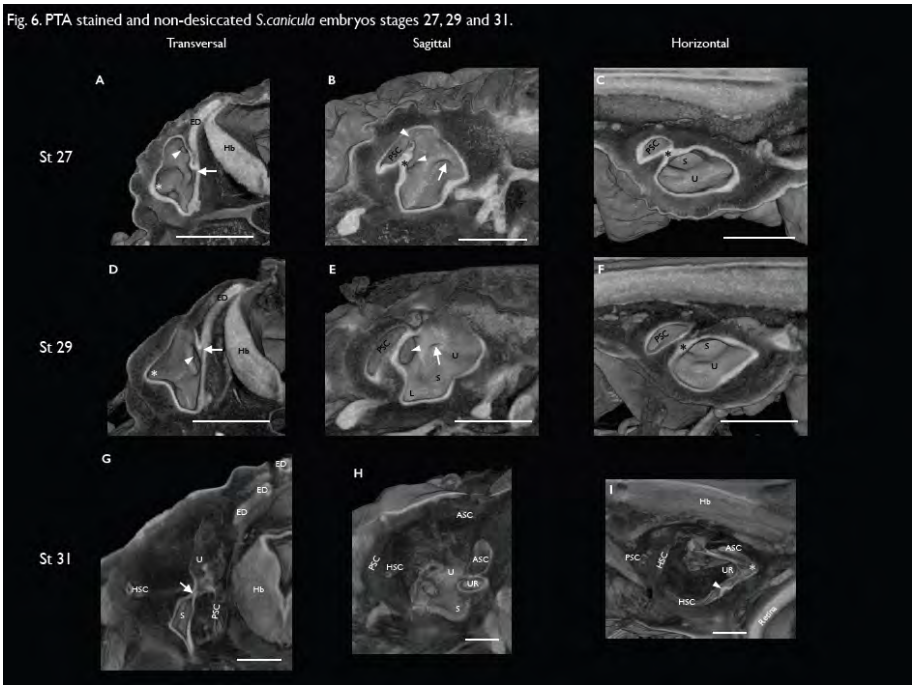
Fig. 6. PTA stained and non-desiccated S.canicula embryos stages 27, 29 and 31.
Transversal
Sagittal
Horizontal
St 27
St 29
St 31
A
B
C
D
E
F
G
H
I
ED
Hb
PSC
HSC
ASC
UR
U
S
L
Radius

Figure 6

Fig. 7.- Sagittal (A) and transverse (H) sections and horizontal external view (O) of a stage 32 embryo stained with PTA and scanned with micro-CT. Fig. A and H indicate the level of Figs. B-G and I-N respectively. By this stage all the structures are completely formed, being visible not only the separated chambers (U, S, L, UR) and canals (ASC, HSC, PSC), but also the sensorial patches within them (B-E, G, I, J, L; white arrowheads). The route of the VIII and IX nerves through the otic capsule is also visible. The volume of the space between the cartilaginous and membranous labyrinths is noticeable in some regions, being occupied by loose mesenchymal tissue (*). Note also the sinuous trajectory of the endolymphatic duct (ED) at its dorsal part and its external openings located in the dorsal region of the head, next to the midline (N, white arrowhead; O, black arrowheads). Scale bar= 2000 µm in A, H, O; 500 µm in B-G, I-N.

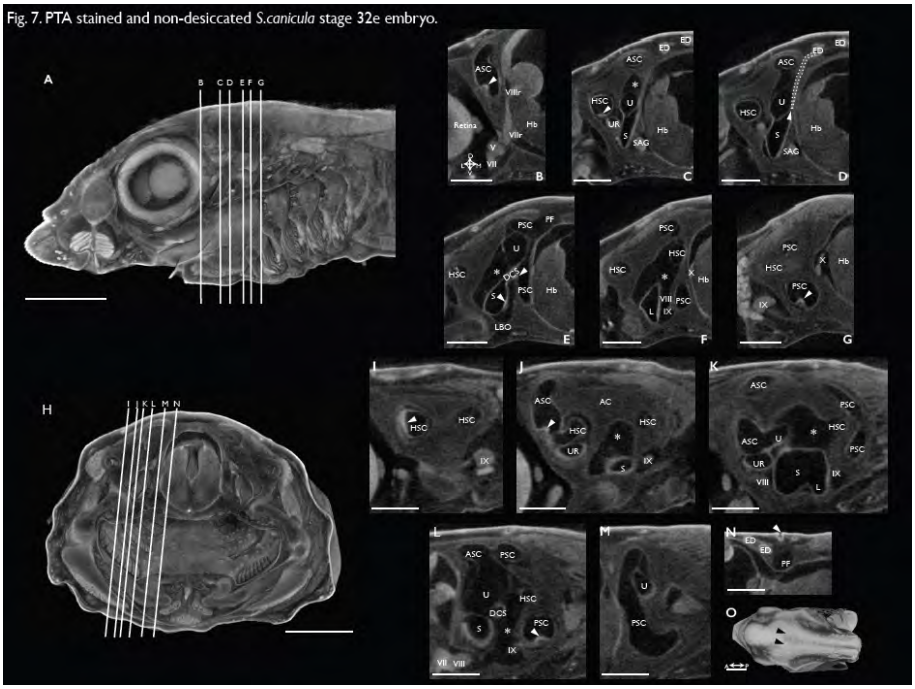
Fig. 7. PTA stained and non-desiccated S.canicula stage 32e embryo.
A
B C D E F G
H
I K L M N
ASC
VIIr
Retina
Hb
V
VII
B
ED
HSC
U
UR
S
SAG
C
D
PSC
PF
DCS
LBO
E
X
VIII
L
IX
F
G
AC
J
K
UR
VIII
L
IX
L
M
N
O

Figure 7

Fig. 8.- Sagittal (A) and transverse (I) sections of a stage 33 embryo stained with PTA and scanned with micro-CT. Fig. A and I indicate the level of Figs. B-H and J-O respectively. At this stage the inner ear is very similar to that observed in post hatching sharks, being the most remarkable new aspect the presence of the irregular-shaped and high-density mineral otoliths located within the utricular recess, the saccule and the lagena (C, D, L-N, black asterisks). Note the wide spaces between the cartilaginous and membranous labyrinths (E-G, L, N, O, white asterisks). Scale bar= 2000 µm in A-I; 500 µm in B-H, J-O.

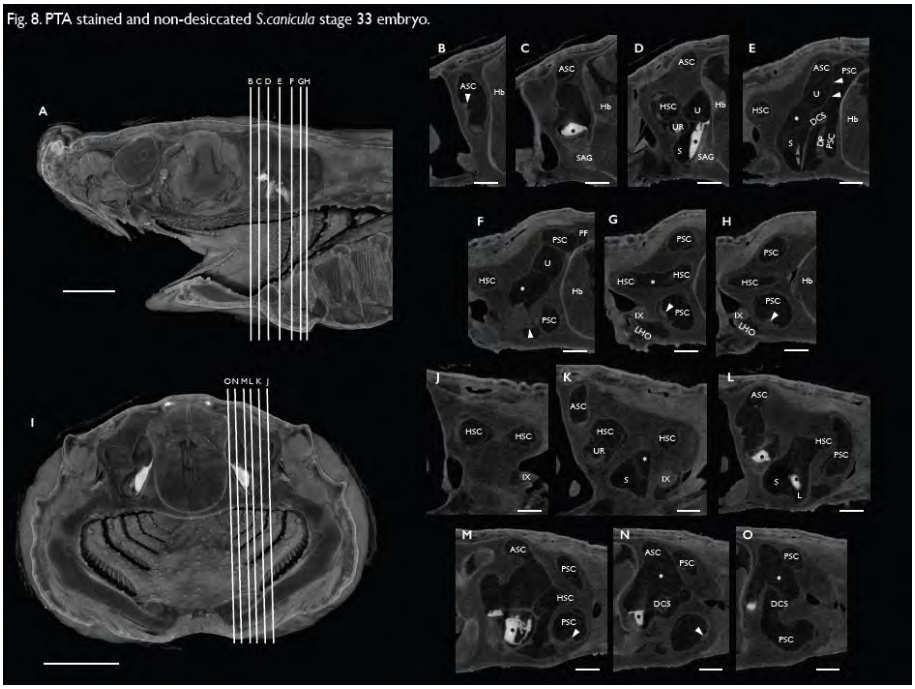
Fig. 8. PTA stained and non-desiccated S.canicula stage 33 embryo.
A
B C D E F G H
I
O N M L K J
B
ASC
Hb
C
ASC
Hb
SAG
D
ASC
HSC
U
Hb
UR
S
SAG
E
ASC
PSC
U
HSC
DCS
Hb
S
PSC
F
PF
PSC
U
HSC
Hb
PSC
G
PSC
HSC
HSC
IX
PSC
LHO
H
PSC
HSC
Hb
PSC
IX
LHO
J
HSC
HSC
IX
K
ASC
HSC
HSC
UR
S
IX
L
ASC
HSC
PSC
S
L
M
ASC
PSC
HSC
PSC
N
ASC
PSC
DCS
O
PSC
DCS
PSC

Figure 8

Fig. 9.- External view (A) and sagittal and transverse sections (B, C) of the head of a juvenile *S. canicula* and transverse (D-H) and sagittal (I-L) sections through an isolated left inner ear of a juvenile scanned with micro-CT after staining with phosphotungstic acid (PTA) (A-C) and unstained after desiccating with HMDS (D-L). Figs. B and C indicate the levels of Figs. D-H and I-L respectively. The thickness of the skin makes the penetration of the PTA more difficult and gives little contrast to deep tissues (C). The desiccated inner ear presents a good contrast and shows a detailed view of all the inner components of the inner ear, specially the otolithic masses (D-F, J, K, white asterisks), and evidences the disposition of the membranous labyrinth (F, G, arrowheads), quite separated from the cartilage in various points (F, G, black asterisks). Note the communication of the horizontal semicircular canal to the posterior region of the utricle (G, star).Scale bar= 2000 µm in A-C; 500 µm in D-L.

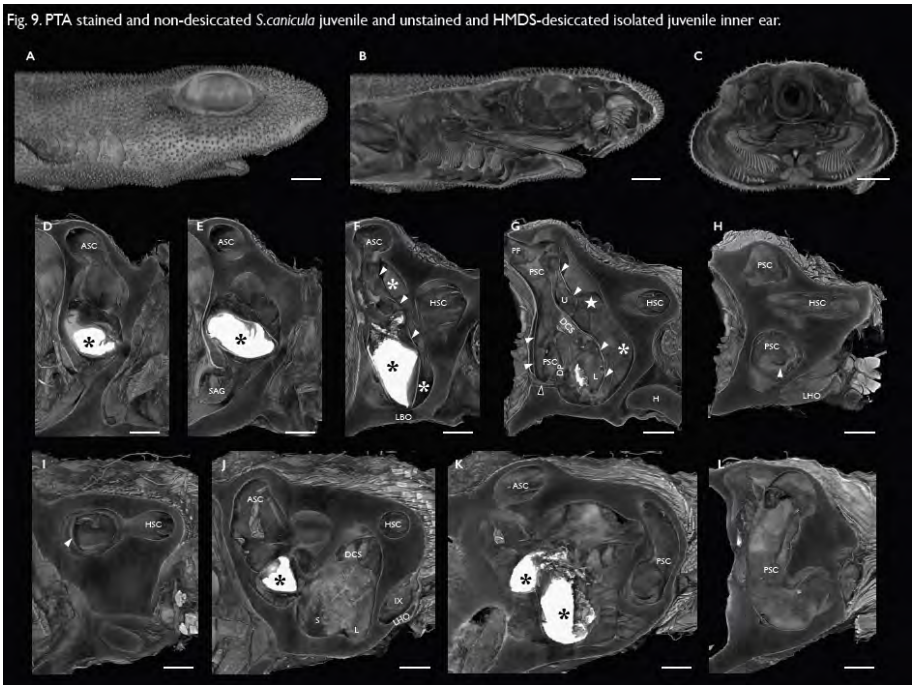
Fig. 9. PTA stained and non-desiccated S.canicula juvenile and unstained and HMDS-desiccated isolated juvenile inner ear.
A
B
C
D
ASC
E
ASC
SAG
F
ASC
HSC
LSO
G
PF
PSC
U
HSC
DCS
PSC
L
H
H
PSC
HSC
PSC
LHO
I
HSC
J
ASC
HSC
DCS
IX
S
L
LHO
K
ASC
PSC
L
PSC

Figure 9

CHAPTER 3

Development of the inner ear innervation in the chondrichthyan *Scyliorhinus canicula*. New perspectives on the vertebrate inner ear evolution

INTRODUCTION

The vertebrate inner ear is a complex three-dimensional sensory organ for the detection of sound, balance and acceleration. It arises from the otic placode, a paired thickening of the head ectoderm derived from the pan-placodal region surrounding the anterior region of the neural plate, which gives rise to all the cranial placodes (Schlosser, 2006; Ladher et al., 2010; Maier et al., 2014;). By the appropriate expression of signals in the surrounding tissues (hindbrain, notochord), some cells of the preplacodal region are induced to form the otic placode and segregated from presumptive cells of other neighbor placodes (trigeminal, epibranchial or lateral line placodes). The thickening of the preplacodal ectoderm forms the otic placode adjacent to the hindbrain, which invaginates to form the otic cup and then the otic vesicle, which gives rise to the membranous inner ear. The sensory neurons of the statoacoustic ganglion (SAG) arise by delamination of neuroblasts produced in thickened areas of epithelial wall of the otic vesicle and their peripheral processes innervate the sensory regions of the otic epithelium where they originated (Torres and Giráldez, 1998; Magariños et al., 2012). Besides the primary ganglion neurons of the SAG, most if not all the cell types of the inner ear epithelium (hair cells and supporting cells of sensory

areas and epithelial cells of non-sensory areas) originate from the otic vesicle walls (Whitfield, 2015; Alsina and Whitfield, 2017). In a next step, the vesicle expand and their walls suffer remodeling to form a complex three-dimensional structure, the membranous labyrinth, with dilated chambers (utricle, saccule, lagena) and three orthogonally arranged semicircular canals, except in agnathans. Sensory patches differentiate in the ampullae at the base of the semicircular canals and in the chambers forming the cristae and maculae, respectively. Sensory hair cells differentiate in these sensory organs. In mammals, the ventral part of the labyrinth grows forming a coiled structure, the cochlea, whose sensory epithelium forms a complex structure, the organ of Corti, which is involved in sound reception. In these animals, the SAG subdivides early in its development to form the cochlear (Corti's) and vestibular ganglia and nerves, forming separated auditory and vestibular pathways, respectively. The accuracy of the development progress is responsible of the correct functioning in the mature animal to process acoustic and vestibular information (reviewed in Rubel and Fritzsch, 2002; Fritzsch and Beisel, 2004; Fritzsch et al., 2002, 2006).

Several studies have reported the development of the inner ear in different tetrapods (*mouse*: Matin and Swanson, 1993;

Morsli et al., 1998; *chick*: Bissonnette and Fekete, 1996; *chamaeleon*: Wever, 1978; *Rana*: Wever, 1983; *Xenopus*: Haddon and Lewis, 1991; Noramly and Granger, 2002; Bever et al., 2003), actinopterigyan fishes (*trout*: Becerra and Anadón, 1993a,b; *zebrafish*: Waterman and Bell, 1984; Haddon and Lewis, 1996, 2002; Bever and Fekete, 2002), sarcopterygian fishes (*Latimeria*: Fritzsch, 1987; Bernstein, 2003), and cyclostomes (Lowenstein et al., 1968; Lowenstein and Thornhill, 1970; Thornhill, 1972; McVean, 1991). However, as far as we know, there are no comprehensive studies in cartilaginous fishes on the normal development of the inner ear, although some of their components have been studied in *Scyliorhinus canicula*, in particular the early expression of certain genes in the inner ear (Mazan et al., 2000; Derobert et al., 2002) and the early development of the otic placode and related ganglia (O'Neill et al., 2007; Baker et al., 2008). Literature concerning the general development of the inner ear of elasmobranchs (sharks, skates and rays) and chimaeras is scarce, but some studies focused on the morphology of the adult inner ear and its connections (Baird, 1974; Tester et al., 1972; Corwin 1977, Boord and Roberts, 1980; Maisey, 2001; Lovell et al., 2007; Evangelista et al., 2010). Comparative analyses have revealed a general gnathostome-type structure of the inner ear in all adult chondrichthyans (cartilaginous fishes), but there are

some differences between elasmobranchs and chimaeras (Baird, 1974; Maisey, 2001). In sharks, skates and rays the posterior semicircular canal is independent from the others and constitutes an almost complete circle, while the horizontal and anterior canals are associated in a common crus (Evangelista et al., 2010) or utricular recess, but in chimaeras the three semicircular canals the pattern is more similar to that observed in primitive bony fishes, with partially fused vertical canals in a *crus communis* (Baird, 1974). The endolymphatic duct also differs between both groups, presenting a straight trajectory in chimaeras, but a recurved trajectory with a dilatation in its dorsal region (the endolymphatic fossa) in elasmobranchs (Baird, 1974, Maisey, 2001).

The sensory organs of the inner ear are innervated by efferent and afferent fiber. The existence of efferent (centrifugal) and afferent terminals at the base of the sensory hair cells has been demonstrated with different approaches (Baird, 1974; Becerra and Anadón, 1993b; Simmons, 2002; Popper, 2017; Fritzsch and Elliot, 2017). Efferent terminals form part of the descending centrifugal pathway from the hindbrain (the octavolateralis efferent system). In cartilaginous fish, as in amphibians, there is extensive overlap between the octavolateralis efferent neurons and the facial branchial motor

nucleus (Roberts and Meredith, 1992; Simmons 2002). Developmental studies in mice have shown that the inner ear efferent neurons represent a specific motor neuron phenotype with common embryological origin with facial branchiomeric motoneurons, which are located in the rhombomere 4, and whose axons exit the brain with the facial-octaval nerve root to the ear (Fritsch and Elliot, 2017). Afferent terminals on the hair cells belong to the bipolar neurons of the SAG, which constitute the afferent system connecting the inner ear sensory epithelium and the brain. These primary sensory neurons send peripheral processes to the otic sensory organs (these ganglion cells have the same place of origin than the sensory cells that innervate, see above) and central projections along the VIII nerve to hindbrain octaval nuclei (Rubel and Fritzsch, 2002; Appler and Goodrich, 2011). The formation of the SAG cells happens along highly regulated sequential steps that include delamination from the otic cup/vesicle epithelia, migration, proliferation and differentiation into ganglion neurons. The processes are similar irrespectively that the otic vesicle was formed by invagination, as in cyclostomes (Thornhill, 1972), amphibians (reviewed in Smotherman and Narins, 2004; *Xenopus*: Haddon and Lewis, 1991; Bever et al., 2003; *Ambystoma*: Norris, 1892) and non-reptile amniotes (mouse: Morsli et al., 1998; chicken: Bissonnette and Fekete, 1996); or by cavitation, as in teleosts

(zebrafish: Waterman and Bell, 1984; Haddon and Lewis, 1996) and reptiles (see review Barald and Kelley, 2004).

In this chapter we analyze the development of the inner ear of *Scyliorhinus canicula* with some molecular markers with the aim of identifying the early events of the formation of the otic epithelium and its neural projections in a basal gnathostome. Our aim has been to characterize the development of the inner ear innervation by profiling the spatiotemporal pattern of distribution of reliable immunomarkers as doublecortin (DCX, a reliable marker of migrating immature neurons and their growing fibers in the catshark; Quintana-Urzainqui et al., 2014a,b) in the developing SAG and otic epithelium of catshark embryos. In addition, we aimed to examine some components of the developing otic system with immunomarkers for proliferating cells (PCNA, proliferative cell nuclear antigen) and early postmitotic neurons (HuC/D). In certain developmental stages we have also analyzed the expression of some genes that play critical roles in inner ear development such as *NeuroD* and *Sox2*, based on the cellular deficit that their deletion causes in the inner ear sensory ganglia and sensory organ of mouse. In mice, *NeuroD* gene encodes a transcription factor that mediates certain aspects of pathfinding and migration as well as survival of the inner ear sensory neurons during differentiation (Liu et

al., 2000; Kim et al., 2001). In embryos of *Scyliorhinus canicula*, *NeuroD* is expressed in all placode-derived cranial sensory ganglia, including the SAG (O'Neill et al., 2007). *Sox2* gene also encodes a transcription factor which is implied in the maintenance of pluripotent stem cells and in the establishment of the neurosensory competence at early stages of inner ear development, being located in prosensory domains during early development, and later in supporting cells of the sensory domains (Millimaki et al., 2010; Neves et al., 2013). With these tools, we described in detail the spatiotemporal dynamics of the derivatives of the otic placode in the shark *S. canicula*. By comparison with available data in other model organisms, we intend to provide an accurate tool for comparing the chronology of the developmental processes in the inner ear among vertebrates. The spatiotemporal characterization of the otic epithelium derivatives and SAG innervation during the embryonic development in a basal gnathostome will provide important information about the evolution of the inner ear in vertebrates.

MATERIAL AND METHODS

Experimental Animals

A total of 25 embryos of the catshark *S. canicula,* also known as the lesser spotted dogfish, from stages 20 to 32 embryos (two st20, three st24, three st25, six st27, four st29, four st31 and three st32). Eggs from different broods and juveniles were raised in fresh seawater tanks in standard conditions of temperature (15–16 ºC), pH (7.5–8.5) and salinity (35 g/L). Embryo staging was done according to Ballard et al. (1993). The following stages were analyzed: stage 20 (characterized by four pairs of unopened pharyngeal pouches visible by translucence), stage 24 (diamond-shaped mouth), stage 25 (four pairs of open pharyngeal clefts), stage 27 (diamond-shaped mouth and primordial gill filaments), stage 29 (mandibular arches crowded into the mouth opening and initial eye pigmentation), stage 31 (detectable rostrum and long branchial filaments). The beginning of stage 32 corresponds to the commencing of the second half of embryonic development, which ends when the external yolk sac is empting and hatching takes place (at stage 34). *S. canicula* embryos were supplied by the Marine Biological Model Supply Service of the CNRS UPMC Roscoff Biological Station (France). Additional embryos

and juveniles were kindly provided by the Aquaria of Gijón, O Grove, and the Aquarium Finisterrae (Spain). Adequate measures were taken to minimize animal pain or discomfort. All procedures conformed to the guidelines established by the European Communities Council Directive of September 22, 2010, (2010/63/UE) and by Spanish Royal Decree 53/2013 for animal experimentation, and they were approved by the Ethics Committee of the University of Santiago de Compostela.

Fixation and sectioning

Embryos were deeply anesthetized with 0.5% tricaine methane sulfonate (MS-222; Sigma, St. Louis, MO) in seawater and separated from the yolk before fixation by immersion (48–72 h depending on the embryo stage) in cold 4% paraformaldehyde (PFA) in 0.1 M phosphate buffer (PB; pH 7.4) containing 1.75% urea (elasmobranch´s PB). Embryos from stage 32 onwards were deeply anesthetized with MS-222 and then perfused intracardially with elasmobranch Ringer's solution (see Ferreiro-Galve et al. 2012) followed by 4 % PFA in elasmobranch´s PB and postfixed in the same fixative for 24–48 h at 4 ºC. The fixative was removed by washing with PB saline (PBS). Samples were dehydrated in graded series of methanol solutions and stored in methanol 100% at -20ºC. The methanol-

stored samples were rehydrated before subsequent processing for immunohistochemistry or *in situ* hybridization. To obtain sections, the tissue was then cryoprotected with 30% sucrose in PB, embedded in NEG 50TM (Thermo Scientific, Kalamazoo, MI, USA) or in OCT compound (Tissue Tek, Torrance, CA, USA), frozen with liquid nitrogen-cooled isopentane, and cut on a cryostat (16–18 µm thick). Parallel series of transverse and sagittal sections were mounted on Superfrost Plus slides (Menzel-Glasser, Madison, WI, USA).

Immunohistochemistry

Sections were pre-treated with 0.01 M citrate buffer (pH 6.0) for 30 min at 90 ºC for heat-induced epitope retrieval and allowed to cool for 20 min at room temperature (RT). Sections were rinsed in 0.05 M Tris-buffered saline (TBS; pH 7.4) for 5 min and treated with 10% H_2O_2 in TBS for 30 min at RT to block the endogenous peroxidase activity. Then, they were rinsed twice in 0.05 M TBS pH 7.4 for 5 min each and incubated overnight at RT in a wet chamber with the primary antibody solutions: rabbit polyclonal anti-doublecortin (DCX, dilution 1/300, catalog No. 4604; Cell Signaling, Beverly, MA); mouse monoclonal anti-human HuC/HuD (HuC/D, dilution 1/100, catalog No. A-21271; Molecular Probes, Eugene, OR); and

mouse monoclonal anti-proliferating cell nuclear antigen (PCNA, dilution 1/100, catalog No. P8825; Sigma, St. Louis, MO). The dilutions were made with TBS containing 15% normal goat serum (Millipore, Billerica, MA), 0.2% Triton-S (Sigma) and 2% bovine serum albumin (BSA, Sigma). Sections were rinsed twice in 0.05 M TBS pH 7.4 for 15 min each, and incubated with secondary antibodies for 1h at RT in a wet chamber. The secondary antibodies were horseradish peroxidase (HRP)-coupled goat anti-rabbit (GAR-HRP; Dako, Glostrup, Denmark; dilution 1/200) and HRP-coupled goat anti-mouse (GAM-HRP; Dako; dilution 1/200) diluted in TBS containing 15% normal goat serum (Millipore), 0.2% Triton-S (Sigma) and 2% bovine serum albumin (BSA, Sigma). After the incubation, the sections were rinsed three times in 0.05 M TBS pH 7.4 for 10 min each. The immunoreaction was revealed by incubation with 0.25 mg/mL diaminobenzidine tetrahydrochloride (DAB; Sigma) in TBS pH 7.4 and 0.00075% H_2O_2 or with SIGMAFAST TM 3, 30-DAB tablets (Sigma) as indicated by the manufacturers. Immunohistochemistry for DCX was also performed on cryostat sections of embryos that had been previously treated for *in situ* hybridization *in toto* for *ScWnt8* and *ScSox2* (see below). Control experiments were carried out by omitting the primary or secondary antibody in the incubations and no immunostaining was detected in any case.

The specificity of the primary antibodies used here has been previously characterized for use in this shark species. For details about the characterization of antibodies against DCX, HuC/D and anti-PCNA, see Pose-Méndez et al. (2014).

In situ Hybridization

We applied *in situ* hybridization (ISH) for the gene *ScNeuroD* (Docampo-Seara et al., 2018) on cryostat sections of stages st24, st25 and st27. This probe was selected from a collection of *S. canicula* embryonic cDNA library (mixed stages, st9 to st22) submitted to high throughput EST sequencing (coordinated by S. Mazan at the Observatoire Océanologique, Banyuls, France). Sense and antisense digoxigenin-UTP-labeled probe were synthesized directly by in vitro transcription using as templates cDNA fragments prepared by PCR amplification. The procedure was carried out following standard protocols [for details, see Coolen et al., 2007, and Ferreiro-Galve et al., 2012]. Briefly, the sections were permeabilized with proteinase K, hybridized with sense or antisense probes overnight at 65 °C, and incubated with alkaline phosphatase-coupled anti-digoxigenin (1/2,000; Roche Applied Science, Mannheim, Germany) overnight at 4°C. The color reaction was performed in the presence of BM-Purple (Roche)

containing levamisol. Finally, sections were dehydrated and coverslipped. Hybridization with the control sense probe did not produce any detectable signal.

Combination of immunohistochemistry for DCX with ISH was performed on sections of stages st20 and st24 embryos processed *in toto* for ISH with *ScWnt8* (a gene specifically expressed in rhombomere 4: Rodríguez-Moldes et al., 2011) and with *ScSox2*. After colorimetric detection of probes, embryos were sectioned on a cryostat in sagittal plane at 18–20 µm thickness, rinsed three times in 0.1M PBS for 10 min each and treated for immunohistochemistry for rabbit anti-DCX as described above. For details, see Rodríguez-Moldes et al. (2011).

Micro-computed tomography

Micro-CT analysis of embryos at stages 20, 24, 25, 27, 29, 31 and 32 was performed for comparison with the sectioned material. Methanol-stored embryos were stained with 1% phosphotungstic acid (PTA) in methanol for 4 days and transferred again to absolute methanol. The scans were performed with a Bruker Skyscan 1172 microtomograph of the Marine Biology Station of the University of Santiago de Compostela at A Graña (Spain) and images were reconstructed

with Recon software and processed with CTAnalyzer software. CTVox and DataViewer software were used for displaying data and obtain serial images along the three axis and three-dimensional (3D) images and videos of the samples.

Imaging

Photographs were taken with an Olympus DP71 color digital camera, fitted to a Provis photomicroscope (Olympus, Tokyo). Sections of embryos at stages 31 and 32 were also analyzed and photographed with an Olympus microscope equipped with Nomarski's differential interference contrast optics (DIC). This imaging technique provides a pseudo three-dimensional appearance of the sample based on the light interference effect that causes that one side of the sample shines while the other side appears darker, allowing the clear appreciation of low-contrasted structures.

RESULTS

The main components of the adult inner ear of *S. canicula* are developed and easily recognizable since late embryos at stage 32 onwards (chapter 2 and present results). The adult inner ear comprises three semicircular canals that present a single dilation, the canal ampullae, each one with its corresponding crista, and the two main ventral chambers, the utricle and the saccule, the latter with the lagena at its caudal end and the utricle with the utricular recess, a rostral bulbous protrusion with lies below the junction of the anterior and horizontal canals. Each one of these chambers and ampullae contains a sensory organ (macula and crista, respectively) innervated by nerve branches of the statoacoustic ganglion. There is also a sensory patch, named *macula neglecta*, located in the edge between the utricle and the saccule, next to the *ductus canalis semicircularis* or posterior semicircular canal duct which communicates the saccule and the posterior canal. Contrarily to the saccular, lagenar and utricular maculae, the macula neglecta is not covered by otoliths or otoconia. The ultrastructure and organization of hair cells of the adult inner ear in *S. canicula* has been studied by scanning electron microscopy by Lovell et al. (2007) and in the shark *Carcharhinus sp.* by Tester et al. (1972) and Corwin (1977), where the precise study reveals that the

presumptive macula neglecta is divided in two sensory patches, something similar to what occurs in many osteichthyans and amphibians.

In order to establish an outline for comparative studies, we have distinguished three periods in the development of the inner ear of the *S. canicula*, based on external features and landmark events, and in the inner ear morphogenesis (chapter 2). In the *first period* (stages 18 to 25), the otic placode invaginates to form the otic pit/cup, which deepens and originates the otic vesicle or otocyst, a spherical cavity surrounded by the otic epithelium. During the *second period* (stages 26 to 31), the cavity and walls of the otocyst expands to form the three semicircular canals and the two large sacks, the saccule (with the lagena) and the utricle, basic structure shared by all the gnathostomes with more or less changes and specialized components. Once the inner ear reached a shape similar to that observed in juveniles, a period of maturation and further growing occurs, the *third period* (stages 32 to 34, prehatching), which has been analyzed here in relation to the earlier periods.

On the basis of expression of immunoreactivity to DCX (expressed in migrating immature neurons and their growing fibers), PCNA (proliferating cells) and HuC/D (early postmitotic

neurons) and that of mRNA of selected developmental genes as *NeuroD* (marker of placode-derived cranial sensory ganglia as SAG) and *Sox2* (expressed in sensory patches) in significant stages, we provide here a cytological and histological description of the main events that take place during the development of the catshark inner ear. We have framed the descriptions of the inner ear into the above mentioned developmental periods, which may serve as a reference for comparative developmental studies.

First period: from otic placodes to otocysts. Stages 18 to 25

The otic placode of **stage 17** *S. canicula* has been at by O`Neill et al. (2007) as "the thickened surface ectoderm by the hindbrain" that presents strong expression of *Pax2*, a paired domain transcription factor known as an early otic placode marker. The micro-CT analysis of *S. canicula* embryos has shown the first morphological signs of invagination of the otic placode at **stage 18** (chapter 2), here considered as the beginning of the first period. At **stage 19**, the primordial SAG is morphologically visible, as demonstrated with micro-CT analysis (chapter 2). At this stage, O'Neill et al. (2007) reported robust expression of *ScNeuroD*, a pan-neuronal marker, in

scattered cells dorsal to the second pharyngeal arch which they considered neuroblasts of the otic placode-derived statoacoustic ganglion (the vestibuloacoustic or VIII ganglion following the nomenclature used by O'Neill et al., 2007).

A previous work of our group on *S. canicula* (Rodríguez-Moldes et al., 2011), showed that in st20 and st24 embryos double-labeled for *ScWnt8* ISH and DCX immunohistochemistry, the DCX-immunoreactive (ir) fibers of the statoacoustic-facial (VII–VIII) nerve exited the hindbrain from rhombomere 4 (r4). A closer re-analysis of such sections, which were obtained in unconventional (midparasagittal/ midhorizontal) planes, reveals that at **stage 20** the otic cup is very close to r4 and to the second pharyngeal arch. Interestingly, some DCX-ir processes appear to join this rhombomere and the otic epithelium (Figs. 1A-C, arrows). Since at this stage the primordial SAG is localized slightly ventral and rostral to the otic cup (Figs. 1D-G), we have identified these few DCX-ir fibers as processes of neuroblasts delaminated from the otic epithelium forming the primordial SAG. Because the scarcity of DCX-ir processes observed in this epithelium, we considered the stage 20 as the beginning of the innervation of the otic cup. At least in part, DCX-ir processes observed at the floor of r4 could belong to the statoacoustic-facial (VII–VIII) nerve roots.

Later in development, at **stage 24**, the presence of DCX-ir processes innervating the otic epithelium is more evident and also in the SAG (Figs. 1H-J). Some DCX-ir ganglion cells in the SAG appear to be the origin of these processes (Fig. 1J). Sagittal sections show a bundle of DCX-ir processes reaching the ventral wall of the otic cup, as well as an important immunoreactivity at the rostral region of the SAG (Figs. 1J, arrowheads). At this stage, we evidence strong *ScNeuroD* expression in the otic epithelium at different levels (Fig. 1K, white and black arrows) and in a mass of cells just adjacent to the ventromedial wall of the otic pit that extends anteriorly, as observed in sagittal sections (Fig. 1K, white arrowheads). This *ScNeuroD* expressing mass of cells appears to correspond to the SAG reported by O'Neill et al. (2007) in a transverse sections of st 24 embryo of *S. canicula* (their Fig 6F). *ScNeuroD* expressing cells have not been described by these authors in the epithelial walls but, interestingly, our results reveal strong *ScNeuroD* expression in scattered cells in the caudodorsal (Fig. 1K, black arrow) and ventrorostral regions of the otic epithelial walls, just adjacent to the SAG (Fig. 1K, white arrow). Micro-CT images at equivalent levels allow to precise the position of the SAG in relation to the otic epithelium (Figs. 1L-O).

At **stage 25**, the innervation of the otic epithelium by DCX-ir processes extends along the ventral part of the just formed vesicle, as can be seen in a series of transverse sections from rostral (Fig. 2A), medial (which correspond with the position of the endolymphatic duct, Fig. 2B) to caudal (Fig. 2C, D**,** arrowheads) levels. There are two main fascicles of DCX-ir fibers entering the otocyst, a rostro-lateral one (Fig. 2A, arrowhead in the detail) and a caudo-medial one (Fig. 2C, arrowhead in the detail). These two fascicles branch off into the epithelia extending as thin branches among the epithelial cells at medial (Figs. 2B, arrowheads in detail) and caudal (Figs. 2C, arrow in detail) levels. At these stage, abundant DCX-ir cells can be seen in the SAG (empty arrowheads in Fig. 2D) among some immunonegative elements. The expression of *ScNeuroD* remains intense in the SAG (Fig. 2E-G, star) and in scattered epithelial cells at the ventral wall of the otic vesicle just adjacent to the SAG (Fig. 2E-F, arrowheads). The location of *ScNeuroD* expressing cells in this ventral wall of the otic vesicle is restricted to the region adjacent to the SAG, and their number, density and intensity decrease notably in the borders of such ventral wall juxtaposed to the SAG (Fig. 2G). The micro-CT analysis is very useful to interpret the spatial organization of the inner ear components labeled with the aforementioned markers. It is evident the spherical shape of the otocyst (Figs. 2H-J) with

the endolymphatic duct arising from the medial wall of the vesicle (Figs. 2H, I; white arrowheads). It is also useful to appreciate the position of the SAG, adjacent to the ventrorostral wall of the vesicle (black star in details of Figs. 2H-I,), but not to its caudal part (Figs. 2J), where expression of *ScNeuroD* which corresponds to the level of figure 2G.

Second stage: the otocyst and the origin of the canals and chambers. Stages 26 to 31.

At **stage 27**, the early morphogenetic events that subdivide the vesicle are evident (see chapter 2). Changes in the otic epithelial walls that lead to the formation of semicircular canals are also seen in transverse and sagittal sections treated for distinct molecular markers (Figs. 3A-N). At this stage, we have observed immunoreactivity to PCNA in the lateral wall of the otic vesicle (Fig. 3A-C; arrowheads), and also in some cells of the SAG that are located in the interface with the otocyst (Fig. 3A-B; arrows). PCNA-ir cells appear absent from the ventral and ventromedial epithelial walls which, as seen in previous stages, contain DCX-ir processes that innervate groups of epithelial cells probably corresponding to primordial sensory patches (Figs. 3D-F, arrowheads). The SAG, which contains dense DCX immunoreactivity (Figs. 3D,E, star), presents early

differentiated neurons, as revealed by the abundant cells labeled with the HuC/D antibody (Figs. 2G-I, arrowheads), which contrasts with the lack of labeling in the otic epithelial walls (Figs. 3G-I). As in previous stages, the expression of *ScNeuroD* remains strong in the SAG (Figs. 3J-N, arrows). The density of cells expressing *ScNeuroD* in the epithelial sensory patches seems higher than in previous stages, especially in the ventrorostral walls (Fig. 3L, arrowheads). Interestingly, a patch of *ScNeuroD* expressing cells is observed in the dorsal walls (Fig. 3N, empty arrowheads), which could correspond to the patch of primordial sensory cells that form the crista of a semicircular canal. The comparison with micro-CT images (O-S) allows to confirm that this dorsal patch of *ScNeuroD*-expressing cells is related to the primordial posterior semicircular canal (PSC), which is formed at this stage (Fig. 3Q, arrow). The analysis through micro-CT also reveals important morphological changes suffered by the otocyst at this stage that will subdivide it into chambers and canals, being anymore a simple sphere (Figs. 3O-Q). The growth of protrusions within the lumen, which appears to happen similarly to that observed in teleosts (Becerra and Anadón, 1993a; Haddon and Lewis, 1996), leads to the formation of a first column (Fig. 3Q, arrowhead) that delimitates the first semicircular canal in this species, the posterior semicircular canal (PSC) (Fig. 3Q, arrow). Buds of the

chambers and of the lateral (horizontal) semicircular canal (HSC) are appreciable too.

At **stage 29**, the subdivision of the otocyst into three chambers (see chapter 2) is quite evident even in sections stained for immunomarkers (Figs. 4A-L). PCNA immunoreactivity is intense in some regions of the otic vesicle epithelium (Figs. 4A-D, arrowheads). These highly proliferating areas correspond to the primordial ampullae of growing semicircular canals, being noticeable the strong PCNA immunoreactivity in the anterior ampulla (Figs. 4A, B; arrowheads) and in the horizontal and posterior semicircular canals (HSC and PSC, respectively**).** The identification of such canals is facilitated by the comparison with micro-CT images (sections in Figures 4A and B correspond to levels between Figures 4M and N, and C and D, roughly related with the levels of sections in Figures 4O and P). The PCNA immunoreactivity is also remarkable in the developing chambers as revealed the intense labeling in the medial wall of the saccule (Fig. 4C). Despite this wide and intense immunoreactivity to PCNA along most of the epithelium, there is a striking lack of PCNA labeling in some areas where the epithelial walls appears notably thick, which correspond to the primordial sensory patches (Figs. 4A, B, C; arrows). The comparative analysis with micro-CT images,

at this stage (Figs. 4M-Q) also suggests that these areas lacking proliferating cells correspond with sensory patches. As in previous stages, some PCNA-ir cells are seen in the SAG (star), especially in its dorsal borders (Figs. 4A, B; empty arrowheads). The distribution of DCX-ir processes in the otic epithelium is much wider than in previous stages (Figs. 4E-H). Numerous DCX-ir processes enter different regions of the otic epithelium. Such regions correspond to the sensory patches of the semicircular canals (cristae) and vestibular chambers (maculae). The anterior ampulla is innervated by DCX-ir processes coming from a rostral DCX-ir bundle (Fig. 4E) that spreads into thin fibers that appear to end on cells of the sensory primordium (arrowheads in upper detail of Fig. 4E). At intermediate levels, a lateral bundle is appreciable below the bud of the horizontal semicircular canal (Figs. 4F, G) and also extends as thin DCX-ir fibers into the epithelium (Fig. 4F, arrowheads in upper detail). Another bundle of DCX-ir fibers courses from the SAG and enters the primordial sensory patch at the medial wall of the saccule (arrowheads in the lower detail of Fig. 4F). The posterior semicircular canal receives also DCX-ir bundles from the SAG at this stage (Fig. 4 H, arrowhead), which also enter deeply in the thickened otic epithelium. The SAG at this stage presents intense DCX immunoreactivity (Figs. 4E, F, arrows), as it is also observed at the rear branch of the otic nerve (Fig. 4G,

arrow) and at the glossopharyngeal nerve (Fig. 4H, arrow). The SAG shows higher HuC/D immunoreactivity than in previous stages (Figs. 4I, J; arrowheads) but, like in earlier stages, HuC/D immunoreactivity is absent in the otic vesicle (Figs. I-L, asterisks). The analysis through micro-CT at this stage helps to recognize the striking morphological changes that led to the subdivision of the otocyst (Figs. 4M-P). Later to the previous formed PSC, the bud of the HSC is quite elongated (Figs. 4N, O, white arrowheads), as well as the endolymphatic duct (Fig. 4N).

By the **stage 31**, the inner ear presents an almost mature aspect, being clearly subdivided (see chapter 2). This stage has been selected as representative of the late events of the otic vesicle and SAG differentiation. Cell proliferation is extensive in the thin epithelial walls as revealed by the presence of areas with numerous PCNA-ir cells (Figs. 5A-D, arrowheads). As in the previous stage described, the expression of PCNA is absent from the sensory patches (Figs. 5A, B, arrows). DCX-ir fibers are clearly innervating specific regions of the inner ear (Figs. 5E-J). Several DCX-ir bundles can be followed from the SAG to the otic epithelia. Some enter rostrally (Figs. 5E, F, arrowheads) and reach the anterior ampulla and the utricular recess walls to branch in thin fibers that innervate the sensory patch of the ASC (arrowheads in upper detail of Fig. 5F) and the primordial

utricular macula (arrowheads in lower detail of Fig. 5F). At intermediate levels, some thin DCX-ir fibers are innervating the primordial saccular macula (black arrowheads in lower detail of Fig. 5G), very close to the rear branch of the statoacoustic and glossopharyngeal nerves (empty and white arrowheads in lower detail of Fig. 5G, respectively), which are also labeled for DCX. In addition, intense DCX immunoreactivity is observed in a newly formed region that protrudes in the edge between the utricle and the saccule (Fig. 5G, arrow). On the basis of its localization, we interpret this area as corresponding to the primordial macula neglecta, which is very close to the duct that communicates to the PSC, similar to that observed by Tester et al. (1972) in adult *Carcharhinus.* Some DCX-ir fibers from the rear branch of the statoacoustic nerve reach the PSC and innervate the posterior crista (Fig. 5H, empty arrowhead), close to the rear part of the glossopharyngeal nerve (Fig. 5H, white arrowhead). The pattern of innervation of DCX-ir fibers along the otic epithelium (Figs. 5I-J, black arrowheads in details) is strikingly coincident with the expression of the gene *Sox2*. The coincident expression is clearly appreciated in the epithelium of the chambers, as the presumptive saccular macula and utricular recess walls (Figs. 5J, empty arrowheads in detail), and also in the ASC and HSC (Figs. 5I and J, empty arrowheads in details). A detailed analysis of the epithelium in these areas that contain

Sox2-expressing cells and DCX-ir innervation reveals that DCX-ir processes extend to apical epithelial levels, and that not all cells at the patches are expressing *Sox2* gene (Figs. 5I, J and details). Moreover, there found no evidences of superficial structures corresponding with differentiated hair cell ciliary bundles even in images taken with differential interference contrast (DIC) microscopy (Figs. 5I´, J). As in previous stages, HuC/D-ir cells are abundant in the SAG (Figs. 5K-M; arrowheads) but they are lacking in the epithelial walls of the inner ear (Figs. 5K-N, asterisks). The visualization of the inner ear at this stage through micro-CT (Figs. 5O-R) evidences the complex morphology reached by the ear, with all the canals and chambers clearly visible, even the utricular recess walls (Fig. 5P).

Third period: from stage 32 onwards.

By **stage 32**, the subdivision of the labyrinth has been completed and presents a mature aspect quite similar to that in posthatching stages. As in previous stages, there is immunoreactivity to PCNA in several parts of the otic epithelium (Figs. 6A-C, black arrowheads). Interestingly, at this stage there are some PCNA-ir cells within the thickened epithelium of the developing sensory patches of the ASC (empty

arrowheads in Fig. 6 A´ and detail of Fig. 6A), the HSC (empty arrowheads in upper detail of Fig. 6B) and the PSD (Fig. 6D, empty arrowhead). Remarkably, this proliferating event in the sensory patches of cristae takes place once the canals are formed and the patches receive afferent fibers. Cell proliferation also persists in the SAG (arrowheads in the lower detail of Fig. 6B) and in the otic nerve (arrow in detail of Fig. 6C). The immunoreactivity to DCX is widely distributed along the inner ear. The anterior crista is innervated by thin DCX-ir bundles that spread in fine processes that ascend into the crista (arrowheads in detail of Fig. 6E). The intermediate region of the inner ear shows abundant DCX-ir fibers (Fig. 6F, arrowheads) that innervate the sensory patches at the utricular (white arrowheads in the left lower detail of Fig. 6F) and saccular maculae (white arrowheads in left upper detail of Fig. 6F). The macula neglecta also presents an intense innervation by DCX-ir fibers (Fig. 6G, white arrowheads). The SAG also maintains the immunoreactivity to DCX (arrowheads in right detail of Fig. 6F), which is also appreciable in the glossopharyngeal nerve (Fig. 6H, arrow). In the caudal region of the inner ear, the posterior canal ampulla receives DCX-ir fibers (detail in Fig. 6H, black arrowheads) which extend till the surface of the posterior crista (white arrowheads in detail of Fig. 6H). The distribution of the HuC/D-ir cells remains as in previous stages,

being intense in the SAG (Figs. 6I-K, stars), but lacking in the otic epithelium (Figs. 6I-K, asterisks). A detailed observation of the sensory areas at this stage reveals the maintenance of the expression of *Sox2* in thickened areas of the otic epithelium (Figs. 6L, M ,N and black arrowheads in details) but, interestingly, such expression seems to have been lost in small patches of cells (arrows in detail of Fig. 6M). In contrast to the former stage, the apical surface of these regions presents a noticed density of structures that may correspond to ciliary bundles of sensory hair cells as revealed by the images obtained with the differential interference contrast (DIC) optic (empty arrowheads in details of L, M and N). The analysis of the inner ear with micro-CT at this stage reveals a very complex structure with a mature-like aspect (Figs. 6O-S). It is noticeable the protrusion of the three cristae within the ampullae (Figs. 6O, P, R, arrowheads), and also the wide spaces filled of very loose mesenchyme and perilymph between the cartilage and the membranous labyrinth in some regions, as over the utricle (Fig. 6M) or lateral to the saccule (Fig. 6N).

DISCUSSION

The use of molecular markers is generalized in developmental studies of the inner ear in model organisms as mouse, chick or *Xenopus*. In fishes, such studies have been almost exclusively restricted to zebrafish (Waterman and Bell, 1984; Haddon and Lewis, 1996, 2002; Bever and Fekete, 2002), which is considered the canonical fish model for developmental studies and, for this, representative of all fish groups. The ancient and highly diversified group of “fishes” includes both the cartilaginous and bony fishes, which show often highly divergent features. Taking into account the great differences that exist between both groups, the use of a single teleost species to represent the largest vertebrate group is clearly limiting. On occasions, there is an excessive use of the term fish in the literature. In some cases, the article titles create false expectative talking about the fish inner ear despite they only contains data about teleosts species (as an example, see Vasconcelos et al., 2016). In other cases, particular events that happen in zebrafish, such as the formation of the otic vesicle by cavitation, are presented as a generalization for all fishes (see Whitfield, 2015, as an example), despite that in cartilaginous fishes the process takes place by invagination and eventual pinching off, as it

happens in amphibians, birds and mammals (Haddon and Lewis, 1991, 1996; Magariños et al., 2012).

In the last decade, a number of developmental studies have been performed in *Scyliorhinus canicula*, and this shark became a reliable biological model representative of chondrichthyans or cartilaginous fish (Coolen et al., 2009). Its coastal abundance, protracted development and the relative large size of the embryonic structures permit to study in detail some developmental processes that could be disregarding in species of rapid development and small size, like zebrafish. Such studies have provided abundant information about the main developmental events in cartilaginous fishes, and helped to better understand the similarities and differences with other model organisms (revised in Rodríguez-Moldes et al., 2017).

Some studies on the evolution of the genetic control of the development of cranial neurogenic placodes and cranial sensory ganglia in vertebrates have provided important information about the early development of the otic placode and derived sensory ganglia in *S. canicula* (O'Neill et al., 2007; Baker et al., 2008). However, there are no comprehensive studies about the development of the inner ear in *Scyliorhinus* or other chondrichthyans, in spite of the importance that this fish group

has to deepen in the knowledge about the development of vertebrates from an evolutionary perspective.

Main developmental events in the catshark inner ear

The present results agree with the observations of O'Neill et al. (2007) in the same species and extend them considerably with regards the ear development. The *S. canicula* inner ear develops from the otic placode, an ectodermal thickening adjacent to the rhombomere 4, which will suffer significant morphogenetic changes. Firstly, the otic placode invaginates into the underlying mesenchyme to form the otic cup or pit, which separated from the skin epithelium and finally will form a spherical epithelial vesicle, the otocyst. Then, the vesicular walls will expand and reorganize to form the membranous labyrinth, a sophisticated structure formed by a series of canals and chambers disposed in a complex three-dimensional arrangement. As previously defined (chapter 2), the events that form the otocyst and SAG from the otic placode, happen during the FIRST PERIOD (*invagination of the otic placode and eventual pinching off to form the otic vesicle or otocyst*). The beginning of the invagination of the otic placode and the eventual closing and pinching off of the otic cup, are comprised in the first period. The formation of the SAG takes place in parallel to the

otocyst formation, the epithelial and ganglionic cells sharing the same placodal origin. Taking into account that signs of invagination of the otic placode are appreciable at stage 18 (chapter 2) but not at stage 17 (O`Neill et al., 2007), we have proposed the stage 18 as the beginning of the first period, ending in the stage 25. The morphological changes taking place from the closure of the otic cup to the mature-like aspect with all the chambers and semicircular canals well differentiated at the end of stage 31 are comprised in the SECOND PERIOD of the inner ear development *(morphogenesis of the chambers and semicircular canals)*. The beginning of the elongation of the dorsal opening of the vesicle into the endolymphatic duct and the emergence and growth of different internal protrusions that eventually fuse and subdivide the otocyst, as seen in chapter 2, establish the beginning of this period. The growth of protrusions creating constrictions between different parts of the otocyst and the proliferation of cells along several areas of the otic epithelium, as reported above, increase the separation of certain areas (i. e., between the utricle and the saccule) leading to the acquisition of a mature-like morphology at the end of this period, in which the innervation pattern of the sensory patches is completed. We have proposed the stage 32 as the beginning of the THIRD PERIOD of the inner ear development *(maturation and growing of the inner ear)* in which the morphological

mature aspect has been reached. The present results provide cytological support for considering the stage 32 as the earliest with visible differentiated sensory patches in the membranous labyrinth.

Formation of the statoacoustic ganglion

The presence of DCX-immunoreactive processes contacting with the otic epithelium and extending into the mesenchyme between the ventromedial walls of the developing inner ear and hindbrain floor (rhombomere 4) at very early stages (st20, early placodal invagination), reveals the appearance of migrating bipolar neuroblasts that appear to delaminate from the ventromedial level of the otic epithelial walls, sending both peripheral and central primordial processes. This marker has previously evidenced the earliest delaminated neurons of the olfactory placode of *S. canicula* (Quintana-Urzainqui et al., 2014) and it has been consistently used in this shark as a marker of migrating neuroblasts (immature neurons) and their growing fibers, as well as a marker of pioneer tracts during brain development (Pose-Méndez et al., 2014; Santos-Durán et al., 2016). Our observations appear to reveal the presence of delaminated neuroblasts of the primordial SAG at st20, taking into account the scarcity of DCX-ir processes in the epithelium

compared with later stages and the short extension of the invasion. If these neuroblasts are the first delaminating cells cannot be confirmed because, unfortunately, we could not analyze stages earlier than s20. Anyway, using the *NeuroD* expression as a marker of cranial sensory ganglia, O'Neill et al. (2007) have described in *in toto* stage 19 embryos of *S. canicula* "a salt-and-pepper patch of robust *NeuroD* expression by the otic developing vesicle" that they interpret as neuroblasts of the otic placode-derived statoacoustic (VIII) ganglion (the vestibuloacoustic or VIII ganglion following the nomenclature used by O'Neill et al., 2007) and of the anterodorsal lateral line ganglion. They do not present results at st20 but at stage 21 they distinguish a dense patch of *NeuroD* expression ventral to the rostral half of the open otic vesicle that belongs to the forming statoacoustic ganglion, and the anterodorsal lateral line placode-derived neurons. Moreover, at st21 O'Neill et al. (2007) also show strong expression of *Tbx3* in the developing otic placode and in the statoacoustic/anterodorsal lateral line ganglionic complex located rostral to it. Thus, although results of O'Neill et al. (2007) correspond to *in toto* embryos and sections appear necessary to check it, as regards the *NeuroD* expression in relation to the developing SAG, it seems that during st19 the earliest events of neuroblast delamination from the otic placode/ pit take place. We interpret that the epithelial cells expressing

ScNeuroD that are close to the SAG represent delaminating neuroblasts and those in the SAG, as cells migrating away from the otic pit to form sensory neurons, similarly to that reported in mouse embryos at E10.5 (Kim et al., 2001). It is interesting to note that these early-delaminated neuroblasts maintain contact with the epithelium from which they originate by means of thin processes, which probably represent the primordial afferent innervation of the otic sensory epithelium.

Later in development, when the placodal invagination is advanced (at st24), the DCX-ir innervation in the otic epithelium has increased, as well as the density of DCX-ir fibers in the bundles that connect the epithelium with the cluster of peripheral DCX-ir neuroblasts. Based on its position, just adjacent to the basal epithelial walls, this cluster corresponds to the primordial SAG described by O'Neill et al. (2007) at the same stage. Since these early embryonic stages, it is possible to recognize fiber bundles emerging from the SAG and projecting to different parts of the otic epithelium (see below).

As development progresses, once the otocyst has been closed, the SAG appears as a compact mass. The presence of HuC/D positive cells at st27 (the earliest analyzed with this immunomarker) indicates that at this stage the SAG contains

young ganglion neurons (early differentiated). Moreover, the coexistence with *ScNeuroD*-expressing cells and DCX-ir neuroblasts suggests the presence of different stages of ganglion cell differentiation in the SAG at this developmental stage.

Innervation pattern during catshark inner ear development

As soon as in stage 20, it is possible to appreciate DCX-ir processes relating the rhombomere 4 (identified by its *ScWnt8* expression; Rodríguez-Moldes et al., 2011) and the otic vesicle epithelium. We have interpreted these processes as belonging to the ganglionic neuroblasts that constitute the primordial SAG and that would be linking the inner ear to the brainstem. Although our results do not allow to confirm the ganglionic origin of these peripheral DCX-ir processes, we consider that most, if not all, belong to delaminated neuroblasts originated from the otic pit/vesicle that are sending processes to both the otic epithelium and the brainstem (r4). Fibers of the inner ear efferent system originate from r4 neurons in all vertebrates studied and they are closely associated with facial motor neurons (reviewed in Simmons 2002; Fritszch and Elliot, 2017). Moreover, developmental studies in mice have shown that the cochlea is innervated by efferent (centrifugal) fibers since as

early as in E12 embryos (Fritsch and Elliot, 2017). Thus, the possibility that part of the DCX innervation of the otic epithelium observed in shark corresponds to early differentiated octavolateralis efferent fibers cannot be ruled out. In the adult catshark, the statoacoustic ganglion neurons appear to outnumber the efferent octavolateralis neurons revealed by tract tracing and choline acetyltransferase immunohistochemistry (Meredith and Roberts, 1986; Anadón et al., 2000). Taking into account the early development of primary ganglionic neurons of the SAG and the abundance of these cells from early development, as revealed markers of early neuronal differentiation as HuC/D and DCX, led us to consider that most the DCX positive innervation of the otic epithelium at early development form part of the afferent system from the SAG.

By stage 25 it is possible to recognize the two main DCX-ir bundles emerging from the SAG as part of the afferent system, which branch and project to anterior and posterior regions of the otic vesicle. The early evidence of these two projections may correspond to the earliest steps of the formation of the anterior and posterior branches of the octaval nerve described in the adult *S. canicula* by Boord and Roberts (1980). Although we have not studied adults and the st25 represents an early developmental stage in which the chambers and canals of the

inner ear are not morphologically identifiable yet, it is coherent with the major pattern innervation described by Boord and Roberts (1980) in elasmobranches, and also in most non-mammalian vertebrates (by other authors): The statoacoustic nerve presents two rami: an anterior ramus that innervates the anterior and horizontal cristae, the utricular macula and the anterior region of the saccular macula; and a posterior ramus that innervates the posterior region of the saccular macula, the posterior crista, the lagenar macula and the macula neglecta. At the adulthood, both rami are intermixed and cannot be separated (reviewed in Smeets et al., 1983).

As development progresses, the increasing number of DCX-ir bundles related to the otic epithelium at discrete thickened areas in the otic epithelial walls may correspond to prospective or developing sensory patches, which contain *Sox2*-expressing cells and non-proliferating cells (see below). The thin DCX-ir fibers that innervate these areas come from peripheral DCX-ir bundles that course between the otic vesicle and the SAG. Thin DCX-ir fibers extend mainly throughout the basal part of the epithelium at such discrete areas but, interestingly, some DCX-ir fibers extend laterally among the epithelial cells, even reaching apical levels of the epithelium. Although more studies are needed to confirm it, the present results are compatible with the

existence of cup-shaped nerve endings surrounding hair cells. Cup-shaped afferent endings (or calyces) located at the base of hair cells, reminiscent to those found around type I hair cells of amniotes, have been characterized in the crista of goldfish (Landford and Popper, 1996).

Formation of the sensory organs

The markers used in this study highlight the existence of morphogenetic changes in the epithelial walls of the otic cup and vesicle that involve expansion in some areas and thickening in others. These changes in the otic vesicle walls are concurrent and clearly related to the formation of the SAG and involve the differentiation of epithelial cells into the different cells types that conform the mature inner ear in chondrichthyans, including sensory (mechanosensory hair cells), and non-sensory cells (such as the support cells of sensory areas and the covering and specialized cells of other parts of the otic epithelium).

The region of the otic cup/vesicle adjacent to the SAG of *S. canicula* contain cells that express the proneural transcription factor *NeuroD*, as seen in sections of the embryos processed for this marker from st24 to st27 (present results) and even in *in toto* embryos (see fig 3E of a st24 in O'Neill et al., 2007). In this

st27 and later in development (stages 29 and 32), neither this region nor other regions of the epithelium contain cells immunoreactive to HuC/D, a marker of early postmitotic neurons, which contrasts to that observed in the SAG that is plenty of HuC/D-ir cells at the stages studied (st27, st29, st31, st32). This observation is indicating that the only primary neurons that differentiated in the inner ear are those of the SAG, similarly to that observed in other vertebrates. The expression of *NeuroD* in the region of the developing inner ear that is source of delaminating neuroblasts is related to the critical role that this transcription factor has in the survival, migration and correct organization of neuronal cells in differentiation in the VIIIth nerve ganglion (Lui et al., 2000; Kim et al., 2001; Huanng and Reichardt, 2003; Kim, 2013). Taking into account such a role of *NeuroD*, its expression in the epithelial region of the catshark otic cup/vesicle just adjacent to the SAG, and the evidence of the two main DCX-ir branches innervating the inner ear from the SAG (present results), we consider that this region originates the neurons of the SAG that innervate the anterior and horizontal cristae, and the utricular and saccular maculae. In addition, our systematic study of serial sections of embryos from stage 24 (vesicle almost closed) to 27 (expansion of the walls to form the pouches of the semicircular canals) processed with the *ScNeuroD* probe, has revealed the existence of epithelial regions

that contain cells expressing *NeuroD* at levels apparently not related to the delamination of neuroblasts to form the SAG. A dorsal region is well recognized in the st27, when the expansion of the otocyst walls is evident and the first signs of the formation of semicircular canal are evident. As far as we known, expression of *NeuroD* has not been reported in inner ear regions not related to delamination of neuroblasts and SAG formation. So, the existence of such singular expression in this region in the catshark could be revealing a different role of NeuroD in the shark inner ear. Other possible interpretation is that the growth of the epithelial walls could have exposed dorsally some regions of the *NeuroD* expressing area observed ventrally at earlier stages. In fact, on the basis of the position, and the relation of the presumptive sensory patches with the areas innervated by DCX-ir fibers (see above), this dorsal *NeuroD*-expressing epithelial region could correspond to the primordial sensory patch of a semicircular canal, perhaps the PSC, which is formed at this stage. Thus, we interpret that this dorsal *NeuroD* expression domain may be related to the posterior crista. The appearance of hair cells in an anterior and a posterior pole in the otocyst of zebrafish (Haddon and Lewis, 1996) points in the same way.

While peripheral neuroblasts (DCX-ir) could be identified at the earlier otic cup stages and mature neuronal cells (HuC/D-ir) are present in the SAG at least from stage 27, we could not assess the differentiation progress in the presumptive or primordial hair cells in the sensory patches, neither maculae nor cristae, with the present markers. However, we have seen that the proliferating cells revealed with PCNA are very abundant along the development of the inner ear at several epithelial regions, but seemed to be absent at the developing sensory patches, which may suggests that the differentiation process of sensory cells is taken place. Particularly, at stage 29, we have identified patches of cells in areas of epithelial thickening that contain PCNA-immunonegative cells, in contrast with the adjacent thinner epithelial walls whose cells are PCNA-immunoreactive at this stage and probably correspond to areas of epithelial expansion. The temporal coincidence between the loss of PCNA immunoreactivity and the detection of differentiation markers such as cyclin-dependent kinase inhibitors has led to consider the loss of PCNA immunoreactivity in cells during development as a sign of differentiation (Ngûyen et al., 2001). Then, the cell patches observed in serial sections of embryos at stages 29 and 31 by their PCNA-immunonegativity may represent areas of postmitotic (differentiating) cells related to sensory patches

forming the hair cells of cristae and maculae. These patches of PCNA-negative cells appear to correspond to areas of DCX innervation, as revealed by a comparative analysis of parallel sections (compare figs 4A and E), although double labeling is necessary to confirm it. It is interesting to note that coinciding with the completion of the complex three-dimensional organization of the labyrinth, when the maturation period starts (st32, beginning of the third period) some sparse PCNA-ir cells could be distinguish in the thickened epithelium of the maculae and cristae. The presence of proliferating cells in the sensory areas could be related to the continuous and proportional growth of the inner ear in later development (and after hatching). It is important to note that concurrently, the epithelial cells in the sensory areas have developed superficial structures probably corresponding to hair cell ciliary bundles, as suggest the filiform protrusions that can be seen at this stage (but not earlier) with the DIC imaging (Figs. 6A, A´). This could mean that the differentiation of the hair cells takes place relatively late, when the canals and cavities of the inner ear are completely formed.

Double labeling experiments have shown that in the catshark, the undifferentiated sensory patches of the embryonic stage 31 can be characterized by their content in cells that express *Sox2* and the abundant DCX-ir innervation that extends

laterally among the differentiating cells, perhaps forming nerve structures similar to afferent calyces contacting hair cells in amniotes (see above). The incidence of the expression of *Sox2* within those immature differentiating sensory patches innervated by the DCX-ir fibers agrees with the role of *Sox2* in the differentiation of the sensory patches in amniotes, where its induced expression is enough to promote the formation of ectopic hair cells (Neves et al., 2011, 2013). The neuronal induction and sensory repression by the interaction of *Sox2* with neurog1/neuroD may explain the apparent incoherence between the role of *Sox2* maintaining the pluripotency state but also inducing differentiation (Neves et al., 2013). The expression of *Sox2* in the sensory patches before the appearance of hair cells in stage 31 but also in the same regions after the differentiation of the first hair cells, agrees with that observed in other species (Millimaki et al., 2010; Neves et al., 2013). Future studies implying the deletion of *Sox2* in the catshark appear necessary to determine if its misexpression causes reduction in hair cells production as in the mouse (Millimaki et al., 2010) or if it does not affect it, as in the zebrafish, where *Sox2* knockdown did not completely block the generation of hair cells, but it seemed essential for the surveillance of the supporting cells (Millimaki et al., 2010). *Sox2* has also been proposed as necessary for the maintenance of the pluripotency of the support cells of the inner

ear. In fact, the regeneration of hair cells in certain species as the zebrafish occurs by transdifferentiation of supporting cells, but not by cell division, and *Sox2* seems necessary for such transdifferentiation and therefore, for the regeneration of the hair cells (Millimaki et al., 2010). So, in this fish species, the role of *Sox2* in the differentiation of hair cells may not be essential, but it seems to be crucial for the transdifferentiation of supporting cells into hair cells.

Our present results reveal that in *S. canicula* the formation of the neuronal cells in the inner ear (in the SAG) precedes the formation of the sensory cells (in the epithelial walls). This early neural delamination and neurogenesis at the otic cup stage that happen in *S. canicula* prior to the formation of the sensory organs appears common with that described in amniotes (reviewed in Schneider-Maunoury and Pujades, 2007) but is different to that observed in zebrafish, where the first hair cells are detectable before the complete formation of the vestibular and auditory regions (Haddon and Lewis, 1996).

Comparison between the early development of the inner ear and that of the olfactory system in the catshark

The comparison between the events of the first period of development of the catshark inner ear (present results) with the first period of development of the peripheral olfactory system defined in the same species (Quintana-Urzainqui et al. 2014a, b) on the basis of the expression of similar immunohistochemical markers (DCX, HuC/D, PCNA), reveals interesting similarities and differences. Main events during this early period of catshark olfactory system account with the formation of the olfactory placode and its invagination, the establishment of a neurogenic region in the olfactory epithelium (first neuronal precursors) and the growing of olfactory axons to form the olfactory nerve, with pioneer axons and neurons (Quintana-Urzainqui et al., 2014a). It happens between the stages st20 (when the optic placode becomes morphological visible) and st24 (formation of the olfactory pit and the olfactory nerve primordium). The comparison with the present results reveals similarities in the developmental processes of olfactory and inner ear sensory systems. In both cases, sensory cells will differentiate in curved epithelial walls originated from a placodal invagination and, during the invagination, some placodal cells delaminate to form or to contribute to the formation of peripheral components of the

corresponding sensory system. In both cases, a neurogenic region is formed in the epithelium that will originate the pioneering neuronal precursors of the peripheral components whose growing axons will form the corresponding nerve: ganglion cells of the SAG in the inner ear, and migrating neurons that accompany the growing of olfactory axons in the case of olfactory system. Interesting differences can be noted in the development of both systems in this shark. In addition to different chronology (the starting of the otic placode invagination happens at st18, earlier than the olfactory placode, which happens at st20), distinctions can be pointed in relation to the completion of the placode invagination. While the otic placode invagination culminates with the formation of a closed vesicle at st25, the invagination of olfactory placode ends earlier (s24), once the olfactory pit/nasal sac is completely formed (before the folding of its walls in lamellae starts). On the other hand, while to the inner ear development, the peripheral neurons of placodal origin will differentiate in bipolar (ganglion) neurons that extend central axons towards targets in the hindbrain and peripheral processes towards the sensory cells of the otic epithelium, in the olfactory epithelium, the neurogenic processes will originate neurons (HuC/D+) of at least two types: sensory neurons that differentiate in the epithelium and stay there as olfactory neurons while their centralward growing axons will

form the olfactory nerve, and the first postmitotic neurons in the olfactory placode that delaminate to pioneer the olfactory pathway across the mesenchyme (some Pax6), or that will form the terminal nerve ganglia. In the otic epithelium the sensory cells differentiated in the otic epithelium have not neuronal nature (HuC/D-).

CONCLUSIONS

The beginning of the induction of the neuronal fate, revealed by the expression of *NeuroD*, is appreciable at very early stages of the otic development, as soon as st20, the earliest stage analyzed in this study. The establishment of the innervation of the inner ear takes place during a long period, about two months long, from the first stages where early DCX-ir fibers appear linking the otic cup to the brain (st20) to the latter stages when the innervation pattern is complete (st32). This process is intimately related to the morphogenetic processes described in Chapter 2, where from a very simple initial structure that gradually grows and subdivides a complex three-dimensional labyrinth is achieved. The innervation of all the sensory areas of this structure increases and new branches appear as the otic vesicle grows and subdivides. When complete, the distribution and number of the sensory organs are similar to that observed in other chondrichthyans, with three otolithic maculae located in the utricular recess, saccule and lagena, a non-otolithic macula neglecta located next to the utriculo-saccular boundary and the ductus connecting the chambers to the PSC, and the three ampullary sensory cristae common to all the gnathostomes.

Cell proliferation is quite abundant during inner ear development in the walls of the labyrinth and also in the SAG, but is striking that the expression of proliferation markers is lacking in presumptive sensory patches until the morphologic development of the ear is completed by the end of the stage 31. Some cells within the thickened maculae and cristae begin to proliferate after this developmental stage. At the same time some differentiated hair cells became distinguishable at the sensory patches. Differentiated ganglion cells are present in the SAG from intermediate stages like st27, indicating that the maturation of SAG cells precedes that of the sensory cells. The delayed maturation of the sensory patches in relation to that of the SAG is also supported by the expression of *Sox2* at late stages in these regions, which indicates the maintenance of pluripotency in cells of the maculae and cristae and also the capacity to originate new sensory hair cells.

LITERATURE CITED

- Alsina B, Whitfield TT (2017) “Sculpting the labyrinth: Morphogenesis of the developing inner ear". *Semin. Cell. Dev. Biol*. 65: 47-59.
- Anadón R, Molist P, Rodríguez-Moldes I, López JM, Quintela I, Cerviño MC, Barja P, González A (2000) Distribution of choline acetyltransferase immunoreactivity in the brain of an elasmobranch, the lesser spotted dogfish (*Scyliorhinus canicula*). *J. Comp. Neurol*. 420:139-170.
- Appler JM, Goodrich LV, (2011) “Connecting the ear to the brain: molecular mechanisms of auditory circuit assembly”. *Prog. Neurobiol.* 93: 488-508.
- Baird IL (1974) “Some aspects of the comparative anatomy and evolution of the inner ear in submammalian vertebrates”. *Brain Behav. Evol.* 10: 11-36.
- Baker CVH, O’Neill P, McCole RB (2008) “Lateral line, otic and epibranchial placodes: developmental and evolutionary links?” *J. Exp. Zool. B. Mol. Dev. Evol.* 310B: 370-383.
- Ballard WW, Mellinger J, Lechenault H (1993) “A series of normal stages for development of *Scyliorhinus canicula*, the lesser spotted dogfish (Chondrichthyes: Scyliorhinidae)”. *J. Exp. Zool.* 267: 318-336.
- Barald KF Kelley MW (2004) “From placode to polarization: new tunes in inner ear development”. *Development* 17: 4119-4130.
- Becerra M, Anadón R (1993a) “Development of the inner ear of the brown trout (*Salmo trutta fario*): I. Gross morphology and sensory cell proliferation”. *J. Morphol.* 216: 209-223.
- Becerra M, Anadón R (1993b) “Development of the inner ear of the brown trout (*Salmo trutta fario*): II.

Cytodifferentiation and innervation of sensory cells". *J. Morphol.* 216: 241-257.

- Becerra M, Anadón R (1993c) "Fine structure and development of ionocyte areas in the labyrinth of the trout (*Salmo trutta fario*)". *J. Anat.* 183:463-474.
- Bernstein P (2003) "The ear region of *Latimeria chalumnae*: functional and evolutionary implications". *Zoology* 106: 233-242.
- Bever MM, Fekete DM (2002) "Atlas of the development of the inner ear in zebrafish". *Dev. Dynam.* 223: 536-543.
- Bever MM, Jean YY, Fekete DM (2003) "Three-dimensional morphology of the inner ear development in *Xenopus laevis*". *Dev. Dynam.* 227: 422-430.
- Bissonnette JP, Fekete DM (1996) "Standard atlas of the gross anatomy of the developing inner ear of the chicken". *J. Comp. Neurol.* 368: 620-630.
- Boord RL, Roberts BL (1980) "Medullary and cerebellar projections of the statoacoustic nerve of the dogfish *Scyliorhinus canicula*". *J. Comp. Neurol.* 193: 57-68.
- Coolen M, Menuet A, Chassoux D, Compagnucci C, Henry S, Lévèque L, Da Silva C, Gavory F, Samain S, Wincker P, Thermes C, D'Aubenton-Carafa Y, Rodríguez-Moldes I, Naylor G, Depew M, Sourdaine P, Mazan S (2009) "The dogfish *Scyliorhinus canicula*, a reference in jawed vertebrates. In: Behringer RR, Johnson AD, Krumlauf RE (eds) Emerging model organisms. A laboratory manual, vol 1. CSHL Press, Cold Spring Harbor, pp 431-446.
- Corwin JT (1977) "Morphology of the macula neglecta in sharks of the genus *Carcharhinus*". *J. Morphol.* 152: 341-62.
- Derobert Y, Plouhinec JL, Sauka-Spengler T, Le Mentec C, Baratte B, Jaillard D, Mazan S (2002) "Structure and expression of three *Emx* genes in the dogfish *Scyliorhinus canicula*: functional and evolutionary implications". *Dev. Biol.* 247: 390-404.

- Docampo-Seara A, Lagadec R, Mazan S, Rodríguez MA, Quintana-Urzainqui I, Candal E (2018) “Study of pallial neurogenesis in shark embryos and the evolutionary origin of the subventricular zone”. *Brain Struct. Funct.* https://doi.org/10.1007/s00429-018-1705-2.
- Evangelista C, Mills M, Siebeck UE, Collin SP (2010) “A comparison of the external morphology of the membranous inner ear in elasmobranchs”. *J. Morphol.* 271: 483-495.
- Ferreiro-Galve S, Candal E, Rodríguez-Moldes I (2012) “Dynamic expression of Pax6 in the shark olfactory system: evidence for the presence of Pax6 cells along the olfactory nerve pathway”. *J. Exp. Zool. B. Mol. Dev. Evol.* 318: 79-90.
- Fritzsch B (1987) ”Inner ear of the coelacanth fish *Latimeria* has tetrapod affinities”. *Nature* 327: 153-154.
- Fritzsch B, Beisel KW (2001) “Evolution of the nervous system. Evolution and development of the vertebrate inner ear”. *Brain Res. Bull.* 55: 711-721.
- Fritzsch B, Beisel KW (2004) “Keeping sensory cells and evolving neurons to connect them to the brain: molecular conservation and novelties in vertebrate ear development”. *Brain. Behav. Evol*. 64: 182-197.
- Fritzsch B, Elliott KL (2017) “Evolution and development of the inner ear efferent system: transforming a motor neuron population to connect to the most unusual motor protein via ancient nicotinic receptors”. *Front. Cell. Neurosci*. 11: 114.
- Fritzsch B, Beisel KW, Jones K, Fariñas I, Maklad A, Lee J, Reichardt LF (2002) “Development and evolution of inner ear sensory epithelia and their innervation”. *J. Neurobiol.* 53: 143-156.
- Fritzsch B, Pauley S, Beisel KW (2006) “Cells, molecules and morphogenesis: The making of the vertebrate ear”. *Brain Res.* 1091: 151-171.

- Haddon C, Lewis J (1991) “Hyaluronan as a propellant for epithelial movement: the development of semicircular canals in the inner ear of *Xenopus*”. *Development* 112: 541-550.
- Haddon C, Lewis J (1996) “Early ear development in the embryo of the zebrafish, *Danio rerio*”. *J. Comp. Neurol.* 365: 113-128.
- Haddon C, Lewis J (2002) “Atlas of the developing inner ear in zebrafish”. *Dev. Dynam*. 223: 536-543.
- Hans S, Irmscher A, Brand M (2013) “Zebrafish Foxi1 provides a neuronal ground state during inner ear induction preceding the Dlx3b/4b-regulated sensory lineage”. *Development* 140: 1936-1945.
- Huang EJ, Reichardt LF (2003) “Trk receptors: roles in neuronal signal transduction”. *Annu. Rev. Biochem.* 72: 609-642.
- Kim WY, Fritzsch B, Serls A, Bakel LA, Huang EJ, Reichardt LF, Barth DS, Lee JE (2001) “NeuroD-null mice are deaf due to a severe loss of the inner ear sensory neurons during development”. *Development* 128: 417-426.
- Kim WY (2013) “NeuroD regulates neuronal migration”. *Mol. Cells* 35: 444-449.
- Ladher RK, O'Neill P, Begbie J (2010) “From shared lineage to distinct functions: the development of the inner ear and epibranchial placodes”. *Development* 137: 1777-1785.
- Lanford PJ, Popper AN (1996) “Novel afferent terminal structure in the crista ampullaris of the goldfish, *Carassius auratus*”. *J Comp Neurol*. 366:572-579.
- Liu M, Pereira FA, Price SD, Chu MJ, Shope C, Himes D, Eatock RA, Brownell WE, Lysakowski A, Tsai MJ (2000) “Essential role of BETA2/NeuroD1 in development of the vestibular and auditory systems”. *Gene. Dev*. 14: 2839-2854.
- Lovell JM, Findlay MM, Harper GM, Moate RM (2007) “The polarization of hair cells from the inner ear of the lesser

spotted dogfish *Scyliorhinus canicula*". *J. Fish Biol.* 70: 362-373.
- Lowenstein O, Osborne MP, Thornhill RA (1968) "The anatomy and ultrastructure of the labyrinth of the lamprey (*Lampetra fluviatilis L.*)". *Proc. R. Soc. Lond. B. Biol. Sci.* 170: 113-134.
- Lowenstein O, Thornhill RA (1970) "The labyrinth of myxine: anatomy, ultrastructure and electrophysiology". *Proc. R. Soc. Lond.* B 176: 21-42.
- Magariños M, Contreras J, Aburto MR, Varela-Nieto I (2012) "Early development of the vertebrate inner ear". *Anat. Rec*. (Hoboken) 295: 1775-1790.
- Maier EC, Saxena A, Alsina B, Bronner ME, Whitfield TT (2014) "Sensational placodes: neurogenesis in the otic and olfactory systems". *Dev. Biol*. 389: 50-57.
- Maisey JG (2001) "Remarks on the inner ear of elasmobranchs and its interpretation from skeletal labyrinth morphology". *J. Morphol.* 250: 236-264.
- Matin P, Swanson GJ (1993) "Descriptive and experimental analysis of the epithelial remodellings that control the semicircular canal formation in the developing mouse inner ear". *Dev. Biol.* 159: 549-558.
- Mazan S, Jaillard D, Baratte B, Janvier P (2000) "Otx1 gene-controlled morphogenesis of the horizontal semicircular canal and the origin of the gnathostome characteristics". *Evol. Dev.* 2: 186-193.
- McVean A (1991) "The semicircular canals of the hagfish *Myxine glutinosa*" *J. Zool.* 224: 213-222.
- Meredith GE, Roberts BL (1986) "Central organization of the efferent supply to the labyrinthine and lateral line receptors of the dogfish". *Neuroscience* 17:225-233.
- Millimaki BB, Sweet EM, Riley BB (2010) "Sox2 is required for maintenance and regeneration, but not initial development, of hair cells in the zebrafish inner ear". *Dev. Biol.* 338: 262-269.

- Morsli H, Choo D, Ryan A, Johnson R, Wu DK (1998) “Development of the mouse inner ear and origin of its sensory organs”. *J. Neurosci*. 18: 3327-3335.
- Neves J, Parada C, Chamizo M, Giraldez F (2011) “Jagged 1 regulates the restriction of Sox2 expression in the developing chicken inner ear: a mechanism for sensory organ specification”. *Development* 138: 735-744.
- Neves J, Vachkov I, Giráldez F (2013) “Sox2 regulation of hair cell development: incoherence makes sense”. *Hearing Res*. 297: 20-29.
- Ngûyen V, Candal-Suárez EM, Sharif A, Joly JS, Bourrat F (2001) “Expression of Ol-KIP, a cyclin dependent kinase inhibitor, in embryonic and adult medaka (*Oryzias latipes*) central nervous system”. *Dev. Dyn*. 222: 439-449
- Noramly S, Granger RM (2002) “Determination of the embryonic inner ear”. *J. Neurobiol.* 5: 100-128.
- Norris HW (1892) “Studies on the development of the ear of Amblysoma”. *J. Morphol*. 7: 23-34.
- O´Neill P, McCole RB, Baker CVH (2007) “A molecular analysis of neurogenic placode and cranial sensory ganglion development in the shark, *Scyliorhinus canicula*”. *Dev. Biol.* 304: 156-181.
- Popper AN (2017) “Auditory System Morphology. Reference Module in Life Sciences “[Internet]. Elsevier; Available from: http://dx.doi.org/10.1016/B978-0-12-809633-8.03030-2
- Pose-Méndez S, Candal E, Adrio F, Rodríguez-Moldes I (2014) “Development of the cerebellar afferent system in the shark *Scyliorhinus canicula*: insights into the basal organization of precerebellar nuclei in gnathostomes” *J. Comp. Neurol.* 522: 131-168.
- Quintana-Urzainqui I, Rodríguez-Moldes I, Candal E (2014a) “Developmental, tract-tracing and immunohistochemical study of the peripheral olfactory system in a basal

vertebrate: insights on Pax6 neurons migrating along the olfactory nerve". *Brain Struct. Funct*. 219: 85-104.

- Quintana-Urzainqui I, Anadón R, Candal E, Rodríguez-Moldes I (2014b) "Development of the terminal nerve system in the shark *Scyliorhinus canicula*". *Brain Behav Evol*. 84:277-287.
- Roberts BL, Meredith GE (1992) "The efferent innervation of the ear: variations on an enigma". In: Webster DB, Fay RR, Popper AN, editors. The evolutionary biology of hearing. New York: Springer-Verlag, p 185–210.
- Rodríguez-Moldes I, Carrera I, Pose-Méndez S, Quintana-Urzainqui I, Candal E, Anadón R, Mazan S, Ferreiro-Galve S (2011) "Regionalization of the shark hindbrain: a survey of an ancestral organization". *Front. Neuroanat.* 7:16.
- Rodríguez-Moldes I, Santos-Durán GN, Pose-Méndez S, Quintana-Urzainqui I, Candal E (2017) ''The brains of cartilaginous fishes'' *Evolution of Nervous Systems* (Vol. 1), ed. J. Kaas (Oxford: Elsevier), 77-97.
- Rubel EW, Fritzsch B, (2002) "Auditory system development: primary auditory neurons and their targets". *Annu. Rev. Neurosci*. 25: 51-101.
- Santos-Durán GN, Ferreiro-Galve S, Menuet A, Quintana-Urzainqui I, Mazan S, Rodríguez-Moldes I, Candal E (2016) "The shark alar hypothalamus: molecular characterization of prosomeric subdivisions and evolutionary trends". *Front. Neuroanat.* 10:113.
- Schlosser G (2006) "Induction and specification of cranial placodes". *Dev. Biol.* 294: 303-351.
- Schneider-Maunoury S, Pujades C (2007) "Hindbrain signals in otic regionalization: walk on the wild side" *Int. J. Dev. Biol*. 51: 495-506.
- Simmons DD (2002) "Development of the inner ear efferent system across vertebrate species". *J. Neurobiol*. 53: 228-250.

- Smeets WJAJ, Nieuwenhuys R, Roberts BL (1983) “The central nervous system of cartilaginous fishes. Structural and functional correlations”. Springer-Verlag Berlin Heidelberg. Chapter 6, pp 40-41.
- Smotherman M, Narins P (2004) “Evolution of the amphibian ear”. G. A. Manley et al. (eds.), Evolution of the Vertebrate Auditory System © Springer Science+Business Media, New York.
- Tester AL; Kendall JI, Milisen WB (1972) “Morphology of the ear of the shark genus *Carcharhinus*, with particular reference to the macula neglecta”. *Pac. Sci*. 26: 264-274.
- Thornhill RA (1972) “The development of the labyrinth of the lamprey (*Lampetra fluviatilis* Linn. 1758)”. *Proc. R. Soc. Lond. B.* 181: 175-198.
- Torres M, Giráldez F (1998) “The development of the vertebrate inner ear”. *Mech. Develop.* 71: 5-21.
- Vasconcelos RO, Alderks PW, Sisneros JA (2016) “Development of structure and sensitivity of the fish inner ear”. *Adv. Exp. Med. Biol.* 877: 291-318.
- Waterman RE, Bell DH (1984) “Epithelial fusion during early semicircular canal formation in the embryonic zebrafish, *Brachydanio rerio*”. *Anat. Rec.* 210: 101-114.
- Webb J, Noden D (1993) “Ectodermal Placodes: Contributions to the development of the vertebrate head”. *Am. Zool*. 33: 434-447.
- Wever EG (1978) “The ear of the chameleon- *Chamaeleo senegalensis* and *Chamaeleo quilensis*”. *J. Exp. Zool*. 168: 423-436.
- Wever EG (1983) “The ear and hearing in the frog, *Rana pipiens*”. *J. Morph.* 141: 461-478.
- Whitfield TT (2015) “Development of the inner ear”. *Curr. Op. Genet. Dev.* 32: 112-118.

FIGURES LEGENDS

Abbreviations: ASC: anterior semicircular canal; Hb: hindbrain; HSC: horizontal semicircular canal; OC: otic cup; PSC: posterior semicircular canal; r4: rhombomere 4; Rh: rhombencephalon; S: saccule; SAG: statoacoustic ganglion; U: utricle; UR: utricular recess.

Flg. 1.- Parasagittal sections labeled with the molecular markers indicated (A-C, H-K) and surface rendering (D-G, L-O) of 3D volumes of reconstructed micro-CT datasets of st20 (A-G) and st24 (H-O) *S. canicula* embryos to show early events of the SAG and otic epithelium differentiation. A-C. Panoramic view (A) and details (B,C) of a st20 embryo to show the early innervation of the otic cup (oc) by DCX-immunoreactive (ir) fibers (arrows). Note also abundant DCX-ir fibers coursing along the basal plate of the rhombencephalon (Rh). The section also shows in blue the expression of *ScWnt8* gene in the rhombomere 4 (r4) and the epithelium of pharyngeal pouches (ph). D-G, Surface (D), parasagittal (E,F) and transversal (G) rendering images of a st20 embryo that help to better interpret the level of the section in A. Note the shape and position of the invaginating otic cup in the rear part of the head (D-E) and the close position of the SAG, slightly ventral and rostral to the cup (E-F). Red line in G indicates the approximate level of the sagittal sections in A-F. H-J. Panoramic (H) and details (I,J) of parasagittal sections of st24 embryo showing DCX-ir fibers in the otic epithelium and SAG. Note some DCX-ir processes innervating the walls of the otic cup (black arrows in H-I) and its periphery (white arrow in I). Abundant DCX-ir fibers are seen in the SAG (H and J) and some DCX-ir cells are distinguished in the SAG close to the otic cup (black arrowheads in J). K. Detail of a sagittal section at the same level of H to show a clear expression of *NeuroD* in the SAG (white arrowheads) and in caudo-dorsal (black arrow) and rostro-ventral (white arrow) regions of the otic cup. L-O. Surface rendering images of a st24 embryo that help to better interpret the level of sections in H and K. At this stage, the otic cup is almost closed, being noted the narrow aperture (white arrowheads). The position of the SAG is appreciated (M and N). Red line in O indicates the level of the sagittal sections in H-N. Asterisk, otic cup; star, SAG. Scale bars = 500 µm in D, E, L, M, O; 200 µm in A, G-I, K, N; 100 µm in B, F, J; 50 µm in C.

Fig. 2.- Transverse sections labeled with the markers indicated (A-G) and 3D rendering of reconstructed micro-CT datasets (H-L) of st25 *S. canicula* embryos to show the DCX-ir fibers innervating the otic vesicle (A-D), the expression of *NeuroD* in the SAG and ventral region of the otocyst (E-G) and the shape and location of the recently closed vesicle (H-L). A-D. Rostral (A) to caudal (C) panoramic and detailed views showing the innervation of the otocyst by DCX-ir fibers (arrowheads) and the abundant DCX immunoreactivity in the SAG (stars), where DCX-ir cells are appreciated (D, outlined arrowheads). Note also DCX immunoreactivity in the hindbrain (Hb). E-G. Panoramic and detailed views to show the maintained expression of *NeuroD* in the SAG (star), and in the ventromedial part of the otic vesicle (arrowheads). Note that the cells expressing *NeuroD* are located in the

region of the otic vesicle which contacts the ganglion (arrowheads) and the intense expression in the cells of the SAG. H-L. Panoramic (H, I, J) and detailed views of reconstructed 3D micro-CT datasets of a st25 *S. canicula* embryo at similar levels to A-G to better understand the levels of the sections and the actual morphology and location of the otocyst. Figs. H, I and J correspond respectively to the levels of sections in Figs. A, B and C. At this stage the otic vesicle presents ovoid-shape and only communicates to the exterior by the elongated endolymphatic duct (arrowheads in H and I). Red lines in lateral (K) and parasagittal (L) panoramic micro-CT views of the st25 embryo indicate the level of the transverse sections. Asterisk, otocyst; star, SAG. Scale bars = 200 µm in H-L (details 100 µm); 100 µm in A-G (details 50 µm).

Fig. 3.- Transverse labeled with the markers indicated (A-K) and parasagittal (L-N) sections and 3D renderized micro-CT images (O-R) of st27 *S. canicula* embryos. A-C. Sections through the otic vesicle and SAG showing distribution of PCNA immunoreactivity. PCNA-ir cells are present in the lateral wall of the otic vesicle (A-C; arrowheads) while few PCNA-positive cells are present in the SAG, especially in the region next to the otocyst (A, B). D-F. Rostral (D) to caudal (F) sections through the otic vesicle and SAG showing intense immunoreactivity to DCX in the ganglion (D and E) and in branches of the otic nerve entering the otic epithelium (D-F, arrowheads). Abundant immunoreactivity to DCX is observed in the hindbrain (Hb in D). G-I. Rostral (G) to caudal (I) sections through the otic vesicle and SAG showing expression of HuC/D in cells of the ganglion (G-I; arrowheads), but not in the otic vesicle(asterisks in G-I). J-N. Transverse (J, K) and parasagittal (L-N) sections showing the expression of *NeuroD* in the SAG (J, K, M, N; arrows) and in the ventral region of the otic vesicle (J-L; arrowheads). Note expression of *NeuroD* also in the dorsal region of the otic epithelium, which appears formed by two patches due to the section plane of the slice (N; outlined arrowheads). O-S. Transverse (O-Q), lateral (R) and parasagittal (S) rendered images obtained through micro-CT showing the location and three-dimensional morphology of the otic vesicle. Various wall folds have begun to protrude into the otocyst, being recognized the two protrusions that contact and fuse to form the first semicircular canal (PSC) (Q; arrowhead). Asterisk, otic vesicle; star, SAG. Red lines in R and S show the level of the transverse sections in O-Q. Scale bars = 400 µm in R; 200 µm in A-C, G-Q; 100 µm in D-F.

Fig. 4.- Transverse sections labeled with the markers indicated (A-L) and 3D reconstructed micro-CT images of st29 *S. canicula* embryos (M-Q) to show the expression of different molecular markers and morphological changes which take place at this stages of the inner ear development. A-D. Sections from rostral (A) to caudal (D) showing the cell proliferation pattern through the immunoreactivity to PCNA in cells of the otic epithelium (A-D, arrowheads) and in some cells of the SAG (A, B; empty arrowheads). PCNA immunoreactivity is absent in areas where the future sensory patches will develop (A-C; arrows). E-H. Panoramic views and details of sections showing DCX-ir fibers entering the otic epithelium (E-H and details; arrowheads). Note the intense DCX expression in the SAG (E, F and details, arrows), otic nerve (G, arrow) and glossopharyngeal nerve (H, arrow). Note also the correspondence between the regions innervated by DCX-ir fibers in E-H and the PCNA-negative regions of A-C. I-L. Rostral (I) to caudal (L) sections to show the intense expression of HuC/D in the SAG (I, J; arrowheads) and its

negativity in the otic vesicle. M-Q. Transverse (M-P) and parasagittal (Q) 3D reconstruction of a micro-CT scanned st29 *S. canicula* embryo to show the morphological changes which have taken place in the otic vesicle in relation to the previous stage reported. Its complex shape and location can be followed along the corresponding to the level indicated in Q (Q; red lines). Note the developing HSC. Asterisk, otic vesicle; stars, SAG. Scale bars = 400 µm in Q; 200 µm in A-P (100 µm in details).

Fig. 5.- Transverse sections labeled with the markers indicated (A-N) and micro-CT 2D transverse images (O-R) and 3D parasagittal volume reconstruction (S) of st31 *S. canicula* embryos to show the late events of the SAG and otic vesicle morphogenesis. A-D. Sections through the inner ear showing the distribution of PCNA-ir cells in various regions of the otic epithelium (A-D, arrowheads). PCNA-ir cells are absent in the primordial sensory patches (A, B, arrows). E-J. Panoramic views and details of transverse sections of the inner ear showing the DCX-ir fibers (E-J and details; arrowheads) innervating the anterior ampullary crista (E-F and details, arrowheads), the presumptive sensory patches of the chambers (F, G and details; black arrowheads) and the posterior ampullary crista (H, empty arrowhead). Note the immunoreactivity to DCX in the ganglion (F, I, J, arrow) and glossopharyngeal nerve (G (detail) and H, white arrowheads), ventrally to the branch that innervates the posterior ampullary crista (G (detail) and H, outlined arrowheads). The innervation pattern of the DCX-ir fibers (I, J and details; black arrowheads) is strikingly coincident with the expression of *Sox2* in the otic epithelium of the chambers and semicircular canals (details of I and J; empty arrowheads). I´, J´. Differential interference contrast (DIC) images of the areas squared in details of I and J, respectively, to show the epithelial surface at the primordial sensory patches. Note the absence of superficial structures (empty arrowheads). K-N. Sections through the inner ear and SAG showing HuC/D immunoreactive neurons in the SAG (K-M, arrowheads). Note the absence of HuC/D-ir structures in the inner ear walls (K-N). O-S. Transverse 2D micro-CT images of the inner ear and SAG (O-P) and parasagittal 3D volume of reconstructed micro-CT datasets of a st31 *S. canicula* embryo for better understanding the morphology and location of the inner ear and its components at this stage. Note the complex structure and subdivision of its cavity in intercommunicated chambers and semicircular canals. Red lines in S indicate the level of the transverse sections. Asterisk, inner ear; stars, SAG. Scale bars = 400 µm in S; 200 µm in A-R (100 µm in details).

Fig. 6.- Transverse sections (A-N) and micro-CT 2D transverse images (O-R) and 3D parasagittal volume reconstruction (S) of st32 *S. canicula* embryos showing the expression of molecular markers and the morphology of the inner ear. A-D. Panoramic views and details of sections showing immunoreactivity to PCNA in cells of the otic epithelium and in the SAG. The immunoreactivity to PCNA continues to be present in the epithelium surrounding the cavities and canals (A-D; black arrowheads). Note also some cells PCNA-ir in the thickened regions of the sensory patches of ASC (detail of A, A´, outlined arrowheads), HSC (detail in B, outlined arrowheads) and PSC (D, outlined arrowhead), where most of cells are PCNA-negative. The SAG and the statoacoustic nerve (arrow in detail of C) also present immunoreactivity to PCNA. E-H. Panoramic views and details to show the immunoreactivity to DCX in the SAG (detail in F, black arrowheads) and in

fibers innervating sensory patches (detail of E and F, G, black arrowheads). Thin DCX-ir fibers enter the sensory patches and reach apical epithelial levels (details of F and H, G, white arrowheads). I-K. Transverse views of the inner ear and SAG showing the immunoreactivity to HuC/D in the SAG (star), in other ganglia and in the brain, but not in the inner ear walls. L-N- Differential interference contrast (DIC) images of the anterior and lateral semicircular ampullae and the utricular recess. The expression of *ScSox2* is present in the sensory patches of the anterior ampullary crista (black arrowheads in detail of L), utricular recess (black arrowheads in detail of M) and lateral crista (black arrowheads in detail of N). All these sensory organs present at this stage (the earliest) bundles of hairs emerging from epithelial cells (empty arrowheads in details).These superficial structures are evident all along the thickened region of the epithelium that defines the sensory patches (empty arrowheads). Note that are even visible at the surface of in small groups of cells in the utricular recess wall that no longer express *ScSox2* (detail of M, arrows). O-S. Transverse 2D micro-CT images of the inner ear and SAG (O-R) and parasagittal 3D reconstruction (S) of a st32 *S. canicula* embryo showing the mature-like aspect of the inner ear and its components. The three sensory cristae are clearly visible protruding into the lumen of the anterior, lateral and posterior ampullae (white arrowheads in O, P and R, respectively). The inner ear has developed all its chambers and is quite similar to posthatching stages. Red lines in P indicate the levels of the transverse sections. Asterisk, inner ear; star, SAG. Scale bars = 2000 µm in S; 500 µm in I-K and O-R; 200 µm in A-H and L-N (100 µm in details) and 50 µm in detail of F.

FIGURES

Fig. 1.- Parasagittal sections labeled with the molecular markers indicated (A-C, H-K) and surface rendering (D-G, L-O) of 3D volumes of reconstructed micro-CT datasets of st20 (A-G) and st24 (H-O) *S. canicula* embryos to show early events of the SAG and otic epithelium differentiation. A-C. Panoramic view (A) and details (B,C) of a st20 embryo to show the early innervation of the otic cup (oc) by DCX-immunoreactive (ir) fibers (arrows). Note also abundant DCX-ir fibers coursing along the basal plate of the rhombencephalon (Rh). The section also shows in blue the expression of *ScWnt8* gene in the rhombomere 4 (r4) and the epithelium of pharyngeal pouches (ph). D-G, Surface (D), parasagittal (E,F) and transversal (G) rendering images of a st20 embryo that help to better interpret the level of the section in A. Note the shape and position of the invaginating otic cup in the rear part of the head (D-E) and the close position of the SAG, slightly ventral and rostral to the cup (E-F). Red line in G indicates the approximate level of the sagittal sections in A-F. H-J. Panoramic (H) and details (I,J) of parasagittal sections of st24 embryo showing DCX-ir fibers in the otic epithelium and SAG. Note some DCX-ir processes innervating the walls of the otic cup (black arrows in H-I) and its periphery (white arrow in I). Abundant DCX-ir fibers are seen in the SAG (H and J) and some DCX-ir cells are distinguished in the SAG close to the otic cup (black arrowheads in J). K. Detail of a sagittal section at the same level of H to show a clear expression of *NeuroD* in the SAG (white arrowheads) and in caudo-dorsal (black arrow) and rostro-ventral (white arrow) regions of the otic cup. L-O. Surface rendering images of a st24 embryo that help to better interpret the level of sections in H and K. At this stage, the otic cup is almost closed, being noted the narrow aperture (white arrowheads). The position of the SAG is appreciated (M and N). Red line in O indicates the level of the sagittal sections in H-N. Asterisk, otic cup; star, SAG. Scale bars = 500 µm in D, E, L, M, O; 200 µm in A, G-I, K, N; 100 µm in B, F, J; 50 µm in C.

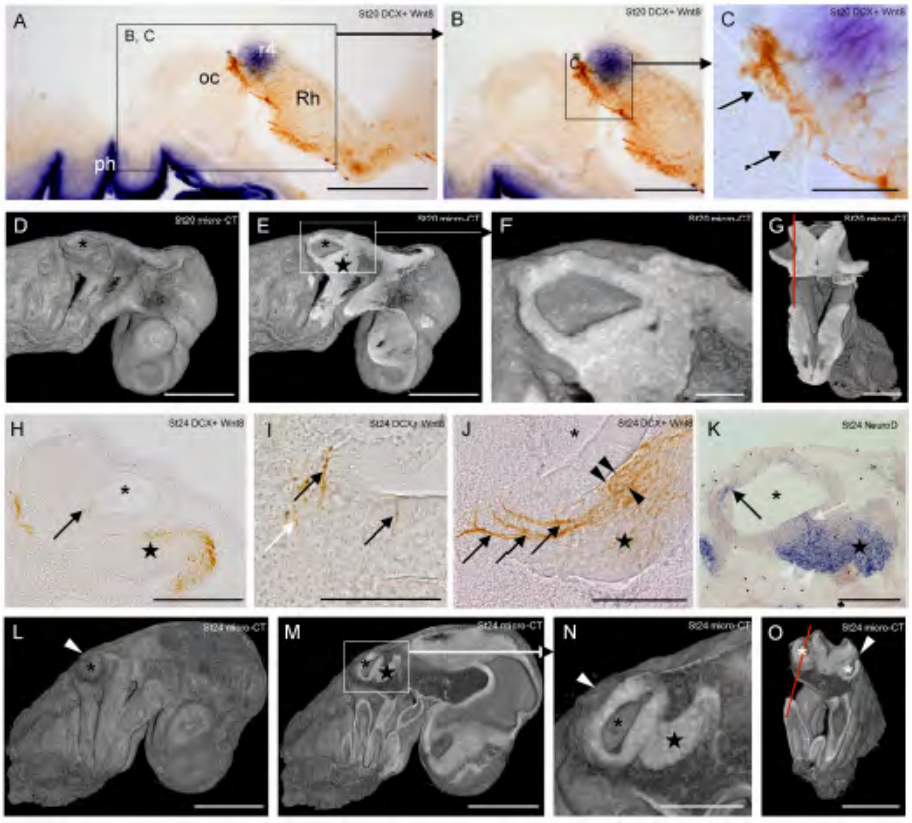

FIGURE 1

Fig. 2.- Transverse sections labeled with the markers indicated (A-G) and 3D rendering of reconstructed micro-CT datasets (H-L) of st25 *S. canicula* embryos to show the DCX-ir fibers innervating the otic vesicle (A-D), the expression of *NeuroD* in the SAG and ventral region of the otocyst (E-G) and the shape and location of the recently closed vesicle (H-L). A-D. Rostral (A) to caudal (C) panoramic and detailed views showing the innervation of the otocyst by DCX-ir fibers (arrowheads) and the abundant DCX immunoreactivity in the SAG (stars), where DCX-ir cells are appreciated (D, outlined arrowheads). Note also DCX immunoreactivity in the hindbrain (Hb). E-G. Panoramic and detailed views to show the maintained expression of *NeuroD* in the SAG (star), and in the ventromedial part of the otic vesicle (arrowheads). Note that the cells expressing *NeuroD* are located in the region of the otic vesicle which contacts the ganglion (arrowheads) and the intense expression in the cells of the SAG. H-L. Panoramic (H, I, J) and detailed views of reconstructed 3D micro-CT datasets of a st25 *S. canicula* embryo at similar levels to A-G to better understand the levels of the sections and the actual morphology and location of the otocyst. Figs. H, I and J correspond respectively to the levels of sections in Figs. A, B and C. At this stage the otic vesicle presents ovoid-shape and only communicates to the exterior by the elongated endolymphatic duct (arrowheads in H and I). Red lines in lateral (K) and parasagittal (L) panoramic micro-CT views of the st25 embryo indicate the level of the transverse sections. Asterisk, otocyst; star, SAG. Scale bars = 200 µm in H-L (details 100 µm); 100 µm in A-G (details 50 µm).

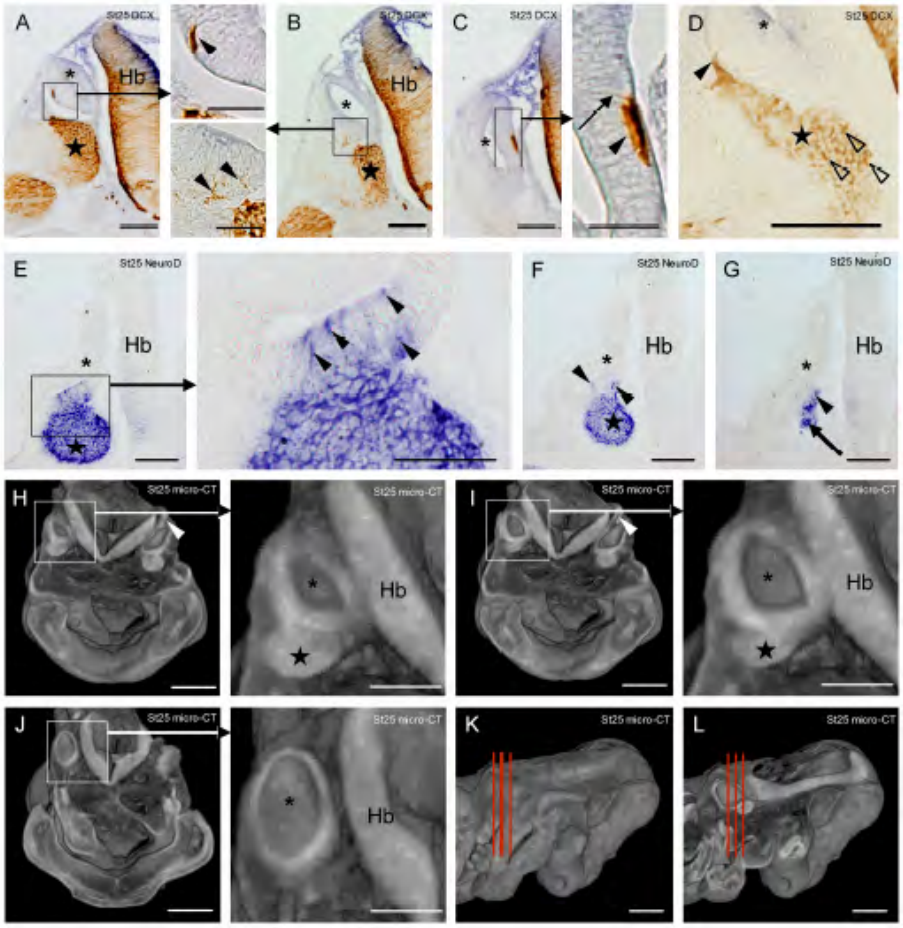
A
St25 DCX
Hb
B
St25 DCX
Hb
C
St25 DCX
D
St25 DCX
E
St25 NeuroD
Hb
F
St25 NeuroD
Hb
G
St25 NeuroD
Hb
H
St25 micro-CT
St25 micro-CT
Hb
I
St25 micro-CT
St25 micro-CT
Hb
J
St25 micro-CT
St25 micro-CT
Hb
K
St25 micro-CT
L
St25 micro-CT

FIGURE 2

Fig. 3.- Transverse labeled with the markers indicated (A-K) and parasagittal (L-N) sections and 3D renderized micro-CT images (O-R) of st27 *S. canicula* embryos. A-C. Sections through the otic vesicle and SAG showing distribution of PCNA immunoreactivity. PCNA-ir cells are present in the lateral wall of the otic vesicle (A-C; arrowheads) while few PCNA-positive cells are present in the SAG, especially in the region next to the otocyst (A, B). D-F. Rostral (D) to caudal (F) sections through the otic vesicle and SAG showing intense immunoreactivity to DCX in the ganglion (D and E) and in branches of the otic nerve entering the otic epithelium (D-F, arrowheads). Abundant immunoreactivity to DCX is observed in the hindbrain (Hb in D). G-I. Rostral (G) to caudal (I) sections through the otic vesicle and SAG showing expression of HuC/D in cells of the ganglion (G-I; arrowheads), but not in the otic vesicle(asterisks in G-I). J-N. Transverse (J, K) and parasagittal (L-N) sections showing the expression of *NeuroD* in the SAG (J, K, M, N; arrows) and in the ventral region of the otic vesicle (J-L; arrowheads). Note expression of *NeuroD* also in the dorsal region of the otic epithelium, which appears formed by two patches due to the section plane of the slice (N; outlined arrowheads). O-S. Transverse (O-Q), lateral (R) and parasagittal (S) rendered images obtained through micro-CT showing the location and three-dimensional morphology of the otic vesicle. Various wall folds have begun to protrude into the otocyst, being recognized the two protrusions that contact and fuse to form the first semicircular canal (PSC) (Q; arrowhead). Asterisk, otic vesicle; star, SAG. Red lines in R and S show the level of the transverse sections in O-Q. Scale bars = 400 µm in R; 200 µm in A-C, G-Q; 100 µm in D-F.

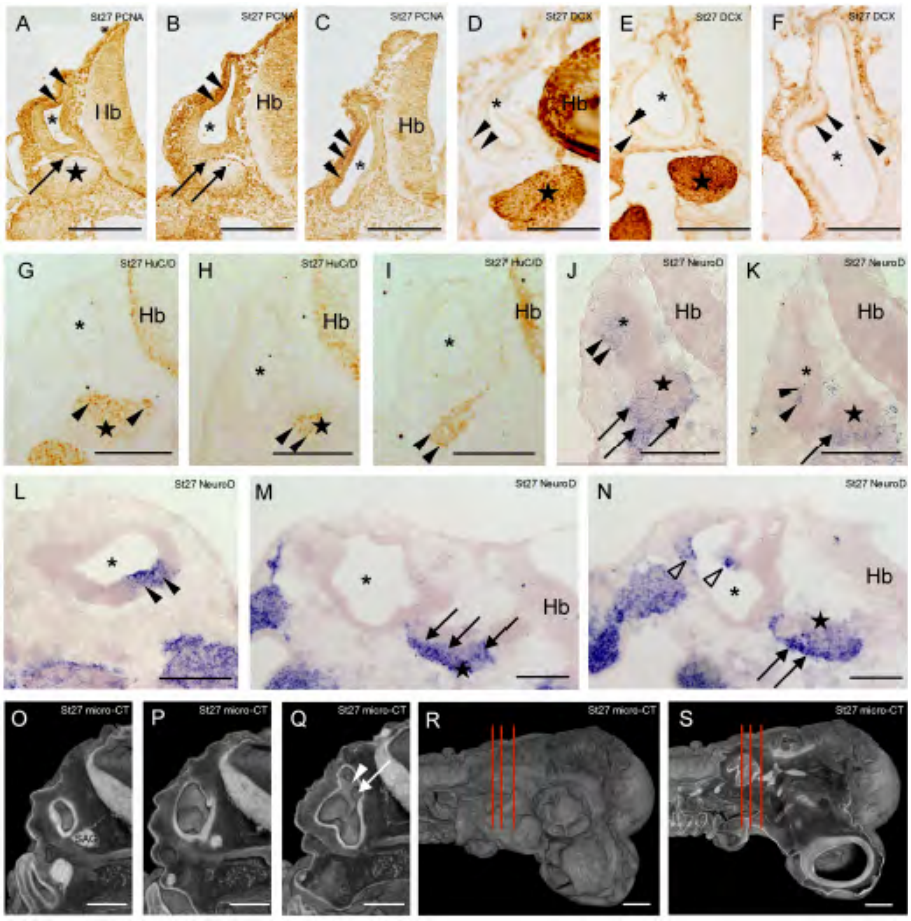
A
St27 PCNA
IIb
B
St27 PCNA
Hb
C
St27 PCNA
Hb
D
St27 DCX
Hb
E
St27 DCX
F
St27 DCX
G
St27 HuC/D
Hb
H
St27 HuC/D
Hb
I
St27 HuC/D
Hb
J
St27 NeuroD
Hb
K
St27 NeuroD
Hb
L
St27 NeuroD
M
St27 NeuroD
Hb
N
St27 NeuroD
Hb
O
St27 micro-CT
P
St27 micro-CT
Q
St27 micro-CT
R
St27 micro-CT
S
St27 micro-CT

FIGURE 3

Fig. 4.- Transverse sections labeled with the markers indicated (A-L) and 3D reconstructed micro-CT images of st29 *S. canicula* embryos (M-Q) to show the expression of different molecular markers and morphological changes which take place at this stages of the inner ear development. A-D. Sections from rostral (A) to caudal (D) showing the cell proliferation pattern through the immunoreactivity to PCNA in cells of the otic epithelium (A-D, arrowheads) and in some cells of the SAG (A, B; empty arrowheads). PCNA immunoreactivity is absent in areas where the future sensory patches will develop (A-C; arrows). E-H. Panoramic views and details of sections showing DCX-ir fibers entering the otic epithelium (E-H and details; arrowheads). Note the intense DCX expression in the SAG (E, F and details, arrows), otic nerve (G, arrow) and glossopharyngeal nerve (H, arrow). Note also the correspondence between the regions innervated by DCX-ir fibers in E-H and the PCNA-negative regions of A-C. I-L. Rostral (I) to caudal (L) sections to show the intense expression of HuC/D in the SAG (I, J; arrowheads) and its negativity in the otic vesicle. M-Q. Transverse (M-P) and parasagittal (Q) 3D reconstruction of a micro-CT scanned st29 *S. canicula* embryo to show the morphological changes which have taken place in the otic vesicle in relation to the previous stage reported. Its complex shape and location can be followed along the corresponding to the level indicated in Q (Q; red lines). Note the developing HSC. Asterisk, otic vesicle; stars, SAG. Scale bars = 400 µm in Q; 200 µm in A-P (100 µm in details).

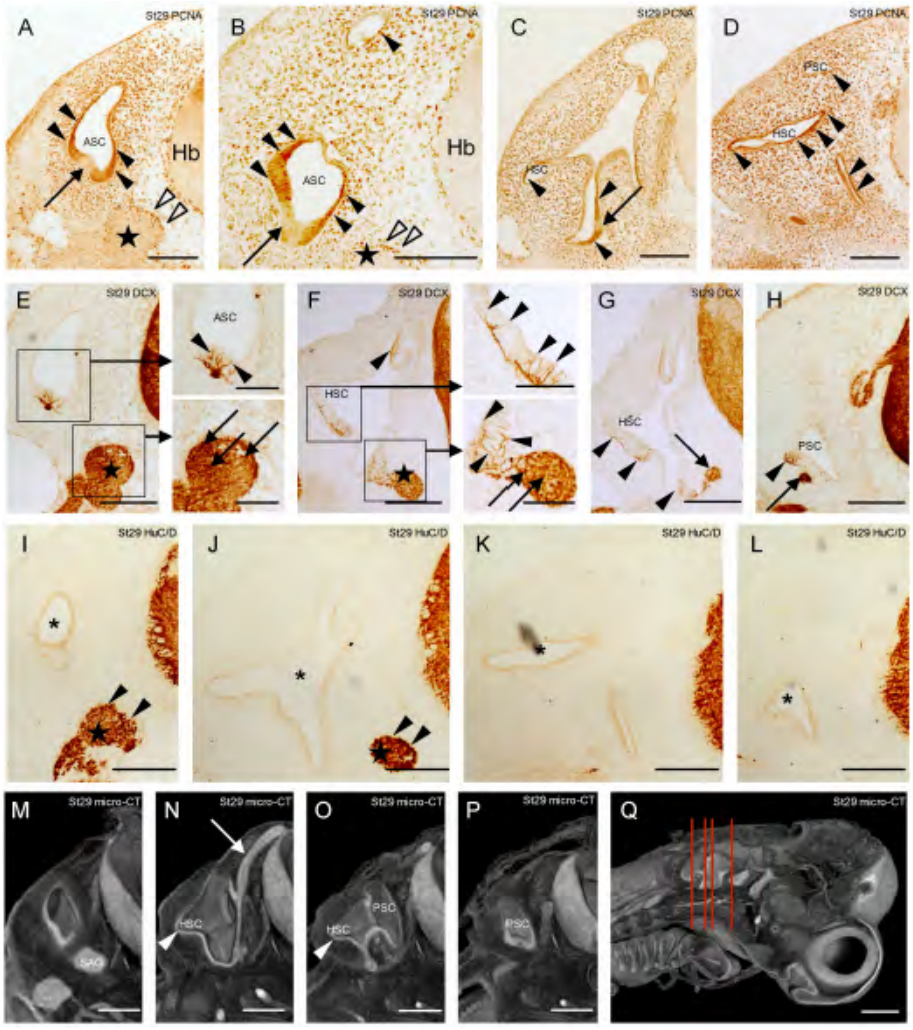
A
St29 PCNA
ASC
Hb
B
St29 PCNA
ASC
Hb
C
St29 PCNA
HSC
D
St29 PCNA
PSC
HSC
E
St29 DCX
ASC
F
St29 DCX
HSC
G
St29 DCX
HSC
H
St29 DCX
PSC
I
St29 HuC/D
J
St29 HuC/D
K
St29 HuC/D
L
St29 HuC/D
M
St29 micro-CT
N
St29 micro-CT
HSC
O
St29 micro-CT
PSC
HSC
P
St29 micro-CT
PSC
Q
St29 micro-CT

FIGURE 4

Fig. 5.- Transverse sections labeled with the markers indicated (A-N) and micro-CT 2D transverse images (O-R) and 3D parasagittal volume reconstruction (S) of st31 *S. canicula* embryos to show the late events of the SAG and otic vesicle morphogenesis. A-D. Sections through the inner ear showing the distribution of PCNA-ir cells in various regions of the otic epithelium (A-D, arrowheads). PCNA-ir cells are absent in the primordial sensory patches (A, B, arrows). E-J. Panoramic views and details of transverse sections of the inner ear showing the DCX-ir fibers (E-J and details; arrowheads) innervating the anterior ampullary crista (E-F and details, arrowheads), the presumptive sensory patches of the chambers (F, G and details; black arrowheads) and the posterior ampullary crista (H, empty arrowhead). Note the immunoreactivity to DCX in the ganglion (F, I, J, arrow) and glossopharyngeal nerve (G (detail) and H, white arrowheads), ventrally to the branch that innervates the posterior ampullary crista (G (detail) and H, outlined arrowheads). The innervation pattern of the DCX-ir fibers (I, J and details; black arrowheads) is strikingly coincident with the expression of *Sox2* in the otic epithelium of the chambers and semicircular canals (details of I and J; empty arrowheads). I´, J´. Differential interference contrast (DIC) images of the areas squared in details of I and J, respectively, to show the epithelial surface at the primordial sensory patches. Note the absence of superficial structures (empty arrowheads). K-N. Sections through the inner ear and SAG showing HuC/D immunoreactive neurons in the SAG (K-M, arrowheads). Note the absence of HuC/D-ir structures in the inner ear walls (K-N). O-S. Transverse 2D micro-CT images of the inner ear and SAG (O-P) and parasagittal 3D volume of reconstructed micro-CT datasets of a st31 *S. canicula* embryo for better understanding the morphology and location of the inner ear and its components at this stage. Note the complex structure and subdivision of its cavity in intercommunicated chambers and semicircular canals. Red lines in S indicate the level of the transverse sections. Asterisk, inner ear; stars, SAG. Scale bars = 400 µm in S; 200 µm in A-R (100 µm in details).

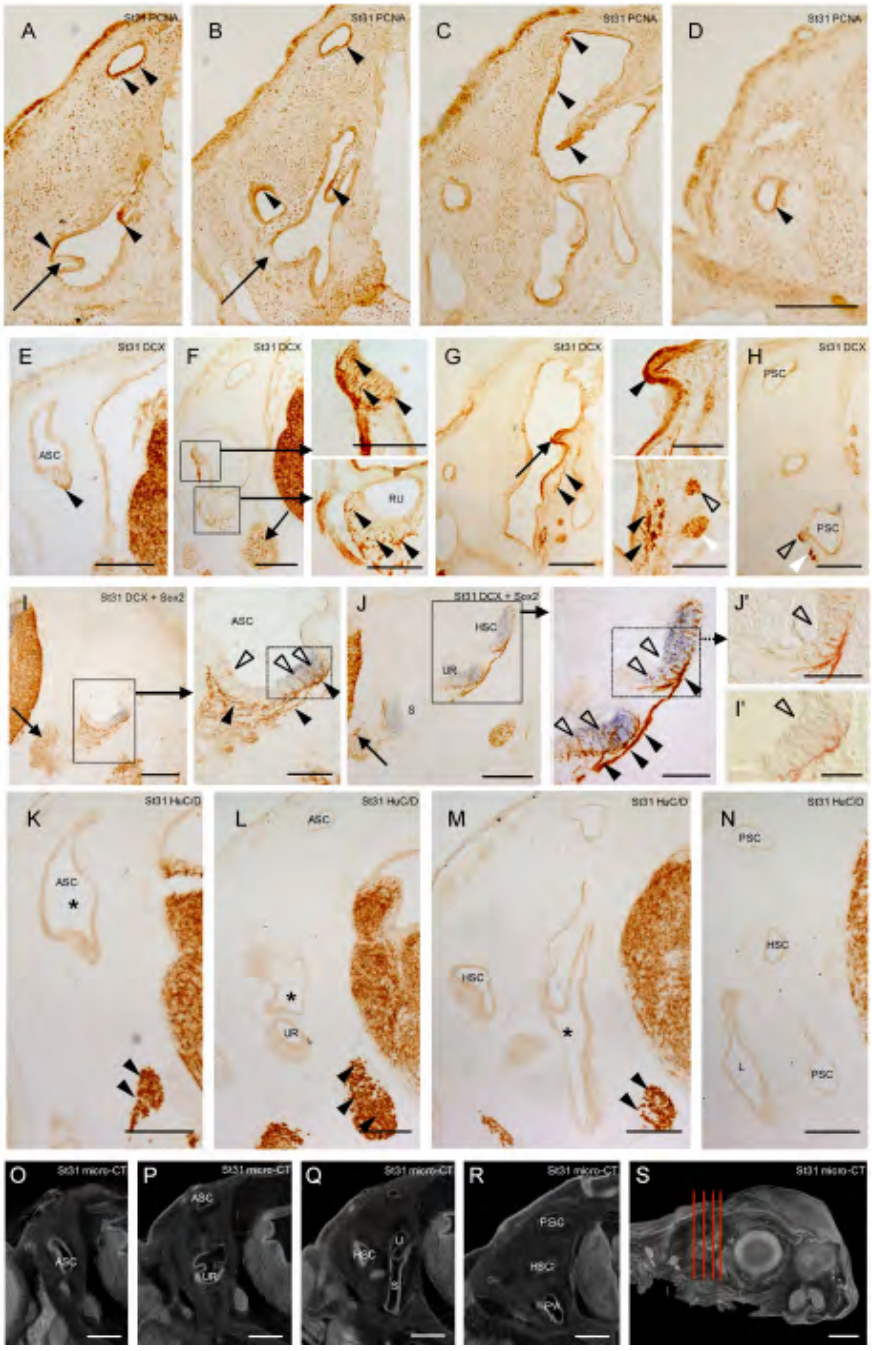
A
St31 PCNA
B
St31 PCNA
C
St31 PCNA
D
St31 PCNA
E
St31 DCX
ASC
F
St31 DCX
RU
G
St31 DCX
H
St31 DCX
PSC
PSC
I
St31 DCX + Sox2
ASC
J
St31 DCX + Sox2
HSC
UR
S
J'
I'
K
St31 HuC/D
ASC
L
St31 HuC/D
ASC
UR
M
St31 HuC/D
HSC
N
St31 HuC/D
PSC
HSC
L
PSC
O
St31 micro-CT
ASC
P
St31 micro-CT
ASC
UR
Q
St31 micro-CT
HSC
U
R
St31 micro-CT
PSC
HSC
PM
S
St31 micro-CT

FIGURE 5

Fig. 6.- Transverse sections (A-N) and micro-CT 2D transverse images (O-R) and 3D parasagittal volume reconstruction (S) of st32 *S. canicula* embryos showing the expression of molecular markers and the morphology of the inner ear. A-D. Panoramic views and details of sections showing immunoreactivity to PCNA in cells of the otic epithelium and in the SAG. The immunoreactivity to PCNA continues to be present in the epithelium surrounding the cavities and canals (A-D; black arrowheads). Note also some cells PCNA-ir in the thickened regions of the sensory patches of ASC (detail of A, A´, outlined arrowheads), HSC (detail in B, outlined arrowheads) and PSC (D, outlined arrowhead), where most of cells are PCNA-negative. The SAG and the statoacoustic nerve (arrow in detail of C) also present immunoreactivity to PCNA. E-H. Panoramic views and details to show the immunoreactivity to DCX in the SAG (detail in F, black arrowheads) and in fibers innervating sensory patches (detail of E and F, G, black arrowheads). Thin DCX-ir fibers enter the sensory patches and reach apical epithelial levels (details of F and H, G, white arrowheads). I-K. Transverse views of the inner ear and SAG showing the immunoreactivity to HuC/D in the SAG (star), in other ganglia and in the brain, but not in the inner ear walls. L-N- Differential interference contrast (DIC) images of the anterior and lateral semicircular ampullae and the utricular recess. The expression of *ScSox2* is present in the sensory patches of the anterior ampullary crista (black arrowheads in detail of L), utricular recess (black arrowheads in detail of M) and lateral crista (black arrowheads in detail of N). All these sensory organs present at this stage (the earliest) bundles of hairs emerging from epithelial cells (empty arrowheads in details).These superficial structures are evident all along the thickened region of the epithelium that defines the sensory patches (empty arrowheads). Note that are even visible at the surface of in small groups of cells in the utricular recess wall that no longer express *ScSox2* (detail of M, arrows). O-S. Transverse 2D micro-CT images of the inner ear and SAG (O-R) and parasagittal 3D reconstruction (S) of a st32 *S. canicula* embryo showing the mature-like aspect of the inner ear and its components. The three sensory cristae are clearly visible protruding into the lumen of the anterior, lateral and posterior ampullae (white arrowheads in O, P and R, respectively). The inner ear has developed all its chambers and is quite similar to posthatching stages. Red lines in P indicate the levels of the transverse sections. Asterisk, inner ear; star, SAG. Scale bars = 2000 µm in S; 500 µm in I-K and O-R; 200 µm in A-H and L-N (100 µm in details) and 50 µm in detail of F.

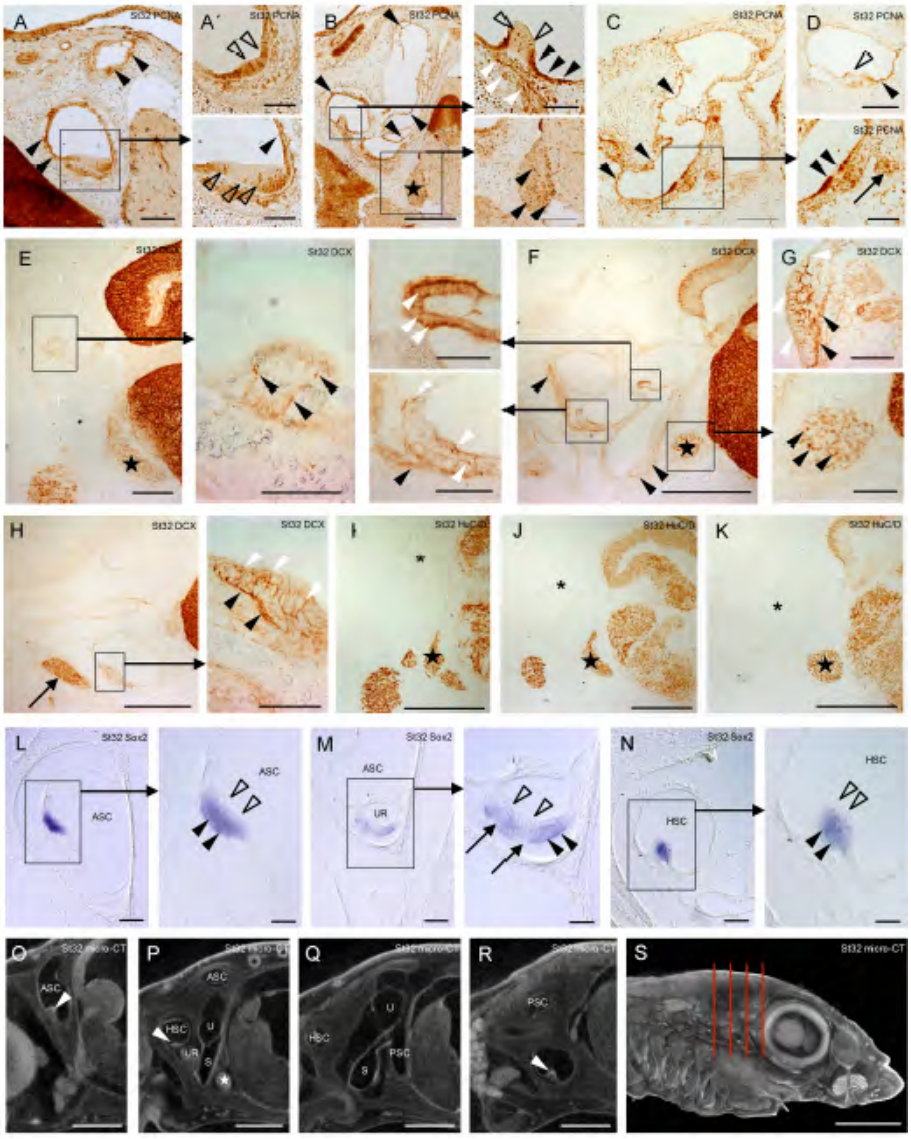
A
St32 PCNA
A'
St32 PCNA
B
St32 PCNA
C
St32 PCNA
D
St32 PCNA
St32 PCNA
E
St32 DCX
St32 DCX
F
St32 DCX
G
St32 DCX
H
St32 DCX
St32 DCX
I
St32 HuC/D
J
St32 HuC/D
K
St32 HuC/D
L
St32 Sox2
ASC
ASC
M
St32 Sox2
ASC
UR
N
St32 Sox2
HSC
HSC
O
St32 micro-CT
ASC
P
St32 micro-CT
ASC
HSC
U
UR
S
Q
St32 micro-CT
U
HSC
PSC
S
R
St32 micro-CT
PSC
S
St32 micro-CT

FIGURE 6

DISCUSSION

GENERAL DISCUSSION

Development of a simple contrast-enhancing and scanning method.

The availability of a procedure for studying complex three-dimensional biological structures like the inner ear is an imperative need. The study of classical histological sections through optic microscopy, despite its excellent resolution and the availability for specific molecular markers such as antibodies or genetic probes against multiple antigens and mRNAs, requires the destruction of the samples. Moreover, the obtained slices of the samples usually present morphological distortions or ruptures, a serious trouble if volumetric reconstruction of the sample is required. Three-dimensional imaging techniques provide a non-distorted and size-calibrated volumetric images of the samples, preserving the volumetric relationship in the original specimen (Metscher, 2009 a). With this in mind, we had to determine which of the available three-dimensional imaging techniques was the most appropriated for our samples and our resources. Micro-computed tomography (micro-CT) and micro-magnetic resonance imaging (micro-MRI) are two 3D imaging techniques that provide high-quality and reliable results of

complex structures, even those composed by soft tissues, and do not require the destruction of the samples for its analysis, allowing the use of the samples for further studies, the combination with other techniques such immunohistochemistry (Metscher, 2011; Metscher and Müller, 2011) or even *in vivo* imaging of samples (De Crespigny et al., 2008; Badea et al., 2008).

Micro-CT appeared to be the most appropriated imaging technique for our samples due to the lower maintenance cost than equivalent micro-MRI, the high resolution, similar to light microscope (Metscher 2009 a, Alba-Tercedor and Sánchez-Tocino, 2011; Metscher and Müller, 2011), the possibility of improving contrast (Babaei et al., 2016; Metscher, 2009 b) and combining with immunohistochemistry (Metscher, 2011; Metscher and Müller, 2011) or even *in vivo* imaging of samples (De Crespigny et al., 2008; Badea et al., 2008).

Micro-CT is useful for analyzing bones, shells and mineralized tissues, but the visualization of soft tissues as early embryos of *S. canicula* is not as cool and requires contrast-enhancing treatment before scanning, as seen in our first attempt with an unstained embryo. Among the different contrast-

enhancing media compatible with micro-CT, we tried staining with Lugol´s solution (IKI), alcoholic iodine (I2M) and phosphotungstic acid (PTA) and also desiccating the samples, but we discarded those that, although efficient, are too hard-working or need special and expensive devices, like the freeze drying or critical point drying (Pawels et al., 2013). Due to the usual shrinkage of soft samples when desiccated, we tried a simple desiccation method using hexamethyldisilazane (HMDS) (Alba-Tercedor and Sánchez-Tocino, 2011; Alba-Tercedor, 2013), which is supposed to prevent shrinkage and is compatible with our methanol-stored samples. Other contrast-enhancing media like gallocyanin-cromallum were discarded due to its low efficiency (Metscher, 2009 a) or to the toxicity or incompatibility of its compounds with methanol, like osmium tetroxide. Stabilization protocols containing acrylamide (Wong et al., 2013) were also discarded due to its toxicity (LoPachin and Gavin, 2012).

The only application of HMDS in non-stained samples produced important distortions in soft embryos, but not in chondrified samples, although the internal contrast was low in both cases and only mineralized structures were appreciated correctly, but thin structures were not visible. If combined with

staining, the contrast was increased, but only in the larger inner structures, while the deep tissues were poorly stained. The contrast-enhancing with PTA prior to desiccation with HMDS slightly prevented the shrinking of the tissues, but only improved the external view. Non-desiccated and stained with I2M soft samples showed a high contrast with almost none shrinking of the tissues and without “stain bleeding”, contrarily to other authors observations (Alba-Tercedor, 2013; Smith et al., 2016). On the other hand, larger and chondrified samples presented lower contrast, but acceptable. When densely chondrified samples were stained with Lugol´s solution, the external appearance presented a high detailed aspect, but the inner regions seemed low-contrasted, maybe because the cartilage reduced the penetration of the solution. PTA seemed to be the best contrast-enhancer for any size of sample, with the advantage of not presenting “staining bleeding” (Smith et al., 2016) and the staining concentrations and times were not critical (Metscher, 2011), although adjusting the staining periods may improve the results in large samples.

The results obtained lead us to establish a simple but effective protocol for improving the contrast and the quality of

the 2D and 3D images provided by micro-CT from embryos and juveniles of *S. canicula*.

General development of the inner ear of *S. canicula*.

The development of the inner ear of chondrychthyans has not been studied as deeply as in other gnathostome groups. Most of the knowledge proceeds from studies of developed inner ears or from studies concerning the development of the whole braincase (Tester et al., 1972; Maisey, 2001, 2004; Lovell et al., 2007; Evangelista et al., 2010). The use of three-dimensional imaging techniques like micro-CT has been increasing in the last years because they allow high-resolution, reliable and reproducible 3D images (Metscher, 2009 a). Once we have developed an appropriated protocol for our samples, as seen above, this technique allowed us to study in detail the formation of the inner ear of *S. canicula* from early embryological stages to post-hatching period. Apart from the morphological development, the obtained data also provide information to compare the development of the inner ear of this chondrichthyan with other groups of vertebrates and to gain knowledge about the evolution of this sense organ.

Similarly to what happens in other vertebrates, the inner ear of *S. canicula* develops from the otic placodes, a pair of thickened regions of the ectoderm adjacent to the hindbrain. Contrarily to that observed in agnathans (hagfishes and lampreys), which present simple inner ears with one or two semicircular canals (Lowenstein and Thornhill, 1970; Thornhill, 1972, McVean, 1991), the inner ear of *S. canicula* meets the requirements of the gnathostome inner ear, including the presence of an horizontal semicircular canal (Mazan et al., 2000). Although some agnathans present common characteristics with gnathostomes, none of them are equivalent to the horizontal semicircular canal (Mazan et al., 2000; Maklad et al., 2014). Among vertebrates, despite the great morphological variability of its inner ears, all of them present the same basic structure, with three perpendicular dorsal semicircular canals, responsible for the detection of the angular acceleration, and a variable number of ventral chambers, responsible for the detection of balance and sound.

At Ballard´s stage 18, the otic placode of *S. canicula* begins to invaginate into an cup or pit. This otic cup closes and forms an ovoid-shape vesicle connected to the exterior by the narrow endolymphatic duct at stage 25, which determines the end of the

first period of the development of the inner ear of *S. canicula.* This invagination process is strikingly different from the cavitation process observed in the otic placodes of teleost fishes and reptiles (Haddon and Lewis, 1996), but similar to the invagination process that occurs in lampreys, amphibians and non-reptile tetrapods (Thornhill, 1972; Haddon and Lewis, 1996; Bissonnette and Fekete, 1996; Morsli et al., 1998).

Despite the invagination process of the otic placodes similar to that observed in other vertebrates, the inner ear of *S. canicula*, as in all the chondrichthyans studied, presents some particularities (Baird, 1974). The endolymphatic duct of *S. canicula* never closes completely, as occurs in all the chondrichthyans (Tester et al., 1972, Baird, 1974). The persistence of the open endolymphatic duct seems to be related to the formation of the endolymphatic fluid and otoliths (Garvin et al., 1988; Eckhardt et al., 2012), but also with the presence of exogenous granules within the inner ear of chondrichthyans (Carlström, 1963; Hanson et al., 1990). Unlike the solid crystallized otoliths of bony fishes or the small otoconia of agnathans and tetrapods (Carlström, 1963; Popper, 2011), the otoliths of *S. canicula* look like aggregated small granules.

The formation of the otic vesicle and the elongation of the endolymphatic duct marks the beginning of the second period of the development of the inner ear of *S. canicula*. As in other vertebrates, the otic vesicle enlarges and modifies its shape by growing protrusions into its lumen and evagination processes that originate the ventral chambers and the dorsal semicircular canals. Two contacting protrusions originate the posterior semicircular canal by stage 27, but the anterior and horizontal canals appear later and approximately at the same time about stage 30. The buds of the chambers begin to arise by stage 27 and by stage 29 are appreciated all the three chambers (utricle, saccule and lagena), but until stage 31 they do not get a developed appearance. The inner of *S. canicula,* like other chondrichthyans (Baird, 1974; Maisey, 2001), is characterized by the presence of the utricular recess, a rostral diverticula which contains the utricular macula and that only a group os osteichthyans, the dipnoans, present (Maisey, 2001).

The order of apparition of the semicircular canals is very variable among vertebrates. In most teleosts, the first canal that appears is the anterior canal and the last os the posterior canal (Waterman and Bell, 1984; Becerra and Anadón, 1993), but there are exceptions to this order in some primitive fishes

(Thomot and Bauchot, 1987) and also in flat fishes, maybe due to the torsion of the head (Becerra et al., 1990). In amphibians, the horizontal semicircular canal uses to appear the first (Haddon and Lewis, 1991), but in birds and mammals it uses to appear the last (Streeter, 1906, Larsell et al., 1936; Bissonnette and Fekete, 1996; Morsli et al., 1998). By the end of stage 31, the gross morphology of the inner ear of *S. canicula* is completed, which marks the end of the second period of its formation.

From stage 32 onwards, the third period of the development begins and the inner ear of *S. canicula* is a miniature of the adulthood and presents some striking characteristics respect to other vertebrates inner ear. The posterior semicircular canal of *S. canicula*, like all the chondrichthyans (Baird, 1974), describes an almost complete circle and avoids the formation of a common cruss with the anterior semicircular canal, like happens in non-choncrichthyan gnathostomes (Baird, 1974, Maisey, 2001). The anterior and horizontal semicircular canals also differ from other gnathostomes because they meet and fuse each other over the utricular recess (Maisey, 2001), instead reaching independently the utricle. Although some bony fishes have a communication between both inner ears that also perceives

vibrations from the swim bladder (Bever and Fekete, 2002; Schulz-Mirbach et al., 2013), none of these structures is present in *S. canicula* nor other chondrichthyan (Baird, 1974, present results). No structure specialized in guiding the sound to the inner ear is present in *S. canicula,* unlike the columnelles or tympanic membranes present in some amphibians (Wever, 1983, Smotherman and Narins, 2004) or reptiles (Wever, 1978; Manley, 2000). There is also no structure resembling the basilar papilla placed in a cochlear duct like occurs in reptiles (Manley, 2000) or the cochlea of birds (Bissonnette and Fekete, 1996) and mammals (Morsli et al., 1998).

Analysis of the expression pattern along the morphogenesis of the inner ear of *S. canicula*.

The use of molecular markers in developmental studies of the inner ear in model organisms like mouse, chicken, *Xenopus* or zebrafish is generalized. From a few years now, the use of *Scyliorhinus canicula* as a model organism for developmental studies due its abundance, easily maintenance, large embryologic period and size and its key phylogenetic position (Coolen et al., 2009). The studies about the embryological development of *S. canicula* provided valuable information for

understanding the differences between chondrichthyans and other vertebrates (reviewed in Rodríguez-Moldes et al., 2017), but there are not deep studies about the development of its inner ear nor other chondrichthyans beyond the development of the cranial placodes and sensory ganglia (O´Neill et al., 2007; Baker et al., 2008).

Once we have previously described the morphological development of the inner ear and determined the three main periods in which it can be divided for a better comprehension, we are well-placed for analyzing the molecular expression patterns and thin aspects of the morphogenesis of the inner ear, including the formation of the SAG, the innervation process and the formation of the sensory organs.

The presence of DCX-immunoreactive (DCX-ir) processes connecting the otic epithelium and the hindbrain at very early stages (st20) reveals the migrating neuroblasts that delaminate from the otic epithelium and form the primordial SAG (present results), similar to the delaminating neurons of the olfactory placode of *S. canicula* (Quintana-Urzainqui et al., 2014). The expression of *NeuroD* in the otic cup by st19 in embryos of *S. canicula* (O´Neill et al., 2007) agrees with the presence of

delaminating neuroblasts that migrate to the SAG, similar to that observed in mouse (Kim et al., 2001). By stage 24 the otic vesicle is almost closed and the DCX-ir fibers innervating the otic epithelium have increased and connect to the migrated neuroblasts, which position agrees with that described at this stage by O´Neil et al. (2007). The SAG becomes a compact mass and by stage 27 presents young ganglion neurons HuC/D-ir. The coexistence of expression of HuC/D-ir neurons, DCX-ir neuroblasts and cells expressing *ScNeuroD* suggests the presence of different stages of differentiating cells in the ganglion.

From the early stage 20, DCX-ir processes are appreciated connecting the otic epithelium and the hindbrain. These processes seem to belong to the first ganglionic neuroblasts that constitute the SAG and that we consider to proceed from the early delaminating neuroblasts from the otic placode/cup. This agrees with studies that show the early innervation of the cochlea in mouse (Fritzsch and Elliot, 2017). By stage 25, two main DCX-ir bundles are recognizable, one projecting rostrally and one projecting caudally to the otic vesicle; which may correspond to the earliest stages of the anterior and posterior branches of the octaval nerve described in the adult *S. canicula*

(Boord and Roberts, 1980) and that coincides with that observed in other vertebrates: an anterior ramus innervating the anterior and horizontal cristae, the utricular macula and the anterior region of the saccular macula; and a posterior ramus innervating the posterior region of the saccular macula, the posterior crista, the lagenar macula and the macula neglecta. In the adulthood, both rami are intermixed and are inseparable (reviewed in Smeets et al., 1983). Later in the development, by stage 31, the DCX-ir bundles from the SAG innervate regions of the otic epithelium which express *Sox2* but lack proliferating (PCNA-ir) cells. The thin DCX-ir fibers extend among the epithelial cells in a compatible way with the existence of calyces located at the base of the hair cells, but further studies are needed.

The morphogenetic events in the walls of the otic vesicle implies expansion in some areas and thickening in others. These changes comprise the differentiation of the epithelial cells in sensory cells, supporting cells and other specialized type of cells. Cells of the otic vesicle adjacent to the SAG express the proneural transcription factor *NeuroD*, (O´Neill et al., 2007, present results). No analyzed stage (st27 and onwards) presented immunoreactivity to the marker of early post mitotic neurons HuC/D in the otic epithelium, but yes in the SAG. *NeuroD* is

needed for the correct survival, migration and organization of neuronal cells (Kim et al., 2001; Kim, 2013). The role of NeuroD, its expression in the otic epithelium in contact to the SAG and the DCX-ir branches innervating the vesicle (present results) suggest that this region originates the migrating neurons of the SAG that innervate the inner ear. Additional regions of the otic epithelium apparently not related to the delimitation of neuroblasts express *NeuroD* at st27, when the formation of the posterior semicircular canal is evident. As far as we know, no expression of *NeuroD* has been reported in regions of the inner ear not related to the delimitation of neuroblasts. A possible explanation is that the morphogenesis of the inner ear could have displaced dorsally the presumptive sensory patch of the posterior semicircular canal that is formed at this stage, which also agrees with the presence of sensorial cells in the anterior and posterior pole of the otocyst of zebrafish (Haddon and Lewis, 1996) and with the expression of certain genes of the Iroquois transcription factor family (Irx1 and Irx3), implied in the maintenance of the proneural and non-proneural identity during the development of the inner ear of the chicken, which are expressed in several sensory patches besides in the acoustic-vestibular ganglion (Cardeña-Núñez et al., 2017).

Although with the present markers we could not describe the differentiation process of the primordial hair cells in the sensory patches, we have seen that the proliferating cells are very abundant along the otic epithelium, but seemed to be absent at the developing sensory patches. The loss pf PCNA-ir and the detection of differentiation markers suggest that the loss pf PCNA immunoreactivity is a sign of differentiation (Ngûyen et al., 2001). The cell patches PCNA immunonegative observed at stages 29 and 31 may be differentiating sensory patches. The coincidence of these PCNA-negativepatches with DCX-ir innervation points in the same way, but double labeling is needed to confirm it. When the gross morphology of the inner ear is completed and the maturation period begins (st32), some PCNA-ir cells appear within these thickened areas, which may be related to the proportional and continuous growth of the inner ear in later development. Filiform structures appreciated with differential interference contrast (DIC) imaging at st32 but not earlier, suggest that the differentiation of the hair cells occurs when the canals and cavities are completely formed.

By stage 31, undifferentiated sensory patches are identifiable by the expression of *Sox2* which coincides with the innervating DCX-ir fibers, revealing the possible contact

structures (calyces) between these innervating fibers and hair cells. The role of *Sox2* in the differentiation of sensory patches in amniotes (Neves et al., 2011, 2013) points in the same way. The maintenance of the expression of *Sox2* in later stages (st32) may be related to the surveillance of supporting cells or the possibility of hair cell regeneration via transdifferentiation sf supporting cells, as occurs in zebrafish (Millimaki et al., 2010).

The early delamination and neurogenesis in the otic cup of *S. canicula* before the formation of the sensory organs is similar to that observed in amniotes (reviewed in Schneider-Maunoury and Pujades, 2007), but different to the early hair cell differentiation in zebrafish (Haddon and Lewis, 1996).

The development of a simple and efficient protocol for staining and scanning embryos and juveniles of *S. canicula* allowed us to obtain high quality images through micro-CT. These images provide a realistic and precise view of the three-dimensional structure of the inner ear at different developmental stages and permit a better comprehension of the spatial expression pattern of different molecular markers.

LITERATURE CITED

- Alba-Tercedor, J, Sánchez-Tocino, L (2011) "The use of the SkyScan 1172 high-resolution micro- CT to elucidate if the spicules of the sea slugs (Mollusca: Nudibranchia, Opisthobranchia) have a structural or a defensive function". *SkyScan Users Meeting* 2011, 113-121.
- Alba Tercedor J (2013) "Study of the anatomy of the common housefly *Musca domestica* Linnaeus, 1758 (Insecta: Diptera, Muscidae) scanned with the Skyscan 1172 high resolution micro-CT". *Bruker Micro-CT Users Meeting 2013,* 275-289.
- Badea CT, Dragonva M, Holdsworth DW, Johnson GA (2008) "In vivo small animal imaging using micro-CT and digital subtraction angiography". *Phys. Med. Biol.* 53: 319-350.
- Baird IL (1974) "Some aspects of the comparative anatomy and evolution of the inner ear in submammalian vertebrates". *Brain Behav. Evol.* 10: 11-36.
- Baker CVH, O'Neill P, McCole RB (2008) "Lateral line, otic and epibranchial placodes: developmental and evolutionary links?" *J. Exp. Zool. B. Mol. Dev. Evol.* 310B: 370-383.
- Ballard WW, Mellinger J, Lechenault H (1993) "A series of normal stages for development of *Scyliorhinus canicula*, the lesser spotted dogfish (Chondrichthyes: Scyliorhinidae)". *J. Exp. Zool.* 267: 318-336.
- Becerra M, Anadón R (1993) "Development of the inner ear of the brown trout (*Salmo trutta fario*): I. Gross morphology and sensory cell proliferation". *J. Morphol.* 216: 209-223.

- Bever MM, Fekete DM (2002) “Atlas of the development of the inner ear in zebrafish”. *Dev. Dynam.* 223: 536-543.
- Bissonnette JP, Fekete DM (1996) “Standard atlas of the gross anatomy of the developing inner ear of the chicken”. *J. Comp. Neurol.* 368:620-630.
- Boord RL, Roberts BL (1980) “Medullary and cerebellar projections of the statoacoustic nerve of the dogfish *Scyliorhinus canicula*". *J. Comp. Neurol.* 193: 57-68.
- Cardeña-Núñez S, Sánchez-Guardado LO, Corral-San-Miguel R, Rodríguez-Gallardo L, Marín F, Puelles L, Aroca P, Hidalgo-Sánchez M (2017) “Expression patterns of Irx genes in the developing chick inner ear”. *Brain Struct. Funct.* 222: 2071-2092.
- Carlström D (1963) “A crystallographic study of vertebrate otoliths”. *Biol. Bull.* 125: 441-463.
- Coolen M, Menuet A, Chassoux D, Compagnucci C, Henry S, Lévèque L, Da Silva C, Gavory F, Samain S, Wincker P, Thermes C, D’Aubenton-Carafa Y, Rodríguez-Moldes I, Naylor G, Depew M, Sourdaine P, Mazan S (2009) “The dogfish *Scyliorhinus canicula*, a reference in jawed vertebrates. In: Behringer RR, Johnson AD, Krumlauf RE (eds) Emerging model organisms. A laboratory manual, vol 1. CSHL Press, Cold Spring Harbor, pp 431-446.
- de Crespigny A, Bou-Reslan H, Nishimura MC, Phillips H, Carano RA, D'Arceuil HE (2008) “3D micro-CT imaging of the postmortem brain”. *J. Neurosci. Methods* 171: 207-213.
- Eckhard A, Gleiser C, Arnold H, Rask-Andersen H, Kumagami H, Müller M, Hirt B, Löwenheim H (2012) “Water channel proteins in the inner ear and their link to hearing impairment and deafness”. *Mol. Aspects Med.* 33: 612-637.

- Evangelista C, Mills M, Siebeck UE, Collin SP (2010) “A comparison of the external morphology of the membranous inner ear in elasmobranchs”. *J. Morphol.* 271: 483-495.
- Fritzsch B, Elliott KL (2017) “Evolution and development of the inner ear efferent system: transforming a motor neuron population to connect to the most unusual motor protein via ancient nicotinic receptors”. *Front. Cell. Neurosci*. 11: 114.
- Garvin JL, Spring KR, Santi PA (1988) “Secretion of endolymph by semicircular canals of the shark”. *Am. J. Physiol.* 255: 711-719.
- Haddon C, Lewis J (1991) “Hyaluronan as a propellant for epithelial movement: the development of semicircular canals in the inner ear of *Xenopus*”. *Development* 112: 541-550.
- Haddon C, Lewis J (1996) “Early ear development in the embryo of the zebrafish, *Danio rerio*”. *J. Comp. Neurol.* 365: 113-128.
- Hanson M, Westerberg H, Öblad M (1990) “The role of magnetic statoconia in dogfish (*Squalus acanthias*)”. *J. Exp. Biol.* 151: 205-218.
- Kim WY, Fritzsch B, Serls A, Bakel LA, Huang EJ, Reichardt LF, Barth DS, Lee JE (2001) “NeuroD-null mice are deaf due to a severe loss of the inner ear sensory neurons during development”. *Development* 128: 417-426.
- Kim WY (2013) “NeuroD regulates neuronal migration”. *Mol. Cells* 35: 444-449.
- Larsell O, McCrady E Jr, Zimmermann (1935) “Morphological and functional development of the membranous labyrinth in the opossum”. *J. Comp. Neurol.* 63: 95-118.

- LoPachin RM, Gavin T (2012) "Molecular mechanism of acrylamide neurotoxicity:lessons learned from organic chemistry". *Environ. Health Perspect.* 120: 1650-1657.
- Lovell JM, Findlay MM, Harper GM, Moate RM (2007) “The polarization of hair cells from the inner ear of the lesser spotted dogfish *Scyliorhinus canicula*”. *J. Fish Biol.* 70: 362-373.
- Lowenstein O, Thornhill RA (1970) “The labyrinth of myxine: anatomy, ultrastructure and electrophysiology”. *Proc. R. Soc. Lond. B. Biol. Sci*. 176: 21-42.
- Maisey JG (2001) “Remarks on the inner ear of elasmobranchs and its interpretation from skeletal labyrinth morphology”. *J. Morphol.* 250: 236-264.
- Maisey JG (2004) “Morphology of the braincase in the broadnose sevengill shark *Notorynchus* (Elasmobranchii, Hexanchiformes), based on CT scanning”. *Am. Mu. Novit.* 3429**:** 1-52.
- Maklad A, Reed C, Johnson NS, Fritzsch B (2014) “Anatomy of the lamprey ear: morphological evidence for occurrence of horizontal semicircular ducts in the labyrinth of *Petromyzon marinus*”. *J. Anat.* 224: 432-446.
- Manley GA (2000) “The hearing organs of lizards”. In: Dooling R, Popper AN, Fay RR, editors. “Comparative hearing: birds and reptiles. Springer Handbook of Auditory Research” p. 139–196.
- Mazan S, Jaillard D, Baratte B, Janvier P (2000) “Otx1 gene-controlled morphogenesis of the horizontal semicircular canal and the origin of the gnathostome characteristics”. *Evol. Dev.* 2: 186-193.
- McVean A (1991) “The semicircular canals of the hagfish *Myxine glutinosa*” *J. Zool. Lond.* 224: 213-222.

- Metscher BD (2009 a) “MicroCT for developmental biology: a versatile tool for high-contrast 3D imaging at histological resolutions”. *Dev. Dynam.* 238: 632-640.
- Metscher BD (2009b) “MicroCT for comparative morphology: simple staining methods allow high-contrast 3D imaging of diverse non-mineralized animal tissues”. *BMC Physiol*. 9:11 doi: 10.1186/1472-6793-9-11.
- Metscher BD (2011) "X-ray microtomographic imaging of intact vertebrate embryos”. *Cold Spring Harb. Protoc.* 12: 1462-1471.
- Metscher BD, Müller GB (2011) “MicroCT for molecular imaging: quantitative visualization of complete three-dimensional distributions of gene products in embryonic limbs”. *Dev. Dynam.* 240: 2301-2308.
- Millimaki BB, Sweet EM, Riley BB (2010) “Sox2 is required for maintenance and regeneration, but not initial development, of hair cells in the zebrafish inner ear”. *Dev. Biol.* 338: 262-269.
- Morsli H, Choo D, Ryan A, Johnson R, Wu DK (1998) “Development of the mouse inner ear and origin of its sensory organs”. *J. Neurosci.* 18: 3327-3335.
- Neves J, Parada C, Chamizo M, Giraldez F (2011) “Jagged 1 regulates the restriction of Sox2 expression in the developing chicken inner ear: a mechanism for sensory organ specification”. *Development* 138: 735-744.
- Neves J, Vachkov I, Giráldez F (2013) “Sox2 regulation of hair cell development: incoherence makes sense”. *Hearing Res*. 297: 20-29.
- Ngûyen V, Candal-Suárez EM, Sharif A, Joly JS, Bourrat F (2001) “Expression of Ol-KIP, a cyclin dependent kinase

inhibitor, in embryonic and adult medaka (*Oryzias latipes*) central nervous system". *Dev. Dyn*. 222: 439-449

- O´Neill P, McCole RB, Baker CVH (2007) "A molecular analysis of neurogenic placode and cranial sensory ganglion development in the shark, *Scyliorhinus canicula*". *Dev. Biol.* 304: 156-181.
- Pauwels E, Van Loo D, Cornillie P, Brabant L, Van Hoorebeke L (2013) "An exploratory study of contrast agents for soft tissue visualization by means of high resolution X-ray computed tomography imaging". *J. Microsc*. 250: 21-31.
- Popper AN (2011) "Auditory system morphology". In *Encyclopedia of Fish Physiology: From Genome to Environment*. Ed. Farrel AP. San Diego: Academic, 252–261.
- Quintana-Urzainqui I, Rodríguez-Moldes I, Candal E (2014a) "Developmental, tract-tracing and immunohistochemical study of the peripheral olfactory system in a basal vertebrate: insights on Pax6 neurons migrating along the olfactory nerve". *Brain Struct. Funct*. 219: 85-104.
- Quintana-Urzainqui I, Anadón R, Candal E, Rodríguez-Moldes I (2014b) "Development of the terminal nerve system in the shark *Scyliorhinus canicula*". *Brain Behav Evol*. 84:277-287.
- Rodríguez-Moldes I, Santos-Durán GN, Pose-Méndez S, Quintana-Urzainqui I, Candal E (2017) ‘‘The brains of cartilaginous fishes’’ *Evolution of Nervous Systems* (Vol. 1), ed. J. Kaas (Oxford: Elsevier), 77-97.
- Schneider-Maunoury S, Pujades C (2007) "Hindbrain signals in otic regionalization: walk on the wild side" *Int. J. Dev. Biol.* 51: 495-506.
- Schulz-Mirbach T, Heß M, Metscher BD, Ladich F (2013) "A unique swim bladder-inner ear connection in a teleost

fish revealed by a combined high-resolution microtomographic and three-dimensional histological study ". *BMC Biol.* 11: 75-87.

- Smeets WJAJ, Nieuwenhuys R, Roberts BL (1983) "The central nervous system of cartilaginous fishes. Structural and functional correlations". Springer-Verlag Berlin Heidelberg. Chapter 6, pp 40-41.
- Smith DB, Bernhardt G, Raine NE, Abel RL, Sykes D, Ahmed F, Pedroso I, Gill RJ (2016) "Exploring miniature insect brains using micro-CT scanning techniques". *Sci. Rep.* 6: 21768-21777.
- Streeter GL (1906) "On the development of the membranous labyrinth and the acoustic and facial nerves in the human embryo". *Am. J. Anat*. 6: 139-165.
- Tester AL; Kendall JI, Milisen WB (1972) "Morphology of the ear of the shark genus *Carcharhinus*, with particular reference to the macula neglecta". *Pac. Sci.* 26: 264-274.
- Thomot A**,** Bauchot R (1987) "L'organogenesis du labyrinthe membraneux chez Polypterus senegalus Cuvier, 1829. (Pisces, Holostei, Polypteridae)". *Anat. Anz*. 164: 189-211.
- Waterman RE, Bell DH (1984) "Epithelial fusion during early semicircular canal formation in the embryonic zebrafish, *Brachydanio rerio*". *Anat. Record* 210: 101-114.
- Wever EG (1978) "The ear of the chameleon- *Chamaeleo senegalensis* and *Chamaeleo quilensis*". *J. Exp. Zool.* 168: 423-436.
- Wever EG (1983) "The ear and hearing in the frog, *Rana pipiens*". *J. Morph.* 141: 461-478.

RESUMEN

RESUMEN

El oído interno de los vertebrados es el órgano responsable de la percepción del sonido, equilibrio y aceleración. Su origen se remonta a la evolución temprana de los vertebrados hace unos 600 millones de años y está presente en todos los vertebrados craneados, desde agnatos como las lampreas y mixines, hasta los vertebrados mandibulados que incluyen a los peces, anfibios, reptiles, aves y mamíferos. El oído interno de todos los vertebrados comprende una región dorsal con un número variable de canales semicirculares, cada uno con una cresta sensorial, y una región ventral con diferentes cavidades y máculas sensoriales otolíticas y no otolíticas, todo ello encajado en una cápsula ótica ósea o cartilaginosa.

A pesar de las diferencias morfológicas entre los oídos internos de los vertebrados, todos ellos se originan a partir de las placodas óticas, un par de engrosamientos del ectodermo adyacentes al rombencéfalo que, mediante un proceso de cavitación (en teleósteos y reptiles) o de invaginación (en lampreas, condrictios y tetrápodos no reptiles), forma la vesícula ótica. Posteriormente, la vesícula ótica aumenta de tamaño y sufre cambios morfológicos que, debido a la expansión diferencial de unas regiones respecto a otras y al crecimiento de protrusiones internas que delimitan los canales semicirculares, dan lugar a la forma madura del oído interno.

El oído interno de los agnatos se caracteriza por ser más sencillo y presentar sólo uno (en mixines) o dos (en lampreas) canales semicirculares

verticales. El oído interno de los mixines tiene forma de anillo irregular, con una cresta sensorial anterior y una cresta sensorial posterior, además de una única mácula sensorial ventral con otoconias asociadas. El oído interno de lampreas presenta dos canales semicirculares verticales, cada uno con una cresta sensorial, y, al igual que los mixines, una única mácula sensorial ventral asociada a otoconias.

Los vertebrados mandibulados tienen un oído interno más complejo que se caracteriza por la presencia de un canal semicircular horizontal dispuesto perpendicularmente a los canales verticales. A pesar de existir una gran variabilidad morfológica entre los oídos internos de los gnatóstomos, todos ellos comparten un patrón básico, con los tres canales semicirculares en la región dorsal y varias cámaras en la región ventral, que es la que mayor diversidad presenta. En peces esta región está constituida por dos grandes cámaras, el utrículo y el sáculo, con una tercera más pequeña, la lagena, asociada a la región caudal del sáculo. Cada cámara contiene una mácula sensorial con otolitos asociados, además de una mácula no otolítica, la mácula neglecta. En algunos teleósteos existe un canal comunicante entre los sáculos de ambos oídos que recibe vibraciones procedentes de la vejiga natatoria a través de los osículos de Webber, que funcionalmente podría ser equivalente al oído medio de los tetrápodos. También existen diferencias morfológicas entre el oído interno de peces teleósteos y cartilaginosos.

El oído de los peces teleósteos, como el de los demás gnatóstomos, no presenta una comunicación directa con el exterior del cuerpo. Por el

contrario, en los peces cartilaginosos, el conducto de invaginación de la copa ótica nunca llega a cerrarse y persiste en el estado adulto como el conducto endolinfático, que conecta el interior del oído con el exterior del cuerpo. Los teleósteos, al contrario, no presentan dicho conducto, aunque desarrollan un tubo ciego que no llega a abrirse al exterior denominado igualmente conducto endolinfático. Además, los elasmobranquios (tiburones, rayas y torpedos) presentan un canal semicircular posterior independiente que describe casi un círculo completo y que se comunica con el utrículo por un único conducto, a diferencia de los holocéfalos (quimeras) teleósteos y tetrápodos, cuyo canal semicircular posterior se fusiona con el anterior en una *cruss commune.*

El oído interno de los tetrápodos presenta una gran variabilidad morfológica, sin embargo, todos comparten a presencia de otoconias en vez de otolitos asociadas a las máculas sensoriales y una estructura cerrada. El conducto endolinfático se cierra y desarrolla una dilatación en su extremo, el saco endolinfático, que no se comunica con el exterior. En anfibios aparecen junto con el utrículo, sáculo y lagena, los recesos de la papila basilar y de la papila anfibia, responsables de la sensibilidad auditiva. Además, con frecuencia presentan estructuras accesorias destinadas a mejorar la audición tanto bajo el agua como en el aire, como membranas timpánicas que transmiten las vibraciones sonoras hasta el oído interno mediante unas columnelas.

Los reptiles son el grupo vertebrado que mayor diversidad presentan en relación a la morfología del oído interno, siendo la mayor innovación la aparición de un conducto coclear que contiene la papila basilar cubierta por una membrana tectorial en su parte proximal y la mácula lagenar en la parte distal. Al igual que otros tetrápodos, presentan estructuras accesorias como membranas timpánicas que mejoran la capacidad auditiva, aunque hay grupos que carecen de dichas estructuras.

El oído interno de las aves presenta una considerable similitud con el esquema general de los reptiles. El oído interno presenta un conducto coclear especializado en la percepción auditiva, con la papila basilar ocupando la mayor parte de su longitud y la lagena localizada en su extremo distal.

Los mamíferos tienen un oído interno complejo, en el que el conducto coclear se alarga y enrolla sobre sí mismo. La cóclea de mamíferos contiene el órgano de Corti, especializado en la percepción acústica, y carece de la mácula lagenar en su extremo distal.

El patrón de desarrollo que transforma la placoda ótica en la vesícula ótica y finalmente el oído interno es compartido por todos los vertebrados. Debido a ello, el conocimiento de los mecanismos morfogenéticos básicos ayudará a comprender las procesos que pueden ser la causa de alteraciones en el sentido de la audición o del equilibrio. La mayor parte de la información sobre el desarrollo del oído interno de los vertebrados procede

de estudios realizados en ratón, pollo y pez cebra. Este último ha sido considerado un modelo canónico para estudios del desarrollo y representativo de todos los peces, a pesar de las importantes diferencias entre el oído interno de los peces óseos y cartilaginosos. La posición filogenética de los peces cartilaginosos la base del linaje gnatóstomo y próximos a la condición ancestral los hace un modelo ideal para el estudio del origen, desarrollo y evolución del oído interno. Entre los condrictios, la pintarroja *Scyliorhinus canicula* es un modelo ideal para estudios morfogenéticos debido a su abundancia, su desarrollo lento con embriones relativamente grandes y la transparencia de los huevos que facilita la identificación de las etapas embrionarias. Estas características han hecho de *S. canicula* un modelo de interés para estudios del desarrollo desde hace décadas. Ante la idoneidad de la pintarroja como organismo modelo, la escasa información sobre el desarrollo del oído de los peces cartilaginosos y la disponibilidad de herramientas genéticas y de microtomografía computerizada (micto-CT), nos planteamos como objetivos desarrollar un protocolo sencillo para mejorar el contraste y la obtención de imágenes mediante micro-CT, aplicar ese protocolo para analizar el desarrollo del oído interno de la pintarroja a lo largo de su etapa embrionaria y juvenil y analizar el patrón de expresión de diferentes marcadores moleculares que participan en el desarrollo del oído interno de esta especie.

Para estudiar estructuras biológicas complejas como el oído interno es necesario disponer de un método capaz de de proporcionar imágenes de alta resolución y que representen la forma real de las muestras. El estudio de

microscópico de secciones histológicas clásicas proporciona una gran resolución y permite el marcaje molecular específico. Sin embargo, requiere el seccionado de las muestras, que pueden sufrir importantes distorsiones o roturas durante el proceso, lo que dificulta una posible reconstrucción volumétrica. Las técnicas de imagen tridimensional proporcionan representaciones volumétricas realistas y no distorsionadas de las muestras. Entre las técnicas disponibles, la micro-tomografía computerizada (micro-CT) y la imagen por micro-resonancia magnética (micro-MRI) proporcionan imágenes de alta calidad y permiten la combinación con técnicas inmunohistoquímicas o la toma de imágenes de animales vivos.

La técnica micro-CT es la más apropiada para nuestras muestras por su alta resolución y reducido coste frente a la micro-MRI equivalente, por lo que es la técnica seleccionada para desarrollar un protocolo sencillo adecuado para estudiar nuestras muestras. El micro-CT una técnica muy adecuada para estudiar estructuras densas o mineralizadas como conchas, huesos o dientes, pero para el estudio de tejidos blandos es necesario el empleo de sustancias que incrementen su contraste. Entre los diferentes medios potenciadores de contraste hemos testado la solución de Lugol, la iodina alcohólica (I2M) y el ácido fosfotúngstico (PTA). También hemos probado la desecación de las muestras con hexametildisilazano (HMDS) por su supuesto efecto protector ante la deformación de las mismas durante su manipulación. Otros medios fueron descartados por su baja eficiencia o por su toxicidad.

Pese a lo esperado, la desecación con HMDS en embriones tempranos provoca grandes distorsiones, mientras que en embriones tardíos ya condrificados no incrementa suficientemente el contraste interno. Cuando se combina la desecación con HMDS con la tinción con PTA, las distorsiones son menores y el contraste mejora, pero sólo en los tejidos superficiales. La tinción de embriones tempranos con I2M muestra un buen incremento del contraste con poca deformación, mientras que en muestras grandes y con mucho cartílago el contraste es menor, pero aceptable. La solución de Lugol empleada como medio de contraste de muestras grandes proporciona unas imágenes con un gran detalle de su superficie externa y zonas superficiales, pero las regiones profundas presentan escaso contraste, posiblemente debido a que el propio cartílago limita la penetración de la solución. El empleo de PTA como medio de contraste proporciona imágenes con buena resolución y contraste en embriones de cualquier tamaño y tiene la ventaja de no sobreteñir las muestras, al contrario que la iodina alcohólica.

Los resultados obtenidos con los diferentes medios de contraste nos permitieron desarrollar un protocolo sencillo para la obtención de imágenes en dos y tres dimensiones con alta resolución en embriones de cualquier etapa del desarrollo y de juveniles de pintarroja, lo que permitió el desarrollo del capítulo 2 de la tesis.

Una vez establecido el protocolo más adecuado para nuestras muestras de *S. canicula*, lo aplicamos para escanearlas en la Estación de Biología Marina de la Universidad de Santiago de Compostela, en A Graña. Los

escaneos fueron realizados con un microtomógrafo Bruker Skyscan 1172 y las muestras analizadas comprenden desde embriones tempranos donde se inicia el desarrollo del oído interno (st18) hasta tardíos y ejemplares juveniles, incluidos algunos oídos diseccionados de juveniles.

Las primeras señales indicando el inicio de la formación del oído interno de la pintarroja se aprecian en la etapa 18 de Ballard, cuando la placoda ótica comienza a invaginarse en forma de copa. Este proceso de invaginación difiere significativamente del proceso de cavitación que sufren las placodas de peces telósteos y reptiles, pero es similar a lo que ocurre en lampreas, anfibios y amniotas no reptiles. La copa ótica se cierra hasta tomar forma de vesícula en la etapa 24, cuando se comunica con el exterior sólo mediante un pequeño orificio, que a partir de la etapa 25 se alarga formando el conducto endolinfático. El cierre de la vesícula y la elongacoón del conducto endolinfático determinan el final de la primera etapa de la formación del oído interno de la pintarroja. Como en los demás condrictios, el conducto endolinfático de la pintarroja nunca llega a cerrarse completamente y se mantiene en la etapa adulta.

Una vez formada la vesícula ótica y la elongación del conducto endolinfático, comienza la segunda etapa de la formación del oído de la pintarroja. Como en los demás vertebrados, la vesícula crece y modifica su forma mediante procesos de evaginación que originan las cámaras centrales y el crecimiento de protrusiones internas que delimitan los canales semicirculares. En la etapa 27 de Ballard se empiezan a apreciar los esbozos

de las cámaras centrales y se produce el contacto entre dos protrusiones, lo que forma un pilar que supone el origen del canal semicircular posterior. Los canales anterior y horizontal no se forman, aproximadamente a la vez, hasta la etapa 30. El orden de formación de los canales semicirculares es muy variable entre los vertebrados. En la mayoría de los teleósteos el primero en formarse es el anterior y el último el posterior, pero hay excepciones como algunos peces primitivos o los peces planos. En anfibios es el canal horizontal el primero en formares, mientras que en aves y en mamíferos suele ser el último en aparecer. Al final de la etapa 31, el desarrollo del oído de la pintarroja completa su segundo periodo de formación, en el que presenta todas sus cámaras y canales ya formados y tiene una apariencia similar al estado juvenil y adulto.

Desde la etapa 32 en adelante comienza la tercera etapa del desarrollo del oído interno de *S. canicula*, en la que se produce la maduración de los órganos sensoriales. A partir de este momento el oído crece en tamaño y completa el desarrollo de las células sensoriales, pero su estructura anatómica ya no se modifica.

La información obtenida en este capítulo sobre la disposición tridimensional de todas las partes del oído interno durante su desarrollo permite una mejor comprensión del patrón de expresión de diferentes marcadores moleculares empleados en el tercer capítulo.

El estudio de marcadores moleculares durante el desarrollo del oído interno de organismos modelo como ratón, pollo, *Xenopus* o pez cebra es generalizado. El estudio del patrón de expresión de marcadores moleculares a lo largo del desarrollo de un pez cartilaginoso como la pintarroja proporciona valiosa información para entender las diferencias entre los condrictios y los demás vertebrados, aunque todavía no se hayan realizado estudios en profundidad sobre el desarrollo de su oído interno.

Una vez descrito el desarrollo morfológico del oído interno y establecidos los tres principales periodos de su formación, podemos analizar los patrones de expresión de diferentes marcadores moleculares que intervienen en su morfogénesis, así como en la formación de galio estatoacústico (SAG), el proceso de inervación y la formación de los órganos sensoriales.

En etapas tempranas del desarrollo embrionario de la pintarroja (st19 y st20), detectamos procesos immunorreactivos a DCX, un marcador de neuroblastos en migración, (DCX-ir) que muestran como neuroblastos se delaminan desde el epitelio ótico y forman el primordio del SAG, así como la expresión de *NeuroD* en la copa ótica, coherente con esa delaminación. Esta delaminación en etapas tan tempranas del desarrollo es similar a la delaminación temprana que ocurre durante el desarrollo del oído interno de vertebrados amniotas.

En la etapa 24 de Ballard, la vesícula ótica está casi cerrada y las fibras DCX-ir procedente del SAG que la inervan se han incrementado notablemente. En la etapa 25 se reconocen dos haces principales DCX-ir, uno proyectando rostralmente y otro caudalmente, que se corresponderían con las primeras etapas de las ramas anterior y posterior del nervio octavo descritas en el adulto de *S. canicula* por otros autores y que también concuerda con lo observado en otros vertebrados: la rama anterior inervando las crestas anterior y horizontal, la mácula utricular y la parte anterior de la mácula del sáculo; y la rama posterior inervando la parte posterior de la mácula del sáculo, las máculas lagenar y neglecta y la cresta posterior. Ambas ramas están intermezcladas y son inseparables en el adulto. En embriones tardíos, las zonas del epitelio ótico inervadas por haces DCX-ir desde el SAG expresan *Sox2*, pero carecen de células proliferantes, al contrario que el resto del epitelio.

Durante el crecimiento de las paredes de la vesícula ótica, unas áreas se expanden y otras se engrosan a medida que las células epiteliales se diferencian en células sensoriales, células de soporte u otro tipo celular. Las células del epitelio ótico adyacentes al SAG expresan el factor de transcripción proneural NeuroD, necesario para la supervivencia celular migración y organización de las neuronas, lo que sugiere que de esta región del epitelio ótico se delaminan las neuronas que forman el SAG e inervan la vesícula ótica. Además, también hay expresión de NeuroD en regiones dorso-caudales del epitelio ótico aparentemente no relacionadas con el SAG en la etapa 27, cuando se forma el canal semicircular posterior. Esa

expresión posiblemente se debe a que durante la morfogénesis de este canal, el primordio del parche sensorial del canal posterior se haya desplazado dorsalmente.

Las células proliferantes (PCNA-ir) son muy abundantes a lo largo del epitelio ótico, pero es llamativa su ausencia en los primordios de las máculas y crestas sensoriales, lo que puede indicar que las células de esas regiones se estén diferenciando en células sensoriales. La inervación de esas zonas no proliferantes en los estadíos 29 y 31 con fibras DCX-ir y la expresión de Sox2, implicado en la diferenciación sensorial, sugiere que esas regiones originarán parches sensoriales. En estadío 32, con el desarrollo morfológico del oído completo, aparecen algunas células proliferantes en las regiones engrosadas del epitelio, posiblemente relacionadas con el crecimiento continuo del oído durante el desarrollo tardío. En esta etapa también se empiezan a apreciar estructuras filiformes en la superficie de estas zonas con microscopía de contraste de fases, lo que indica que las células sensoriales ciliadas empiezan a formarse cuando los canales y cámaras completan su desarrollo morfológico. Así mismo, el mantenimiento de la expresión del factor de transcripción Sox2 en estas zonas posiblemente esté relacionado con el mantenimiento y supervivencia de las células de soporte y con la posibilidad de que la celular ciliadas se regeneren mediante la transdiferenciación de células de soporte, como ocurre en otras especies. Esta diferenciación tardía de las células ciliadas de la Scyliorhinus canicula contrasta con la diferenciación temprana que ocurre en peces teleósteos.

Este estudio ha permitido desarrollar un protocolo sencillo para aumentar el contraste y escanear mediante micro-CT muestras de ejemplares de Scyliorhinus canicula en cualquier momento de su desarrollo. Este protocolo ha permitido obtener imágenes de alta resolución de diferentes etapas del desarrollo de la pintarroja y a partir de ellas describir de forma precisa y realista el desarrollo del oído interno. El estudio de los patrones de expresión de diferentes marcadores moleculares en diferentes etapas del desarrollo, con el apoyo de la descripción morfológica proporcionada por las imágenes obtenidas con los escaneos, ha permitido una mejor comprensión del desarrollo del oído interno de la pintarroja y también comparar los resultados obtenidos con otros animales modelo para entender mejor la evolución del oído interno de los vertebrados.

CONCLUSIONES

CONCLUSIONES

1. El empleo de medios de contraste para muestras escaneadas mediante microtomografía computerizada ha resultado ser un método eficiente para obtener imágenes bidimensionales y tridimensionales del desarrollo embrionario de *Scyliorhinus canicula*, desde el tejido blando de las etapas tempranas hasta muestras de juveniles completamente condrificadas, y particularmente, para el estudio de estructuras tridimensionales complejas y frágiles como el oído interno. Todo ello demuestra la utilidad de esta técnica con diferentes tipos de muestras, no solo con las mineralizadas como conchas, huesos o dientes, sino también con tejidos blandos, aunque se debe aplicar algún medio de contraste.

2. Después de probar diferentes métodos de secado y medios de contraste para obtener imágenes mediante micro-CT de embriones y juveniles fijados del tiburón *Scyliorhinus canicula*, hemos determinado que el protocolo más eficiente y sencillo para obtenerlas a partir de embriones de distintas etapas del desarrollo y oídos diseccionados es la tinción con ácido fosfotúngstico, aunque la tinción con yodina también proporcionó resultados aceptables.

3. La aplicación de medios de contraste y protocolos de escaneo adecuados a embriones y juveniles de *Scyliorhinus canicula* ha

permitido obtener las primeras imágenes de alta resolución del desarrollo global del oído interno de un condrictio, desde etapas embrionarias tempranas, cuando la placoda empieza a invaginarse, hasta la etapa juvenil, cuando el oído interno es una miniatura del estado adulto. El análisis de las imágenes bidimensionales y tridimensionales obtenidas ha hecho posible la elaboración de una descripción realista y detallada de la morfogénesis del oído interno del tiburón *S. canicula*, reconocido como la especie representante del grupo de los peces cartilaginosos.

4. El desarrollo del oído interno de *S. canicula*, a diferencia de lo observado en peces óseos y reptiles, ocurre por un proceso de invaginación de la placoda ótica similar a lo observado en lampreas y tetrápodos no reptiles. Este desarrollo comienza en etapas tan tempranas como el estadío 18 de Ballard y comprende aproximadamente un tercio del periodo embriológico completo, hasta que el oído interno alcanza un aspecto similar al maduro al final de la etapa 31.

5. Con el fin de proporcionar un marco comparativo, el proceso de desarrollo del oído interno de *S. canicula* puede dividirse en tres periodos de acuerdo con los cambios morfológicos que ocurren y en base a características externas y eventos de referencia. El primer periodo comprende desde la etapa de placoda hasta la formación de la

vesícula ótica al en la etapa 25de Ballard; el segundo periodo comprende la transformación de la vesícula redonda en la etapa 25 en un oído similar al maduro al final de la etapa 31 de Ballard; y el tercer periodo comienza en la etapa 32 e implica el crecimiento de acuerdo al tamaño corporal y la maduración de los órganos sensoriales.

6. En este estudio se ha demostrado que en el estadio 32 de Ballard se reconoce la morfología madura del oído interno, con tres canales semicirculares perpendiculares y tres cámaras ventrales: el utrículo (con el receso utricular), el sáculo, localizado ventralmente al utrículo y conectado con él mediante un conducto estrecho; y la lagena en la parte posterior del sáculo y conectado con él mediante un espacio amplio. Esta organización se corresponde con las características generales de los gnatóstomos,

7. El canal semicircular posterior es casi un círculo completo conectado con el utrículo por un solo conducto, e implica la ausencia de la *cruss commune* entre la rama anterior del canal semicircular posterior y la rama posterior del canal semicircular anterior, como ocurren en vertebrados no elasmobranquios. Al contrario que en tetrápodos y peces óseos, el canal semicircular anterior y el canal semicircular horizontal se encuentran y fusionan sobre el receso utricular, lo que puede distinguirse desde el estadio 32, que hemos

identificado como el comienzo de la maduración de los órganos sensoriales.

8. El oído interno de *S. canicula* se comunica con el exterior mediante el conducto endolinfático, una reminiscencia del proceso de invaginación que nunca se cierra completamente. El conducto endolinfático emerge desde la pared medial del sáculo y discurre dorsalmente, tomando una trayectoria sinuosa en su región dorsal, antes de abrirse al exterior en lo alto de la cabeza, próximo a la línea media. Este estudio revela que el conducto endolinfático se forma como consecuencia del proceso de invaginación y no se trata de un nuevo conducto.

9. Este es el primer estudio describiendo el origen, desarrollo y conexión entre los componentes del oído interno del tiburón *S. canicula*. Basándonos en los patrones de expresión de ciertos marcadores como DCX, HuC/D y *NeuroD* en el **primer periodo** del desarrollo del oído interno, hemos identificado la formación de las neuronas primarias del ganglio estatoacústico, originadas por delaminación desde el epitelio ótico, similar a lo observado en otros vertebrados.

10. El desarrollo de la inervación del oído interno ocurre durante un largo periodo, aproximadamente dos meses, desde las primeras

etapas en las que fibras immunorreacivas a la DCX aparecen uniendo la copa ótica con el cerebro (st20), hasta las etapas tardías en las que el patrón de inervación está completo (st32). La inervación de todas las áreas sensoriales de esta estructura se incrementa y aparecen nuevas ramas a medida que la vesícula ótica crece y se subdivide. Cuando se completa, durante el **segundo período**, todos los órganos sensoriales que se están diferenciado, reciben inervación del ganglio estatoacústico.

11. La maduración de los órganos sensoriales tiene lugar durante el **tercer período**, siendo su distribución y número similares a las de otros condrictios, con tres máculas otolíticas localizadas en el receso utricular, el sáculo y la lagena; una mácula neglecta no otolítica localizada cerca del límite utrículo-sacular y el conducto que conecta las cámaras con el canal semicircular posterior; y tres crestas sensoriales ampulares comunes a todos los gnatóstomos.

12. La proliferación celular es muy abundante durante el desarrollo del oído interno en las paredes del laberinto y también en el ganglio estatoacústico, pero no aparece en los parches sensoriales presuntivos hasta que el desarrollo morfológico está completo al final de la etapa 31. En la etapa 32, algunas células de las máculas y crestas engrosadas empiezan a proliferar. Al mismo tiempo, se pueden

distinguir algunas células ciliadas diferenciadas en los parches sensoriales.

13. La formación del ganglio estatoacústico comienza en etapas tempranas del primer periodo y continúa por delaminación durante el segundo periodo. Células ganglionares diferenciadas están presentes en el ganglio desde etapas intermedias como st27, indicando que la maduración de las células del ganglio precede a la de las células sensoriales.

14. La maduración retrasada de los parches sensoriales en relación a la maduración del ganglio también es evidenciada por la expresión de *Sox2* en etapas tardías en estas regiones, lo que indica el mantenimiento de la pluripotencialidad en células de las máculas y las crestas y también la capacidad de originar nuevas células ciliadas.

15. Los resultados obtenidos proporcionan datos abundantes y útiles para comparar con el desarrollo del oído interno en otros organismos modelos y también para incrementar nuestro conocimiento sobre la evolución del desarrollo de este órgano sensorial. Este trabajo muestra la utilidad de los estudios 3D para aumentar el conocimiento sobre el desarrollo de estructuras complejas y sienta la base para la implementación de un atlas del desarrollo del oído interno de *S. canicula*.

CONCLUSIONS

CONCLUSSIONS

1. The use of contrast-enhancing methods associated for scanning samples through micro-CT has proved to be an efficient way to obtain two-dimensional and three-dimensional images of the embryonic development of *Scyliorhinus canicula*, from the soft tissue of the earlier stages to the fully chondrified juvenile samples, and particularly, for the study of complex and fragile three-dimensional structures as the inner ear. This shows the usefulness of this technique for different kind of samples, not only for mineralized samples like shells, bones or teeth, but also soft tissues, although some contrast-enhancing method must be applied.

2. After testing different methods of drying and contrast enhancement for micro-CT imaging of fixed embryos and juveniles of the shark *Scyliorhinus canicula*, we have determined that the most efficient and simple protocol for obtaining the images from embryos at different developmental stages and isolated inner ears is the staining with phosphotungstic acid, although iodine staining also provided acceptable results.

3. The application of appropriated contrast-enhancing and scanning protocols to embryos and juveniles of *Scyliorhinus canicula* has allowed to obtain the first high-resolution images of the global

development of the inner ear of a chondrichthyan, from early embryonic stages, when the otic placode starts to invaginate, to juvenile stage, when the inner ear is a miniature of the adulthood. The analysis of the two-dimensional and three-dimensional images obtained has made possible to elaborate a realistic and detailed description of the morphogenesis of the inner ear in the shark *S. canicula*, recognized as the species that represent the cartilaginous fish group.

4. The development of the inner ear of *S. canicula*, at different to that observed in bony fishes and reptiles, takes place by an invagination process of the otic placode similar to that observed in lampreys and non-reptilian tetrapods. This development begins at early stages, at least as soon as Ballard´s stage 18, and comprises approximately one third of the entire embryological period, until the inner ear reaches a mature-like aspect at the end of stage 31.

5. In order to provide a comparative framework, the developmental process of the inner ear of *S. canicula* may be divided in three main periods according to the morphological changes that happen and on the basis of external features and landmark events. The first period comprises from the placodal stage to the formation of the otic vesicle at Ballard´s stage 25; the second period comprises the transformation of the round vesicle at stage 25 into a mature-like

inner ear at the end of Ballard´s stage 31; and the third period begins at stage 32 and implies growth according to the body size and the maturation of the sensory organs.

6. In this study we have shown that at Ballard´s stage 32 the mature morphology of the inner ear is recognized, with three perpendicular semicircular canals and three ventral chambers: the utricle (with the utricular recess), the saccule located ventral to the utricle and connected to it by a narrow duct; and the lagena at the rear part of the saccule and connected to it by a wide space. This organization corresponds to the general characteristics of the gnathostomes.

7. The posterior semicircular canal is almost a complete circle connected to the utricle by a single duct, and implies the absence of a *cruss commune* between the anterior branch of the posterior semicircular canal and the rear branch of the anterior semicircular canal, as happens in non-elasmobranch vertebrates. In contrast to tetrapods and bony fishes, the anterior semicircular canal and the horizontal semicircular canal meet and fuse over the utricular recess, what can be distinguished from stage 32 onwards, which we have identified as the beginning of the maturation of the sensory organs.

8. The inner ear of *S. canicula* is communicated to the exterior by the endolymphatic duct, a reminiscence of the invagination process that never closes completely. The endolymphatic duct arises from the medial wall of the saccule and goes dorsally, taking a sinuous trajectory at its dorsal region, before opening to the exterior on the top of the head, next to the midline. This study reveals that the endolymphatic duct is formed as consequence of the invagination process and that it is not a new duct.

9. This is the first study detailing the origin, development and connexion between the components of the inner ear. On the basis of the expression pattern of certain markers like DCX, HuC/D and *NeuroD* in the **first period** of the development of the inner ear, we have identified the formation of the primary neurons of the statoacoustic ganglion, originated by delamination from the otic epithelium, similar to that observed in other vertebrates.

10. The development of the innervation of the inner ear takes place during a long period, about two months long, from the first stages, where fibers immunoreactive to DCX appear linking the otic cup to the brain (st20), to the latter stages when the innervation pattern is complete (st32). The innervation of all the sensory areas of this structure increases and new branches appear as the otic vesicle grows and subdivides. When complete, during the **second period**, all the

sensory organs that are differentiating receive innervation from the statoacoustic ganglion.

11. The maturation of the sensory organs takes place during the **third period**, being its number and distribution similar to that observed in other chondrichthyans, with three otolithic maculae located in the utricular recess, saccule and lagena; a non-otolithic macula neglecta located next to the utriculo-saccular boundary and the ductus connecting the chambers to the posterior semicircular canal; and the three ampullary sensory cristae common to all the gnathostomes.

12. Cell proliferation is quite abundant during inner ear development in the walls of the labyrinth and also in the statoacoustic ganglion, but is lacking in presumptive sensory patches until the morphologic development of the ear is completed, by the end of the stage 31. By stage 32, some cells within the thickened maculae and cristae begin to proliferate. At the same time, some differentiated hair cells became distinguishable at the sensory patches.

13. The formation of the statoacoustic ganglion begins at early stages of the first period and continues by delamination during the second period. Differentiated ganglion cells are present in the statoacoustic ganglion from intermediate stages like st27, indicating

that the maturation of statoacoustic ganglion cells precedes that of the sensory cells.

14. The delayed maturation of the sensory patches in relation to that of the statoacoustic ganglion is also evidenced by the expression of *Sox2* at late stages in these regions, which indicates the maintenance of pluripotency in cells of the maculae and cristae and also the capacity to originate new sensory hair cells.

15. The results obtained provided abundant and useful data for comparing with the development of the inner ear in other model organisms and also to increase our knowledge about the evolution of the development of this sense organ. This work shows the usefulness of 3D studies for gaining knowledge about the development of complex structures and lays the groundwork for the implementation of an atlas of the developing inner ear of *S. canicula.*